UNIVERSITY OF LEICESTER

Macrophages as a Replicative Niche During Systemic Bacterial Infection

Thesis submitted for the degree of Doctor of Philosophy at the University of Leicester

By

Joseph Jack Wanford BSc

Department of Genetics and Genome Biology, University of Leicester

March 2020

Abstract

Bloodborne bacterial pathogens are exposed to multiple macrophage-mediated clearance mechanisms in organs including the liver and spleen. Some pathogens – termed intracellular pathogens – are known to resist intracellular killing and persist within cells during the pathogenesis of infection. Extracellular pathogens are not widely considered to survive and replicate within macrophages. In this thesis, I report that two typically extracellular pathogens *Streptococcus pneumoniae* and *Klebsiella pneumoniae* have key phases of infection within tissue macrophages. For *S. pneumoniae,* I demonstrate that following infection of mice, bacteria can replicate within CD169-positive metallophilic macrophages and red pulp macrophages, but are efficiently cleared by SIGN-R1-positive marginal zone macrophages in the spleen. CD169+ macrophages were shown to be a critical safe haven for pneumococci prior to invasive disease, as blocking these cells with a monoclonal antibody prevented disease. Replicative foci within CD169-positive macrophages were shown to be hidden from neutrophil surveillance which may facilitate pneumococcal immune evasion in the early hours of infection. Instead, for *K. pneumoniae*, I demonstrate that hypervirulent strains (hv*Kp*) – characterised by their hypermucoid capsules – replicated within splenic macrophages and Kupffer cells in the liver, while non-hv strains did not. Replication of hv*Kp* within Kupffer cells formed a focal point for resistance to neutrophil-mediated killing, which led to the formation of tissue abscesses comparable to that which is observed in human disease. I developed a model of *ex vivo* human spleen perfusion, and porcine spleen-liver co-perfusion which allowed the translation of our murine findings for both pathogens to the human host. Together, this thesis identifies the within-macrophage niche as a safe haven for two bacterial species traditionally considered to be extracellular during the pathogenesis of infection. This work will open new research opportunities in the short term and facilitate the development of novel treatment strategies in the future.

Acknowledgements

As with all large bodies of work, this thesis would not have been possible without the help of a huge number of mentors, and lab mates. First, I thank my supervisor Professor Marco Oggioni, for encouraging my curiosity, and for his enthusiasm for my work. I am grateful to my second supervisor Dr Christopher Bayliss for providing an alternate perspective on science. I greatly benefitted from the constructive project feedback from my probation panel, Dr Julie Morrissey, Professor Peter Andrew, and later Dr Andrew Millard. I am thankful for the advice and mentorship of Professor Edward Richard Moxon, and Dr Luisa Martinez-Pomares throughout the course of this project, which also benefitted from the collaboration of Dr Wen Chung, and Professor Ashley Dennison, without whom the perfusion work would not have been possible.

Without all members, past and present of lab 121, this thesis would have been half as productive, and twice as miserable. I thank Giuseppe Ercoli for his teaching, Luke Green for his advice and dad jokes in the early stages of my PhD, Neelam Dave for keeping me on my toes with 10000 questions per day, Megan De Ste Croix for tolerating my messiness, Charlotte Davison for the beauty of her singing, Liam Crawford for even worst jokes than Luke, and Alan for playing football with me in the office. I am especially thankful to David Carreno, Ryan Hames, and Zydrune Jaisinaite, with whom I shared this project, for their assistance, dedication, Eurovision updates, and grime bars.

This thesis would not have been possible without the continued encouragement of my friends and family. I am immeasurably grateful to my parents Nicola and Adrian Wanford, my sister Madeleine Wanford, and my grandparents Terrance and Susan Perrin for their unerring love and support, and for continually pretending to be interested in my work. Lastly, I am especially thankful to Lily Patrick for tolerating my ever increasing stress levels, and for her unwavering love, support, and communication in a made up language.

Table of Contents

Figure list

Table list

Abbreviations

Abbreviations	Meaning
CSF	Cerebrospinal fluid
PAMP	Pathogen Associated Molecular Pattern
PRR	Pattern Recognition Receptor
LPS	Lipopolysaccharide
TLR	Toll-like Receptor
CD	Cluster of Differentiation
ROS	Reactive Oxygen Species
KO	Knock Out
IL	Interleukin
MHC	Major Histocompatibility Complex
IFN	Interferon
TNF	Tumour Necrosis Factor
PMN	Polymorphonuclear
RPM	Red Pulp Macrophage
MMM	Marginal Metallophilic Macrophage
MZM	Marginal Zone Macrophage
WT	Wild Type
IV	Intravenous
LD	Lethal Dose
BHI	Brain Heart Infusion
LB	Luria Bertani
hv	Hypervirulent
CR	Carbapenem Resistant
CAT	Casein Tryptone Broth
LPM	Low Phosphate and Magnesium
OD	Optical Density
PBS	Phosphate Buffered Saline
CFU	Colony Forming Units
mAb	Monoclonal Antibody
MOI	Multiplicity of Infection
N/A	Not Applicable
IgG	Immunoglobulin G
IHC	Immunohistochemistry
MIC	Minimum Inhibitory Concentration
MBC	Minimum Bactericidal Concentration
HRP	Horseradish Peroxidase
ELISA	Enzyme-Linked Immunosorbent Assay
MDR	Multi-drug Resistant

Abbreviations are shown in order of appearance.

Chapter 1: Introduction

The Host Defence Against Systemic Bacterial Pathogens

1 Chapter 1: Introduction

1.1 General Introduction

Bacteria are a domain of prokaryotic organisms which have been co-evolving with eukaryotes for millions of years [1]. In the majority of cases, bacteria co-exist symbiotically within sites of the host exposed to the environment such as the nasopharynx and the gut. Frequently, bacteria cross barriers in the gut, nasopharynx and skin to enter sterile sites such as the blood and CSF. This event leads to series of complex interactions of the pathogen with the host. In the majority of cases, the host pathogen interaction is self limiting, and efficiently resolved by the immune system. In rarer cases, bacteria are able to either overwhelm, or subvert active immune responses to proliferate in sterile sites, leading to pathology. The immune system, is a complex network of cells and effector molecules that are geared towards responding to pathogens and clearing them from systemic sites (the innate response), and also to prime the body from future attack from pathogens (the adaptive response). There are a number of organs in the body which are highly specialised for the immune response to infection, both in their mechanical, anatomical, and cellular functions. This thesis will examine the role that macrophages in the spleen and liver, play in the defence against invasion by the two major pathogens *Streptococcus pneumoniae*, and *Klebsiella pneumoniae.* Furthermore, I will try to demonstrate the dual edged sword scenario of these pathogens in their interactions with macrophages, whereby they can be manipulated to facilitate pathogenesis.

1.2 Macrophages in Defence of Bacterial Infection

1.2.1 The macrophage

Macrophages are professional phagocytes with complex ontology. The previous model for macrophage development stated that they were derived from monocytes, which terminally differentiate upon inflammation. Recent studies have indicated that many tissue-resident macrophages specifically, in fact originate from early development in the yolk sac – the membrane outside of the human embryo connected to the midgut – and not from circulating monocytes from the bone marrow [2]. Furthermore, later during development macrophages can be derived from fetal liver produced monocytes [3], before being replenished by bone marrow derived monocytes after birth in the neonate and in fully developed adults [4]. In many cases,

it is unclear whether tissue macrophages derived in early development are functionally distinct from macrophages replenished from circulating monocytes. Furthermore, the origins of the numerous heterogenous populations of macrophages in tissues remain unclear (e.g. yolk sac vs fetal liver). The ontogeny of macrophages in different tissues have been reviewed elsewhere [5], and a diagrammatic representation is shown in Figure 1. Macrophages are an extremely diverse set of cells, and tissue resident cells in particular become very specialised to specific functions depending on their anatomical location, ranging from tissue homeostasis [6], killing of pathogens [7], antigen presentation [8], and wound healing [9]. The roles of specific macrophage populations in innate and adaptive immunity relevant to the context of this thesis will be discussed in detail later in this chapter. One common feature of all macrophages is their ability to perform phagocytosis of foreign antigens, or apoptotic self antigens and blood cells. This thesis and the sections to follow will focus on the interaction of tissue resident macrophages with bacterial pathogens.

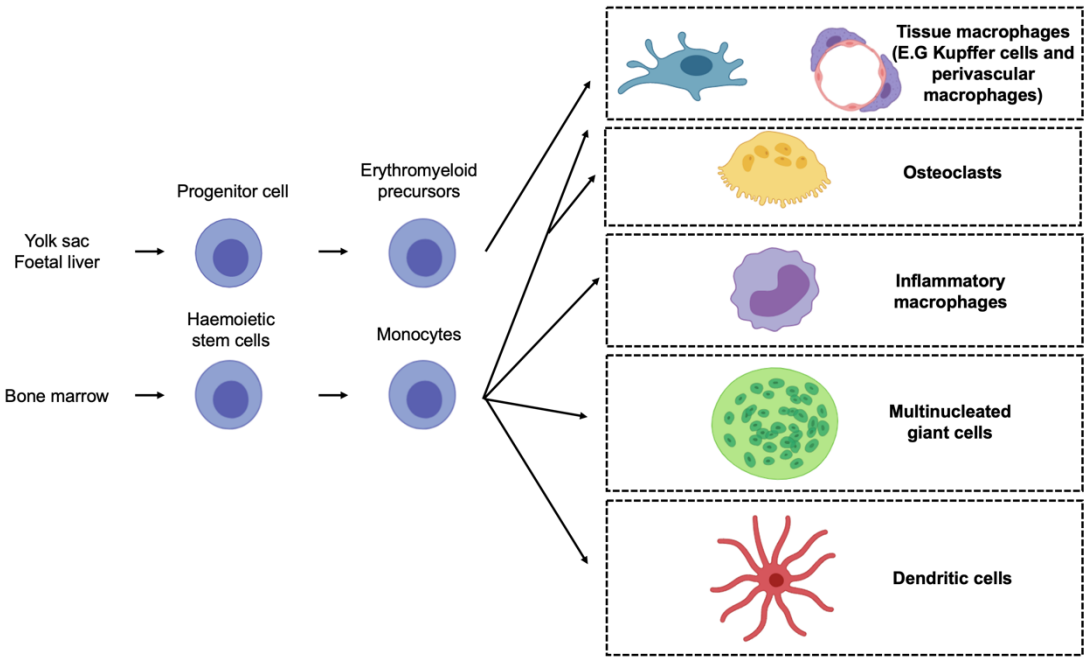

Figure 1 - *Ontology of tissue macrophages and other mononuclear phagoctyes.* Cell types are labelled with non-bold text. Figure was adapted from [10] and was produced in Biorender. Arrows indicate proven cell lineages.

1.2.2 **Phagocytosis**

1.2.2.1 **Foreign antigen recognition and uptake**

Phagocytosis originates from the Greek word 'phago' (to devour), and is the active process of engulfing foreign material. To undergo phagocytosis, macrophages must first recognise foreign particles. In non-immune organisms, this can occur via the recognition of pathogen specific surface structures which can be differentiated from host cell structures, termed Pathogen Associated Molecular Patterns (PAMPs), which are identified by Pathogen Recognition Receptors (PRRs) on the macrophage surface. PAMPs can be non-self surface sugars such as bacterial lipopolysaccharide (LPS) [11], surface proteins, or apoptotic host cells which lose expression of the self recognition molecule α2,6-terminal sialic acid [12, 13]. One common example of bacterial recognition by macrophages is the binding of LPS by Toll-like Receptors (TLR) 2 and 4 [14], and components of the Gram-positive cell wall by TLR2 [15]. An additional mechanism of foreign particle recognition is via opsonin receptors on the surface of the macrophages. Opsonisation of foreign particles is mediated by either binding of antibody (providing cross talk between adaptive and innate immunity) [16], or by deposition of complement [17]. Macrophages express different repertoires of both Fc (the host recognition portion of the antibody molecule) and complement receptors which can facilitate recognition of opsonised pathogens. Specific macrophages receptors of tissue resident cells will be discussed later in this section. It should be noted that there is an enormous gap in our knowledge of macrophage uptake pathways, and the subsequent subcellular events, following phagocytosis mediated by opsonins vs PRPs. Therefore, the phagocytic pathway described in detail below is predominantly that of the antibody-mediated pathway. The phagocytic uptake pathway determines a number of facets of phagocytosis, one of which is speed of phagosome processing – Fc-receptor mediated phagosome maturation for example is far quicker than complement mediated uptake [18]. It should be noted that a number of bacterial pathogens manipulate mechanisms of macrophage uptake via both coating their surfaces with host mimetics [19], and preventing antibody-mediated opsonisation by antigenically varying host structures [20].

Following recognition of foreign particles by any of the above mechanisms, macrophages undergo extensive actin polymerisation, mediated by a number of

cellular GTPases (e.g Rac1, Rac2, and Cdc42) [21]. Cdc42 is a direct binding partner of Wiskott-Aldrich syndrome protein (WASP) which directly initiates actin polymerisation via its interaction with the Arp2/3 complex [22], which are nucleation sites for new actin filaments. This leads to invagination of the macrophage membrane, forming the so called 'phagocytic cup', which encompasses the foreign antigen [23]. Closing of the phagocytic cup, leads to formation of the early phagosome, which can then undergo maturation events leading to bacterial cell death and antigen processing.

1.2.2.2 **Phagosome maturation**

Following phagocytosis, the subcellular composition of the phagosome is extremely dynamic, and is altered multiple times to make it inhospitable for microbes – a process driven by multiple fusion events with host cell compartments. Here I will described a generalised process of phagosome maturation, including the host proteins involved in 3 parts: the early phagosome, the late phagosome, and the phagolysosome. Killing mechanisms will be described in section 1.2.2. Following phagocytosis, the so called nascent, early phagosome is primarily made up of cell membrane, and as such its proteome consists of surface proteins [24]. Phagosome maturation through stages from early endosomes, to phagolysosomes is mediated by GTPases from the Rab family. Rab5 for example mediates the fusion of early phagosomes with endosomes by engaging EEA1 [25]. In addition to EEA1, Rab5 also facilitates the recruitment of type III PI3K human vacuolar protein-sorting 34 [26]. This protein generates phospholipids which recruit a number of other proteins involved in phagosome maturation [27, 28]. As phagosome maturation progresses, Rab5 co-localisation is lost, and Rab7 is recruited which facilitates the fusion of the phagosome with lysosomes [29]. Throughout this process, luminal pH decreased which activates a number of within-phagosome proteins with acidic pH optima (see below). It should be noted that macrophages which have been classically activated (see section 1.2.3) show different kinetics of phagosome maturation to M2-like cells [30, 31].

1.2.2.3 **Killing mechanisms in the macrophage phagolysosome and bacterial strategies to evade killing**

Owing to the diverse nature of pathogens, and their different resistances to environmental stress, macrophages have developed a repertoire of mechanisms for killing pathogens. Not all pathogens are equally susceptible to these individual mechanisms, and successful clearance is usually a product of multiple killing mechanisms, and collaboration between macrophages and other immune cells. Following successful passage of bacteria to the phagolysosome, pathogens are exposed to nutrient starvation, acidification and toxification, and a vast number of anti-microbial effector molecules [32]. A diagrammatic representation of the killing mechanisms described below are shown in Figure 2.

1.2.2.3.1 **Nutrient starvation/nutritional immunity**

The phagosome has a number of transporters embedded within its membrane which actively remove nutrients, limiting their availability. Iron is a critical metal for microbial metabolism, and is essential for survival in many pathogens, through regulation of the *fur* regulon [33]. The phagosome becomes increasingly depleted in cations such as iron and manganese during the maturation process. The NRAMP-1 (natural resistance-associated macrophage protein 1) becomes enriched on the phagosomal membrane as it matures and becomes fused with lysosomes [34]. This protein is an active transporter of cations, and pumps iron out from the phagosome into the cytosol [35, 36]. This iron is then sequestered by additional cytosolic chaperones for storage, which limits the availability of this critical metal to bacteria both with the phagosome, and in the host cell cytoplasm. Furthermore, iron is exported from the cell as a whole by the Ferroportin protein which is under the transcriptional control of a number of immune modulators [37, 38]. In response, bacteria have co-evolved a number of acquisition systems to compete for iron which will be discussed later in this thesis. Bacteria such as *Salmonella ssp.* for example, in response to vacuole acidification and nutritional starvation, switch on expression of specific genes, and become non-replicating persisters [39–41]. Not only does this allow *Salmonella* to persist within the phagosome, but it renders them resistant to many antibiotics which rely on active replication for their activity [42, 43].

1.2.2.3.2 **Acidification and toxification**

During the process of maturation, the phagosome becomes increasingly more and more acidic, a process which is mediated by the vacuolar ATPase which pumps H+ into the phagosome [44, 45]. Furthermore, as the phagosome matures the membrane becomes less permeable, maintaining protons and the resulting acidic pH within the membrane. There are a wide spectrum of microbes which are able to resist acidic pH to varying degrees. Many bacteria which are not able to resist acidic pH have developed mechanisms to prevent maturation of the phagosome, reducing their need for acidic pH resistance. *Salmonella ssp.* for example are know to secrete effector proteins via their two Type 3 Secretion Systems (T3SS) – SPI-1 and SPI-2 – which modulate host cell biology [46]. Many of these factors are thought to work in tandem to prevent fusion of the *Salmonella* containing vesicle (SCV) with lysosomes via extensive actin remodelling [47]. Enteric bacteria are highly pH resistant [48, 49], owing to their inhabitation of the gastric tract, where acidic pH is commonplace. Common mechanisms of acid tolerance in these bacteria include the generation of protective clouds of ammonia [50]. Bacteria such as *S. pneumoniae* which colonise the nasopharynx do not possess such tolerances and are therefore highly susceptible to low pH within macrophages [51].

Trace metals such as copper and zinc, which are essential bacterial co-factors in small quantities, can be toxic in high quantities. Macrophages utilise a number of transporters to import copper [52] and zinc to the phagosome, and form a toxic environment for the bacteria within. Proteins of the SLC3OA family are transporters of zinc [53], and function both to efflux them from the cell, thus limiting trace amounts of metal in the cytosol which would be beneficial to microbial growth, and to import them within the phagosome to toxic concentrations for the bacteria. Supporting this, many bacteria encode efflux pumps for metals such as zinc [54] and copper [55] which are critical for within-macrophage survival *in vitro* [56], and for virulence *in vivo* [57].

1.2.2.3.3 **Anti-microbial reactive oxygen species**

Reactive oxygen species (ROS) have long known to be critical to the immune control of pathogens. Macrophages produce a number of reactive species, which work in tandem to kill pathogens, in addition to the release of protein-based antimicrobial

compounds into the phagosome. Additionally, other phagocytes such as neutrophils, and dendritic cells, as well as non-phagocytic cells produce reactive species in varying levels. Here I will discuss a few of the ROS based-mechanisms employed by macrophages to kill pathogens. During maturation of the phagosome, NADPH oxidase 2 (NOX2) is assembled on the phagosomal membrane, but is also present on the whole cell membrane [58, 59]. NOX2 catalyses the conversion of intracellular O_2, into the reactive oxygen species O_2 ·- [60] which is subsequently converted into hydrogen peroxide (H_2O_2) by superoxide dismutase (SOD) [61]. High concentrations of ROS in the phagosome are microbiocidal, but there have been a number of recent advances in the field demonstrating that lower concentrations of cytosolic ROS, are involved in a number of additional cellular and global immune processes such as macrophage activation [62], and chemotaxis (reviewed in detail by Dupret-Crochet *et al.* 2013). A second pathway for production of reactive species, is the inducible nitric oxide synthase (iNOS) pathway [63], which although similar to NOX2 in its requirement for NADH, is distinct in that it produces reactive nitrogen species (NO.). These two pathways work in tandem to control pathogens, are tightly regulated by a number of physiological stimuli, and consist of multiple signalling cascades (reviewed in detail by Gang., 2004).

The mechanisms by which reactive species kill bacterial pathogens is hotly debated [64], and is likely dependent on the pathogen in question, the quantity of ROS they are exposed to, and the phagocyte subset in question. The majority of our understanding of the bactericidal activity of reactive species, comes from studies of *E. coli,* and *Salmonella spp* and a small number of immortal macrophage cell lines. ROS can damage bacterial enzymes which utilise iron as a co-factor via fenton chemistry leading to defects in bacterial metabolism [65]. Furthermore, the hydroxyl radicals produced by fenton chemistry reactions between iron and H_2O_2, are highly bactericidal by damaging DNA [66]. Furthermore, H_2O_2 is capable of direct interaction with cysteine residues of bacterial proteins which can also damage the cell. Many of the toxic activities of reactive species are not limited to bacteria, therefore their close control within the phagosome is important to the viability of the host cell [67].

Bacterial resistance to reactive species can be mediated by prevention of phagosome maturation, thereby preventing toxic exposure to these compounds, as is employed

by *Salmonella ssp* [68] – although these bacteria also possess systems for detoxifying ROS [69], and the Salmonella-containing vacuole is not entirely ROS negative [70].

1.2.2.3.4 Macrophage cell death, inflammasome-mediated pyroptosis and recruitment of granulocytes

The macrophage response is not always sufficient for the control of intracellular pathogens (see later in this thesis). A number of pathogens have been shown to trigger different mechanisms of cell death such as apoptosis or pyroptonecrosis [71–74], which whilst mechanisms of microbicide themselves [75], also mediate the release of inflammatory mediators, which can lead to neutrophil chemotaxis to the site of infection [76]. Dockrell and colleagues [77–79] demonstrated with a combination of macrophage depletion, knock out mice lacking microbiocidal mechanisms, and inhibitors of apoptosis, that apoptosis mediates the killing of intracellular pneumococci in the absence of additional inflammatory influx. The initial clearance of pneumococci is facilitated by the phagolysosome (see above). The capacity for killing within the phagosome is limited, and following prolonged resistance to killing of intracellular bacteria, there is a downregulation of anti-apoptotic proteins, leading to programmed cell death, resulting in killing of the bacterium [80]. Some macrophage subsets are known to activate 'inflammasomes' following microbial challenge. Inflammasomes are host cell receptor-sensor complexes which recognise microbial pathogens, activate caspase-1, which can eventually lead to cell death and inflammatory cytokine production [81]. NLRP3 is one such inflammasome complex [82] which following challenge with pathogens such as *S. pneumoniae* and *S. aureus* elicits IL-1β production [83, 84], which leads to the chemotaxis of neutrophils and in some models the resolution of infection. Importantly however, the inflammatory response elicited by NLRP3 can also be pathological [85], and inhibitors of this complex are being considered as an adjunctive therapy for pneumococcal meningitis [82, 86].

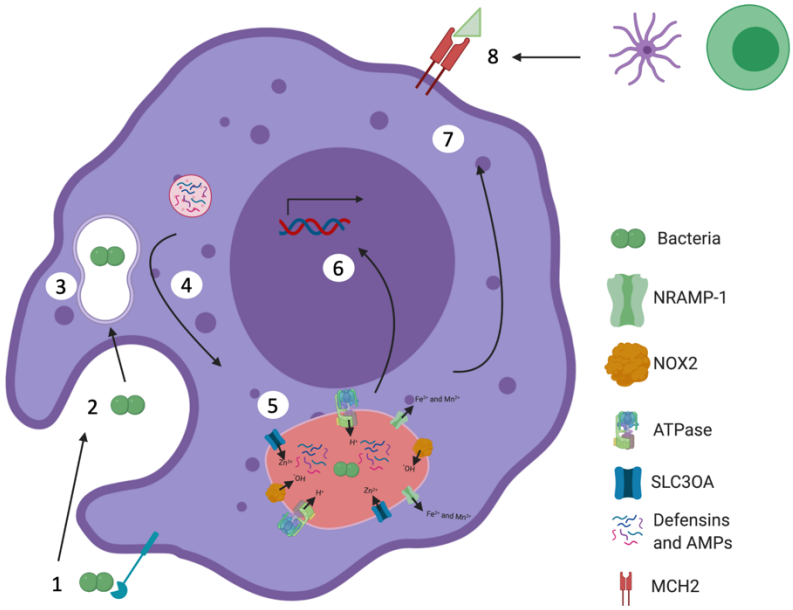

Figure 2 - *Mechanisms of macrophage killing*. Figure was made using Biorender. The meanings of symbols are explained in the legend. (1) engagement of bacteria by surface phagocytic receptors, (2) invagination of the cell membrane to form the phagocytic cup, (3) suspension of bacterial within early phagosome, (4) fusion of early phagosome with lysosomes, (5) recruitment of proteins and killing mechanisms to the late phagosome, (6) activation of cytokine transcription, (7) trafficking of antigens to the cell membrane, (8) presentation of antigens on the cell surface to cells such as T cells. The size of the phagosome surrounding bacteria is not representative, and is only large so as to fit images of possible effectors.

1.2.3 **Macrophage activation: the M1 and M2 continuum**

Macrophages are exposed to a wide variety of stimuli, and as such require different behaviours and production of downstream effectors to respond to these stimuli. Early studies indicated that following initial infection of macrophages with *Listeria monocytogenes*, that the secondary infection was met with a more microbiocidal response [87] – a phenomena that would later be come to known as 'classical activation' of the macrophage, or M1 activation. Later studies demonstrated that IL-4 and IL-13 stimulation of macrophages enhanced antigen presentation of Major Histocompatibility Complex 2 (MHCII), and reduced the production of pro-inflammatory cytokines, which was entirely distinct from the phenotype presented by M1 macrophages [88]. This 'alternate activation' led to what became known as the M2 state. It should be noted that multiple subtypes of macrophage activation exist, and that M1 and M2 is not an all or nothing situation, rather a continuum by which

macrophages continually fine tune their phenotypic response to diverse stimuli [89]. Further, much work on the M1-M2 dichotomy has been performed with immortal cell lines, and it is unclear whether diverse populations of tissue macrophages adhere to this continuum. The pathogen-ligand interactions, molecules, and cytokines known to polarise macrophages have been reviewed elsewhere [90], and I will describe a few of these below.

1.2.3.1 **Induction and downstream effectors of the M1-like state**

The M1-state is considered a microbiocidal response against invading pathogens, for which a full-blown inflammatory response is required for clearance. Macrophages can be polarised to the M1 state by exposure to LPS [91], interferon gamma [92] produced by T cells for example, or by the global inflammatory cytokine Tumour Necrosis Factor Alpha (TNF-α) [93]. Stimuli of the M1 state can be classified based on their ability to initiate a pro-inflammatory response. In the case of IFN-λ, this cytokine is directly recognised by interferon receptor which sets a cascade of signalling events resulting in transcription of pro-inflammatory cytokines [94], and enhanced activity of endosomal trafficking proteins [95]. Furthermore, antigenic stimuli such as LPS are recognised by pattern recognition receptors. LPS for example is recognised by Toll-Like Receptor 4 (TLR4), and engagement of this receptor leads to synthesis of M1-like pro-inflammatory cytokines [91], mediated by similar intracellular signalling pathways similar to that of the interferon pathway [96–98]. Firstly, the M1 like state enhances the microbiocidal response such as iNOS production within the phagolysosome, enhancing the killing of intracellular pathogens [99]. The M1 state is also associated with enhanced release of pro-inflammatory cytokines such as IL-1, TNF-α, IL-6, and IL23 [100, 101]. This cytokine profile is associated with enhanced Th1 responses [102].

1.2.3.2 **Induction and downstream effectors of the M2-like state**

M2 polarisation is a highly complex network of stimuli and different downstream effectors, and as such has been subdivided into M2a, M2b, and M2c [89]. Functions of some of the cytokines and receptors produced and expressed by differentially activated macrophages will be discussed in section 1.2.4. Whilst M2-activated

macrophages differ in their phenotype, they can be defined by the prototypical marker Arginase-1 [103]. Arginase-1 is an enzyme which catalyses the conversion of L-arginine to L-ornithine and urea. One function of arginine-1 is thought to be the feeding of L-ornithine into the collagen synthesis pathway which may facilitate tissue repair [104] – a phenotype heavily associated with M2 polarisation. Additional functions of arginine-1 include dampening of T-cell proliferation, and the depletion of NO (the progenitor of NOS [105].

1.2.3.2.1 **M2a**

M2a polarisation (also known as alternate activation) is induced potently by exposure of macrophages to the two cytokines IL-4 and IL-13 [106], which are produced in abundance by T-cells in a positive feedback loop [107]. M2a polarisation produces a number of effector receptors and cytokines involved in Th2 responses, allergic responses, and restriction of parasites through encapsulation. This is achieved by enhanced production of IL-10 [108], and IL-1 receptor agonist, enhanced expression of MHCII on the cell surface, and enhanced expression of the immune receptors mannose receptor [88] and Cluster of Differentiation 163 (CD163) [109]. M2a cells are also known to produce large amounts of the cc family of chemokines such as CCL17/18 which help mediate the Th2 responses [110].

1.2.3.2.2 **M2b**

M2b polarisation (also know as type II activation), is associated with Th2 activation and immunoregulation, and is induced by engagement of TLR with microbial ligands, or engagement of immune complexes via IgG receptors [111]. M2a activation is associated with secretion of IL-10 [112], IL-1, and TNF-α [113], in addition to the chemokine ligand CCL1 [114]. M2b cells also express large amounts of surface CD80, CD86, and MCHII [111].

1.2.3.2.3 **M2c**

M2c macrophages (also known as de-activated macrophages) are heavily associated with a lack of inflammation [115], but rather with matrix deposition and the remodelling of tissue in response to damage. M2c is induced by the anti-inflammatory cytokine IL-10 [116], and results in the additional expression of IL-10 in a positive feedback loop,

and the production of extracellular matrix components such as matrix versican which facilitate wound healing [117].

1.2.4 **Cytokine and chemokine production**

Macrophages are uniquely positioned in the tissue not only to respond to initial challenge by pathogens, but also the coordination of adaptive and continued innate immune responses, by the secretion of cytokines. A vast amount of work has been performed, documenting cytokine secretion in immortalised macrophages, and of readily available primary cultures of cells such as bone-marrow derived macrophages. The dynamics and repertoire of cytokine production of lesser populations of tissue macrophages, in response to diverse stimuli is less understood. Here I will describe the cytokine response of 'typical macrophages', and responses of specific macrophage populations will be described later in this chapter. Macrophages are able to response to inflammatory (e.g. pathogens) and non-inflammatory (e.g. host cells) stimuli and co-ordinate their cytokine response accordingly.

1.2.4.1 **Pro-inflammatory cytokines produced by macrophages**

Inflammatory stimuli such as phagocytic processing of bacterial PAMPs lead to the production of cytokines which co-ordinate inflammatory reactions. Macrophages are major producers of tumour necrosis factor (TNF), IL-1, 6, 8, and 12 for example which elicit different activities on neighbouring cells [118]. Activities of cytokines are largely overlapping, and the full complexity of regulation of the cytokine network, and their downstream effects are poorly understood. Furthermore, the functions of many cytokines are pleiotropic, having both pro, and anti-inflammatory functions, adding further complexity the their functional characterisation [119]. TNF for example is perhaps the best understood cytokine, is canonically pro-inflammatory and has a number of global activities. These include but are not limited to: neural activities such as the suppression of appetite [120], and the induction of fever [121], vasodilation which allows extensive infiltration of neutrophils to the inflamed area [122], and the induction of apoptosis in infected cells [123]. Conversely, a major function of the structurally unrelated, pro-inflammatory cytokine IL-12 is to stimulate Th1 cells [124] – a major arm of cellular immunity. This differs from the activities of TNF in that it relies less heavily on the promotion of cell death and inflammatory cell infiltration, and

instead relies on the induction of intracellular killing through IFN- γ production by T cells [125].

1.2.4.2 **Anti-inflammatory cytokines produced by macrophages**

As discussed below (section 1.5.2) the dysregulated production of pro-inflammatory cytokines has been implicated in a number of pathologies. Additionally, many pro-inflammatory cytokines set off a cascade of events which exacerbates inflammation. The immune system therefore requires mechanisms to reduce existing inflammation, and also to facilitate cellular events which do not require a large scale inflammatory response. These are often mediated by regulatory molecules known as anti-inflammatory cytokines. One example of an anti-inflammatory cytokine is the IL-1r antagonist which is produced by macrophages among other cells, in response to IL-4 exposure [126, 127]. Binding of IL-1r antagonist to IL-1r helps to modulate the pro-inflammatory effects of the IL-1 response.

1.2.4.3 **Chemokines produced by macrophages**

Chemokines are immunomodulatory molecules and co-receptors which facilitate the chemotaxis and attachment of inflammatory cells to sites of infection. Both classically and alternatively activated macrophages produce chemokines in response to infection. One example is the production of CXCL1 by macrophages in response to microbial challenge, which facilitates the chemotaxis of neutrophils to the inflamed area [128]. This is beneficial as synergy between macrophages and neutrophils have been shown to have enhanced microbiocidal activity [129].

1.2.5 **Antigen presentation**

Following intracellular killing of bacterial pathogens via the phagolysosomal pathway described above, bacterial factors are degraded into small antigens (such as peptides) by vacuolar enzymes such as the cathepsins [130, 131]. These antigens are sequestered into endosomal compartments where they can interact with MHCII molecules [132, 133]. Antigen-MHC complexes can then be shuttled to the surface to via the endoplasmic reticulum pathway, where they are surfaced expressed [134]. This allows their recognition by T-lymphocytes which can then facilitate subsequent immune responses [135]. In the case of cytosolic antigens, such as invading viruses

and bacteria that have escaped the lysosomal trafficking system, the MHCI pathway is initiated and facilitates antigen presentation [136].

1.2.6 **Neutrophil-mediated killing**

Neutrophils or polymorphnuclear cells (PMNs) are phagocytes of the granulocyte lineage, specially adapted to the innate response to pathogen invasion. Neutrophils are the most abundant phagocytic cell in mammals, and make up between 55-80% of circulating white blood cells [137]. They are relatively small (~12μm diameter) and have lobe nuclei, differentiating them from mononuclear cells such as monocytes. Neutrophils are considered the most bactericidal of innate immune cells, and have evolved a plethora of killing mechanisms. Neutrophils are rapidly chemotactically recruited to sites of infection, mediated by expression of a number of receptors for chemokines and adhesion molecules [138]. Neutrophils are capable of phagocytosis and intracellular killing of pathogens mediated by reactive species [139], but also have extracellular mechanism of killing. PMNs are characterised by a large number of cytosolic granules containing defensins and degradative enzymes – such as the protease neutrophil elastase [140] – for the killing of bacterial pathogens [141]. At sites of infection, the contents of these granules are released, along with fibres composed primarily of DNA known as NETs. This process of 'NETosis' [142] entraps pathogens and renders them targets for the bactericidal contents of the granules which are sequestered to the NETs. It should be noted that many of these effectors also mediate host tissue damage, and therefore the control of their release is tightly regulated, and often intertwined. For example, in meningitis, neutrophils are the major effector mediating the inflammatory response which is eventually responsible for damage to brain tissue. One mechanism neutrophils possess to dampen continued inflammation is to trigger apoptosis following intracellular microbial killing. This facilitates clearance of both dying cell and bacteria without continuing tissue damage [143].

1.3 **The Spleen**

1.3.1 **Anatomic organisation and vasculature**

The spleen is a secondary lymphoid organ positioned in the upper left quadrant of the abdomen [144]. Historically, the spleen has been considered a major organ involved in filtration of pathogens, red blood cells, and cellular debris from the blood [145]. Blood

flow through the spleen is a key facet in the response of this organ to pathogens, and is extremely complex with both an open, and closed circulation, highly adapted to facilitate both adaptive, and innate immune responses [146, 147]. In mice, blood enters the closed circulation of the spleen through the major splenic artery, before branching into the trabecular arteries, surrounded by areas of white pulp. These arteries then leave the white pulp via arterioles, which gradually lose their walled structure, and drain into the venous marginal sinus surrounding the white pulp area, where they are exposed to a diverse population of tissue macrophages. Blood then drains into the open circulation of the splenic red pulp, which is home to macrophages, and neutrophils, before re-entering the circulation via the major splenic vein [148].

1.3.2 Cellular composition of the white pulp, marginal sinus, and red pulp of the spleen

In mice the white pulp is a lymphocyte rich tissue that consists of the peri-arteriolar lymphoid sheathes which are made up of T cell populations, and B cell follicles [149] (Figure 3). The unique position of these cell populations at the early stages of the splenic vasculature, and their close association with macrophages of the splenic marginal zone mean they are perfectly placed to receive presented antigens, and begin to coordinate adaptive immune responses to infection, via the production of antibodies against invading pathogens [150]. The marginal zone is a critical micro-compartment positioned for sampling of foreign antigens [151]. In mice, the white pulp-facing wall of the marginal sinus is lined with metallophilic macrophages (MMM; Figure 3), identified by expression of the lectin receptor CD169 (sialoadhesin), which are thought to have a critical role in antigen presentation to follicular B cells and the subsequent humoral immune response, and coordination of the early innate recruitment of immune effectors such as dendritic cells and neutrophils [152]. The opposing side of the marginal sinus is lined by marginal zone macrophages (MZM), delineated by expression of the C-type lectin SIGNR-1 [153] (Figure 3). MZMs have been shown via depletion studies to be critical in the innate immune clearance of bacterial pathogens, indicating that their role is geared more towards initial control of infection, as opposed to the role of humoral immune responses thought to dominate in the MMM macrophages [154]. The splenic red pulp is home to a more diverse set of cells. The majority population are the red pulp macrophages which are interspersed

along the splenic sinuses. In mice, these cells are differentiated from MMMs and MZMs by their expression of the scavenging receptor F4/80. They are uniquely exposed to large pools of blood and are thus highly adapted to filtration, iron scavenging, and recycling of apoptotic cells and platelets [155]. Also in the red pulp are a large population of resident neutrophils [156], and a pool of mobile monocytes in the cords of bilroth, which can response to localised and systemic infection respectively.

1.3.3 **Species differences**

The majority of immunological characterisation of the spleen, and work to decipher the pathogenesis of invasive pneumococcal disease have been conducted in mice. Whilst these models are readily available and extremely useful tools, they are not perfect as murine and human splenic anatomy, and immunology are distinct [157]. Pigs are emerging as a translational models, and are a model used in this thesis [158]. In mice, the marginal zone of the spleen is extremely pronounced, forming a ring-like structure consisting of the MMM and MZMs respectively [159]. In humans this area is less pronounced – CD169+ macrophages are arranged around the peri-arteriolar lymphoid sheathes (PALS), a feature that is shared with the porcine model [160]. Furthermore, humans lack a clear homologous population of SIGN-R1+ macrophages [161]. Indeed the human SIGN-R1 homolog, DC-SIGN is restricted to dendritic cells, and is lowly expressed in the spleen [162]. Reagents to characterise porcine immune cell populations are lacking, which has hampered the identification of an analogous cell population in the pig spleen. Considering the red pulp, morphology between pig, mouse and human seems far more conserved than components of the marginal sinus [157]. Humans have a far more pronounced sinusoidal endothelium which are closely associated with the red pulp macrophages when compared to mice which show limited expression of endothelial markers in the red pulp. The expression of markers in the porcine red pulp is still yet to be full explored due to the lack of availability of anti-porcine monoclonal antibodies. Lastly, humans and pigs have been shown to have a larger percentage of circulating neutrophils when compared to their murine counterparts [163]. A diagrammatic representation of the structure of the murine and porcine spleen are shown in Figure 3.

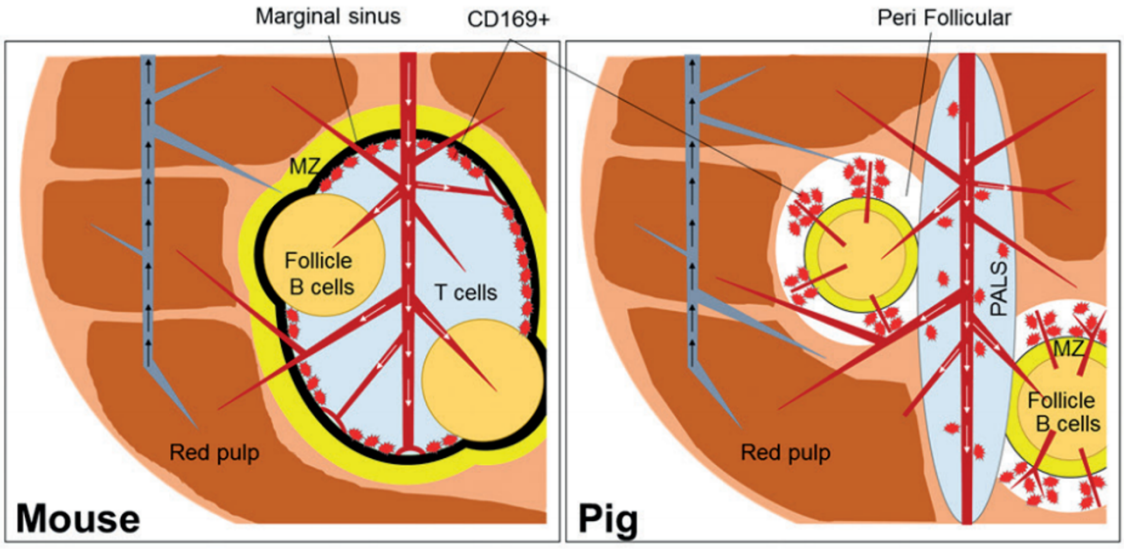

Figure 3 - *Comparative anatomy of the murine and porcine spleen*. T cell areas are shown in grey, B cells are shown in dark yellow, CD169+ macrophages are shown in red, marginal zone-like areas are shown in light yellow, splenic red pulp is shown in brown.

1.3.4 **Splenic macrophages and resident endothelial cells as immune sentinels**

1.3.4.1 **Marginal Metalophillic Macrophages**

As described previously, MMMs are characterised by expression the receptor CD169 (sialoadhesin, or Siglec-1), and are positioned at the inner most wall of the marginal sinus. CD169 is a Pattern Recognition Receptor (PRR), which binds to several linkages of sialic acid [164], and has been demonstrated to be a receptor for bacteria such as *Campylobacter jejuni* [165], and *Neisseria meningitidis* [166], but also for sialyated viruses such as HIV-1 [167]. Their very location, close to the splenic follicular B cells, and the T-cell area in the white pulp, is in accordance with their involvement in antigen presentation and the coordination of the adaptive immune response. Veninga *et al.* (2015) [168] used monoclonal antibodies, to target antigens to different macrophage subsets in the spleen. They observed that targeting of antigen to CD169+ macrophages in the spleen induced high affinity antibody production, and the persistence of specific germinal centre B cells, definitively demonstrating the critical role of these macrophages to humoral immunity. Confirming their specific role in

antigen presentation, and not to microbial killing, Phan *et al.* (2009) [169] demonstrated that CD169+ macrophages had low lysosomal activity, and that foreign antigens, rather than being processed in the phagosome, were often retained on the surface of the cell.

1.3.4.2 **Marginal Zone Macrophages**

Marginal zone macrophages are positioned at the marginal sinus directly adjacent to MMMs, and in mice are identified by expression of the C-type lectin SIGN-R1. Studies of *S. pneumoniae* have indicated that SIGN-R1 is a direct receptor of the pneumococcal polysaccharide capsule [170], and that antibody-mediated blockade of the receptor prevents uptake of bacteria. Further studies have shown that depletion of MZM *in vivo* leads to far shorter survival times in an intravenous model of sepsis [154]. There are several studies which demonstrate the likely reason SIGN-R1+ macrophages are so proficient in control of pneumococcal disease. Firstly, Delamarre *et al.* (2005) [171] demonstrated that SIGN-R1+ macrophages have high lysosomal activity, indicating they are efficient intracellular killers of bacteria. Secondly, Kang *et al.* (2006) [172] found that the SIGN-R1 receptor itself is a potent player in a non-canonical pathway for the fixation of complement to the pneumococcal polysaccharide without the presence of antibody.

1.3.4.3 **Red Pulp Macrophages**

Red pulp macrophages (RPM) are interspersed homogenously within the sinusoidal system of the splenic red pulp, placed to filter red blood cells and apoptotic host cells from the open circulation. RPMs are differentiated from other splenic macrophage populations by their expression of the prototypical macrophage marker F4/80 in mice [173], and by expression of CD163 in humans [174] and pigs [175]. Red pulp macrophages appear less geared to deal with microbial challenge, in part due to their reduced expression of PRPs when compared to marginal zone macrophage populations. Instead, the role of red pulp macrophage has been considered as the filtration of ageing red blood cells which accumulate in the red pulp, but also the phagocytosis of apoptotic host cells [176, 177]. Red pulp macrophages are however capable of producing pro-inflammatory cytokines and chemokines following microbial

challenge, and are known to be a major focal point for the chemotaxis of neutrophils which patrol the red pulp [156, 178].

1.3.4.4 **Splenic endothelial cells**

The innate immune functions of the splenic sinusoidal endothelial cells remains relatively unexplored, although studies have indicated that they express immune molecules and PRPs. Human, but not murine splenic sinusoidal endothelial cells in human [179] express mannose receptor (CD206), a key molecule for the detection of mannosylated pathogens such as selected serotypes of *S. pneumoniae* via their capsular polysaccharide [180, 181]. Interestingly, in mice, red pulp macrophages and not endothelial cells express this marker in the spleen [182]. The intrinsic function of the sinus systems which is given structural stability by the endothelial cells allows sequestration of pathogens and apoptosis host cells in the red pulp, and in this light sinusoidal endothelial cells can be seen as sentinels which immobilise pathogens for processing by professional phagocytes. Sinusoidal endothelial cells in the spleen can also produce pro-inflammatory cytokines during infection, and upregulate expression of chemotactic receptors mediating neutrophil recruitment [183].

1.4 **The Liver**

1.4.1 **Anatomic organisation and vasculature**

The liver is located in the upper right section of the abdomen, directly adjacent to the diaphragm [184]. The liver performs a plethora of functions related to filtration of the blood, protein synthesis, and aiding in digestion. The liver in man is made up of 4 lobes, which are irrigated by two major blood vessels; the portal vein (which provided 80% of total blood input) carrying nutrients from the digestive system, and the hepatic artery which brings oxygen rich blood from the heart [185]. Upon entering the liver, each of these vessels initially divide into left and right sides, irrigating the respected lobes of the liver. The hepatic and portal vessels run antiparallel to the bile ducts, forming the hepatic triad [186]. These vessels run at the hexagonal borders of lobuli – the functional units of the liver. From these vessels, blood reaches the hepatic sinusoids which are lined by hepatocytes, Kupffer cells, and sinusoidal endothelial cells. The sinusoids then drain into the central hepatic vein where it leaves the liver and re-enters the circulation. As the liver is present at the intersection of both portal

and hepatic artery blood, it is exposed to incoming nutrients and antigens from the gut (portal), and from the systemic circulation (hepatic artery). In light of this, it is a critical organ for filtration of gut pathogens which have translocated across the gastrointestinal epithelium (such as members of the Enterobacteriaceae)[187], and also pathogens which have traversed from the lung/nasopharynx directly into the bloodstream, or from the lymph.

1.4.2 **Cellular composition**

The major cells of the liver, making up 70-80% of the organs biomass are the hepatocytes. Hepatocytes are the major structural component of hepatic lobuli, and their main function is protein synthesis, metabolism, and the production of bile (Figure 4) [188]. Their direct exposure to blood places them in the optimal position to process nutrients and detoxify the blood of substances such as alcohol. The liver sinus system is delineated and given structural integrity by sinusoidal endothelial cells (LSECs) [189]. LSECs sit between hepatocytes and the systemic circulation of the lumen, perfectly situated for interaction with foreign antigens (Figure 4). They lack a canonical basement membrane which leaves a loose space between the base of the LSECs and the hepatocytes termed the space of Disse [190] (Figure 4). Next to the hepatocytes at the hepatic lobuli, and sitting on the wall of the liver sinusoids are the Kupffer cells (Figure 4). Kupffer cells are tissue resident macrophages named after their discoverer Karl Wilhelm von Kupffer in 1876 [191]. Kupffer cells are a more homogeneous population of macrophages when compared to the spleen, and are identified by expression of F4/80 in mice [192]. Kupffer cells are a major player in the recycling of senescent red blood cells in the circulation [193, 194], but also have a major part in the clearance of pathogens [195]. Similarly to the spleen, the liver is home to a resident population of neutrophils, which have been shown to work in tandem with Kupffer cells to facilitate clearance of pathogens from the circulation [196].

1.4.3 **Species differences**

Anatomical structure of the liver is highly conserved among mammals. In general, the major difference between the human/porcine and murine liver are the lack of lobation in the former, and the existence of lobation in the latter [197]. Despite this, the differences in liver anatomy are mainly a numbers game, in that with the larger size of

the liver (humans vs mice for example), there are simple more functional liver units, rather than a difference in their core anatomy. A recurring theme is the lack of understanding of the expression of cell surface markers in the porcine vs mouse liver due to the lack of available monoclonal antibodies for their characterisation. Some work has demonstrated different patterns of gene expression in human and mouse liver cells by single cell RNA sequencing, although these studies are still in their infancy, and direct spatiotemporal analysis of these cell populations remains unexplored [198].

1.4.4 Cellular basis for immune surveillance in the liver

1.4.4.1 Kupffer cells

Kupffer cells – named after their discoverer Karl Wilhelm von Kupffer – are the single macrophage population in the liver which line the sinusoids. Kupffer cells have a diverse number of functions in the liver. They have a typically tissue-resident macrophage phenotype, and are identified by expression of F4/80 [192] similar to the splenic red pulp macrophages – both of which line sinus systems. Kupffer cells have a role in clearance of mannosylated antigens from the blood stream, as evidenced by their expression of the mannose receptor (CD206) [199]. Furthermore, Kupffer cells express a repertoire of complement receptors, indicating their critical role in opsonic uptake of pathogens [200]. Kupffer cells are regularly exposed to mannosylated ligands, in the form of microbial LPS originating from the gut, and draining to the liver [201].

1.4.4.2 Liver sinusoidal endothelial cells (LSECs)

The position of LSECs in direct contact with the hepatic circulation, rich with antigens from the gut via the portal vein, puts them in an ideal position to participate in the innate immune response [190]. Unlike endothelial cells present in vessels external to immune organs, LSECs express a repertoire of immune recognition molecules such as toll-like receptors (TLRs)[202] mannose receptor (CD206)[203], and inflammatory cell adhesion molecules [204]. This positions them for the recognition of pathogens and to facilitate the chemotactic response of neutrophils [205]. Furthermore, they express high level of major histocompatibility complexes 1 and 2. They have been

demonstrated to efficiently demonstrate extracellular antigens to circulating T cells, leading to immune tolerance [6]. It is tempting to speculate that LSEC induced tolerance to antigen may dampen the immune response to pathogens allowing them to persist in this organ.

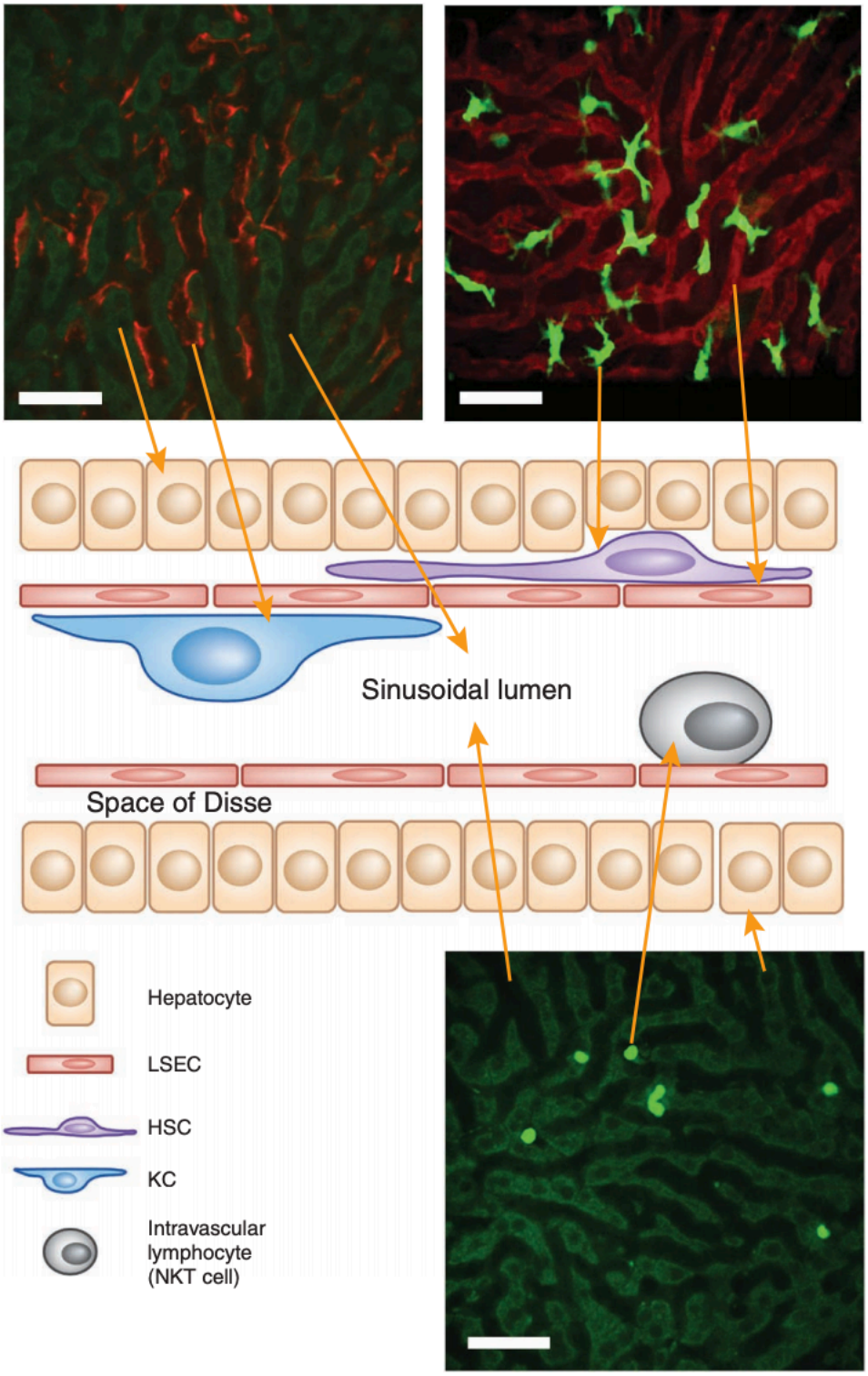

Figure 4. *Cellular composition of the murine liver. Images in this liver were acquired following immunostaining of Kupffer cell, hepatocyte, liver sinusoidal endothelial cells, hepatic stellate cell, and Natural Killer T cell (NKT) populations and visualisation by spinning disk intravital microscopy [206]. A diagrammatic figure of these cells is provided in the centre of the figure and provides reference to the microscopy figures.*

1.5 Bacteria Induced Sepsis

1.5.1 Symptoms, cause and risk factors

Sepsis is a dysregulated immune syndrome in response to infection, differentiated from the commonly termed septicaemia in that it is caused by the bodies response to challenge, and is not the challenge itself [207, 208] Sepsis has an extremely high mortality rate if not caught early, and can cause long lasting sequalae in survivors [209]. Sepsis is an inflammatory condition, and as such the symptoms include fever, increased heart rate, rapid breathing, confusion, and metabolic acidosis, all of which can culminate in organ failure [210]. Sepsis is a cascade of immunological dysfunctions, which are maintained either by sustained infection – such as bacteraemia – or the inability to dampen immune function following successful control of systemic pathogen challenge. Sepsis can be caused by infection with a plethora of bacterial pathogens [211]. The common nature of this disease to multiple infectious organisms indicates common molecular mechanisms employed within the host, which is a theme discussed in this thesis. The etiology of sepsis varies by location and is influenced by a number of socioeconomic factors. Major causes of sepsis however include *Escherichia coli*, *Staphylococcus aureus*. *S. pneumoniae*, and *Klebsiella pneumoniae* [211].

By far the greatest cause of sepsis is systemic bacterial infection [212]. As described earlier, bacterial surface molecules trigger inflammation as a mechanism for control of infection. The recognition of such molecules by immune cells such as macrophages leads to the production of different repertoires of cytokines, which have global inflammatory and also anti-inflammatory effects on cells in other organs. Sepsis arises when the process becomes uncontrolled, and the body can not effectively regulate its inflammatory response [213].

1.5.2 **The role of cytokines in sepsis**

Cytokines play a major role in regulation of innate, and also adaptive immune responses, through the initiation of signalling cascades in neighbouring, and also global immune cells (see above). Following translocation of bacteria to the blood, they are recognised by innate immune cells such as macrophages, monocytes, neutrophils, and dendritic cells. Each of these cell populations has a different role in the control of infection, and therefore produces a different repertoire of cytokines. It is the bodies job to regulate this process, despite the fact that different bacteria, have different tropisms for each of these cell populations. I have already described that different populations of macrophages even within a single organ (the spleen for example), produce different cytokines. However in this context our understanding of the pathophysiology of sepsis is exceptionally poor, as we have limited knowledge of the tropism of pathogens to different innate immune cells, the dynamics of infection across these populations, and the downstream implications for cytokine production. Much of the research on cytokine productions is limited to cell lines, and to majority populations of primary innate cells. TNF-α is an example of a cytokine with a profound role in the pathology of sepsis. TNF-α is produced by macrophages (which are also extremely responsive to this cytokine), and functions by inducing cell proliferation, differentiation and programmed cell death (apoptosis) [123]. It is a massively pro-inflammatory cytokine, and acts as a global regulator of inflammatory cytokine production. Not surprisingly due to its heavily pro-inflammatory nature, TNF-α is also a biomarker for sepsis [214], and contributes to the sustained inflammation which characterises this disease [215]. Tracey *et al.* (1987) [216] demonstrated that pre-treatment of baboons with a TNF-α neutralising antibody protected baboons from sepsis induced by challenge with *E. coli*. Indeed, TNF-α directed therapeutics have been proposed as a therapeutic target for a number of inflammatory diseases including sepsis and crohn's disease [217]. This same paradigm of neutralising as a therapeutic strategy has been observed in a number of pre-clinical studies for other cytokines (such as IL-17)[218], but as of yet, therapeutically targeting cytokines is not a licenced approach to sepsis treatment. This is likely due to the fact that while uncontrolled cytokine production is pathogenic, their regulated production is also key to orchestrating successful immune responses. Despite years of research, treatment of sepsis has scarcely improved, and multiple clinical trials at improving therapeutic intervention have failed [219, 220].

1.6 Population Bottlenecks During Bacterial Pathogenesis

1.6.1 Introduction to bottlenecks

Population bottlenecks are arbitrary reductions in size, which reduce population diversity, and are predominantly discussed in the context of evolutionary genetics and founder effects [221]. The founder effect is where few organisms from population A, establish a new colony (population B) with reduced genetic diversity, for example the movement of a few early humans to a new island [222]. This concept has been applied to bacteria and their transmission between, and translocation within hosts [223][224, 225]. Studies utilising modelling approaches and experimental models of infection in a number of bacterial pathogens have indicated that at doses of bacteria around the LD_{50} – the dose required to induce disease in 50% of animals – that the disease population is caused by a single organism [223, 226][227]. This implies a stringent population bottleneck within the host in the early stages after infection – a facet of pathogenesis that is largely overlooked. Population bottlenecks are significant because (1) they represent the optimal time for therapeutic intervention; it is easier to clear a few founding organisms than a large biomass, and (2) they help to understand the key cellular players in disease pathogenesis, which may open the door to developing new therapeutic interventions.

1.6.2 Examples of microbial infection bottlenecks

1.6.2.1 ***Haemophilus influenzae***

Moxon and Murphy (1978) [228] conducted a thorough investigation of population bottlenecks occurring during the pathogenesis of *Haemophilis influenzae* type b (Hib) bacteraemia and meningitis, following intranasal inoculation. They demonstrated that at low dose inoculation, blood cultures were dominated by one of either streptomycin resistant, or streptomycin sensitive bacteria indicating a population bottleneck following translocation from the lung. They also demonstrated this same phenomena using organisms cultured from the cerebrospinal fluid (CSF) of rats. Interestingly, when blood cultures were monoclonal, the same strain was cultured from the CSF indicating meningitis in this model had arisen from the hematogenous route. More importantly when the blood culture was not monoclonal, they observed some cases of monoclonal meningitis indicating that there is also a bottleneck between the blood and the CSF.

These observations are a perfect example of how studies of within host bacterial population diversity can inform understanding of disease pathogenesis.

1.6.2.2 ***Salmonella* ssp.**

Salmonella are the quintessential example of an intracellular pathogen capable of manipulating host cell biology to facilitate pathogenesis. *Salmonella* are fascinating organisms to study with respect to population bottlenecks, due to their frequent translocation between host compartments during disease pathogenesis. The theory of independent action, which was built upon by others including Moxon and colleagues, was first coined by Meynell *et al.* (1957) [223] with respect to *Salmonella* infection. Using isogenically tagged WT *Salmonella* strains and powerful statistical analysis, Han Lim *et al.* (2014) [229] later demonstrated that after oral challenge, multiple population bottlenecks were observed during the pathogenesis of infection. Bottlenecks were observed in establishing colonisation of the gut, in translocation to the system compartment via the Peyer's patch, and in invasion of the liver and spleen. Phenomena such as this are largely considered non-selective and stochastic, but the authors demonstrated the roles of selection in population bottlenecks. They demonstrated that following anti-*Salmonella* vaccination of mice, within-host populations of bacteria demonstrated different levels of diversity than those within naïve mice. Additional studies of *Salmonella*, have demonstrated that these bottlenecks are largely imposed by uptake of bacteria by phagocytic cells, where *Salmonella* can proliferate away from the attack of the innate immune system – an observation common to many unrelated pathogens. Further, Rossi *et al.* [43] demonstrated that antimicrobial treatment with drugs acting on either a fast, or slow growing variant of *Salmonella* impacted treatment outcome with the latter persisting in the tissue for days after therapy. This provides therapeutic implications for the shuttling of populations of *Salmonella* with heterogeneous growth rates into host cell compartments, and their survival during therapy [43, 230].

1.6.2.3 **Additional pathogens undergoing within host bottlenecks**

Characterisation of infection bottlenecks are widespread in the literature. Pollit *et al.* [231] demonstrated that following infection of mice with *Staphylococcus aureus*, that individual abscesses in the kidneys were founded by single bacterial cells. Further

work by this group [232] demonstrated the role of sub-curative doses of antibiotic during staphylococcal infection played in the clonal expansion of resistant organisms, highlighting that close attention should be paid to within-host infection dynamics in optimising treatment regimens. In the case of the Gram-negative pathogen *E.coli,* Schwartz *et al.* [233] demonstrated that uropathogenic strains cause cystitis dominated by a single bacterial clone, and Pluschke *et al* [234] alluded to the monoclonal nature of bacteraemia in rats following infection with serotype K1 isolates.

1.6.2.4 ***Streptococcus pneumonia*e: a basis for this project**

Considering the eclipse phase of pneumococcal bacteraemia first reported by Wright *et al.* (1927), Gerlini and colleagues (2014) [235] aimed to characterise this within-host population bottleneck, and in particular the host and bacterial factors playing key roles. The authors performed 1:1:1 infections of mice with isogenic mutants tagged with three different antibiotic resistance cassettes. At intravenous (IV) doses around the LD_{50}, they were able to demonstrate that the bacteraemia population which emerged after the eclipse phase was dominated by one resistant mutant. Statistical analyses of these data indicated that the population bottleneck required to reduce resistance diversity to a single strain was most likely to be mediated by a single bacterium. They then demonstrated through infection of mice depleted of neutrophils that although bacteria were cleared gradually over the first 12h of infection, it was far less efficient than in neutrophil competent mice. Conversely, depletion of macrophages completely abolished clearance capacity of the mice, and in fact an increase in bacterial counts in the blood was observed up to 8h post infection when the mice had to be killed. Together, these data demonstrated a stringent population bottleneck after IV infection, and that macrophages were the critical cell type underpinning this reduction in population size. Population bottlenecks are likely widespread during many stages of the pneumococcal life cycle, as Kono *et al.* [236] have also demonstrated a stringent bottleneck during transmission of pneumococci from infected mice, to uninfected littermates.

1.7 **Aims and Objective**

At the start of this thesis, I joined a project which aimed to understand the contributions of intracellular replication of typically extracellular bacteria to pathogenesis, which is

described in detail in section 3.1.5. The overarching aim of this thesis was to further charecterise both the host and bacterial factors underpinning a pneumococcal infection bottleneck in the spleen, to translate these observations to the human host, and to determine if other typically extracellular pathogens replicate within tissue macrophages *in vivo*.

The specific objectives of this thesis were:

(1) To charecterise the contribution of CD169+ splenic macrophages and the pneumococcal virulence factor NanA to disease pathogenesis in mice
(2) To establish a novel, *ex vivo* model to study intracellular replication of pneumococcus in the human spleen
(3) To investigate whether the typically extracellular pathogen *Klebsiella pneumoniae* exploits tissue macrophages to mediate pathogenesis

Chapter 2: Materials and Methods

2 Chapter 2: Materials and Methods

2.1 Bacterial Strains, Culture Conditions, and Standard Growth Media

For studies of *S. pneumoniae,* the serotype 2 strain D39, its genetically modified derivatives were used, in addition to the serotype 4 strain TIGR4 (Table 1). *S. pneumoniae* strains were routinely cultured in Brain-Heart Infusion broth (BHI; Oxoid), and BHI-agar (Oxoid) supplemented with 3% (v/v) defibrinated horse blood (Thermo), and selective antibiotics where appropriate (Table 2).

Table 1 - *WT pneumococcal strains used in this work, and mutants produced in this thesis.*

Strain name	Serotype	Comment	Source
D39	2	WT	[237]
R6	Non-encapsulated	D39-derived capsule mutant	[237]
DP1004	Non-encapsulated	D39-derived capsule mutant, streptomycin resistant	[238]
TIGR4	4	WT	[239]
D39Δ*nanA*	2	D39-derivative with 5' insertion of Janus cassette. No amino acid deletion.	This work
D39Δsial	2	D39-derivative minus AAs 290-786	This work
D39Δlect	2	D39-derivative minus AAs 76-282	This work
DP1004Δsial	Non-encapsulated	DP1004-derivative minus AAs 290-786	This work
DP1004Δlect	Non-encapsulated	DP1004-derivative minus AAs 76-282	This work

WT; wild type, serotypes were determined previously in the references literature, clean; no cassette remaining, AAs amino acids

Table 2 - *Antibiotics used for selection in pneumococcal transformations with the Janus system*

Antibiotic	Stock concentration	Working concentration
Kanamycin	50 mg/mL	500 µg/mL
Streptomycin	20 mg/mL	500 µg/mL

Both antibiotics were dissolved in water. Both antibiotics were purchased from Sigma.

For studies of *Klebsiella pneumoniae*, I used 11 human clinical isolates of *Kp*, encompassing 5 serotypes including hypermucoviscous/hypervirulent (hv*Kp*) K1 and K2 isolates, carbapenem multi-drug resistance (CR*Kp*) KL17, KL103 and KL107 isolates, and the K6 *K. quasipneumoniae* ATCC 700603 susceptibility testing

reference strain (Table 3). Explanations of strain nomenclature can be found in chapter 4. Clinical isolates were a kind gift of Professor Gian Maria Rossolini (University of Florence). Strains of *Kp* were grown in BHI broth for liquid culture with 400 revolutions per minute (RPM) shaking, and on Lysogeny Broth Agar (LA, Oxoid) as a solid medium at 37ºC. All bacterial strains were stored at -80ºC, in BHI broth supplemented with 10% (v/v) glycerol for short term storage, or 25% (v/v) glycerol (Sigma) for long term storage. Virulence and antimicrobial gene profiles have been published previously in the references included in the table.

Table 3 - *Klebsiella pneumoniae isolates used in this thesis, and their relevant metadata and phenotypic charecterisation*

Strain name	Serotype	ST	Source	Mucosity phenotype	Resistance phenotype	Carbapenemase genes	Virulence genes	Genome accession	Reference
NTUH-K2044	KL1: O1v2	23	Human, blood, Taiwan	●	-	-	*ybt, iuc, iro, rmpA, rmpA2*	AP006725.1	[240]
RM1628	KL1: O1v2	1861	Human, blood, Italy	●	-	-	*ybt, clb, iuc, iro, rmpA, rmpA2*	JAALJC000000000	[241]
SGH10	KL1: O1v2	23	Human, liver abscess, Malaysia	●	-	-	*ybt, clb, iuc, iro, rmpA, rmpA2*	NZ_CP025080.1	[242]
GMR151	KL2: O1v2	25	Human, blood, Italy	●	ESBL	-	*iuc, iro*	JAALJD000000000	N/A
HMV-1	KL2: O1v1	86	Human, blood, Italy	●	-	-	*ybt, iro, rmpA*	JAALCW000000000	N/A
HMV-2	KL2: O1v2	65	Human, blood, Italy	●	-	-	*iuc, iro*	JAALCV000000000	N/A
KPC157	KL107: O2v2	512	Human, rectal swab, Italy	-	CR	bla_{KPC-3}	-	JAALCU000000000	N/A
KKBO-1	KL107: O2v2	258	Human, blood, Italy	-	CR	bla_{KPC-3}	-	GCA_000495875.1	[243]
KK207-1	KL107: O2v2	258	Human, blood, Italy	-	CR	bla_{KPC-2}	-	GCA_001399815.1	[243]
HS11286	KL103: O2v2	11	Human, sputum, China	-	CR	bla_{KPC-2}	*ybt*	NC_016845.1	[244]
DG5544	KL17: O1v1	2502	Human, rectal swab, Italy	-	CR	bla_{KPC-3}	*ybt*	GCF_003227695.1	[245]
KPC58	KL17: O1v1	101	Human, blood, Italy	-	CR	bla_{KPC-2}	*ybt*	JAALCT000000000	N/A
KPC284	KL17: O1v1	101	Human, blood, Italy	-	CR	bla_{KPC-2}	*ybt*	JAALCS000000000	[246]
ATCC 700603	KL6: O3/3a	498	Human, urine, USA	-	ESBL		-	NZ_CP014696.2	[247]

Abbreviations: ESBL, extended-spectrum β-lactamase; CR, carbapenem-resistant; *ybt*, yersiniabactin; *iuc,* aerobactin; *iro*,salmochelin; *clb*, colibactin; *rmpA*, regulator of mucoid phenotype. ●; hypermucoid. Serotypes, phenotypic characterisations, and genomic characterisations were performed by the group of Professor Gian Maria Rossolini.

2.2 Additional Culture Mediums

2.2.1 Casein tryptone broth

For *S. pneumoniae* I used the minimal media casein tryptone broth (CAT) which allowed for supplementation with either N-Acetyl-Mannosamine or glucose which would either yield or overcome respectively carbohydrate catabolite repression of the neuraminidase operon [248]. CAT medium was made by dissolving 0.3g Yeast Extract (Oxoid), 4g Bacto Casitone (Becton Dickinson, USA), 4g Tryptone (Oxoid), and 2g NaCl in 400 mL of dH2O before autoclaving. The sterilised medium was then supplemented with 3% 0.5M K2HPO4 to buffer the medium, and 0.2% final wt/v of the sugar of interest.

2.2.2 Low phosphate and magnesium broth

For assessment of *K. pneumoniae* growth in medium mimicking host cell compartments, I used the Low Phosphate and Magnesium (LPM) medium previously described in the context of *Salmonella* genes known to be expressed within macrophages [249]. LPM medium consisted of 5 mM KCl, 7.5 mM $(NH_4)_2SO_4$, 0.5 mM K_2SO_4, 38 mM glycerol (0.3% v/v), 0.1% casamino acids, and 8 µM $MgCl_2$, 337 µM PO_4^{3-}. pH 5 medium (phagosome mimicking was made by titration of 80 mM MES to pH 5.8, whilst pH 7 medium (endosomal mimicking) was made by titration 100 mM Tris-HCl for titration to pH 7.0

2.3 Growth Assays Measuring Optical Density

For assessing bacterial growth in medium, mouse/pig serum, and mouse/pig whole blood, bacterial strains were first streaked onto their respective agars and incubated o/n. The following day, colonies were resuspended in PBS (MP Bio), and diluted to an OD_{600nm} of 0.2, and diluted 1:100 into the test medium to give an approximate starting inoculum of ~ 10^5 CFU/mL. Samples in broth were arrayed into clear, flat-bottomed 96 well microtiter plates (Nunc), and placed into a plate reader (Eon, Biotek) set to 37ºC, and their OD_{600nm} values were continually monitored every 5 minutes for 24h. The same protocol was followed for both *S. pneumoniae* and *K. pneumoniae.* For quantification of growth dynamics, OD values were plotted on a logarithmic scale in Microsoft Excel to identify the period of exponential growth. Doubling time in the exponential growth period was then calculated using the following equation:

Generation time (minutes) = (1/((LOG(B) – LOG(b))/(0.301*t))*60

Where B = optical density at end point

b = optical density at start point

t = time (hours)

2.4 **Murine Sepsis Model**

2.4.1 **CD1 mice**

For the preparation of mouse infection stocks, single colonies of *Klebsiella* from overnight plates were inoculated into fresh BHI, and incubated overnight (o/n). The following morning, samples were diluted 1:100 into fresh BHI, and cultured until an optical density (OD_{600nm}) of 0.3. Instead, pneumococci were directly diluted 1:100 from frozen stocks, and grown to an OD_{600nm} of 0.4 without an o/n incubation step. Samples of both bacteria were then frozen at -80 ºC, with 10% glycerol (Thermo). The following day, single aliquots of the infection stock were thawed at room temperature, serially diluted, and plated to determine the exact bacterial concentration.

All animals used in this study were handled in accordance with the UK home office license P7B01C07A. Procedures and experiments were also approved by the local University of Leicester Ethics committee. Animals were either culled at pre-determined time points, or when they displayed moderate signs of disease, as is outlined in the project license.

I used a published intravenous model of bacterial sepsis in 6-8 week old CD1 swiss mice [250, 251] which were bred in house at the University of Leicester Pre-Clinical Research Facility. Briefly, infection stocks of both bacteria species were thawed, and diluted in PBS to give an inoculum containing 10^7 CFU/mL. Mice were infected with 100 µl of this suspension (10^6 CFU/mouse) through the lateral tail vein. Mice were then monitored for signs of disease regularly throughout the infection time course. At pre-determined time points, mice were anaesthetized, and blood removed by cardiac puncture using 23-gauge needles (Medicina), and placed into microcentrifuge tubes (Sigma) containing 50 units of heparin (sigma). Tissues were taken post mortem, and either homogenized in BHI + 10% glycerol for enumeration of CFU, or flash frozen in

Optimum Cutting Matrix (Fisher Scientific) using 2-methyl butane (sigma) and dry ice for microscopy analysis.

2.4.2 **Sample size calculations**

Mouse group sizes were calculated using pilot data generated previously in our lab. The online tool ClinCalc was used for power calculations. Briefly, parameters used for the calculator were: difference between 2 group means (log_{10} of 2), standard deviation (log_{10} of 1), statistical power (0.8), and an alpha level of 0.05. The output of this calculation was a group size of 5 mice, which was used for subsequent experiments.

2.4.3 **CL57BL/6 and CL57BL/6-$Sn^{-/-}$ mice**

To investigate the role of the macrophage restricted marker CD169 (sialoadhesin) in pneumococcal infection, we performed experiments in collaboration with Professor Paul Crocker at the University of Dundee in homozygous sialoadhesin deficient mice and their WT littermates in the CL57BL/6 background. The method of construction of CL57BL/6-$Sn^{-/-}$ has been reported previously [252]. This same study also demonstrated that $Sn^{-/-}$ have a marginal increase in the relative number of T cells in their spleens compared with WT mice. Infection stocks for intravenous infection in these mice were prepared in Leicester as above and shipped to Dundee on dry ice. The group in Dundee performed intravenous infection with 10^6 CFU of D39, and harvested blood and spleen at 6h post infection. Blood samples were diluted 1:10 in BHI + 10% glycerol, whilst spleens were coronally halved, with half being placed into 1 mL of BHI + 10% glycerol and frozen at -80 ºC, and the other half being flash frozen in OCT. All samples were shipped to Leicester, and were processed for enumeration of CFU and confocal microscopy by myself. Freezing spleens using the above conditions has no effect on the viability of bacteria in the tissue (Oggioni lab, unpublished data).

2.4.4 **Receptor blockade and survival experiments**

CD169 blockade experiments were performed as previously described [253]. Briefly, we intravenously injected 10 µg of anti-CD169 mAb (Rat IgG2a,k, Clone: 3D6.112), or isotype matched control (Rat IgG2a, clone RTK2758) 30 minutes prior to intravenous infection with 10^6 CFU *K. pneumoniae* NTUH- K2044 or *S. pneumoniae* D39, before

taking and processing samples as described above. To determine therapeutic efficacy of antibody blocking, some mice were monitored for their survival over a 72h time period. Mice were culled and scored as not surviving when they reached moderate signs of disease in accordance with the project licence.

2.5 **Preparation of Serum Samples**

Serum samples from mice, and from abattoir sourced pigs were prepared as follows. Samples were collected into sterile Eppendorf or falcon tubes (Corning) respectively, without anti-coagulant, and were left to clot at room temperature for 30 minutes. Samples were then centrifuged at 400 x G for 30 min at 4 °C, before aliquoting the serum supernatant into fresh tubes and storing at -80 °C.

2.6 ***Ex vivo* Whole Murine and Porcine Blood Growth Assays**

Mouse blood was obtained from CD1 mice (as above), by cardiac puncture under terminal anaesthesia. For growth assays, to prevent coagulation, mouse blood was immediately placed into tubes containing hiriduin (Sarstedt), as heparin has been demonstrated to be an inhibitor of complement [254]. 200 µL of sera, or whole blood were arrayed into round bottom 96 well plates and inoculated with ~10^5 CFU of bacterial suspension in PBS, which was obtained from thawing pre-prepared infection stocks. At pre-determined time points, a 20 µl sample was removed, serially diluted, plated on the relevant agar plate, and left to incubate overnight for enumeration of bacterial colonies.

2.7 **Murine Neutrophil Isolation and Killing Assay**

Blood was collected from CD1 mice by cardiac puncture in EDTA vacutainers (BD Diagnostics-Preanalytical Systems, UK). To isolate neutrophils [129], 12 ml of Histopaque-1077 (Sigma-Aldrich, UK) was placed in a 50-ml Falcon tube (BD Biosciences, UK), and 12 ml of Histopaque-1119 (Sigma-Aldrich, UK) was layered beneath with a glass Pasteur pipette. Whole mouse blood (~4 ml) diluted 1:1 with Hanks Balanced Salt Solution (HBSS) without Ca_{2+}/Mg_{2+} was layered over the Histopaque-1077 layer, and the tube was centrifuged at 700 × *g* with slow acceleration and no braking for 30 min at room temperature. The neutrophil layer was collected and washed once with HBSS without Ca^{2+}/Mg^{2+}. Red blood cells were lysed in 0.2% saline

at room temperature for 1 min. An equal volume of 1.6% saline was added to the cells to equilibrate the solution, and cells were washed once with HBSS without Ca^{2+}/Mg^{2+}. Two more washes were carried out in the buffer or medium required for the assay (HBSS with Ca^{2+}/Mg^{2+}). Confocal microscopy using the anti-mouse Ly6G antibody (table 4) of cells were routinely used to assess the purity of neutrophils following isolation.

For infection assays, frozen stocks of *Kp* were thawed, pelleted by centrifugation, and suspended in HBSS with Ca^{2+}/Mg^{2+} before infecting neutrophils at an MOI of 10. Samples were taken at regular intervals for enumeration of CFU. A no neutrophil control was included in all experiments.

2.8 **Immunohistochemistry and Histology Analysis**

10 µm organ sections were mounted onto microscope slides following sectioning with a Leica cryostat (CM1850UV). All subsequent steps were performed at room temperature. Sections were left to dry for 10 min, before fixation with 4% paraformaldehyde (Sigma) for 20 min. Sections were washed 3x in PBS (Sigma), before permeabilisation of the sections with PBS + 0.1% triton-X100 (Sigma) for 10 min. Sections were then blocked with PBS + 5% goat serum (Sigma) for 45 min and were subsequently incubated with primary antibody diluted in the blocking buffer for 1 h. Sections were then washed 3x in PBS, before a 45-min treatment with fluorophore-conjugated secondary antibodies. Sections were subsequently washed 3x with PBS, before a final wash with H_2O. Lastly, samples were mounted with prolong antifade mountant with DAPI (Molecular Probes, Fisher scientific). All antibodies and reagents used in this study are shown in Table 4.

Table 4 - *Primary antibodies and fluorescence reagents used in this thesis*

Antibody/reagent (clone)	Target	Dilution	Conjugate	Catalogue	Supplier
Primary antibodies					
Rat anti-mouse CD169 (3D6.112)	CD169+ MΦ	1:200	None	MCA884GA	Biorad
Rat anti-mouse F4/80 (A3-1**)**	RP MΦ/Kupffer cells	1:200	None	MCA497RT	Biorad
Rat anti-mouse MARCO (ED31)	MZM MΦ	1:200	None	MCA1849T	Biorad
Rabbit anti-K1 *Klebsiella*	*Kp* serotype K1	1:500	None	Gifted	SSI
Rabbit anti-K2 *Klebsiella*	*Kp* serotype K2	1:500	None	Gifted	SSI
Rabbit anti-type 2 pneumococcus	Serotype 2 pneumo	1:500	None	N/A	SSI

Rabbit anti-type 4 pneumococcus	Serotype 4 pneumo	1:500	None	N/A	SSI
Rabbit anti-pan *Klebsiella*	*Kp*	1:200	None	aBii0947	Abcam
Rat anti-mouse Ly-6G (1A8)	Neutrophils	1:200	None	MCA711A647	Biorad
Mouse anti-porcine CD169 (3BI1/11)	CD169+ MΦ	1:200	None	MCAII316GA	Biorad
Mouse anti-porcine CD163 (2AI0/11)	CD163+ MΦ	1:200	None	MCAII311GA	Biorad
Mouse anti-porcine granulocytes (2BII)	Granulocytes	1:200	None	MCAII600GA	Biorad
Mouse anti-human CD206 (15-2)	Splenic endothelia	1:200	None	MCA2155	Biorad
Mouse anti-human CD163 (EDHu-1)	RP MΦ	1:200	None	MCA1853	Biorad
Sheep anti-human CD169	CD169+ MΦ	1:100	None	AF5197	R&D
Secondary antibodies and reagents					
Goat anti-rat IgG - 647	Rat primary antibody	1:500	Alexafluor 647	A-21247	Thermo
Goat anti-rat IgG - 568	Rat primary antibody	1:500	Alexafluor 568	A-11077	Thermo
Goat anti-rabbit IgG - 488	Rabbit primary antibody	1:500	Alexafluor 488	A-11008	Thermo
Goat anti-mouse IgG - 568	Mouse primary antibody	1:500	Alexafluor 568	A-21124	Thermo
Phalloidin	Actin	1:100	Alexafluor 647	AII2287	Thermo
Texas red conjugation kit	N/A	N/A	Texas red	aBi95225	Abcam
FITC conjugation kit	N/A	N/A	FITC	aBi02884	Abcam
DAPI	Nuclei	N/A	DAPI-405	D9542	Sigma

Abbreviations: SSI; Statens Serum Institute, FITC; Fluorescein isothiocyanate, IgG; immunoglobulin G

2.9 **Rabbit IgG Purification and Fluorophore Conjugation**

For bacterial staining of *K. pneumoniae* K1 and K2 co-infected organs using two anti-sera raised in rabbits, we purified IgG from the sera, and conjugated them to fluorophores. Briefly, 20 µl of sera was mixed with 100 µl of protein-G agarose (Roche), and left at 4 ^{o}C overnight with gentle shaking. Protein G bound antibody was subsequently pelleted at 3000 x G for 2 minutes at 4 ^{o}C and washed 3 x in PBS. Purified IgG was eluted in dH_2O with 100 mM glycine at pH 2.7 for ten minutes with frequent agitation. Agarose beads were pelleted, and the IgG-containing supernatant was combined 1:1 with 1M Tris at pH 8.0. Protein concentration of the IgG preparation was determined by Bradford assay, using bovine serum albumin as a standard. Purified anti-K1 and K2 IgG were conjugated with texas red, and FITC respectively using the easy FITC/texas red labelling kits (Abcam) according to the manufacturer's

instructions. IHC using these purified, conjugated sera were performed as described above, with the absence of a secondary antibody staining step.

2.10 Confocal, and Whole Tissue Scanning Microscopy, and Image Analysis Software

For analysis of bacterial distribution in the tissue, whole immunostained tissue sections were imaged on a Vectra Polaris digital pathology system (Perkin Elmer; hereafter referred to as 'slide scanner') using the 40x/NA=0.75 objective and Opal480, 520, 620, and 690 filter cubes. In addition to their use in determining whole tissue bacterial distribution, slide scans were used to select regions of interest for confocal analysis. For analysis of bacterial distribution across macrophage subsets in slide scans of murine and porcine tissue, Fiji [255] was used (see below). To delineate subcellular localisation of bacteria, Z-stacks of tissue samples stained with macrophage surface markers were acquired with an FV1000 Olympus Confocal laser scanning microscope using a 40x/Na=1.3 or 60x/NA=1.35 objective. Confocal microscopy images were visualized using Fluoview (Olympus), and were exported as .tif files for additional downstream analysis. 3D visualisation of Z-stacks was performed using Imaris 3D V9.4 reconstruction software (Bitplane, Switzerland). For light microscopy imaging of hemotoxylin and eosin stains, we used a fully motorized Nikon eclipse Ti microscope, with a Nikon DS-Fi2 colour camera, using a Plan Apo TIRF 100X oil objective.

2.11 Image Analysis Pipelines

For quantitative analysis of the co-localisation of bacteria with cell populations of interest in Vectra Polaris slide scans, we developed an analysis pipeline in Fiji. Briefly, images which were co-stained for bacteria and different cellular markers were separated into their respective channels. The cell area pertaining to the marker of interest was selected by applying a fluorescence threshold to the channel. This selection was then applied to the bacterial channel, and the total number of bacterial particles was analysed. Comparison of multiple markers, in conjunction with the number of bacteria present in the whole tissue, allowed us to apply percentage co-localisation values of bacteria with cellular markers. This pipeline is outlined in Figure 5. Analysis specific to experiments in this thesis are described in their respective results sections.

(A) Image with bacteria and marker of interest

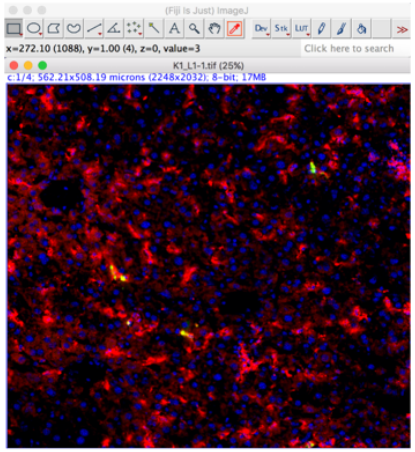

(B) Isolation of channel of interest

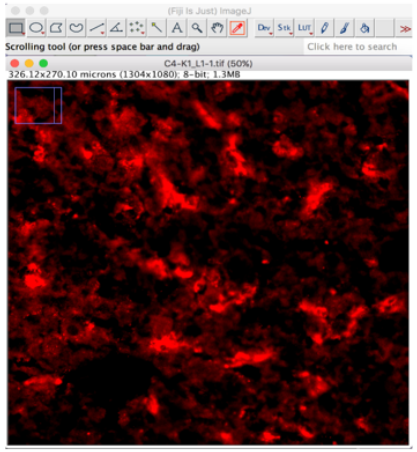

(C) 'Thresholding' of marker

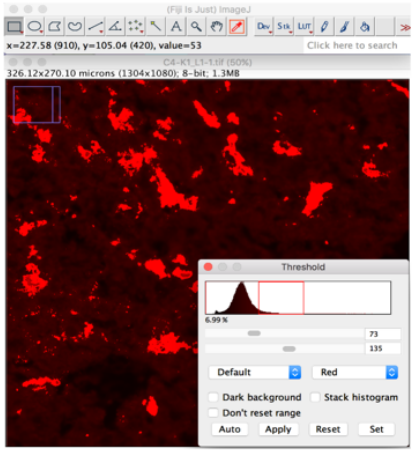

(D) Create selection using thresholded image

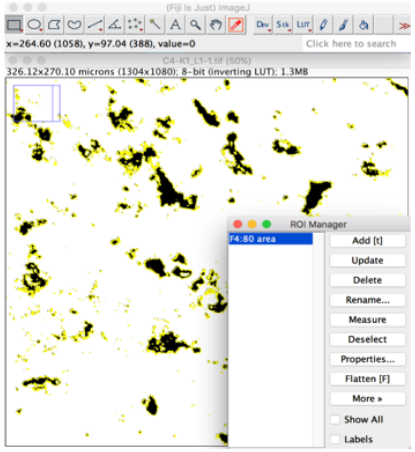

(E) Isolation of bacteria channel

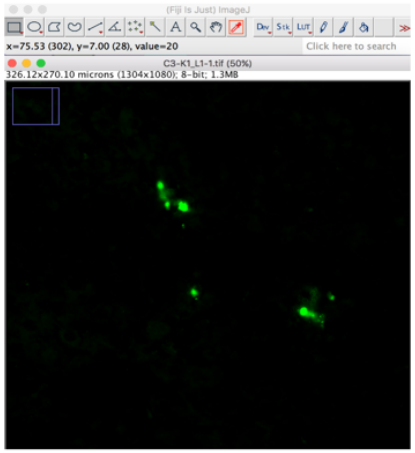

(F) Imposition of marker selection, on thresholded bacteria channel

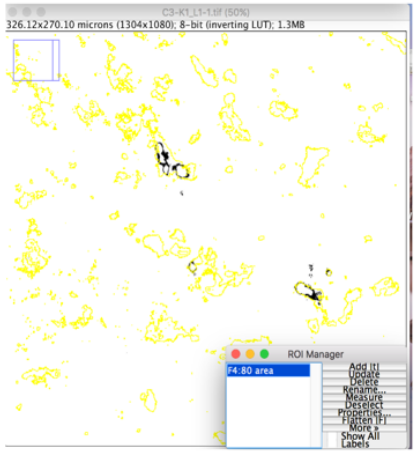

(G) Set parameters for particle size analysis

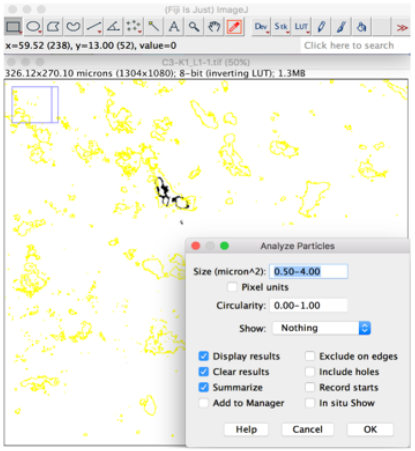

(H) Analyse bacterial particles in marker selection

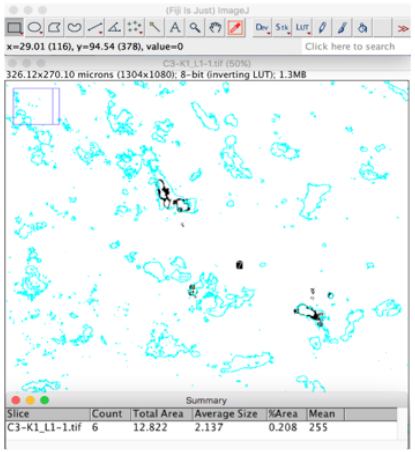

Figure 5 - *Fiji analysis pipeline for analysing distribution of bacteria in tissue.* (A) First, a multi-colour channel image is required which includes a bacterial stain, and a stain which delineates a marker of interest. (B) Next the channel which identifies the cellular marker should be isolated using the split channels function, before (C) thresholding the image to highlight only the cell area above an arbitrary fluorescence threshold. (D) This thresholded images is then used to produce a region of interest (roi) selection. (E-F) This selection can then be applied to the bacterial fluorescence channel, before particle size analysis is performed (G-H) with suitable parameters for the bacterium of interest.

2.12 *Ex vivo* Porcine Organ Perfusion Experiments

2.12.1 Porcine organ retrieval

We adapted our previously published model of a porcine spleen perfusion to include the porcine liver in the same circuit [256, 257]. Pigs of the breed “Large White” (45-60 kg) from Joseph Morris Abattoir (South Kilworth, Leicestershire) were slaughtered following routine protocols to reduce suffering and stress as outlined by UK and EU laws. Pigs were euthanized by exsanguination from the jugular vein after stunning, and ~3L of autologous blood was collected in a container containing 25000 units of Heparin. Splenectomy was performed close to the hilum following midline laparotomy. The main splenic artery was cannulated *in situ*, whilst all other arteries were carefully ligated and divided, prior to organ removal and perfusion with 500 mL soltran preservative solution (Baxters, UK). To retrieve the liver, the diaphragm and pleurae were divided, and subsequently the supra-hepatic inferior vena cava, thoracic aorta, and oesophagus were ligated. The portal vein and hepatic artery were then cannulated, and all additional vasculature was clamped and divided together with conjoining non-vascular tissue. The liver and gall bladder were removed *en bloc*, and both vessels were flushed with 500mL of soltran solution. Organs were then transported to the lab under sterile conditions and on ice. For all organ retrievals performed in this study, the cold ischemia time was less than 30 minutes. All other surgical procedures performed during organ retrieval were performed with the contribution of the surgeon Dr Wen Chung from the Hepato-Pancreato-Biliary unit of the Leicester General Hospital and have been described elsewhere [258].

2.12.2 **Normothermic porcine liver-spleen co-perfusion and *ex vivo* infection**

In the lab of the Hepato-Pancreato-Biliary unit of the Leicester General Hospital (PI Prof Ashely Dennison), each vessel was flushed with 500 mL of saline solution, before being connected to a custom extracorporeal circuit (Medtronic Inc, Minneapolis, MN, USA), which contained 3L of autologous pig blood. We ensured normothermia using a heat bath (set to 37 ºC), and physiological oxygenation using an oxygenator providing 2 L/min of O_2. Perfusion pressure was set to 80 Hg/mm for the length of the experiment, and the flowrate through each vessel was monitored at hourly intervals. We performed perfusion experiments for up to 6h (~1h stabilisation, and 5h infection). Autologous blood was recirculated to all vessels via the main circuit reservoir. To the circuit we also added $NaHCO_3$ to minimise the effect of tissue acidosis, and Flolan (Epoprostenol sodium; GSK) to facilitate vasodilation and effective oxygenation of the tissues. Throughout the perfusion period, we also monitored pH, haemoglobin oxygenation, lactate production and levels of physiological electrolytes using a Radiometer ABL90 series, to confirm maintenance of physiological blood gas parameters. Once a stable perfusion flow rate, and blood gas parameters had been achieved (~30 minutes of perfusion), we infected the circuit with 6.5 x 10^7 CFU of *K. pneumoniae* strain GMR151. We subsequently sampled blood and obtained multiple independent tissue biopsies at 30 minutes, 1, 2, 3, 4, and 5h post infection. Blood was serially diluted and plated on LA plates to determine bacterial concentrations. Tissue biopsies were either homogenised, serially diluted and plated to determine bacteria concentration, or were flash frozen in OCT for IHC analysis.

2.12.3 ***Ex vivo* human spleen perfusion, infection, and sample ethics**

The Health Research Authority approved in 2018 a trial with Prof Oggioni as chief investigator to collect human spleens to explore during *ex vivo* perfusion the events during the early phases of invasive infection [259]. Human spleen samples were taken from patients undergoing elective splenectomy in the context of pancreatic disease in a clinical trial, under the Research Ethics Committee (REC) number 18/EM/0057. Spleens were surgically removed *en bloc* in accordance with standard practises of the University Hospitals Leicester. The major splenic artery was immediately cannulated, flushed with Soltran preservative solution, and was transported to the lab on ice for

perfusion experiments. *Ex vivo* human spleen perfusion was performed as above with the following modifications. A paediatric perfusion circuit was used, which had only a single connection to the vessel, and subsequently lacked the reservoir used for perfusion of the portal vein above. The circuit was perfused with the artificial perfusate Hemopure® (HbO2 Therapeutics, Souderton, PA, USA) to facilitate tissue oxygenation. The components of hemopure are displayed in Table 5. The circuit was infection with pneumococci direct from frozen stocks, and samples were taken as above for analysis.

Table 5 - *Components of the artificial perfusate Hemopure®*

Component	Volume / concentration
Lactated Ringers Solution	500 mL
Water for Infection (WFI)	100 g/dL
Purified bovine hemoglobin	13 g/dL
Sodium Chloride	114 mmol/L
Sodium Hydroxide	11 mmol/L
Potassium Chloride	4 mmol/L
Calcium Chloride	1.6 mmol\L
Sodium Lactate	27 mmol/L
N-acetyl-Lcysteine	200 mg/dL

Components of hemopure were taken from the manufacturers booklet, and were not empirically determined by me

2.13 Cell Culture Techniques and Pneumococcal Phagocytosis Assays

J774A.1 macrophages were routinely cultured in Roswell Park Memorium Institute Medium (RPMI; Gibco)+ 10% Fetal Bovine Serum (FBS) at 37 degrees Celsius and 5% CO_2. For phagocytosis assays [260], cells were seeded in cell culture grade flat bottomed 96 well plates (Fischer Scientific) at 10^5 cells/mL overnight. The following day, cells were washed 3x in PBS, and fresh medium was added before infecting with a multiplicity of infection of 10 of pneumococci. Infections were left for 45 minutes before either lysis with 0.1% saponin (adherent), or a 30 min treatment with 200 µg/mL gentamicin (Sigma), and 5 µg/mL penicillin (Sigma). Following cell lysis, serial dilutions were performed and plated on blood agar plates for enumeration of bacteria.

2.14 Modifications for *K. pneumoniae* Phagocytosis Assays

Phagocytosis assays with the J774A.1 cell line and *K. pneumoniae* were performed as above, but with the following modifications. Following bacterial inoculation at an MOI of 10, plates were centrifuged at 200 X G to synchronise infection. 'Adhesion' steps were performed for 1h, and due to the high level of drug resistance in this species, antibiotic treatments were determined empirically depending on the strain (see section 4.2.2). For time course experiments, after the initial antibiotic step to kill extracellular bacteria, media were replaced with gentamicin at the minimum inhibitory concentration to prevent bacterial outgrowth, but not to penetrate the cells.

2.15 Microbroth Dilution Antibiotic Susceptibility Assays

The susceptibility of both *S. pneumoniae* and *K. pneumoniae* strains to antibiotics were determined by the broth microdilution assay in accordance with standard protocols from the European Committee on Antimicrobial Susceptibility Testing (EUCAST). The assays were used to determine the minimum inhibitory concentration (MIC) and minimum bactericidal concentration (MBC) of drugs being assayed. All antibiotics were purchased from Sigma Aldrich, and stock solutions were made by suspending lyophilised drug in the solvent recommended by the manufacturer.

2.15.1 Preparation of bacterial inoculum and reading of MIC

Briefly, bacterial strains were plated onto their respective media as outlined in section 2.1, and incubated overnight. The following day, colonies were resuspended in PBS to an OD_{600nm} of 0.2. Cultures were then diluted 1:100 into the medium required in the assay giving an approximate bacterial concentration of 10^5 CFU/mL. 100 µl of the inoculum was then dispensed into wells of a 96 well plate containing 100 µl of pre-prepared serial dilutions of antibiotic. Triplicate negative control wells were included and consisted of just culture medium. Triplicate positive control wells consisted of 100 µL culture medium, and 100 µL bacterial suspension. Plates were then incubated statically at 37 °C with 5% CO_2 overnight. The following day MICs were scored as the first concentration of antibiotic to prevent turbid growth of the bacterium.

2.15.2 **Determination of MBC**

To determine the MBC of the bacterium, cultures from the MIC plate were spotted onto fresh agar plates and incubated overnight. The following day, the CFU/mL in each dilution well was calculated, and compared to the inoculum. A reduction of 2-logs or more in CFU from the inoculum was scored as the MBC.

2.16 **Construction of *nanA* Mutants in *S. pneumoniae* Using the Janus System**

This thesis produced three constructs which were used for disruption of the gene encoding pneumococcal neuraminidase NanA*,* and deletion of its two functional domains respectively, in two independent strain backgrounds (D39; encapsulated, DP1004; unencapsulated). Below I describe the strategy for construction of cassette marked mutants, and subsequently clean deletion mutants in pneumococcus. Further detail on the specific construction of mutants in *nanA* can be found in results section 2.16.

Sung *et al.* (2001)[261] first described the development of a negatively selectable system for construction of markerless mutations in *S. pneumoniae.* The so called 'Janus cassette' incorporates a kanamycin resistance marker (*aphIII*), and a WT copy of the *rpsL* gene (encoding for the ribosomal S12 protein) which confers sensitivity to streptomycin. Transformation of this cassette, flanked by sequences homologous to flanking sequences of the pneumococcal target gene, into a strain harbouring a mutant *rpsL** allele (*rpsL**; point mutation conferring streptomycin resistance) allows recombinogenic integration of the construct into the chromosome. These disruption mutants are resistant to kanamycin, but sensitive to streptomycin because of the dominance of the *rpsL* WT allele in the cassette. Transformation of these disruption mutants with a construct consisting of gene flanking sequence, but not the Janus cassette, allows for selection of 'clean mutants' which have lost the cassette by recombination and now have only the streptomycin resistance allele of *rpsL*.

2.16.1 **Primer design**

Primers for amplification of the Janus cassette, and of flanking sequences – including sequence overlapping with the Janus cassette to mediate ligation – for the different constructs are displayed in Table 6. Primers were designed using the online tool

Primer3 [262], and were ordered from SigmaAldrich. Lyophilised primers were suspended in ultrapure water to a stock concentration of 100μM, and working stocks were diluted in dH_20 to a final concentration of 10μM.

Table 6 - *Primers used for construction of nanA mutants*

Primer name	Sequence	Purpose
Janus casssette		
MD014	GTTTGATTTTTAATGGATAATGTGATATAATCT	Amplification of Janus cassette
MD015	GGCCCCTTTCCTTATGCTTTTG	
nanA sialidase KO		
*nanA*_Sial_F1	CCAAGAGATTACTATGCACGA	Amplification of US flank with overlap
*nanA*_Sial_R1_Jan	AGATTATATCACATTATCCATTAAAAATCAAACCGTTTTCTCTGTTAAAGCCGC	
*nanA*_Sial_F2_Jan	CAAAAGCATAAGGAAAGGGGCCGCTCCAACCCTTCAATTGG	Amplification of DS flank with overlap
*nanA*_Sial_R2	TGTTTCAGGAAGTGCCTGC	
nanA sialidase clean		
*nanA*_Sial_R1_Clean	CCAATTGAAGGGTTGGAGCCGTTTTCTCTGTTAAAGCCGC	Amplification of DS flank without overlap
*nanA*_Sial_F2_Clean	GCGGCTTTAACAGAGAAAACGGCTCCAACCCTTCAATTGG	
nanA lectin KO		
*nanA*_Lect_F1	GGATTGAGCAGGAAGTATG	Amplification of US flank with overlap
*nanA*_Lect_R1_Jan	AGATTATATCACATTATCCATTAAAAATCAAACTCGTGCATAGTAATCTCTTGG	
*nanA*_Lect_F2_Jan	CAAAAGCATAAGGAAAGGGGCCGCGGCTTTAACAGAGAAAACG	Amplification of DS flank with overlap
*nanA*_Lect_R2	GAAGTAGATATTGCCTAGTAATTGG	
nanA lectin clean		
*nanA*_Lect_R1_Clean	CGTTTTCTCTGTTAAAGCCGCTCGTGCATAGTAATCTCTTGG	Amplification of DS flank without overlap
*nanA*_Lect_F2_Clean	CCAAGAGATTACTATGCACGAGCGGCTTTAACAGAGAAAACG	

KO; knock out mutant with integration of cassette and disruption of gene, clean; following deletion of target region and excision of cassette, US; upstream, DS; downstream. All primer sequences are expressed 5' → 3'. Sequences of homology to either the Janus cassette (KO mutants) or to chromosomal sequence (clean mutants) are underlined in the respective sequence

2.16.2 High fidelity Polymerase Chain Reaction (PCR) and fragment ligation

PCR amplification of sequence for use in the construction of mutants was performed with the high fidelity Phusion PCR polymerase (Thermo). PCR master mixes consisted

of: 2 μM concentrations of each forward and reverse primer (see Table 6), in addition to 0.2M dNTPs, 0.02 units of polymerase, 1x High Fidelity Buffer, and approximately 100ng of template DNA. PCR amplification was performed using an Eppendorf Mastercycler Pro (Eppendorf). Denaturation of template DNA was performed at 94 °C for 15 seconds, followed by 30 cycles of denaturation at 94 °C for 15 seconds, annealing at a primer-dependent temperature for 15 seconds, and extension at 72 °C for 1 minute per kilobase of sequence amplified. A final extension at 72 °C was performed for 5 minutes. All PCR amplicons were resolved on 1% agarose (SeaKem LE Agarose, Lonza, USA) gels and sized using a 1 kb DNA size standard (HyperladderI). For assembly of 2-3 PCR amplicons to make transformation constructs, purified DNA from each amplicon – which contained flanking sequences complementary for one another – were added in equal volumes to a PCR reaction, with forward and reverse primers spanning the whole construct. Amplification yielded a full length product which was suitable for transformation.

2.16.3 **Preparation of competent pneumococcal cells**

Frozen stocks of pneumococci at an OD_{600nm} of 0.3 were thawed and diluted 1:100 into fresh BHI. Cultures were then incubated as above (section 2.1) until an OD_{600nm} of 0.03-0.05, and were subsequently diluted 1:10 into BHI supplemented with 0.1% (v/v) of 1M $CaCl_2$, 0.4% (w/v) Bovine Serum Albumin, and 0.2% (v/v) glucose, and incubated for a further 60 min. Samples were then frozen at -80 °C with 10% (v/v) glycerol.

2.16.4 **Transformation and selection of marked and unmarked mutants**

For marked mutants, frozen stocks of WT pneumococcal competent cells were thawed and incubated for 45 min following addition of 5 μL of construct DNA at a concentration approximately 20 ng/mL, and 5 uL of Competence Stimulating Peptide variant 1 (CSP1) at a concentration of 25 μg/mL. Transformation mixes were subsequently plated in a stepwise fashion. Briefly, 5 mL of BHI agar was added to a petri dish and allowed to dry at room temperature. 100 μL of the transformed pneumococci were than mixed carefully with 2 mL of BHI supplemented with 400 μL of horse blood. This mixture was then combined with 10 mL of BHI-A supplemented with 500 μg/mL

Kanamycin before layering onto the agar plate, leaving to dry, and incubating o/n. Single colonies were then patched onto fresh plates containing kanamycin and streptomycin to confirm resistance to the former, and sensitivity to the latter, before making frozen stocks.

Unmarked mutations were then constructed by making competent cells from marked mutants as above, and transforming them with a construct consisting of only the two flanking regions, with no Janus cassette. This enabled selection of markerless mutants which had excised the Janus cassette and had subsequently lost resistance to kanamycin, but gained resistance to streptomycin.

2.16.5 **Sanger sequencing**

Sanger sequencing was used to confirm gene disruption/deletion. Sequence of interest was PCR amplified as above using flanking primers displayed in Table 6. 5 µL of PCR amplicon (~ 25 ng/mL) was sent with 5 µL of forward and reverse primer (5 µM; in separate reactions) for Sanger sequencing by GATC sequencing. Sequence chromatograms were visually interrogated using A Plasmid Editor (APE; [263]), and .fasta files were queried against their respective reference genome by nucleotide BLAST [264].

2.16.6 **Preparation of pneumococcal protein lysates and western blot analysis**

For analysis of NanA protein production by pneumococcus, colonies were suspended in 10 mL CAT medium supplemented with 0.2% (wt/v) N-Acetyl-Mannosamine – which induces expression of neuraminidase – and cultured to OD_{600nm} of 0.2. Samples were then pelleted by centrifugation at 13000 RPM for 10 minutes in an Eppendorf 5424R bench top centrifuge, before resuspending in SDS and boiling at 100 °C for 10 minutes to extract protein. Protein concentrations were determined using NanoDrop ND-1000 spectrophotometer. 50 µg of pneumococcal protein lysate from each strain was loaded onto a commercially available, pre-prepared polyacrylamide gels (Biorad) and subject to electrophoresis, before transferring onto polyvinylidene fluoride (PVDF) membrane (activated in methanol for 2 minutes) using ice-cold transfer buffer (Biorad). Transfers were conducted for 1 hour at 100 V before blocking the membrane for 1 h in blocking buffer (PBS, 0.5% Tween-20 (Sigma), 5% Milk (Oxoid). The membrane was incubated with a 1:3000 dilution of anti-NanA antisera in blocking buffer for 1 h with gentle

shaking. Membranes were washed thrice with PBST (PBS + 0.1% (v/v) Tween-20) for 5 min with gentle shaking. The membrane was then incubated with a 1:10000 concentration of horseradish peroxidase (HRP)-conjugated secondary antibody, in blocking buffer for 1 h with gentle shaking. Then the membrane was washed thrice in PBST and then the reaction was detected using EZ-Chemiluminescence Kit (Geneflow, UK) and photographic film (Thermo).

2.17 **Multiplex Murine Cytokine Immunoassay**

The cytokine concentrations of mouse sera following infection with *S. pneumoniae* in this thesis was determined using a commercially available, multiplex immunoassay for 23 murine cytokines (Biorad; M60009RDPD) using the Luminex Magpix system (Luminex). Mouse serum samples were prepared as described above (section 2.5). Samples were analysed as per the manufacturers instructions. A standard curve was generated in Microsoft Excel using the fluorescence values from the in-kit cytokine standard controls. Raw samples fluorescence values were converted to concentrations by imputing them into the equation of the line generated from the standard curve. A subset of samples were analysed in technical duplicate, and very little variation was observed.

2.18 **Whole Cell Enzyme-Linked Immunosorbent Assay (ELISA)**

This thesis utilised Enzyme-Linked Immunosorbent Assays (ELISAs) to determine titres of antibody against whole bacterial strains in both murine and porcine serum. Whole bacterial strains were used to coat medium binding ELISA plates (Costar).

2.18.1 ***S. pneumoniae*** **inoculum preparation and plate coating**

For *S. pneumoniae,* strains were streaked onto BA plates, and incubated overnight at 37 °C with 5% CO_2. The following day, a sweep of colonies were inoculated into fresh BHI broth, incubated, and grown to an OD_{600}nm of 0.4. Samples were then pelleted at 13000 RPM for 10 minutes (as above), washed 3x in PBS, and resuspended in PBS to a final OD_{600}nm of 0.4. 100ul of bacterial suspension was dispensed into wells of the ELISA plate, which were then incubated o/n at room temperature to coat. The following day, un-coated bacteria were removed, wells were washed 3x with PBS, and samples were fixed for 20 min at room temperature with 100 µL of 4% PFA (Sigma).

Wells were washed an additional 3x with PBS before proceeding with the ELISA protocol (section 2.18.3).

2.18.2 *K. pneumoniae* inoculum preparation and plate coating

For *K. pneumoniae,* strains were streaked onto LA plates, and incubated overnight at 37°C. The following day, single colonies were inoculated into 5mL of LB broth, and incubated o/n at 37 °C. The following day, samples were sub-cultured 1:100 into fresh LB broth, and grown at 37 °C until an OD_{600} of 0.4. Samples were then pelleted at 3000 X G for 10 minutes, washed 3x in PBS, and resuspended in dH_2O to a final OD_{600nm} of 0.4. 100µl of bacterial suspension was dispensed into wells of the ELISA plate, which were dried o/n at room temperature in a biological safety cabinet to coat. The following day, samples were fixed in 100 µL of methanol, and left to dry o/n in a BSc. The following day, un-coated bacteria were removed, wells were washed 3x with PBS before proceeding with the ELISA protocol (section 2.18.3).

2.18.3 ELISA protocol

All steps of the ELISA protocol were performed at room temperature. Coated wells were first washed 3x with PBS supplemented with 0.05% (v/v) tween20 (Sigma; hereafter referred to as 'wash buffer'). Wells were then incubated for 1h with 100µl of PBS supplemented with 5% (w/v) skimmed milk powder (Oxoid), 0.05% (v/v) tween20, and 0.001% (v/v) naïve goat serum (Sigma), to block non-specific binding sites (hereafter referred to as 'blocking buffer'). Samples were then probed for 1h with 50 µl of the sera of interest, diluted 2 fold in blocking buffer starting from 1:8, to a maximum dilution of 1:16384, including a no sera negative control. Plates were then washed 3x in wash buffer, and probed for 1h with a secondary antibody conjugated with horseradish peroxidase raised against either murine (Sigma), or porcine (Abcam) IgG (diluted 1:40,000 and 5000 respectively). Samples were then washed 3x in wash buffer, and incubated for 10 min with 50 µl of tetramethylbenzidine (TMB; Sigma). The reaction was then stopped by adding 50 µL of 1M sulphuric acid (Sigma), before measuring the absorbance at 450nm using an Eon (Biotek) plate reader. All ELISAs were performed in at least duplicate. All sera, secondary antibodies, and relevant controls used in ELISA experiments are shown in Table 7.

Table 7 - *Serum samples and reagents used for whole cell ELISA*

Sample ID	Host species	Comment/reactivity	Catalogue number
Sera			
GFPS	Pig	From gnotobiotic pigs, kind gift of Andrew Rycroft	N/A
VPS1	Pig	From adult pigs vaccinated with *K. pneumoniae* ST25	N/A
PSP1	Pig	Sera from pig used for 1st pig spleen perfusion experiment	N/A
PSP2	Pig	Sera from pig used for 2nd pig spleen perfusion experiment	N/A
PSP3	Pig	Sera from pig used for 3rd pig spleen perfusion experiment	N/A
Antibodies			
α-pig IgG HRP	Goat	Secondary antibody against porcine IgG conjugated with HRP	AB6915
α-mouse IgG HRP	Rabbit	Secondary antibody against mouse IgG conjugated with HRP	A9044

Abbreviations: HRP; horse radish peroxidase, VPS; vaccinated pig sera, GFPS; germ free pig sera, PSP; pig spleen perfusion, IgG; immunoglobulin G

2.19 **Statistical Analysis**

All data reported in this thesis were statistically analysed using Graphpad Prism (version 8.3.1). Briefly, data were first tested for normality using a Shapiro-Wilk test. Normally distributed comparing 2 variables were analysed using a students t-test. Parametric data comparing 3 or more column variables were analysed using an ANalysis Of VAriance (ANOVA) test with Holm-Sidak's multiple comparisons test, whilst non-parametric data were analysed using a Kruskall-Wallis test with Dunne's multiple comparisons.

Chapter 3

Macrophages in the pathogenesis of pneumococcal infection

3 Chapter 3: Macrophages in the pathogenesis of pneumococcal infection

3.1 Introduction to Chapter

3.1.1 *Streptococcus pneumoniae*: the organism and its pathogenesis

Streptococcus pneumoniae (*Sp*), also known as 'the pneumococcus', is a Gram-positive, facultatively anaerobic, diplococcus of the *Streptococcus mitis* group [265] originally designated *Diplococcus pneumoniae* because of its presentation as diplococci [266]. The closest related organism to the pneumococcus is *Streptococcus mitis*, a commensal of the human oropharynx [267]. The pneumococcus is a transient, asymptomatic coloniser of the human nasopharynx [268]. In rare cases, the pneumococcus disseminates to the lower respiratory tract, causing pneumonia [269]. In approximately 20-30% of cases of pneumococcal pneumonia, pneumococci cross the epithelial barrier into the blood stream, causing bacteraemia (hereafter also referred to as invasive pneumococcal disease) which is associated with worsened disease outcome [270]. Pneumococci also cause meningitis which stems either from their translocation across the blood brain barrier (BBB) during bacteraemia [271], or directly from the middle ear [272]. The exact site of pneumococcal entry to the brain remains unclear. Invasive pneumococcal disease cases are associated with community acquired pneumonia [273]. Cases of pneumococcal bacteraemia without a clear primary source have been reported and are referred to as 'occult bacteraemia' [274]. The most common pneumococcal disease is otitis media, which is the primary reason for visits to general practitioners (GPs) by children. Pneumococcal disease is most common in children, and the elderly [275].

To initiate an infection, pneumococcus must first successfully transmit to a new host, which is thought to be mediated by droplets arising from sneezing, or by close contact with colonised individuals [276]. Pneumococci then establish a state of transient colonisation in the nasopharynx – termed the carriage state. People are thought to be transiently colonised by multiple pneumococcal strains throughout their life [277], but carriage events are predominantly monoclonal at any one time [278]. To cause an infection, pneumococci must become capable of dissemination to the lower respiratory tract. The mechanisms of dissemination to the lower respiratory tract are not fully elicited. One factor influenced pneumococcal dissemination is co-infection with

influenza virus [279], which leads to inflammation, and the release of sialic acid from host cells mediated by viral neuraminidase [280] – both conditions which are thought to favour disruption of the carriage state and mobilisation of pneumococci to the lung [281]. Pneumococci must then undergo a translocation event across the respiratory epithelium into the blood stream to cause bacteraemia [282] and – pertaining to the hypothesis that meningeal invasion originates from primary bacteraemia – an additional translocation event across the blood brain barrier to cause meningitis [283], all whilst evading the innate and adaptive immune responses [284]. These steps in pathogenesis are likely mediated by a number of host and microbial factors. Pneumococcal factors with known roles in the pathogenesis of disease are discussed in detail below.

3.1.2 **Key virulence determinants of *S. pneumoniae***

A vast wealth of scientific literature has been devoted to characterising the roles of surface proteins, metabolic factors, and surface modifying enzymes in the pathogenesis of bacterial disease. Each pathogen has a diverse set of 'virulence factors' involved in interaction with host cells, but many of these factors across species have common mechanisms of action. The commonality of these mechanisms implies intrinsic susceptibilities of the human host, that are readily exploited by a diverse set of pathogens. Below I will review in detail, select virulence factors of the pneumococcus of relevance to this thesis. Additional virulence factors have been described elsewhere and include the surface proteins PavA and Eno (fibrinogen and plasminogen binding respectively), and PspA which prevents surface binding of complement component C3 [285].

3.1.2.1 **Capsular polysaccharide**

Capsules are sugar-rich layers outside of the bacterial cell membrane, and peptidoglycan layer of the Gram-positive cell wall [286]. They consist of repetitive oligosaccharide subunits arrayed into complex polysaccharides [287]. For *Streptococcus pneumoniae,* almost 100 capsular serotypes have been described [288], and their ability to natural transformation of long DNA fragments [289] mean novel capsule types are regularly described [290]. The majority of pneumococcal capsules are covalently attached the outer cell wall subunit (peptidoglycan) [291],

although examples of non covalently linked capsules exist (e.g. serotype 3) [292]. Capsule has long known to be a major virulence factor for pneumococcus [293, 294] which is evident (1) from experimental models of infection where capsule mutants are avirulent [237, 295, 296] and (2) clinical invasive disease isolates are extremely rarely non-encapsulated – non-encapsulated strains tend to only cause non-invasive infections such as otitis [297]. In early studies, the capsule was first shown to be highly anti-phagocytic in hosts negative for anti-capsule antibodies [298]. This activity extends to macrophages [299], and neutrophils [300]. The activity is thought to be due to the highly charged nature of capsule, which prevents strong interactions with host cell receptors [301]. Another virulence strategy conferred by pneumococcal capsule is the prevention of complement and antibody recognition [302]. Of particular relevance to this thesis, different host phagocyte C-type lectins – a major class of receptors for recognising pathogen carbohydrates – differ in their affinity for pneumococcal capsule [303, 304]. For example, SIGN-R1 – a major receptor of marginal zone macrophages – differs in its affinity for capsule types [170], leading to ineffective non-canonical complement fixation [172], and phagocytic killing by this cell type (see section 1.3.4). Secondly, mannose receptor (CD206) expressed by subsets of tissue macrophages in the spleen and endothelial cells in the liver (see section 1.4.4) bind pneumococcal capsule types with varying efficiency [180]. Regulation of capsule biosynthesis is complex [305], and is highly dynamic during pneumococcal infection [306].

3.1.2.2 **LytA**

The release of bacterial surface fragments such as peptidoglycan and teichoic acids which elicit a pro-inflammatory response is a major step which exacerbates the inflammation characterising pneumococcal disease [307]. Pneumococci grown in liquid culture upon reaching the stationary phase of growth undergo spontaneous autolysis [308]. Autolysin has been shown to be mediated by LytA, an amidase which cleaves pneumococcal peptidoglycan [309]. Deletion of LytA results in virulence attenuation in murine models of infection, in which more efficient clearance from the airways is observed [310]. The virulence capacity of LytA is unclear, but is thought to be due to it mediating release of the diverse virulence factor pneumolysin (see below) [311].

3.1.2.3 **Pneumolysin**

S. pneumoniae strains encode a highly conserved, pore-forming toxin which has shown to be a major virulence factor [312] – pneumolysin. Pneumolysin is a pore forming toxin [313, 314] inhibited by cholesterol [315] and is closely related to listeriolysin O encoded by the Gram-positive pathogen *Listeria monocytogenes* [316]. Pneumolysin is a 53 kiladalton protein with a number of functions with defined roles in pneumococcal pathogenesis. At high concentrations pneumolysin is lytic to all eukaryotic cells with cholesterol-containing membranes [317] a feature which renders it highly cytotoxic at stages of infection with high bacterial burdens such as the later stages of septicaemia. At non-lytic concentrations, pneumolysin is highly inflammatory, and leads to the production of pro-inflammatory cytokines [318], and the induction of host cell death [319]. In early studies, Paton *et al.* (1983)[320] first demonstrated that pneumolysin was capable of inhibiting the bactericidal activity of neutrophils by preventing oxidative burst. Of interest to this thesis, Baba *et al.* (2002) [321] demonstrated that pneumolysin initiated an inflammatory reaction in splenic macrophages characterised by increased secretion of interferon gamma.

3.1.2.4 **Pneumococcal neuraminidase**

Pneumococci encode many systems for the cleavage of host glycoconjugates and uptake of sugars which can be used for metabolism [248]. One such family of systems – pneumococcal neuraminidases – cleave host terminal sialic acids and are major virulence factors in experimental infection [322]. Pneumococci encode up to 3 neuraminidases: *nanA*, *nanB*, and *nanC*. *nanA* yields a protein product of 672 amino acids and is encoded by all pneumococci [323] and is the gene whose deletion gives the most profound attenuation in virulence [324]. *nanB* codes for a 697 amino acid protein and is only encoded by 96% of pneumococci, while *nanC* is encoded by only 51% of pneumococci and encodes a 740 amino acid protein [325]. Differences in the three neuraminidase proteins arise from their specificities for different linkages of sialic acid in the host. NanA is a promiscuous sialidase with specificity for multiple linkages of sialic acid [326]. Contrastingly, NanB and NanC are specific for R2,3-sialosides [327]. The final products of sialic acid catabolism of these enzymes has been described by Xu *et al* [328]. Neuraminidase proteins contain two major functional domains, a C-terminal lectin like domain which binds sialic acid, and an N terminal

catalytic domain which cleaves the sugar from host glycoconjugates [327]. Myriad roles for neuraminase (mostly NanA) in pneumococcal virulence have been described. Manco et al [329] showed that following both intravenous and intranasal infection of mice, that *nanA* and to a lesser extent *nanB* deletion mutants had lower organ loads, and longer survival times. Dalia *et al* [330] demonstrated a role for NanA in resisting the opsonophagocytic activity of neutrophils by reducing complement deposition on the cell surface. Uchiyama *et al* [331] demonstrated a key role for NanA in binding to brain endothelial cells mediating CNS invasion.

3.1.3 **Treatment and prevention of pneumococcal disease**

3.1.3.1 **Antibiotic therapy**

Treatment of pneumococcal disease varies worldwide, but has traditionally been achieved by use of a beta-lactam (e.g penicillin, or ampicillin) [332]. Penicillin non-susceptibility [333] is widespread among pneumococci mediated by mutations in penicillin binding proteins (PBPs)[334]. In most cases, penicillins can still be used for treatment of penicillin non-susceptible isolates, because the levels of resistance conferred are still far lower than the peak serum concentrations of the drug during treatment [335]. In many cases, use of penicillin is substituted for use of the cephalosporin ceftriaxone because of their longer half-life *in vivo* [336]. Macrolides (such as clarithromycin or azithromycin) can be an effective treatment for pneumococcal disease [337]. Resistance to macrolides in the pneumococcus can be conferred by (1) active efflux of the drug from the bacterium which confers low levels of resistance to 1-4 mg/L of drug and is predominantly mediated by acquisition of the *mef* gene encoding a major facilitator family efflux protein [338], and (2) modification of the ribosomal target site which confers high level resistance to >128 mg/L of drug and is predominantly mediated by acquisition of the *erm* gene encoding a ribosome methylase [339]. In many places in the UK, low severity community-acquired pneumonia is treated by oral amoxicillin monotherapy, which is combined with a macrolide such as azithromycin in the case of high severity pneumonia [340]. In the case of septic clinical presentations, therapy in the UK is generally started with the carbapenem antibiotic meropenem [341], and can be de-escalated following diagnosis of pneumococci.

3.1.3.2 **Vaccination**

The pneumococcal capsule has long been known to elicit antibodies which protect from systemic disease [342]. Pneumococcal vaccines consisting of purified capsular polysaccharide were first implemented in the 1940s predominantly in the elderly [343]. To date, polysaccharide vaccines such as Pneumovax23 are still in use in the UK in elderly demographics [344]. A major drawback of polysaccharide vaccines are their relative inefficacy in eliciting protective antibodies in children [345] – a demographic who carry a large proportion of the disease burden [346]. Conjugate vaccines – polysaccharides covalently linked to highly immunogenic proteins [347] - against *Haemophilus influenzae* type b had been highly effective in eliciting protective antibody response in children [348], and so this approach was applied to the pneumococcus. Since January 2020, pneumococcal conjugate vaccine 13 (PCV13) has been part of the UK childhood vaccination schedule and is effective in prevention of bacteraemic disease in infants [347, 349]. Both capsular polysaccharide vaccines whilst effective in preventing septic disease, have only a modest effect in protection against pneumonia, and in preventing pneumococcal carriage [350]. An issue with both polysaccharide and conjugate vaccines are their reliance on the capsule as the protective antigen. As described above, pneumococci encode a wide variety of structurally diverse capsules. Further, the ability of pneumococci to uptake large fragments of DNA (which can encompass large portions of the capsule locus) mediates serotype conversion, leading to the emergence of vaccine escape strains [351, 352]. Development of vaccines based on conserved protein antigens would be advantageous as it would provide broad strain coverage, but such vaccines have showed limited success due to their poor immunogenicity in infants and genetic sequence diversity [353, 354]. Whole inactivated cell/attenuated vaccines are being developed for pneumococcus [355], and have found success in the case of *Salmonella* [356], but at present are still in pre-clinical development.

3.1.4 **The spleen and macrophages in pneumococcal disease**

It has been long known that the spleen plays a critical role in the host defence against invasive pneumococcal infection [357]. This was first observed clinically in that patients who undergo splenectomy rapidly undergo overwhelming sepsis in the first

24h after surgery [358, 359], due to the loss of pneumococci-specific B memory cells [360]. Later, Brown *et al.* (1981) [361] demonstrated that in a Guinea pig model of infection, that radiolabelled organisms were closely associated with the spleen, but not the liver. Furthermore, as animals which had undergone splenectomy, were infected with more virulent organisms, the liver was increasingly inefficient in compensating in clearance of the blood, indicating a dominant role for the former organ and not the latter [361]. Later studies demonstrated the critical role of SIGN-R1+ marginal zone splenic macrophages and resident splenic neutrophils in facilitating the clearance capacity of this organ in mice [154]. As described in section 1.6.2, initial clearance of bacteria by the spleen is associated with later recurrence of a monoclonal bacteraemia [235]. Until recently, an extra-vascular niche of organisms seeding the blood after this initial clearance remained unclear.

3.1.5 Intracellular replication of pneumococcus in splenic macrophages: Ercoli *et al.* (2018)

This thesis follows on from work conducted by Prof Marco Oggioni's group - predominantly Dr Giuseppe Ercoli. We published this work (Ercoli *et al.* 2018) [362] in the journal Nature Microbiology, and here I will summarise the key findings which preceded the work performed by me in this thesis. The work by Gerlini *et al.* (2012) demonstrated (1) a role of macrophages in the initial defence against invasive pneumococcal infection, and (2) the existence of a single cell bottleneck in the pathogenesis of invasive pneumococcal infection. The human/murine host is extremely competent in the clearance of bacterial infection, as evidenced by the high infectious dose 50 (LD_{50}) required to initiate disease (10^5 CFU/mouse; Gerlini *et al.* 2015). In light of this, in an immune-competent host, how could bacteraemia be initiated by a single bacterial cell? Ercoli *et al.* hypothesised that there had to be an extravascular reservoir of pneumococci, responsible for the single cell bottleneck, which could then be the population to initiate disease. The subsequent investigations indicated that at the point of the 'eclipse phase' of pneumococcal disease – where no cultivable bacteria are found in the blood (Figure 6a) – that the spleen still contained high bacterial titres (Figure 6b). Confocal microscopy analysis of the spleen indicated that clusters of pneumococci could be found associated to splenic macrophages (Figure 6ci), and that over an infection time course (from 30 minutes, to 8 hours)

(Figure 6cii-v), these clusters of pneumococci increased, providing the first evidence that whilst the spleen is a major organ for pneumococcal clearance, it was likely also permissive to intracellular replication. To decipher if these clusters were replication events initiated by a single founder bacterium, or multiple phagocytic events, the authors conducted a co-infection of mice with a 1:1 mix of pneumococci labelled with either GFP or RFP (Figure 6d). This experiment revealed that clusters of pneumococci were always formed of a single colour, indicating that the bacteria were actively replicating. At this point, I joined this project, and aimed to determine the mechanisms underpinning the permissive nature of specific subsets of macrophage to pneumococcal infection.

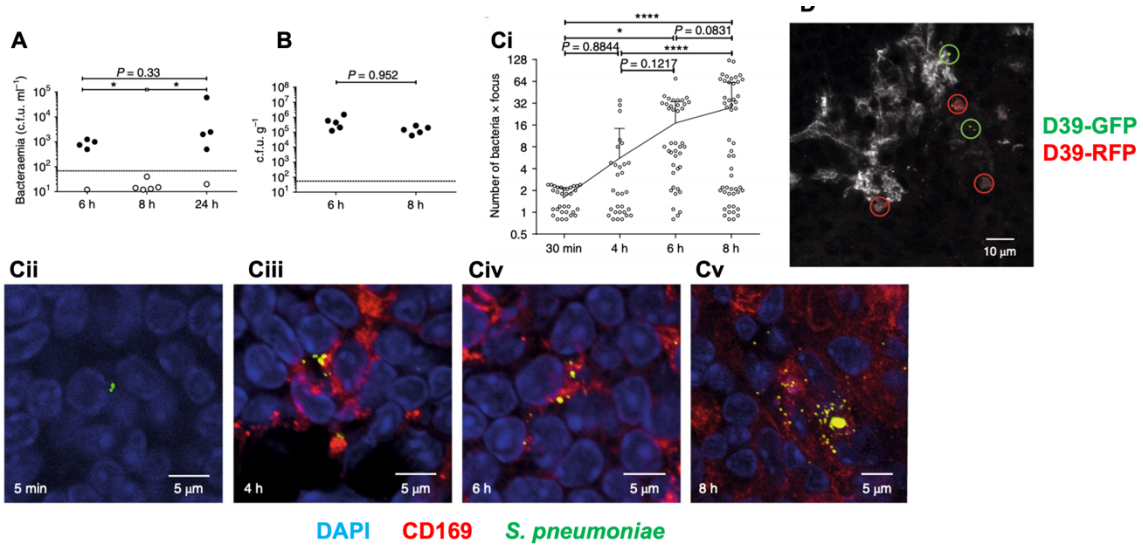

Figure 6 - *The eclipse phase of pneumococcal pathogenesis as reported by Ercoli et al. (2018).* (A) shows the bacterial counts in mouse blood after intravenous infection. (B) shows the bacterial counts recovered from the spleen at 6 and 8h post infection. (C) shows an analysis of the number of bacteria associated to single phagocytes over an infection time course (i) which is exemplified in images (ii-v). (D) shows a representative immunofluorescence section from a mouse spleen following co-infection with a 1:1 mix of D39-GFP and D39-RFP.

3.2 Results

3.2.1 Time course analysis of splenic infection in mice

First, I aimed to characterise the dynamics of *S. pneumoniae* clearance from the blood, and uptake by the spleen following intravenous infection. To achieve this, groups of 5 mice were inoculated with 10^6 CFU of serotype 2 strain D39 through the lateral tail vein, and samples of blood and spleen were taken for enumeration of CFU at 6h, 8h, 12h, 16h, 24h post infection, and one group was sacrificed at the severity limit (moderate signs of disease; hereafter referred to as end-point). I observed that pneumococci were gradually, logarithmically (as evidenced by the linear line on a logarithmic scale) cleared from the blood until at 8h post infection, at which time bacteria were below the limit of detection (Figure 7a; the 'eclipse phase'). This coincided with an increase in bacterial counts in the spleen at 6 and 8h post infection. Importantly, at these early time points when spleen counts were positive, bacteria could not be cultured from liver, brain, or kidney [235]. Further, microscopy investigation [362] performed previously by Dr Giuseppe Ercoli indicated that bacterial counts in the spleen were a product of intracellular replication of organisms, and not just survival of the inoculum. At 12h post infection, bacterial counts in the spleen decreased, which correlated with an increase in bacterial counts in the blood (Figure 7a). Thereafter, counts in both the spleen and the blood increased until the experimental end point. When considering the disease course, and survival times (as determined by the severity limit of the license), mice only began to show signs of disease post-24h, with one mouse in 20 infected reaching the endpoint at this early time point (Figure 7b). The majority of mice began to reach the endpoint at 48h post infection, with a single mouse being culled 2 hours earlier. These data demonstrate that mice have a crucial dynamic phase of infection in the early stages after intravenous inoculation, which is asymptomatic until the 24h after infection. Further, it shows that clearance of bacteria from the blood inversely correlates with the presence of live bacteria in the spleen warranting microscopy-based investigation of bacterial fate in this organ.

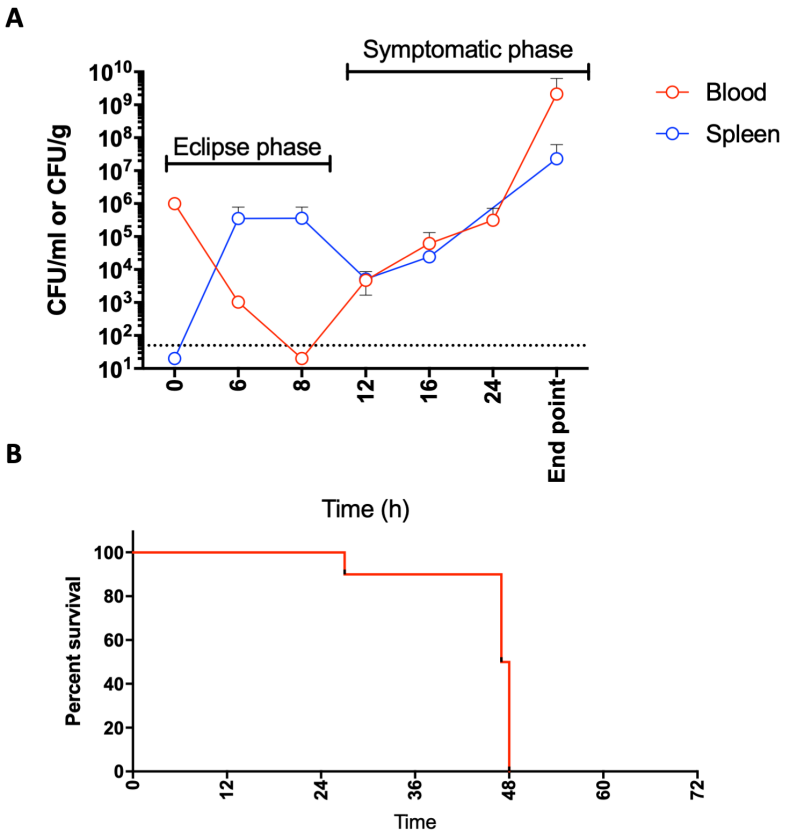

Figure 7 - *Infection time course of CD1 mice with Streptococcus pneumoniae strain D39.* (A) groups of 5 mice were infected with 10^6 CFU of D39 through the lateral tail vein and were killed for sampling at 6h, 8h, 12h, 16h, 24h, and at the experimental end point. Blood samples were taken by cardiac puncture under terminal anaesthesia at predetermined time points and plated to enumerate CFU (red line). Spleens were taken post mortem, homogenised a plated for their CFU (blue line). (B) 10 mice were infected as above and were monitored across the infection time course for signs of disease. Animals were killed when they showed moderate signs of disease in line with the home office license. The % survival times of animals are displayed on an Kaplan Meier plot. Infection experiments reported in panel A were performed with the help of Dr David Carreno.

3.2.2 **Cytokine production following pneumococcal infection**

Cytokines are major regulators of innate and adaptive immunity. To gain insight into the cellular signalling mechanisms occurring during this infection time course, I analysed the production of 23-cytokines and chemokines using a multiplex Luminex assay, in serum samples from un-infected mice, and from mice infected for 6h, 24h, and the experimental end point. Serum concentrations of cytokines are plotted along

side blood and spleen CFU counts in Figure 8. Description of the functions of cytokines included in the 23-plex Biorad kit can be found in Table 8.

Cytokine	Comment	Exemplar functions	Reference
IL-1α	IL-1 family	Acute phase; fever and inflammation	[363]
IL-1ß	IL-1 family	Apoptosis; secreted during NLRP3 pyroptosis	[364]
IL-8	Chemokine	Granulocyte chemotaxis	[138]
IL-17a	IL-17 family	Th17 response; promote inflammatory cytokine production	[365]
TNF-α	Global regulator	Fever; inflammation; cell death	[366]
IFN- γ	Globally pro-inflammatory	Macrophage, NKTC and neutrophil activator	[367]
MIP-1a	CCL family chemokine	Produced by macrophages, chemokine	[368]
IL-9	Common γ-chain receptor ligands	Pleiotropic; prevents apoptosis	[369]
IL-2		T-cell modulation	[370]
IL-4		Lymphocyte stimulation	[371]
IL-13	Shared receptor	Allergic response; IgE production	[372]
IL-5		IgA secretion	[373]
IL-3	Common ß-chain receptor ligands	MHCII induction, Mac + Neu activation	[374]
M-GM-CSF		Growth factor	[375]
M-G-CSF		Granulocyte production	[376]
IL-10	IL-10 family	Downregulation of Th17 cytokines	[377]
IL-12	IL-1 family	Induction of IFN- γ production	[378]
IL-12 (p70)		Induction of IFN- γ production	[379]
RANTES	CCL family chemokine	T cell, eosinophil, and basophil chemotaxis	[380]
Kc	CXC family chemokine	Neutrophil chemotaxis	[381]
Eotaxin	CCL family chemokine	Eosinophil chemotaxis	[382]
MCP-1	CCL family chemokine	Monocyte chemotaxis	[383]

Table 8 - *Cytokines analysed with the Biorad 23-plex kit.*

NKTC; natural killer T cell, NLRP3; NOD-, LRR- and pyrin domain-containing protein 3, CCL family; contain 2 cysteine-cysteine bonds at their N terminus, CXC; separation of N terminal cysteines with another amino acid

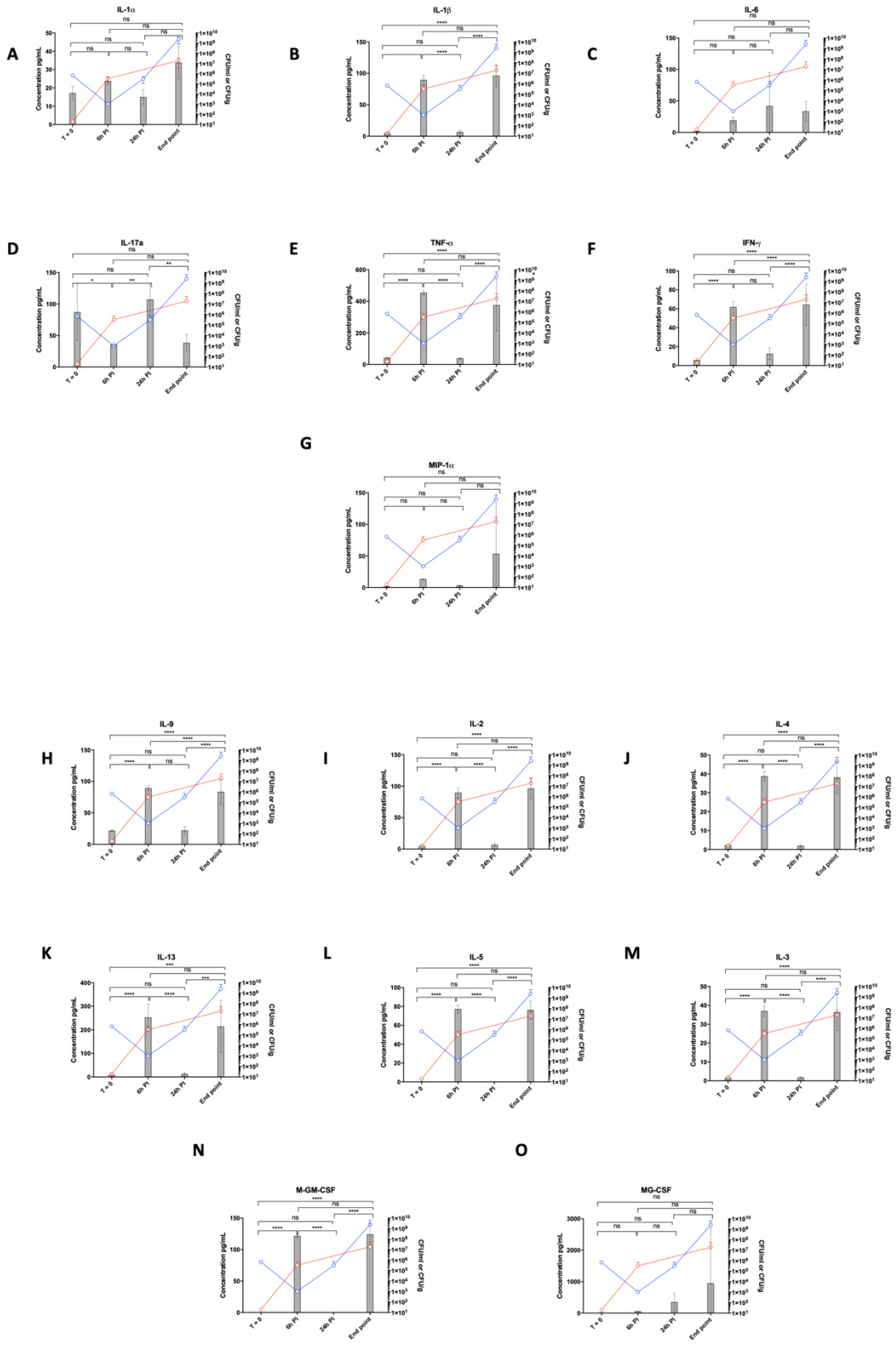
A
IL-1α
B
IL-1β
C
IL-6
D
IL-17a
E
TNF-α
F
IFN-γ
G
MIP-1α
H
IL-9
I
IL-2
J
IL-4
K
IL-13
L
IL-5
M
IL-3
N
M-GM-CSF
O
MG-CSF
Concentration pg/mL
CFU/ml or CFU/g
T = 0
6h PI
24h PI
End point

Figure 8 - *Time course analysis of cytokine production following intravenous infection of mice.* Sera were taken from mice by cardiac puncture under terminal anesthesia at 6h post infection and at the experimental end point when they displayed moderate signs of disease. Sera were also taken pre-infection and at 24h post infection by tail bleed. Samples were analysed using the Luminex 23-plex cytokine kit as per the manufacturers instructions. Data are representative of 5 mice per group. Cytokines analysed were IL-1α (A), IL1ß (B), IL-6 (C), IL-17a (D), TNF-α (E), IFN- γ (F), MIP-1a (G), IL-9 (H), IL-2 (I), IL-4 (J), IL-13 (K), IL-5 (L), IL-3 (M), M-GM-CSF (N), MG-CSF (O), IL-10 (P), IL-12 (Q), IL12-p70 (R), RANTES (S), Kc (T), eotaxin (U), MCP-1 (V). Statistical significance between time points were determined using a 1-way ANOVA. ****; P<0.00005, ***; P<0.0005, **; P<0.005, *; P<0.05, ns; non significant.

3.2.2.1 **Pro-inflammatory cytokine production**

For 3 of 8 pro-inflammatory cytokines assayed (IL-1ß, TNF-α, and IFN-γ), an interesting phenomenon was observed. These cytokines were present in negligible amounts in the pre-infection samples, which significantly increased at 6h post infection. Despite this, at 24h post infection (after the eclipse phase) a significant reduction in production of these cytokines was observed. It is tempting to speculate that the reduction in cytokine production at this time point is due the lack of bacteria in the blood, and that this facilitates pneumococcal persistence in the tissue. These cytokines then increased at the later stage of infection, by which point bacteria had been present in the blood for greater than 24h. For IL-1α, IL-6, and MIP-1a there was no significant change in cytokine production across the time course. For IL-17a, a different pattern was observed; cytokine concentration significantly decreased from pre-infected to 6h PI, and then significantly increased from 6h to 24h PI, and finally decreased again from 24h, to the experimental end point.

3.2.2.2 **Production of anti-inflammatory cytokines and those implicated in humoral immunity**

For 7 of 8 cytokines implicated in adaptive immune responses, the same phenomena was observed as above. IL-9, IL-2, IL-4, IL-13, IL-5, IL-3, and M-GM-CSF displayed significant increase in cytokine concentration from pre-infection to 6h PI, which then significantly reduced at 24h post infection, and increased again at the experimental endpoint. Instead, MG-CSF showed no significant changed in cytokine concentration throughout the experimental time course, although a single mouse at the later time point displayed high concentrations of this cytokine. The anti-inflammatory cytokine IL-10 significantly increased in concentration from 0 to 6h post infection. It then

decreased to pre-infection levels at 24h post infection, before increasing at the experimental endpoint. Instead IL-12 concentrations stayed static until 6h post infection, but then increased significantly at 24h post infection.

3.2.2.3 **Production of chemokines**

Chemokines are important for the directional movement of inflammatory cells to infected areas. For the T-cell chemoattractant RANTES, a significant increase in production was observed between 6h and 24h post infection. The neutrophil chemoattractant KC increased in concentration from 0 to 6h post infection. The eosinophil attractant eotaxin significantly decreased at 6h and 72h post infection. There was no significant change in MCP-1 concentration across the infection time course.

3.2.3 **RPM and MMMs, but not MZMs are permissive to pneumococcal replication**

Following on from my observation that live bacteria are present in the spleen despite negative blood counts, and the observation by Ercoli *et al* (2018) that pneumococci are capable of replication within splenic macrophages (see section 3.1.5 for further details), I aimed to determine which macrophage cells types in this organ were permissive to intracellular replication. For this, spleens from mice infected intravenously for 6h with strain D39 were stained with antibodies for 3 different macrophage populations: RPMs (F4/80+), MMMs (CD169+, CR-Fc+) and MZMs (MARCO+, unstained compartment between CR-Fc, and F4/80+ cells) known to be present in the spleen (see introduction), in conjunction with staining for bacteria. I documented the size of bacterial foci (number of bacteria per infected macrophage) associated with these different macrophage populations (Figure 9a). I observed that both CD169+ metallophilic macrophages, and F4/80+ red pulp macrophages contained clusters of bacteria ranging from 1-25, with no significant difference between these groups. Instead, MZMs only contained either single, or double bacteria, which was significantly less than both MMMs, and MZMs. Representative confocal microscopy images of foci in these cells are shown in Figures 9b-c.

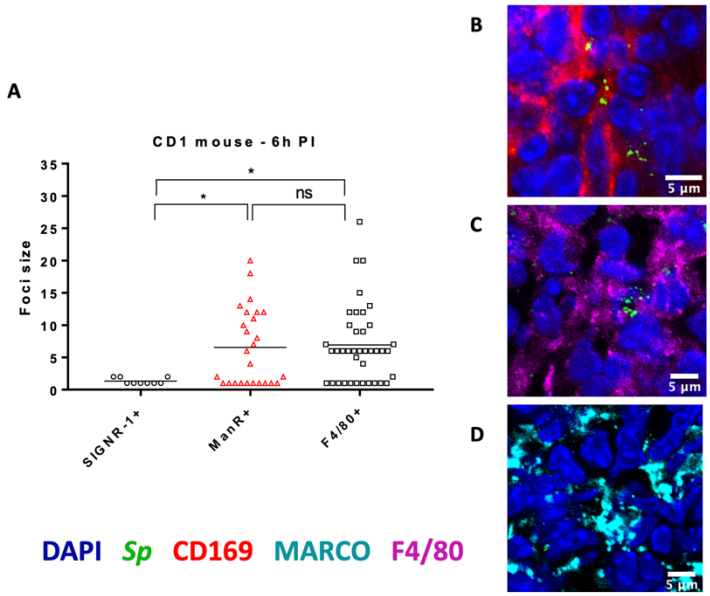

Figure 9 *- Pneumococcal foci formation in splenic tissue macrophages.* (A) Spleens from mice infected intravenously for 6h with 10^6 CFU of *S. pneumoniae* D39 were stained for different macrophage populations, and the number of bacteria associated with individual macrophages was counted from 30 random fields of view with a 60x objective using an Olympus confocal microscope. Data are representative of 3 mice. Statistical significance were determined with an ordinary 1-way ANOVA. *; P<0.05, ns; non-significant. Representative pneumococcal foci associated with CD169 (B), F4/80 (C), and SIGN-R1 (D) positive cells. Scale bars are 5um in width.

3.2.4 **Intracellular localisation of *Sp* in macrophages**

To determine if bacteria found associated with the three macrophage populations in the spleen were intracellular or surface bound, I performed Z-stack microscopy of bacterial found in 6h-infected mouse spleens associated with CD169+, F4/80+, and SIGN-R1+/MARCO+ membrane markers which delineate these macrophage subpopulations. I then reconstructed these Z stacks into 3D images to identify the subcellular localisation of bacteria. I observed that intracellular bacteria could be observed within CD169+ (Figure 10a), MARCO+ (Figure 10b), and F4/80+ (Figure 10c) macrophages. It should be noted that bacteria were not exclusively intracellular, and examples of extracellular bacteria could be found across spleen sections. Use of

a high-resolution confocal imaging systems, systems capable of imaging bacterial infection in real time will be required to delineate the full extent of intracellular vs extracellular bacteria in pneumococcal spleen infection. The balance of intracellular to extracellular organisms is likely to be dependent on inoculum size, and in this context a dose response experiment should be planned, as our infection doses are much above an LD_{50}.

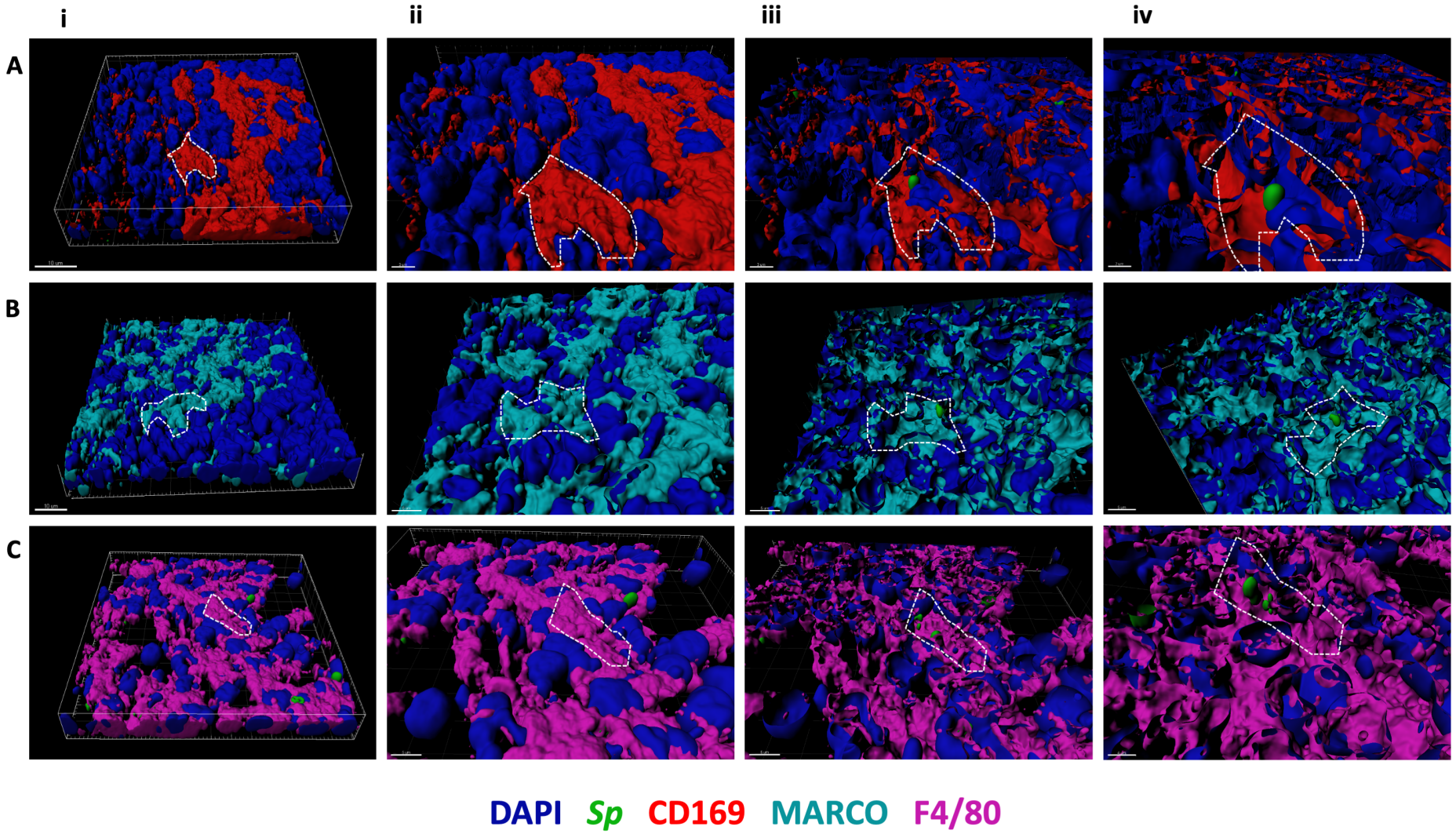
i
ii
iii
iv
A
B
C
DAPI Sp CD169 MARCO F4/80

Figure 10 - *Intracellular localization of pneumococci in splenic macrophages.* Representative Z stacks of pneumococci present in immunostained, 6h infected mouse spleen sections were imaged using an Olympus confocal microscope. Sections were imaged every 0.25 μm, and Z stacks were reconstructed into 3D images using Imaris (see methods). From left to right an artificial cut downwards into the tissue shows bacteria confined within the membrane stains of CD169 (A), SIGN-R1 (B), and F4/80 (C) positive macrophages. Data are representative of bacteria found in 3 independent mouse spleens. Scale bars are 10 μm (i), and 5 μm (ii-iv) respectively. Outlines of cells of interest are highlighted by dotted white lines.

3.2.5 **Foci formation is strain and capsule independent**

The factors encoded by the accessory genome, including many surface proteins and the capsule, all contribute to differences in the virulence potential of distinct phylogenetic pneumococcal lineages [384]. To determine if foci formation in the spleen was dependent on pneumococcal serotype or limited to the type 2 D39 laboratory strain, I infected mice with 10^6 CFU of the Type 4 strain TIGR4 which is known to cause disease in mice [235], and R6, a capsule-null derivative of D39 known to be defective in virulence [296], for 6h before harvesting blood and tissue for analysis. Figure 11b shows that CD1 mice were able to efficiently clear both encapsulated strains to a comparable extent, but that the capsule null strain was completely eradicated from the circulation at 6h post infection. Both encapsulated strains had comparable spleens counts (Figure 11a), but interestingly, there was no significant difference in splenic CFU between the two encapsulated strains and the capsule null strain indicating that capsule is not a major determinant of intracellular survival. When analysing spleen sections by confocal microscopy (Figure 11c; R6, and 10d; TIGR4) it became apparent that in analogy to what I had observed for D39, that both TIGR4 and R6 were capable of foci formation in CD169+ macrophages. These data indicate that the contribution of the capsule to virulence is likely due to its anti-phagocytic properties with ‘killer phagocytes’, and not due to an ability to modulate biology of the macrophage to facilitate intracellular replication. Future work should experimentally confirm at which point virulence attenuation of the capsule mutant occurs through the use of time course infections.

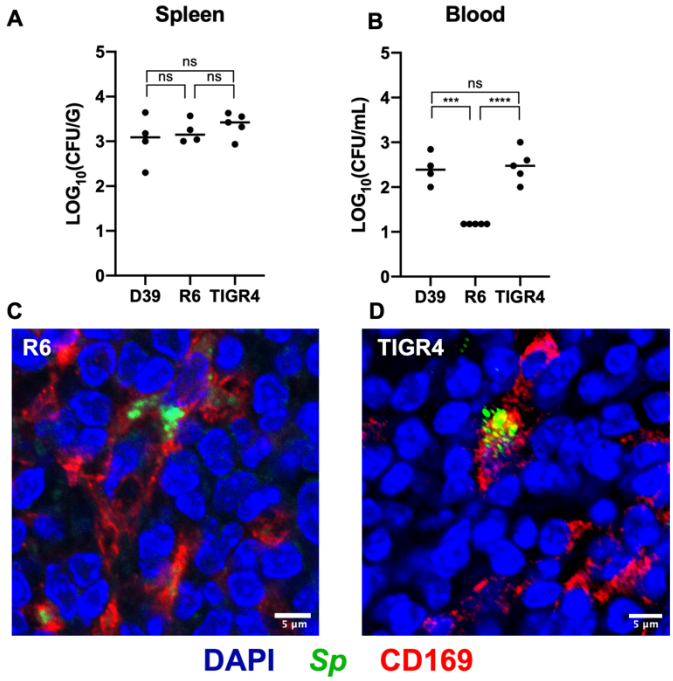

Figure 11 *- Foci of infection formed by the non-encapsulated D39 derivative R6, and the type 2 encapsulated TIGR4*. Mice were infected intravenously with 10^6 CFU of D39, R6, and TIGR4 through the lateral tail vein. At 6h post infection, blood was taken by cardiac puncture for CFU determination, and spleens were taken for homogenization and enumeration of CFU and microscopy. The Log10 transformed CFU/G of spleen are shown in (A), whilst the Log10 CFU/mL of blood are shown in (B). Statistical analysis were performed using an ordinary one way ANOVA. Ns; non-significant, ***; P<0.0005, ****; P<0.00005. Spleen sections from R6 (C) and TIGR4 (D) infected mice were immunostained using antibodies specific for CD169, type 2 capsule (TIGR4; green), and nuclei (DAPI; blue). The R6 derivative using in this experiment expressed GFP, and was constructed by Dr Giuseppe Ercoli.

3.2.6 CD169+ macrophages are the origin of invasive pneumococcal disease in mice

In section 3.2.3, I demonstrated that CD169+ and F4/80+ macrophages both harboured permissive replication of pneumococcus. I therefore aimed to identify which macrophage population played a major role in the pathogenesis of disease. Previous studies of both murine and porcine viral infections have indicated that CD169 – the defining receptor for metallophilic macrophages – functions as a receptor for entry of HIV-1 and Porcine Reproductive and Respiratory Syndrome Virus (PRRSV) into metallophilic macrophages [167, 385]. Further studies have indicated that specific

engagement of CD169 by PRRSV dampens type 1 interferon responses facilitating reduced viral clearance in these cells but not others [386]. Studies have also demonstrated that blockade of CD169 with a monoclonal antibody (clone 3D6.112 for mice), prevented viral entry and protected mice from viremia [387]. I therefore aimed to determine if a receptor blockade could alter the course of pneumococcal infection, as a tool to delineate the specific contribution of this cell marker to disease.

3.2.6.1 **CD169 receptor blockade**

Mice were dosed IV with 10 µg of anti-CD169 monoclonal (clone 3D6.112) antibody (henceforth referred to as 'blocking antibody') or the same concentration of an isotype (IgG2a) matched control, 30 minutes prior to IV infection with 10^6 CFU of D39. Bacteraemia were quantified by plating of serially diluted blood taken by tail bleed at 24 hours on blood agar plates followed by counting of CFUs (Figure 12a). CD169 is also expressed on macrophages in the perivascular area of the brain, and in subcapsular sinus macrophages of the lymph nodes. The brain is independent of the spleen in our intravenous model, and previous quantitative culture of lymph nodes following IV infection with pneumococcus revealed no live bacteria in this niche. Furthermore, BLASTp query of the murine CD169 sequence revealed no significant hits in the pneumococcal proteome, therefore the antibody is unlikely to effect the bacteria. I therefore conclude that any phenotype observed in these experiments is directly due to effects of the antibody in the spleen. The data clearly demonstrate that the majority of mice treated with the blocking antibody (9/10 mice) were completely protected from bacteraemia, as no bacteria could be cultivated from their blood, in contrast to the control group where levels of bacteraemia ranging from 10^3-10^9 CFU/mL were observed. Survival of mice was monitored over a 72 hour period (Figure 12b), and indicated that as expected, mice given the blocking antibody (and which were devoid of bacteraemia) survived significantly better than those given the blocking antibody (P= 0.0005; Mantel-Cox test). Finally, both blood and spleens were plated to determine the number of CFU at the experimental end point (Figure 12c). The data show that in agreement with the 24h blood counts, mice in the blocking group were devoid of bacteraemia when compared with the controls. Most interestingly though, administration of blocking antibody resulted in significantly lower cultivable bacteria in the spleens at the experimental end-point, indicating that specifically CD169+

macrophages, and not the red pulp macrophages – which also display foci formation – are the origin of invasive disease in these mice. This blocking antibody has been previously demonstrated to bind the sialic acid binding domain of sialoadhesin (Figure 12d)[388], but blocking antibodies are also know to mediate inhibition by steric effects. This warrants functional investigation of the role of this marker in infection (see section 3.2.6.3).

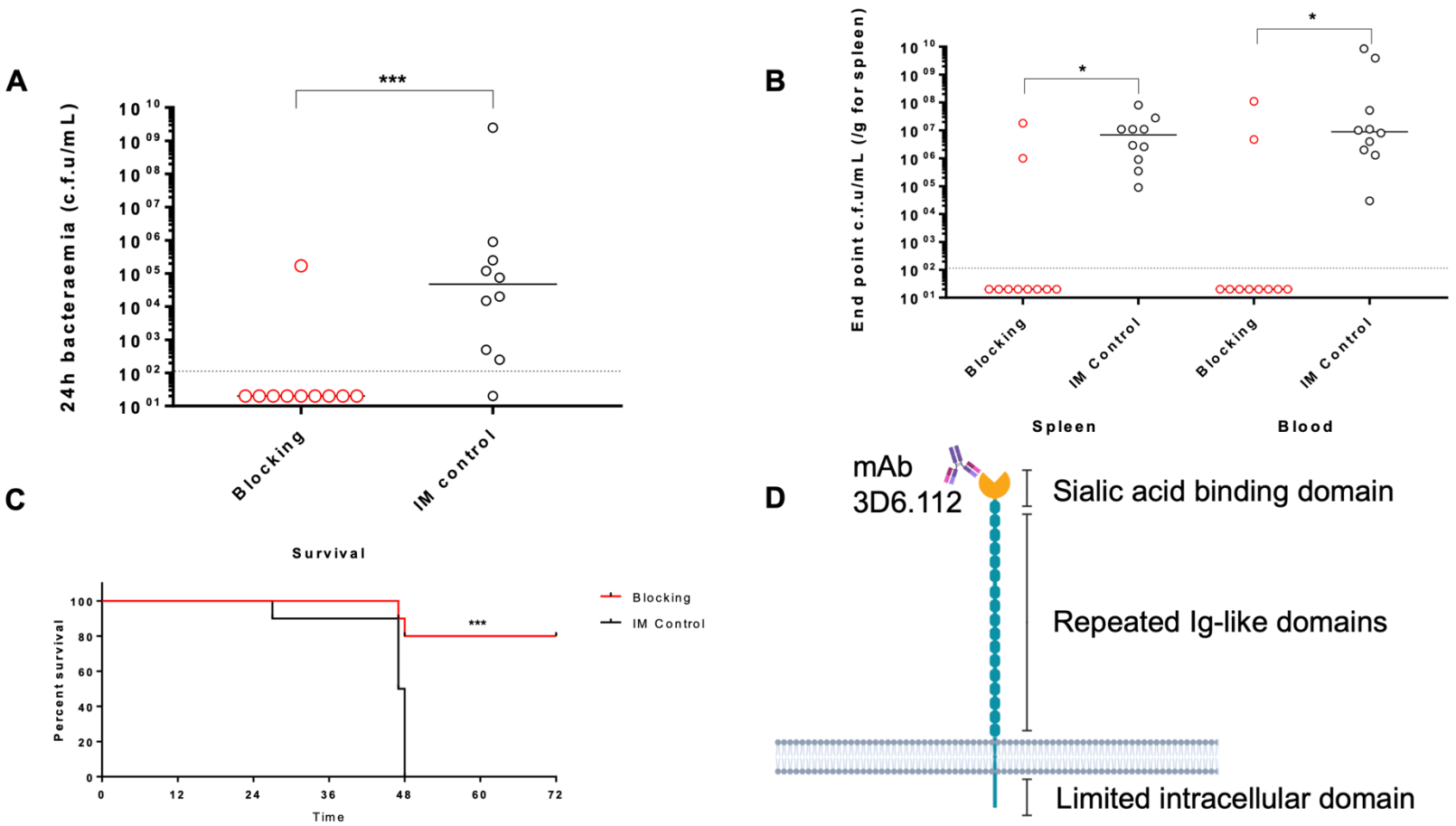
A
24h bacteraemia (c.f.u/mL)
***
Blocking
IM control
B
End point c.f.u/mL (/g for spleen)
*
*
Blocking
IM Control
Blocking
IM Control
Spleen
Blood
C
Survival
Percent survival
Time
***
Blocking
IM Control
D
mAb
3D6.112
Sialic acid binding domain
Repeated Ig-like domains
Limited intracellular domain

Figure 12 *- CD169 blocking inhibits pneumococcal infection of the spleen and correlates with protection from disease.* 6-8 week old CD1 mice were intravenously infected with either anti-CD169 blocking antibody, or IgG isotype matched control through the lateral tail vein, 30 minutes prior to infected with 10^6 CFU of D39 through the opposite tail vein. Blood were taken by tail bleed at 24h post infection for enumeration of bacteremia (A). Statistical significance were determined by 1-way ANOVA. ***; P<0.0005. Mice were monitored for signs of disease up to 72h post infection. Mice were killed when they showed moderate signs of disease in accordance with the home office license. At death, blood were taken by cardiac puncture under terminal anesthesia, and spleens were taken post mortem and homogenized in BHI +10% glycerol. Blood and spleen homogenates were serially diluted and plated for enumeration of CFU (B). Statistical significance were determined by 1 way ANOVA. *; P<0.05. Survival of mice was monitored up to 72h post infection, and are plotted on an Kaplan Meier graph. ***; P<0.0005. In all cases, individual mice which received blocking antibody are represented by red data points, whereas those which received the isotype matched control are indicated by black points. (D) shows the putative binding site of the anti-CD169 blocking antibody to be the sialic binding domain of CD169. The sialic acid binding domain is represented using an orange symbol, whereas immunoglobulin like domains are shown using navy rectangles.

To determine the longevity of receptor blockade, I stained spleens from both mice which were given blocking antibody, and an isotype matched control with only the complimentary secondary antibody to determine whether antibody remained bound in the spleen (Figure 13). Fluorescent signal was found in the blocking treated spleens even 72 hours after infection (Figure 13a), compared to the IMC group which had no fluorescent signal (Figure 13b). This indicates that the anti-CD169 antibody persists on the surface of splenic macrophages for a minimum of 3 days post administration.

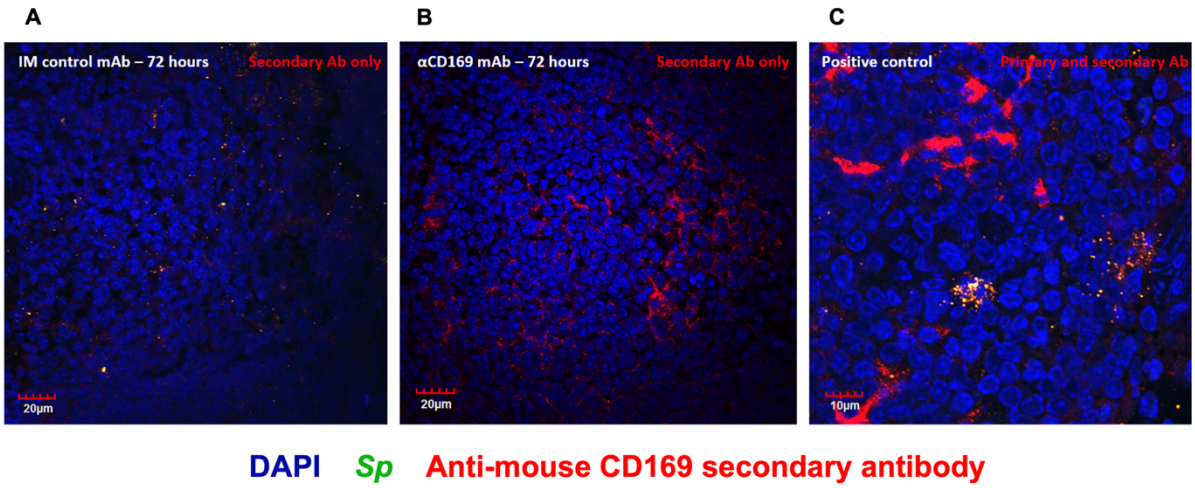

Figure 13 - *Longevity of anti-CD169 blocking antibody binding*. Spleens from mice either treated with anti-CD169 antibody or isotype matched control were frozen in OCT, sectioned, and immunostained. For the positive control sections the same immunostaining protocol as outlined in the methods was followed. For Isotype matched control and blocking antibody treated spleens, the immunostaining protocol was followed but only with incubation using the secondary antibody. Isotype matched control spleens are shown in (A), anti-CD169 antibody treated sections in (B), and the positive control in (C). The scale bar size is indicated in the bottom left of each figure.

3.2.6.2 **Neutrophil distribution in infected and un-infected mouse spleens**

Next I sought to determine why CD169+ macrophages specifically were the permissive cell responsible for invasive disease, despite the fact that both MMMs and RPM are permissive to replication. I hypothesised that due to their unique location adjacent to the marginal sinus – a region containing only 10-30% of total splenic blood at any one time [389] –there may be a less neutrophil chemotaxis, a major facet of the innate immune response [139, 235]. Spleens from both un-infected, 6 hours infected, and 8 hour infected mice were stained for neutrophils, and CD169 to de-lineate the marginal sinus and provide microarchitectural context. Figure 14a shows a marginal zone from an uninfected animal demonstrating that mice have a resident neutrophil population in the red pulp of the spleen and that inflammation is not a requirement for

the recruitment of neutrophils. A section from a 6h infected mouse (Figure 14b) indicates that a higher density of neutrophils are present in the red pulp, but that they are not chemotactically drawn to infectious foci in the marginal zone. At no point can neutrophils be seen co-localising with CD169+ cells, despite infection in these cell types (dashed white circle). Furthermore, I show quantitatively that the density of neutrophils in the spleen increases (Figure 14e), from a mean of 0.0005 neutrophils/μm at 6h post infection, to 0.001 neutrophils/μm at 8 hours post infection. This observation is consistent with the line of thought that neutrophils are actively recruited to the spleen from the circulation to combat infection. Most strikingly however, when analysing the number of neutrophils recruited to pneumococcal foci in either marginal zone (Figure 14c) or red pulp foci (Figure 14d), the distribution of neutrophils drastically changed. Foci of infection which formed in the red pulp were significantly more likely to be surrounded by neutrophils (Figure 14f), and indeed this recruitment increased over time. Foci of infection formed in the marginal zone however, were completely devoid of neutrophils, even at 8 hours post infection. This indicates that the inability of CD169+ macrophages to control pneumococcal infection, may stem from an inability to recruit neutrophils to the marginal zone to facilitate clearance.

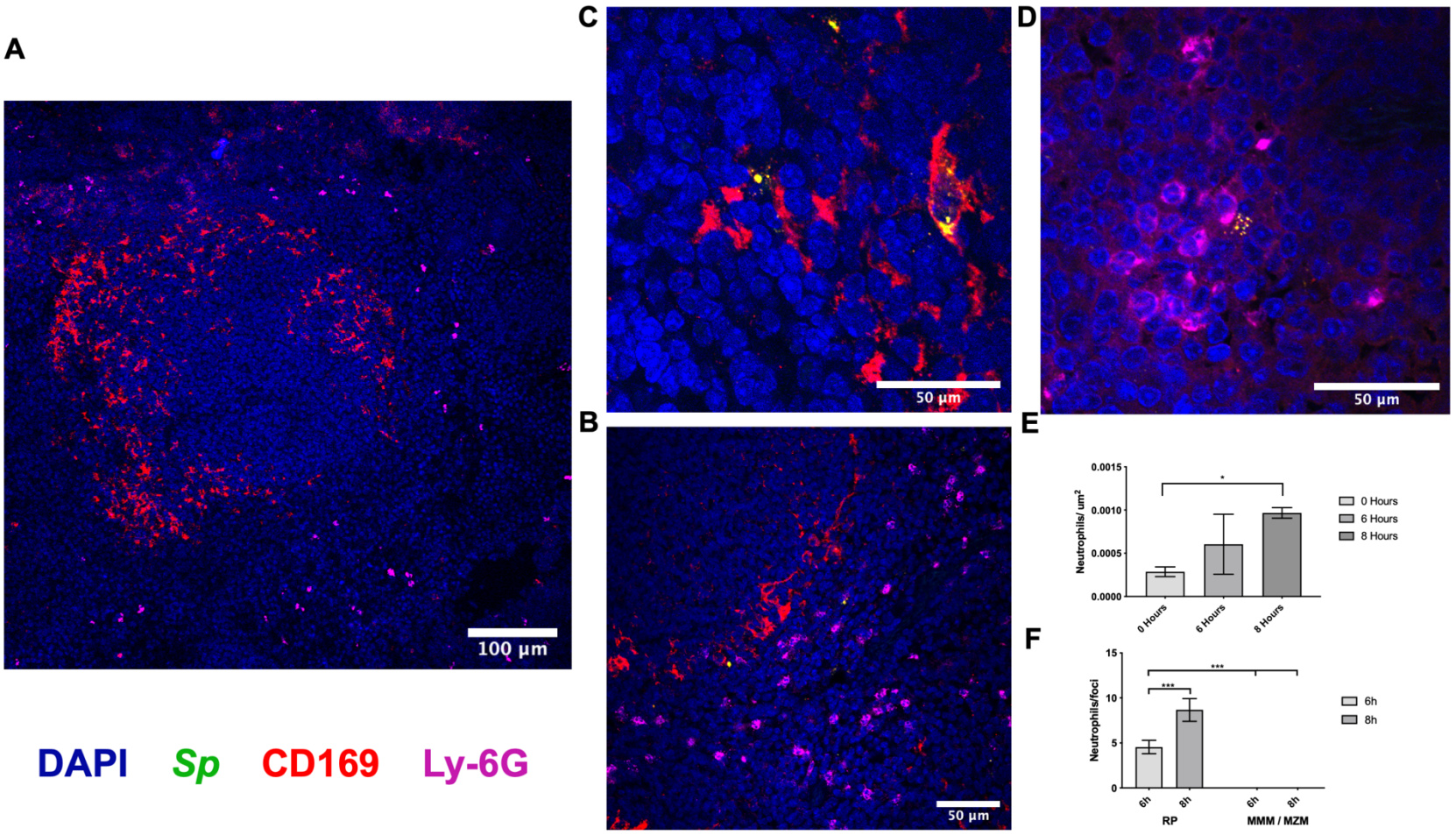
A
100 µm
DAPI Sp CD169 Ly-6G
C
50 µm
D
50 µm
B
50 µm
E
Neutrophils/ um²
0.0015
0.0010
0.0005
0.0000
*
0 Hours
6 Hours
8 Hours
F
Neutrophils/foci
15
10
5
0
***
***
6h
8h
RP
MMM / MZM

Figure 14 - *Dynamics of neutrophil influx to different compartments of the murine spleen.* (A) Spleen section from an uninfected mouse stained with antibodies against CD169, Ly-6G (neutrophils) and DAPI. The scale bar is 100 μm and shows an entire lymphoid follicle and surrounding sinus. (B) Immunostained tissue section from an 8h infected mouse, showing the intersection between the marginal zone and the splenic red pulp with a high density of nuclei. (C-D) exemplar foci of infection formed in a CD169+ and red pulp macrophage population respectively showing neutrophil chemotaxis in the latter but not the former. (E) quantification of neutrophil influx to the murine spleen after infection. 20 random fields of view form a 20x objective were analysed from multiple tissue sections stained with CD169 and neutrophils. The total neutrophil signal area were identified using Fiji. Statistical significance were determined using and ordinary 1 way ANOVA. *; P<0.05, ***; P<0.0005. (F) stratification of neutrophil influx by infected macrophage cell tyoe. Foci of infection were identified in CD169+, SIGN-R1+ and F4/80+ macrophages and the neutrophil signal area in the surrounding area (a circle with a 25 μm diameter) were analysed using Fiji. Statistical significance were determined using a 2-way ANOVA.

3.2.6.3 **Infections of Sialoadhesin-deficient mice**

Next, I aimed to determine if CD169 (the receptor) or merely metallophilic macrophages were the crucial factor defining permissive replication. This work was performed in collaboration with Professor Paul Crocker at the University of Dundee, who has established an sialoadhesin negative mouse strain [252]. Dr Sarah Thompson (University of Dundee) infected C57BL/6 and C57BL/6$^{(Sn\ -/-)}$ [252] mice with D39 (stocks were prepared by me in Leicester), and prepared frozen samples both for microscopy analysis and CFU enumeration, and sent the samples to Leicester for analysis to be performed by me. At 6h post-infection, both blood and spleen counts were indistinguishable between the WT and $Sn^{-/-}$ mice (Figure 15a). I analysed the size of foci in each macrophage compartment (Figure 15b) which indicated there was no difference in foci size between the same cells between WT and $Sn^{-/-}$ mice, however there were differences between macrophage compartments in both mouse strains. Finally, following processing of tissue sections for confocal microscopy, I counted the number of foci localising to each macrophage cell type. As these macrophage populations make up different proportions of the total tissue area; MMMs (~6%), MZMs (~4%), and RPM (~15%), I normalised the bacterial association data to the total volume of the spleen made up by each cell type [362]. This analysis revealed no difference between the distribution of bacteria in the spleens (Figure 15c), and indeed foci were readily observed in metallophilic macrophages (detected with the CR-F*c* reagent which binds sulfated glycans on MMMs) in both WT and $Sn^{-/-}$ mice (Figures

15d and e). This indicates that although CD169+ macrophages are heavily involved in disease, CD169 specifically may not be the major receptor for bacterial entry. Furthermore, this demonstrates that the effect observed following treatment of mice with the blocking antibody was likely mediated by steric effects.

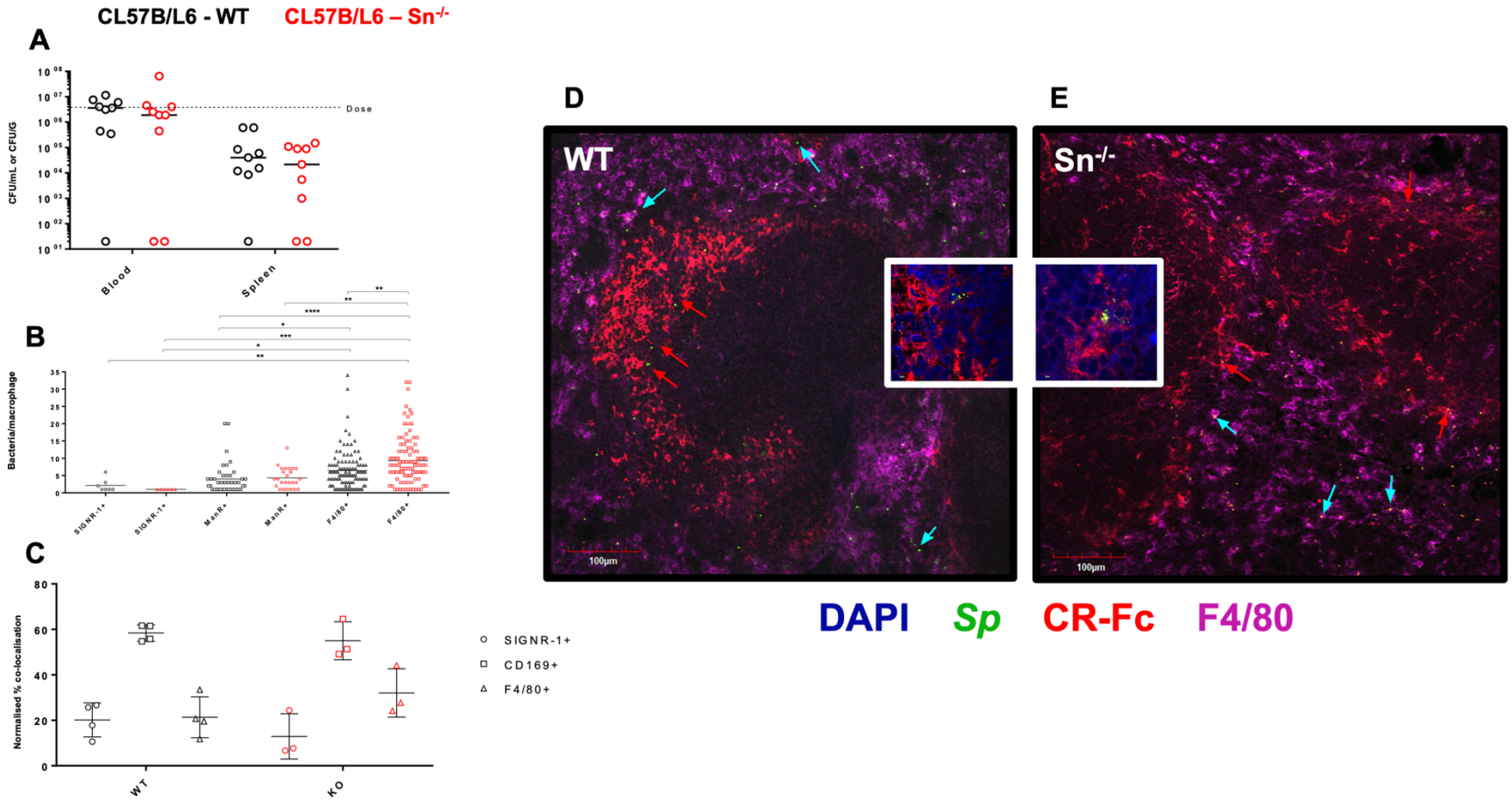
CL57B/L6 - WT
CL57B/L6 – Sn-/-
A
CFU/mL or CFU/G
Dose
Blood
Spleen
B
Bacteria/macrophage
SIGNR-1+
SIGNR-1+
MnrR+
MnrR+
F4/80+
F4/80+
C
Normalised % co-localisation
WT
KO
SIGNR-1+
CD169+
F4/80+
D
WT
100µm
E
Sn-/-
100µm
DAPI
Sp
CR-Fc
F4/80

Figure 15 - *Analysis of bacterial burden and splenic foci formation in C57BL/6 WT and $Sn^{-/-}$ mice.* Groups of 8-12 week old WT and $Sn^{-/-}$ mice in the C57BL/6 background were infected intravenously via the lateral tail vein with 10^6 CFU *S. pneumoniae* D39. At 6h post infection, mice were blood were taken by cardiac puncture under terminal anesthesia, and their spleens removed aseptically post mortem. Blood were serially diluted and plated for enumeration of CFU, whilst spleens were homogenized in BHI+10% glycerol before serially diluting and plating. Infections and sample collection were performed at the University of Dundee in collaboration with Professor Paul Crocker, but were processed and analysed in Leicester. (A) bacterial loads in the blood and spleens of WT and $Sn^{-/-}$ KO mice. Individual WT mice are indicated by black circles, whereas KO mice are indicated by red points. All differences between WT and $Sn^{-/-}$ mice were non-significant my 1-way ANOVA. (B) size of macrophage associated bacteria foci in WT and $Sn^{-/-}$ mice. 30 random fields of view from immunostained sections were imaged using a 60x objective on an Olympus confocal microscope. The number of bacteria/cell were counted by eye and were stratified by the three macrophage cell types MZM, MMMs, and RPM. Statistical analysis were performed using 1-way ANOVA. *; P<0.05, **; P<0.005, ***; P<0.0005, ****; P<0.00005. (C) Analysis of bacterial distribution across the three splenic macrophage subsets. The % co-localization of bacteria with different macrophages is shown, following normalization for the area taken up by that macrophage subset. Spleens from both WT (D) and $Sn^{-/-}$ (E) mouse spleens were immunostained to de-lineate marginal metalophillic macrophages (CR-Fc; red), nuclei (DAPI; blue), and bacterial type 2 capsule (green). Exemplar bacterial co-localization with MMMs are indicated by red arrows, whereas examples of co-localization of bacteria with RPM are indicated by blue arrows. In each image, insets show representative foci of infection in MMMs in each mouse strain. Scale bars are 100 μm.

3.2.7 The role of pneumococcal neuraminidase in splenic macrophage infection

CD169 is a sialic-acid binding lectin. Interactions with pathogenic bacteria – such as *Campylobacter jejuni* and *Haemophilus influenzae* [165, 166], with this receptor have been dependent on the presence of sialic acid within the bacteria's capsular polysaccharide or lipopolysaccharide. *S. pneumoniae* strains have no sialic acids on

their surface, however they do encode three sialidase/neuraminidase proteins with sialic acid binding domains [323]. I hypothesized that interaction of pneumococci with CD169 may be facilitated by the principal neuraminidase (NanA) – a known virulence factor and adhesin in pneumococcal colonization and infection (see section 3.1.2).

3.2.7.1 **Construction of *nanA* deletion mutants**

To determine the potential role of specific functional domains of NanA, I constructed clean targeted deletions of both the sialic acid binding, and catalytic domain of the protein, as well as a mutant defective in the whole *nanA* gene in both the D39 and the non-encapsulated D39 derivative DP1004. A generic neuraminidase structure containing these two domains is shown in Figure 16a. The methodology underpinning construction of the mutants is described in methods section 2.16. I then confirmed targeted deletion of the individual domains by Sanger sequencing. Figure 16b shows a nucleotide BLAST of the sequenced fragment of two of the mutants constructed in the non-encapsulated DP1004 background against the WT sequence. This indicates a large deletion in each strain which pertain to those encoding for the lectin-like and sialidase domains respectively. To confirm that the deletion of nucleotide sequence led to the effective translation of smaller NanA proteins, I performed Western blot analysis probing lysates from each strain grown in the sugar N-acetyl mannosamine which has been shown to induce expression of neuraminidase locus with an anti-NanA antisera [390]. Despite the unfortunately poor quality of Western blot, the *nanA* interruption mutant displayed no obvious bands (Figure 16c). A *nanB* mutant which was included as a control showed similar size bands to the WT lysate. Importantly, the deletion mutants showed bands of 100 and 70 Kilodaltons respectively which matched the predicted protein size deduced from the Sanger sequencing data.

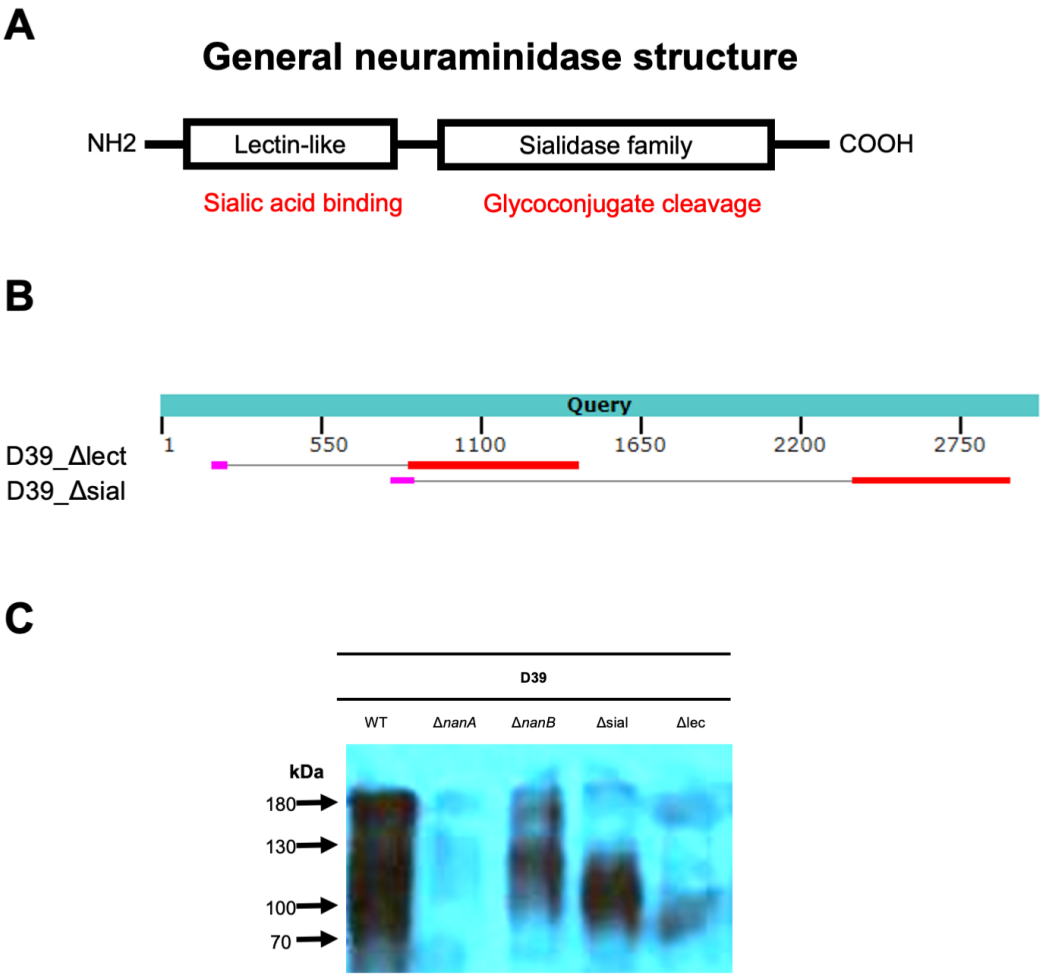

Figure 16 *- Construction of mutants in the neuraminidase nanA in encapsulated S. pneumoniae D39*. (A) General structure of pneumococcal neuraminisase, with an N-terminal lectin-like domain responsible for the binding of sialic acid, and a C-terminal sialidase family domain responsible for cleaving sialic acid from host N- and O-linked glycosides. (B) Deletion of each domain was performed as described in the methods section. Amplification of the *nanA* locus was performed with primers lying outside of both deletions, and was subject to Sanger sequencing. Nucleotide BLAST alignment of these sequences shows targeted deletion of sequences corresponding to the N terminal, and C terminal stretch of *nanA* respectively. (C) confirmation of full length and truncated NanA protein expression in WT strains and their respective mutants was performed by Western blot with NanA-specific anti-sera,. For all panels, identical sequencing and Western blot results were obtained for D39 and the unencapsulated derivative DP1004.

3.2.7.2 **Infection of mice with *nanA* mutants**

I then intravenously infected mice with WT D39, and three *nanA* mutants; one lacking the N-terminal lectin-like (sialic acid binding) domain, one lacking the C-terminal

sialidase domain, and one complete gene knock-out. Spleens from these mice were then analysed by confocal microscopy, and the relative proportions of bacteria associated with CD169+ macrophages were enumerated. Figure 17 demonstrates that in line with our hypothesis, deletion of the lectin domain significantly reduced association with CD169+ cells at 6h post infection, in comparison to the sialidase mutant which displayed comparable co-localisation to the WT. It should be noted that despite this reduction in association, no single mutant was completely unable to form foci in CD169 cells. Further work should include characterisation of the effect of *nanA* deletion on infection dynamics in the spleen over a relevant time course. Due to timing constraints, this was not performed for this thesis.

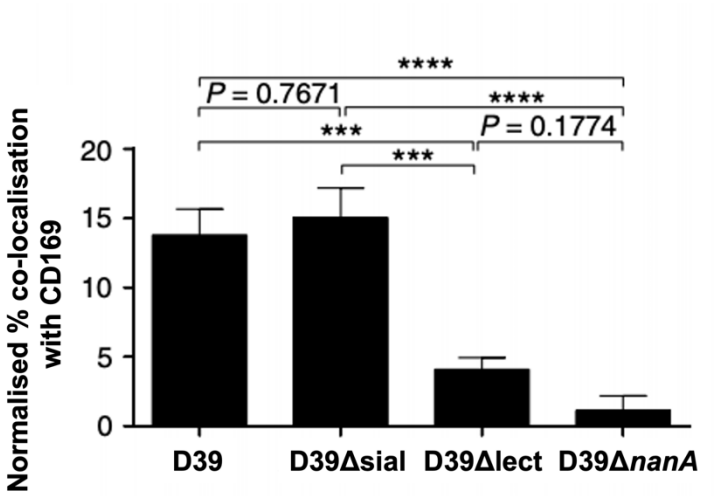

Figure 17 - *Co-localisation of nanA deletion mutants with CD169 in the spleen*. Spleens from at least 3 individual mice, infected with WT D39 and its 3 mutants, were stained for CD169 and the pneumococcal capsule. At least 30 fields of view were analysed for each samples. The % co-localisation of bacteria with CD169 is reported following normalization for the area of CD169 in each image. Statistical significance were determine by 1-way ANOVA. ***; P<0.0005, ****; P<0.00005.

3.2.7.3 Survival/growth of *nanA* mutants in whole blood, BHI broth, and CAT supplemented with either Glc or ManNAc

Previously, *nanA* deletion mutants were shown to be cleared more quickly from the blood following intravenous, and intranasal infection [329]. Furthermore, *nanA* mutants were also impaired in their ability to resist neutrophil attack [330]. I therefore aimed to determine if the inability of *nanA* mutants to establish infection in splenic tissue macrophages was due to a direct effect on spleen cells, or because of an impaired survival in blood leading to reduced bacterial uptake. Blood from CD1 mice was taken by cardiac puncture in tubes containing hirudin (an anti-coagulant with no effect on compliment activity). Blood samples were then inoculated with 10^5 CFU of DP1004 WT or *nanA* mutants, and serial dilutions were plated every 2 hours for 6 hours. Figure 18a shows that both the WT and all *nanA* mutants were capable of survival in blood and growth in *ex vivo* whole blood. This provides imperative to study the role of NanA in survival within the tissue, rather than in the blood. Control growth experiments in minimal media (CAT) supplemented with either glucose (Figure 18b) or N-Acetyl-Mannosamine (Figure 18c) and rich media (BHI; Figure 18d), demonstrated indistinguishable growth kinetics between the mutants and their WT counterparts.

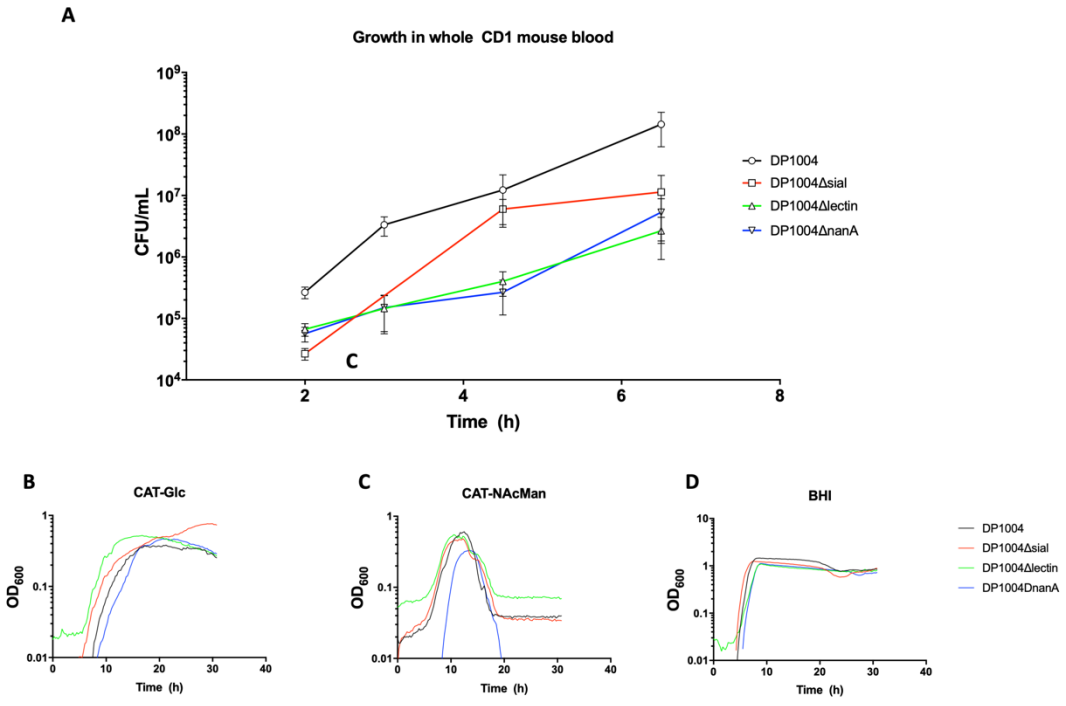

Figure 18 - *Survival and growth of DP1004 and its nanA deletion derivatives*. Growth curves in whole blood (A), BHI (B), CAT-ManNac (C), and CAT-glucose (D) were performed as described in section 2.3. Growth curves in blood were determined by quantitative bacterial culture, whilst those in media were determined by optical density. WT; black line, sialidase mutant; red line, lectin mutant; green line, *nanA* knock out; blue line. Error bars show the standard deviation of 3 independent biological replicates. Error bars are omitted from growth curves in media. For all panels, comparable results were obtained for D39 and the unencapsulated derivative DP1004.

3.2.7.4 **Adhesion of *nanA* mutants to J774a.1 macrophages *in vitro***

Next, I sought to determine if the mutant deficient in the lectin-like doman of NanA was reduced in co-localisation to CD169+ macrophages due to an inability to establish initial adherence to cells. I used the murine macrophage-like cell line J774.A for adhesion/invasion assays, with DP1004 and its lectin domain deficient mutant following growth in either minimal media containing N-Acetyl-Mannosamine (which upregulates neuraminidase expression; CAT-ManNAc) or glucose (which represses neuraminidase expression' CAT-Glc) [390]. The non-encapsulated derivative DP1004 was selected for phagocytosis assays because the capsule is known to reduce rates of phagocytosis, and I wanted to maximise potential interaction of pneumococci with host cells. WT pneumococci grown in CAT-ManNAc adhered significantly better to J774a.1 cells than its glucose grown counterparts (Figure 19a). The WT grown in CAT-ManNAc also adhered significantly better to J774a.1 cells than the lectin mutant grown in the same medium. Interestingly, growth of both the WT and the lectin mutant in CAT-Glc resulted in an equally low adherence to J774a.1 cells, demonstrating a correlation of ManNAc-induced gene expression with ability to adhere to macrophages. The same pattern between strains was observed when considering the intracellular organisms; CAT-ManNAc grown wild types invaded significantly better than the mutant, and this difference was abolished when strains were grown in glucose (Figure 19b). Finally, when determining the ratio of adherent to invasive bacteria, both the WT and the lectin mutant, grown in CAT-ManNAc, displayed significantly increased the proportion of intracellular bacteria (Figure 19c), indicating that whilst likely not entirely due to NanA, that transcriptional changes due to growth on different sugars may influence invasion of murine macrophages.

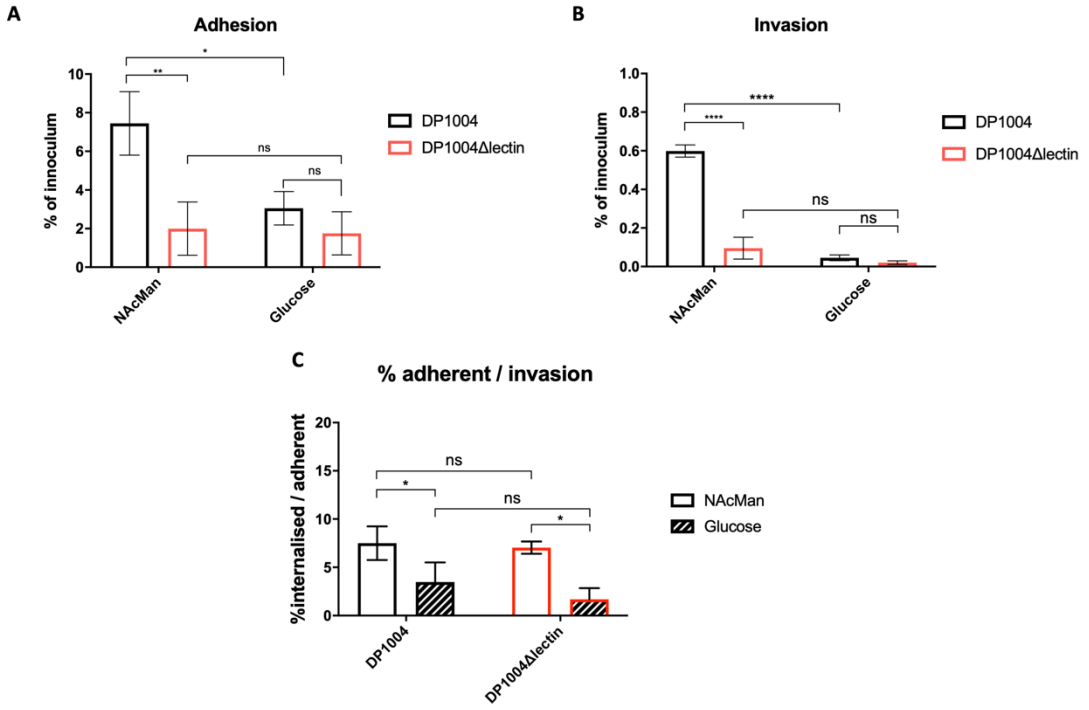

Figure 19 *- J774a.1 adhesion invasion assays using WT and NanA lectin-deficient pneumococci.* (A) adhesion of WT (black bar) and NanA lectin-deficient (red bar) pneumococci grown in either CAT-Glc or CAT-ManNac after 45 minutes of *in vitro* infection at an MOI of 10. (B) determination of intracellular bacterial loads after 30 minutes of gentamicin treatment. Colours and preparation of bacteria are the same as for panel A. (C) the number of intracellular organisms expressed as a percentage of the total adherent organisms. Non-filled bars show strains which were grown in CAT-ManNAc, whilst filled bars show those grown in CAT-Glc. All experiments were performed in biological triplicate. Error bars represent standard deviation. Statistical significance were analysed by 2-way ANOVA with Tukey's multiple comparison test.

3.2.8 **Establishment of a model of *ex vivo* human spleen perfusion**

3.2.8.1 **Model development and rationale**

As described in section 1.3.3, murine spleens differ considerable to human spleens in their tissue microarchitecture, and immune cell composition [157]. Pigs are emerging as a translational model for human disease due to the high similarity in their immune cell repertoires [391]. During this thesis, myself and members of the lab worked to develop a model of *ex vivo* porcine organ perfusion using organs sourced from the abattoir [392]. In this work, I was able to inoculate porcine spleens through the natural, intravenous infection route. I observed replication of pneumococcus in these tissues, in close analogy to what was observed in mice. During the course of

this thesis, our laboratory was granted permission to conduct a clinical trial (REC: 18/EM/0057) whereby spleens taken from patients undergoing elective splenectomy during distal pancreatomy could be used experimentally. Using these *ex vivo* organs I aimed to establish a normothermic model of perfusion mode for human organs comparable to that published by Chung and Wanford for porcine organs [392]. Briefly, fully intact organs were provided to us by the Hepatobiliary & Pancreatic surgery team at University Hospitals of Leicester General Hospital. Organs were retrieved using standard surgical procedures in line with the National Health Services (NHS) standard practise. *Ex vivo*, the splenic artery was immediately cannulated, and the organ was flushed with Soltran (Baxters) preservative solution. Organs were then transported to the lab on ice, and connected to a custom *ex vivo* normothermic perfusion circuit (see section 1.12) and perfused with the artificial perfusate Hemopure. The composition of Hemopure can be found in the materials and methods section 1.12. Images of the *ex vivo* perfusion circuit, in addition to exemplar images of human spleens being connected to the circuit are shown in Figure 20a. A diagrammatic representation of the components of the *ex vivo* perfusion circuit can be found in Figure 20b. We monitored the flow rate through the circuit following connection of human spleens, and observed physiological flow rate throughout the time course (Figure 20c). All work pertaining to the human spleen perfusion model was performed with the help of Dr David Carreno, Mr Ryan Hames, and Miss Zydrune Jasiunaite.

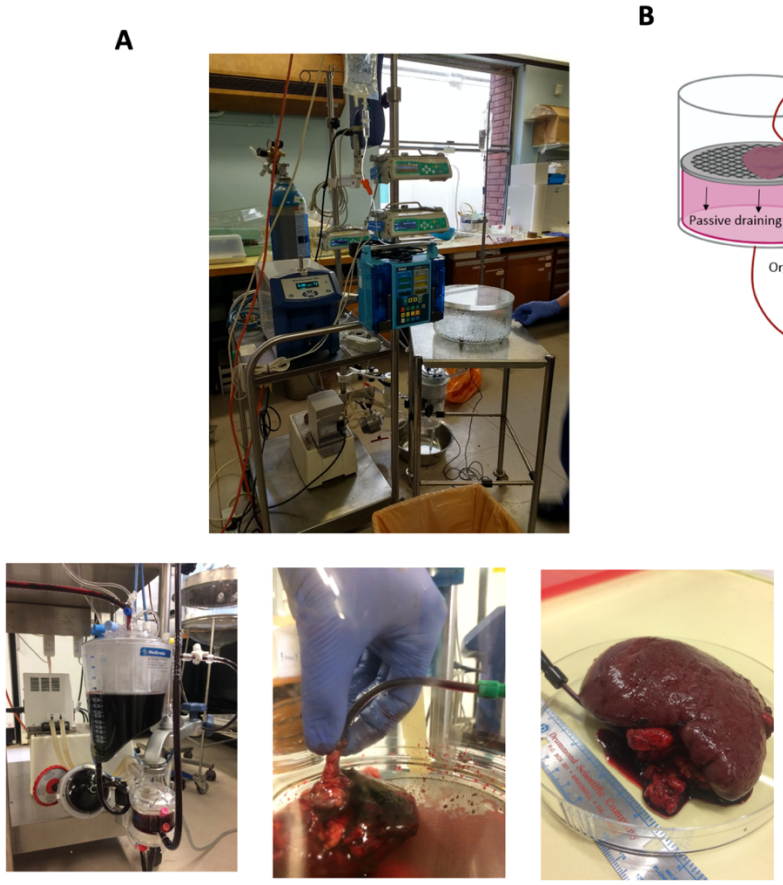
A
B
Splenic artery
Pressure monitor
Bacteria inlet
Oxygenator
O_2
Infusion Apparatus
Control console
Flow rate 0.4 L/min
Spleen pressure 80 mmHg
Passive draining of blood
Organ chamber
NaCl
NaCl + heparin
Pump
Water bath
Blood reservoir
C
Infection
Flow rate (L/min)
0.0
0.2
0.4
0.6
0
1
2
3
4
5
Time (h)

Figure 20 - *A normothermic perfusion model of infection in ex vivo human spleens*. (A) Images of a typical human spleen perfusion circuit, including the hemopure reservoir, cannulation of the splenic artery, and a representative image of a human spleen used for perfusion. (B) diagrammatic representation of the human spleen perfusion circuit. (C) flow rate (L/min) of hemopure through the *ex vivo* spleen perfusion circuit. Representative of 3 uninfected human spleens.

3.2.8.2 Blood gas parameters and maintenance of physiological histology during *ex vivo* perfusion

To confirm that organs remained physiologically active during *ex vivo* perfusion, I analysed blood gas parameters from samples of Hemopure taken throughout a time course using a Radiometer ABL90 series which is used clinically for the analysis of human blood. I observe that Hemopure pH remained static and physiologically relevant along the perfusion time course (Figure 21a). Blood concentration of Hemoglobin (ctHb) significantly decreased from ~130 g/L to ~100 g/L at 3h after infection (Figure 21d). The functional saturation of Hemoglobin by oxygen (FO2Hb) significantly decreased from 85% to 75% after 3h of perfusion (Figure 21g). Concentrations of the ions Na^+, Ca_2^+ and Cl^- remained static and physiologically relevant across the time course. (Figures 21 l, m and n) The methemoglobin saturation increased from t=0 to t=3h (Figure 21j), confirming previous difficulties with long term perfusion of the human spleen compared with other organs (Dennison lab, unpublished observations). All other blood gas parameters remained stable across the perfusion time course, indicating that physiological conditions can be maintained during *ex vivo* human spleen perfusion.

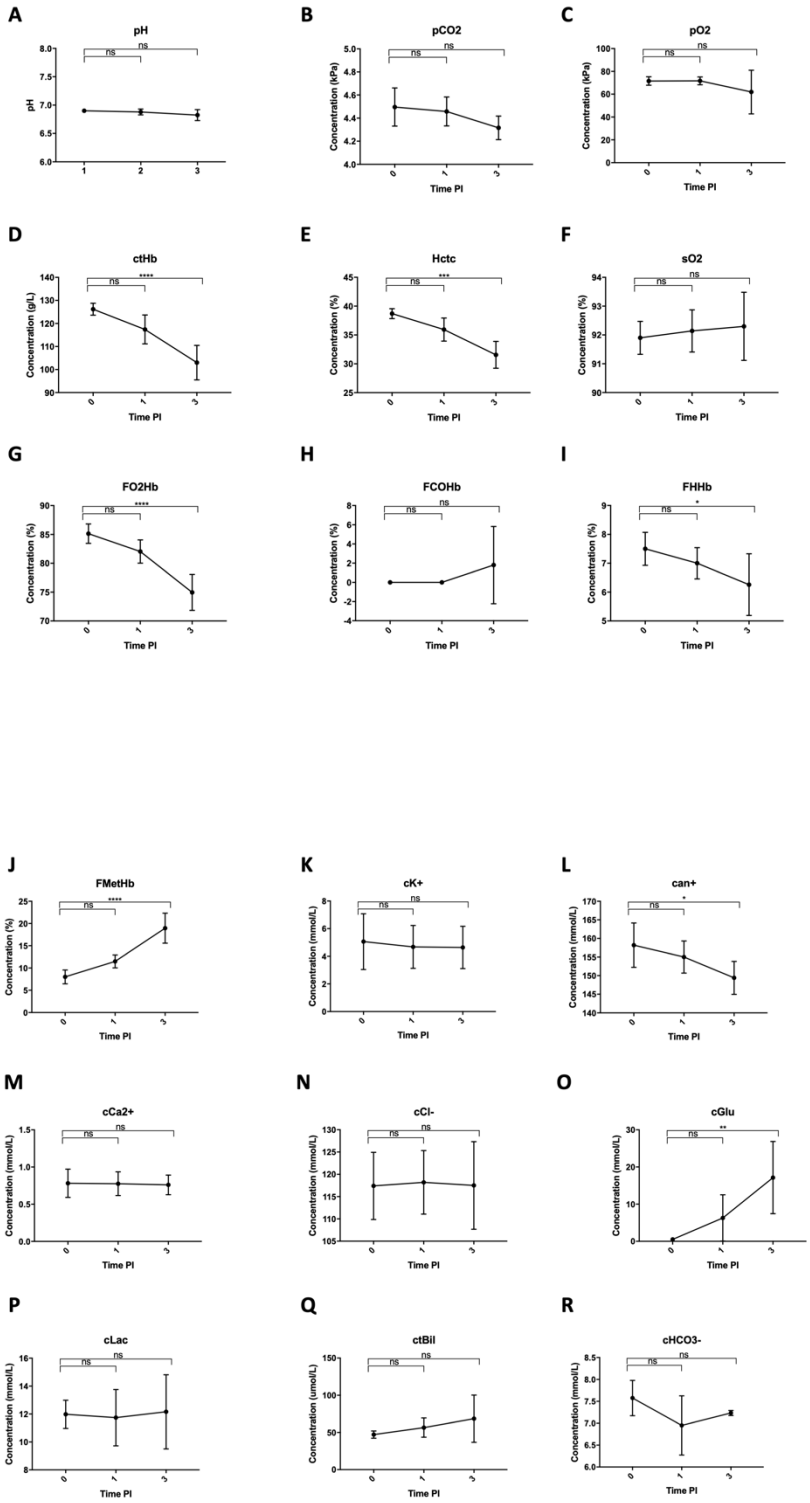

Figure 21 - *Blood gas analysis of hemopure following ex vivo perfusion of 3 uninfected human spleens*. Blood was taken and analysed with the *Radiometer ABL90 series* system in the ICU at the University of Leicester for pH (A), partial pressure of carbon dioxide (pCO2; B), partial pressure of oxygen (PO2; C), total

hemoglobin (ctHb; D), ration between erythrocytes and volume of blood (hctc: E), saturation of hemoglobin with oxygen (sO2; F), fractional oxyhemoglobin (FO2Hb; H), fractional carboxyhemoglobin (FCOHb; I), fractional deoxyhemoglobin (FHHB; G), methemaglobin concentration (FMetHb; J), potassium concentration (cK+; K), sodium concentration (cNa+; L), calcium concentration (cCa2+; M), chloride concentration (cCl-: N), glucose concentration (cGlu; O), lactate concentration (cLac; P), bilirubin concentration (ctBil; Q), bicarbonate concentration (cHCO3-; R). PI; post infection. Statistical comparison between 1, and 3h PI was compared to the time 0 value by 1-way ANOVA. *; P<0.05, NS; non-significant.

To determine if splenic tissue maintained healthy histological features during *ex vivo* perfusion, I performed haematoxylin and eosin staining of un-infected tissue before and after 5h of perfusion. Pre-perfusion, there was a clear distinction between lymphoid tissue and the splenic red pulp (Figure 22a). Higher magnification indicated central arterioles were intact and cells displayed healthy morphology (Figure 22b). At 5h post infection, an undistinguishable tissue microarchitecture was observed with no clear abrasions or necrotic lesions (Figure 22c), and at higher magnification cell morphology remained unchanged, and central vessels remained intact (Figure 22d). For evaluation of the H&E stains I received analytical training from Professor Kevin West (Histopathologist; University Hospitals Leicester).

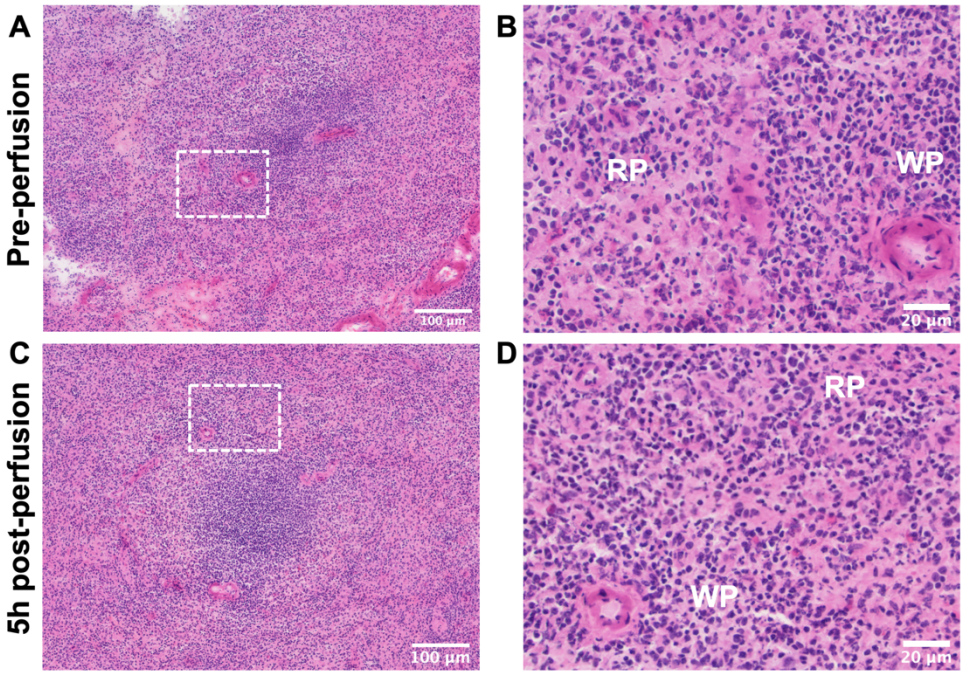

Figure 22 - *Hemotaxylin and eosin staining of human spleens before and after ex vivo perfusion.* Biopsies from human spleens before and after infection, were sectioned and subject to H&E staining. Samples were then imaged using the Vectra Polaris Digital Pathology System with a 40x objective. (A) Panel A shows an image of pre-perfusion spleen with a central follicular arteriole in the centre of the image. The scale bar is 100 μm. The dotted white line is the area shown in B. (B) higher magnification image of pre-perfusion spleen showing the border of the white and red pulp with a central arteriole visible on the right side of the image. The scale bare is 20 μm. (C) Panel C shows the red and while pulp of an H&E stain from a 5h perfused spleens sample, with a 100 μm scale bar. The dotted while line displays the area shown in D. (D) shows the border of the red and white pulp post perfusion, with a 20 μm scale bar.

3.2.8.3 **Optimisation of bacterial growth in hemopure**

To determine the utility of the human spleen perfusion model to study pneumococcal pathogenesis, I determined the survival and growth kinetics of a set of diverse pneumococcal strains in Hemopure supplemented with different combinations of cell culture medium (Figure 23). The conditions tested were neat Hemopure (HP) supplemented with 0.2% glucose (black lines; listed only as Hemopure on the graph), HP + 10% RPMI (yellow lines), HP supplemented with 20% RPMI (brown line), HP + 10% DMEM-F12 cell culture medium (light blue line), HP + 20% DMEM-F12 (dark blue), and BHI as a positive control for growth. The data indicate that all strains were either defective in growth, or reduced in CFU in Hemopure + 0.2% glucose alone. Supplementation with 10% RPMI resulted in bacteria replication but to a lesser extend than both HP + 20% RPMI, HP + 10% DMEM-F12, and HP + 20% DMEM-F12 which resulted in replication times comparable to that of *ex vivo* blood. These data indicate that *ex vivo* perfusion experiments using *S. pneumoniae* as the model organisms should be conducted using Hemopure supplemented with at least 20% cell culture medium.

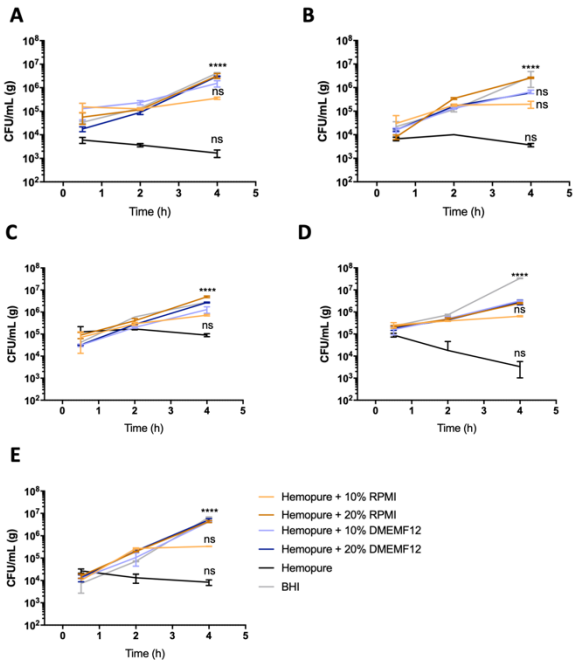

Figure 23 - *Optimisation of pneumococcal growth in the artificial perfusate hemopure*. Approximately 10^6 CFU of pneumococcal strains BHN418 (A; serotype 6B), LgST215 (B; serotype 19F), SP14-BS69 (C; serotype 14), TIGR4 (D; serotype 4), and D39 (E; serotype 2) were inoculated into BHI (grey colored line), hemopure (black colored line), hemopure supplemented with 10% RPMI, (light orange colored line), hemopure + 20% RPMI (dark orange colored line), hemopure + 10% DMEMF12 light blue colored line), and hemopure + 20% DMEMF12 (dark blue colored line) and samples were taken for enumeration of CFU on blood agar plates at 30 minutes, 2h, and 4h post inoculation. Analysis of bacterial grown in supplemented hemopure was performed by myself, Dr David Carreno, and Mr Ryan Hames.

To determine if Hemopure was a suitable candidate perfusion medium for experiments with other bacterial pathogens, I also determined the growth kinetics of *K. pneumoniae* and *L. monocytogenes* in neat Hemopure. Both representative strain for *K. pneumoniae* (ATCC 700 603) and *L. monocytogenes* (CC4 - 0360) were capable of replication in Hemopure with both strains increasing in CFU ten fold over a 4h time period (Figure 24). This indicates the human spleen perfusion model is translatable to studies of other bacterial pathogens.

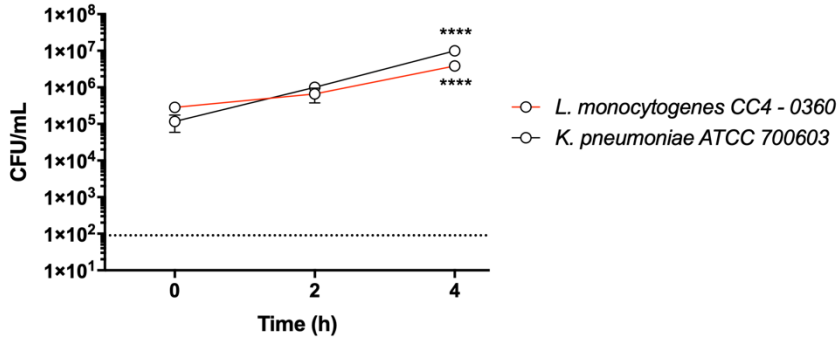

Figure 24 *- Growth of K. pneumoniae and L. monocytogenes in hemopure*. Approximately 10^5/mL CFU of *K. pneumoniae* strain ATCC 700603 (black line), and *L. monocytogenes* strain CC4-0360 (red line) were inoculated into 10 mL hemopure and incubated for 4h at 37 °C with 5% CO_2. Samples were serially diluted and plated on LA plates at 0h, 2h, and 4h post inoculation. Statistical analysis of growth were performed by 2-way ANOVA. ****; P<0.00005.

3.2.8.4 ***Ex vivo*** **perfused spleens possess pneumococcal clearance capacity**

To determine if *ex vivo* perfused human spleens possessed capacity for clearance of *S. pneumoniae* as they do *in vivo*, I analysed the number of colonies recovered from Hemopure and tissue biopsies following infection of the circuit with the serotype 4 pneumococci TIGR4. This experiment was performed using supplementation of hemopure with 10% DMEM, conditions which favour pneumococcal growth rates comparable to that in blood. The data indicate that bacteria were entirely cleared from the circulation by 2h post infection (Figure 25a; blue line). Instead, in the spleen bacterial counts initially reduced, but persisted in the tissue until the experimental end point beyond organisms in the perfusate (Figure 25a; red line). Expression of these data as a percentage of the input inoculum (Figure 25b) indicate that already by 30 minutes post infection, the spleen is able to filter and kill ~80% of invading bacteria, as the sum of total organisms in both the whole spleen is less than 20% of the input.

Further, whilst uptake of organisms from the circuit is efficient, the dynamics of killing of organisms whilst in the tissue is appears to change with time. Between 30 minutes, and 2h post infection bacteria are killed at a far greater rate than between 2 and 4h post infection providing imperative to study pneumococcal interactions with macrophages in this system at the single cell level. These data demonstrate that *ex vivo* perfused human spleens maintain clearance capacity, validating their use in the study of blood filtration of pathogens.

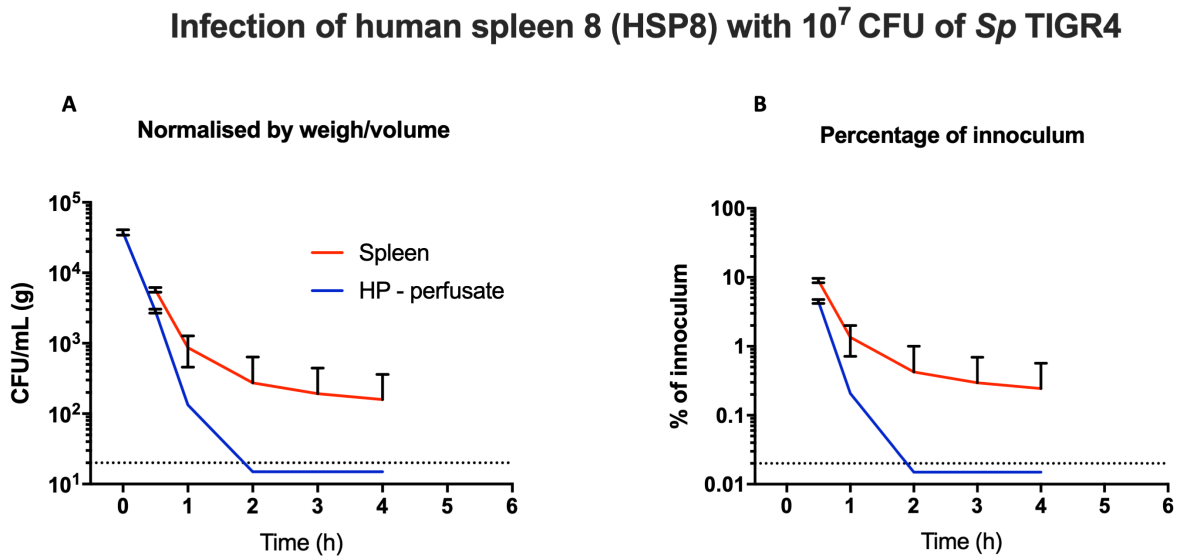

Figure 25 - *Clearance capacity of ex vivo perfused human spleens*. (A) Following infection of either the circuit, or *in vitro* Hemopure supplemented with 10% DMEM to a starting concentrations of ~10^5 CFU/mL, samples of Hemopure, tissue, and in vitro Hemopure were taken at pre-determined time points for enumeration of CFU. The limit of detection is shown by the dotted line. Spleen counts are shown by a red line, Hemopure used for perfusion by the blue line, and *in vitro* Hemopure by a black line. (B) shows the CFU recovered from splenic biopsies and hemopure as a percentage of the total 10^7 CFU inoculum which was injected into the 500 mL of hemopure circuit.

3.2.8.5 Human splenic macrophages co-localise with pneumococcus after *ex vivo* infection

Studies of the *ex vivo* human spleen perfusion model are ongoing in our lab. Here I describe some preliminary observations following microscopy analysis of human spleens 5h post *ex vivo* infection with D39. Staining of human spleen sections with an

antibody against CD206 indicated clear labelling of sinusoidal endothelial cells in the spleen (Figure 26ai, individual channels of zoomed composite image shown in ii-v). Some co-localisation of pneumococci with this marker was observed (red arrows), consistent with the known role of CD206 in binding of pneumococcal capsule. Staining with a polyclonal antisera raised against human CD169 showed clear localisation of these cells to peri-arteriolar lymphoid sheathes directly adjacent to lymphoid follicles (Figure 26bi) consistent with what has been previously reported [160]. Figures 26bii-v show clear co-localisation of pneumococci with CD169+ macrophages, eluding to their capacity for phagocytosis of pneumococci in this *ex vivo* model. Lastly, staining of red pulp macrophages with an antibody targeted against CD163 indicated their distribution across the splenic red pulp, outside of the lymphoid follicles (Figure 26c). Again for this cell type, co-localisation with pneumococci was observed indicating functional activity of macrophages in the *ex vivo* model. Quantitative analysis of bacterial co-localisation with macrophage populations, and the propensity for within cell replication are ongoing.

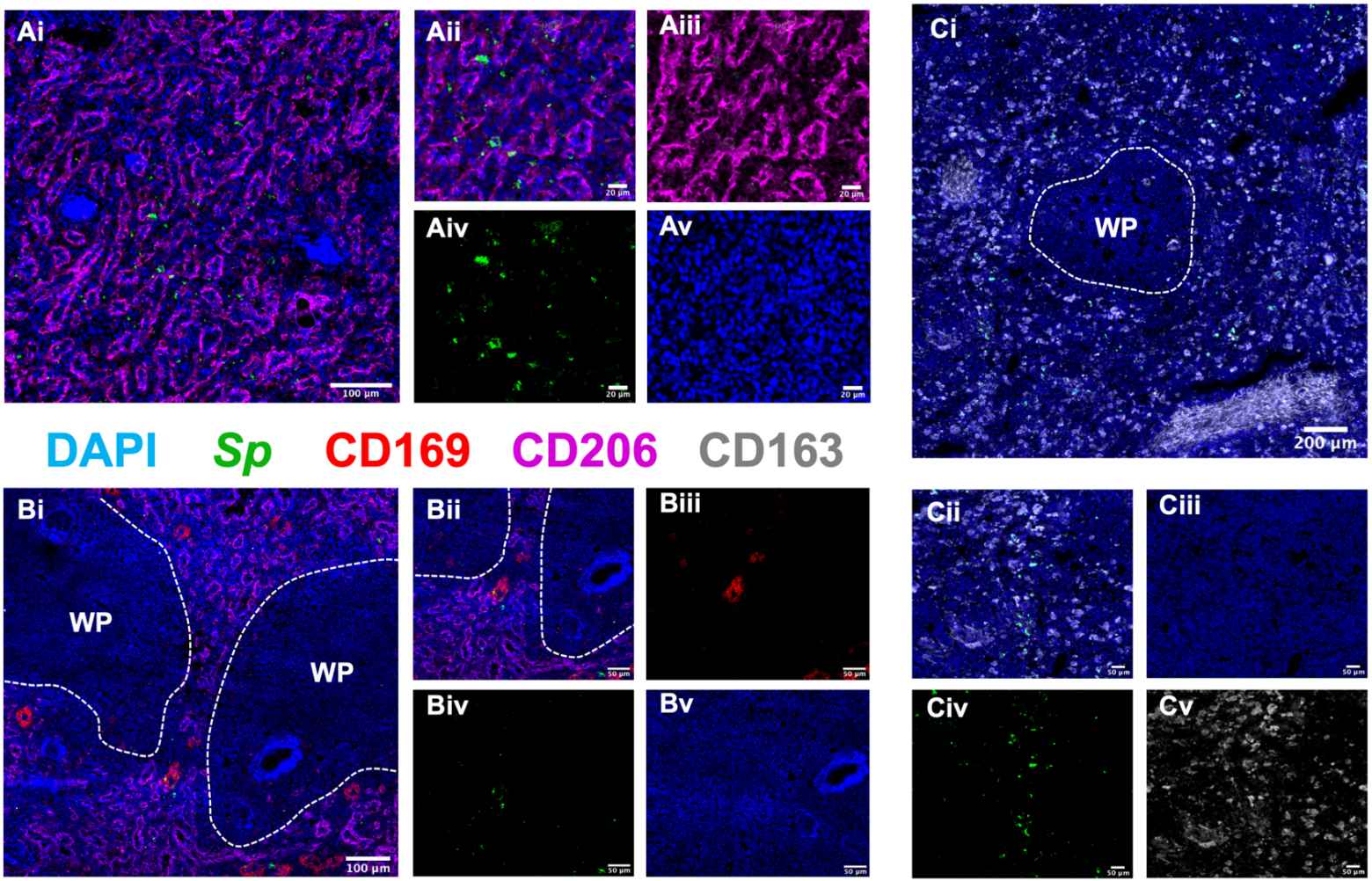
Ai
Aii
Aiii
Aiv
Av
Ci
WP
200 µm
DAPI
Sp
CD169
CD206
CD163
Bi
WP
WP
100 µm
Bii
Biii
Biv
Bv
Cii
Ciii
Civ
Cv

Figure 26 *- Representative co-localisation images of pneumococci with human macrophages.* Sections of human spleen at the experimental end point where prepared, and stained with antibodies/reagents raised against CD206 (A; magenta), CD169 (B; red), CD163 (C; grey), pneumococcal capsule (all panels; green) and nuclei (blue). Samples were images using the Vectra Polaris slide scanner, and analysed in Fiji. Scale bar sizes are indicated in the figure. Areas of splenic white pulp are outlined with a dotted white line. Individual channels of the composite image are shown.

3.3 Discussion of Chapter

3.3.1 Hiding from the host: population bottlenecks and within macrophage replication as an immune evasion strategy

In this chapter, I have described the critical role of macrophages in the imposition of a population bottleneck during systemic *S. pneumoniae* infection. Infection bottlenecks have been described for a number of bacterial pathogens (see section 1.6) [225, 227, 229, 235]. A key theme in our study and those before us are that the host is efficient in clearing the initial challenge, but is ill prepared for clearance of the re-emerging secondary infection. I propose that persistence within macrophages of a minority of bacteria during clearance from the blood may function to hide from host innate immune effectors, whilst the majority of cleared bacteria deplete these different effector systems. Cytokines are immunoregulatory molecules with critical roles in the response to infection, with one of these myriad functions being enhancing the microbiocidal potential of macrophages [118, 393]. My data indicates that for strain D39 (serotype 2) and the mouse strain CD1, a microbial bottleneck is associated with a reduced production of a number of cytokines from 6h to 24h post infection. The imposition of a bottleneck during experimental infection in mice is often serotype specific, and dependent on the line of mouse used [235, 394]. This reduction in cytokine production is not observed following infection of the C57BL/6 mouse line with D39 [395], a strain combination in which no bottleneck is observed. It is tempting to speculate that the initial clearance of blood in the former model leads to a dampened cytokine response that is advantageous for bacterial outgrowth later during infection. Indeed, typically intracellular pathogens such as *Salmonella* are known to inhibit cytokine production by inhibiting intracellular bacterial processing, and promoting the non-inflammatory apoptosis pathway [396, 397]. This may represent a hitherto unrecognised mechanisms of immune evasion for the pneumococcus, in that replication within macrophages is not only an immune protected niche, but also promotes a hospitable inflammatory environment for later proliferation. Two other potential mechanisms for

evasion of immune responses following re-emergence of bacteria in the blood are (1) the depletion of complement (2) or the exhaustion of macrophage killing capacity during primary challenge. Jubrail *et al.* [80, 398] previously demonstrated that following challenge with *S. pneumoniae* and *S. aureus*, that tissue macrophages only having a finite killing capacity, and that complete elimination of bacteria required additional killing mechanisms such as the induction of apoptosis [77, 78]. Furthermore, Boldock *et al.* [399] demonstrated that co-administration of a commensal, non-virulent organism with *S. aureus* in mice, dramatically reduces the LD_{50} of the virulent *S. aureus* strain, which was dependent in their model on macrophages in the liver. Extrapolating these observations to our model, we could speculate that initial challenge prior to the bottleneck exhausts splenic macrophage killing capacity, diminishing their capacity to deal with secondary challenge following bacteria re-emergence. Lastly, in a similar scenario, high dose infection has been shown to deplete serum complement components [400, 401]; Oggioni, Unpublished data). It could be the case that initial challenge depletes the host of complement such that their levels are low enough to impair secondary clearance following bacterial re-emergence.

3.3.2 **How reflective is the intravenous model?**

The most common route of systemic pneumococcal infection in humans is translocation from the lungs during pneumonia [269]. In this case, pneumococci must overcome immune barriers in the form of clearance by alveolar macrophages, and the barrier functions imposed by lung epithelial cells to continually seed the blood [402]. The work in this thesis utilised the intravenous infection model, in which the lung is directly bypassed, in lieu of bacteria being delivered directly into the systemic circulation at high numbers. I selected the intravenous model as it allows for details examination of the fate of organisms at the exact point of translocation to the blood. In the case of the pneumococcal mouse pneumonia model [329], mice consistently develop bacteraemia, but the time at which this occurs following challenge is variable between mice by as much as 12-24h, making it difficult to study the fate of organisms immediately following translocation to the blood. Unpublished data from our lab indicate that following intranasal infection of mice, bacteria can be detected in the splenic macrophages of some mice as early as 24h after challenge. Further work will

be required to determine the role of the spleen as a 'bacterial safe haven' prior to bacteraemia following pneumonia.

3.3.3 **Discussion of tissue macrophage susceptibility to infection**

My data demonstrate that whilst all splenic macrophage populations can undergo phagocytosis of pneumococcus, a distinct dichotomy exists in their ability to control infection with MMMs and RPM being permissive to replication, but SIGN-R1 macrophages not.

I have demonstrated that RPM are permissive to pneumococcal infection. The position of RPM in the sinusoidal open circulation of the spleen positions them for filtration of blood, including the removal of erythrocytes [159, 174]. Less attention has been paid to the role of RPM in the clearance of infectious agents. RPM are known to play a role in the clearance of *Plasmodium falciparum* from the blood stream, a phenomena attributed to their tropism for red blood cells [403]. In the case of bacterial pathogens, they appear to be less well adapted, likely in part due to their reduced expression of specific pattern recognition receptors when compared to marginal zone macrophages [155, 404]. Denniset *et al* [156] demonstrated that depletion of MZM, and MMMs but not RPM using different concentrations of clodronate liposomes decreased survival times of mice infected with *Sp* indicating a minor capacity for RPM in bacterial clearance. Our CD169 blocking experiment indicates that despite the inefficient killing of *Sp* by RPM, that foci in the red pulp do not give rise to bacteraemia. I observe that a key difference in the tissue context between MMMs and RPMs is the recruitment of neutrophils, in that the former does not demonstrate an observable chemotaxis of these cells but the latter does. In agreement with our observations, Denniset *et al.* [156] also demonstrated chemotaxis to the splenic red pulp. Contrary to what I report however, they show that rather than pneumococcus being intracellular, that neutrophils pluck bacteria from the surface of red pulp macrophages. Replication within macrophages in the red pulp appears to be stochastic – not all infection events result in foci. It may be that in cases where bacteria are effectively killed, they remain extracellular as described by Denniset, but not in the case of the foci I see which arise by intracellular replication. Macrophages are known to produce chemokines for neutrophils [79], and indeed my data show an increase in neutrophil chemokines during infection. In particular, whilst not experimentally demonstrated in this thesis,

pneumococci are known to activate the NLRP3 inflammasome in some lung macrophage subsets which results in IL-1ß production [83, 85]. This has not been experimentally demonstrated in the spleen. IL-1ß is chemotactic for neutrophils [405], it would therefore be tempting to speculate that pneumococci do not activate CD169+ macrophage inflammasomes. We cannot also discount that neutrophils have a physical barrier to CD169+ foci in the marginal zone. Difficulty in culture of primary metalophilic macrophages currently hampers the study of chemokine production by these cells in response to infection. Future work may involve pharmacological inhibition of NLRP3 in mice, followed by spatiotemporal analysis of neutrophil recruitment in the spleen.

Lanoue *et al.* reported that SIGN-R1+ MZMs were critical to the control of invasive pneumococcal infection, as KO mice had significantly shorter survival times than WT mice following infection [154]. Further work demonstrated a precise role for the SIGN-R1 receptor-mediated phagocytosis of pneumococcus [170]. An additional role for SIGN-R1 in pneumococcal clearance was described by Kang *et al.* , who demonstrated that its role in initiating complement deposition to the bacterial cell surface [172]. Together these data demonstrate MZMs are specially adapted for interaction with, and clearance of the pneumococcus. Non-specifically, Delamarre *et al.* (2005) demonstrated that MZMs have high lysosomal activity hinting at their propensity to be highly microbiocidal [171]. Kang *et al* described that sequence variation in SIGN-R1 between mouse strains determined specificity for pneumococcal capsule and outcome of infection [170, 172]. This may explain our observations that CD1 and C57BL/6 mice differ in their ability to impose a bottleneck during D39 infection. Interestingly, investigations of aged and young mice indicate a loss of MZMs and an accumulation of fibroblasts in the splenic marginal zone, which correlates with the heightened susceptibility to infection in the elderly [406]. My data together with those described above demonstrate the key role for MZMs in imposition of the splenic bottleneck during infection.

Prior to this thesis, the role of CD169+ macrophages in pneumococcal infection was unclear. Studies of other typically extracellular pathogens such as *Campylobacter jejuni* [407], and *Neisseria meningitidis* [166] have demonstrated their uptake by CD169+ macrophages mediated by surface sialic acid, but no studies have analysed

bacterial fate within these cells. Previous work, and their localisation close to B cell follicles indicate that a predominant role for CD169+ macrophages is in antigen presentation rather than microbicide [152, 167, 252], indeed they have been shown to have low lysosomal activity [169]. My data demonstrating that treatment with an anti-CD169 blocking antibody abolishes disease demonstrates the key role for this cell type in providing the replicative niche that eventually seeds bacteraemia. Our data are in contrast with that of Perez et al. [408] who demonstrated that following *Listeria monocytogenes* infection, CD169+ macrophages effectively control infection, and coordinate immune cell re-distribution to resolve infection. Infection of a MMM depleted mouse strain (DTR in the CD169 reading frame + administration of toxin) [409] revealed that these mice had higher bacterial counts than their WT counterparts. It is unclear whether this is due to targeted depletion of CD169+ cells, or off target depletion of SIGN-R1+ cells via known leaky expression of the DTR promoter. Our antibody blocking data suggest that for pneumococci, these cells instead of regulating innate immunity to infection, are actually a privileged site for bacterial replication. A question that remains is: what interaction of pneumococci with these cells mediates permissiveness. To decipher these susceptibilities, technologies such as flow cytometry would need to be developed to enable RNA sequencing of different cell tissue populations infected with pneumococcus to identify pathways differentially regulated in resolved, vs non-resolved infections. Flow cytometric analysis of CD169+ splenic macrophages was attempted by our group, but proved unsuccessful, as MMMs are but a fraction of the total macrophage cell population. Studies of PRSS have indicated that engagement of CD169 by the virus dampens type 1 interferon responses [386] – a key pathway for clearance of intracellular pathogens. It is tempted to speculate that this is a mechanism for the permissive nature of MMMs, but interactions of pneumococci which remodel spleen macrophage biology have yet to be reported.

3.3.4 Host factors in internalisation of pneumococcus: phagocytosis or cell invasion?

The neuraminidase NanA is a known virulence factor in experimental pneumococcal infection [329]. NanA has catalytic specificity for a wide array of sialic acid linkages, and is likely to mediate interaction with of a number of different host cells during infection making assignment of phenotypes to this protein in virulence *in vivo* difficult

[310, 330, 331]. Despite the lack of availability of primary MMM cultures, my data demonstrate a role for NanA in infection of MMMs *in vivo*, particularly its lectin-like domain. In close analogy, Uchiyama *et al.* [331] demonstrated that the lectin-like domain, but not the sialidase domain mediated interaction of pneumococci with brain endothelial cells. Both ours and their data demonstrate that NanA functions as a pneumococcal adhesin in the absence of catalytic activity. I hypothesise that NanA functions as an adhesin for CD169 macrophages, and that in its absence, the lack of adhesion to this permissive cell type is outweighed by the affinity of SIGN-R1+ macrophages to pneumococci which facilitate clearance.

Whilst not investigated in this thesis, the pore forming toxin pneumolysin may be a candidate factor mediating survival with macrophages. The homologous toxin Listeriolysin form *L. moncytogenes* mediates escape from intracellular vacuoles, and facilitates survival [410]. Pneumolysin production may be afforded in macrophages if rapid oxidative burst does not immediately kill pneumococci. Further investigation of this phenomena would require a model of MMM culture. Subramanian *et al.* [181] demonstrated that pneumolysin binding to alveolar macrophage mannose receptor mediated delivery of pneumococci to a non-lysosomal compartment which mediated their survival. Mannose receptor is also expressed on RPM in mice [411], and binding of pneumoylsin in this context may facilitate the survival within this cell type observed in my work.

3.4 **Future work**

3.4.1.1 **The need to establish a model of metalophilic macrophage culture**

Throughout the course of this thesis, myself and colleagues attempted the primary culture of CD169+ macrophages derived from murine and human spleen. This proved problematic because of the relative proportion of the cell type in the spleen – they are a minority population. Further, FACS based enrichment of these cell types was not achieved, and has not been achieved to my knowledge in any other group. A key follow on from this thesis, should be the identification of the specific pathways involved in the resistance of pneumococci to killing by specific macrophage cell types. It would be fascinating to know whether or not specific bacterial factors and responsible for intracellular replication within tissue macrophages, or whether there is a mechanistic basis for the inability of these cells to kill bacteria. Further, as I have demonstrated a

difference in neutrophil influx across the spleen, it would be interesting to see if there are specific cytokine responses of CD169+ cells to infection which determine the resolution of infection – particularly with respect to the NLRP3 inflammasome which has a known role in neutrophilic inflammation.

3.4.1.2 Host directed therapeutics and optimised antibiotic therapy for transient intracellular pathogens

Development of therapeutics for bacterial infection should be tailored to specific mechanisms of pathogenesis. At present, the standard treatment regimen for pneumococcal infection is a beta-lactam, in particular low severity community acquired pneumonia, – which are well known to have inefficient penetration within host cells including macrophages. The identification of an intracellular reservoir of pneumococcus in the spleen warrants the consideration of the use of antibiotics which penetrate macrophages effectively. Macrolides in particular are know to penetrate 30-100 times within macrophages. Macrolides are already in use for moderate and high severity pneumonia cases and may benefit from their introduction also to low severity pneumonia to prevent disease progression. Further, the identification of a monoclonal antibody in this thesis which protects mice from disease warrants the investigation of potential for use of host directed therapeutics, particularly those which prevent interaction of bacteria with permissive cells in the host.

Chapter 4

Within-Macrophage Persistence During *K. pneumoniae* Pathogenesis

4 **Chapter 4:** Within Macrophage Persistence During *K. pneumoniae* Pathogenesis

4.1 **Introduction to Chapter**

Klebsiella pneumoniae (*Kp*) are a species of Gram-negative rod shaped bacteria of the family *Enterobacteriaceae* – a group which also includes the *Salmonella*, *Yersinia*, and *Escherichia* genera. *K. pneumoniae* can be found as part of the normal human microflora in the skin [412], and gastric tract [413], and are also capable of persistence in the environment [414]. Indeed, soil-borne *K. pneumoniae* have an important environmental role in nitrogen fixation [415]. *K. pneumoniae* are also important nosocomial pathogens, capable of causing infections such as pneumonia, and urinary tract infections, in addition to serious systemic infections such as bacteraemia and meningitis [416, 417]. *K. pneumoniae* are not only human restricted and are also causes of disease in other animals such as pigs [418, 419]. For *Kp* there are two major routes of infection. Bacteria can either translocate across the respiratory epithelium in the lung into the blood stream where they are free to infect sterile sites following a pulmonary infection [420]. On the other hand, *Kp* are readily found in the human gut, and from this infection focus, they can cross the gastric epithelium into the circulation where they can disseminate to the liver and spleen [421]. In particular, there are two major clinical problems associated with *K. pneumoniae* caused by two distinct sets of strains which will be discussed in detail below.

4.1.1 **HV *K. pneumoniae* (hv*Kp*)**

Hypervirulent *K. pneumoniae* are a group of strains which have a unique clinical presentation compared to other *K. pneumoniae* infections [422]. HV*Kp* – unlike other *Kp* – cause infections in otherwise healthy, immunocompetent individuals [423]. They are unique in that infection presents with the formation of splenic and hepatic tissue abscesses that are very difficult to treat both surgically and chemotherapeutically, and are frequently associated with metastasis [416, 424]. Tissue abscesses due to HV*Kp* were first reported in Taiwan in 1998 [425], but they have steadily become a huge clinical concern not only across Asia [426], but now also in Europe where they are the largest cause of hepatic abscess in the UK. HV*Kp* typically express K1 and K2 capsule types, and have enhanced capsule expression mediated by the predominantly plasmid-borne allele of the regulator *rmpA* which gives them a hypermucoid phenotype and is enriched in strains causing pyogenic liver abscess [427]. This phenotype is

confirmed by the string-test method, whereby a positive reaction is given if a colony on a plate can be stretched greater than 5mm with a microbiological loop [428]. An example of a string test for 1 positive and one negative strain used in this study are shown in Figure 27. Definition of HV*Kp* is based not only on the type of capsule they express, but also genetically by the repertoire of virulence genes these strains encode [429]. More worrisome, is that there are now reported of HV*Kp* which encode extended spectrum beta-lactamase genes (ESBL) conferring resistance to beta-lactam antibiotics, and strains encoding multi-drug resistance plasmids [430]. There is the very real possibility then, that hypervirulent strains capable of causing infections in immunocompetent people in the community, may arise, for which there are no treatment options.

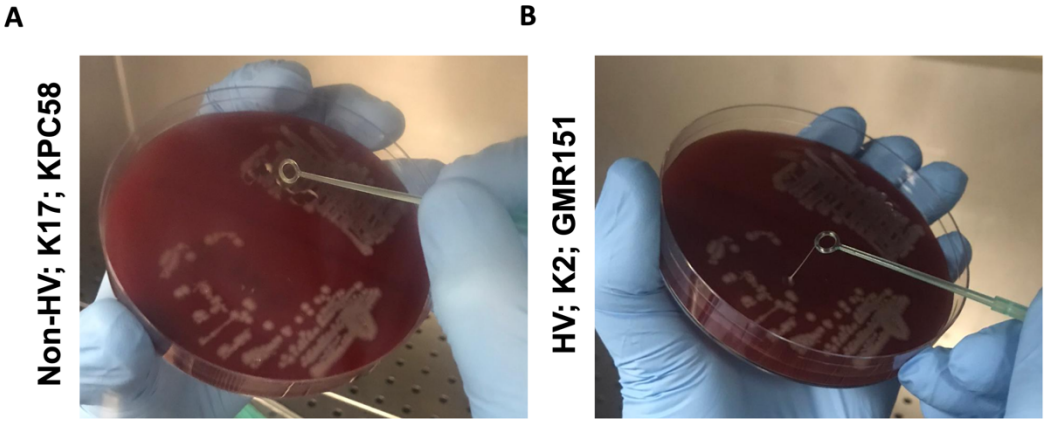

Figure 27 - *The string test for hypermucosity*. Example of a positive string test for serotype K2, hv*Kp* strain GMR151 (A), and a negative string test from the serotype K17 non-hv*Kp* strain KPC58 (B). Bacteria were streaked onto blood agar plates and incubated overnight at 37 °C. The following morning, a disposable microbiology loop was touched to the colonies, and a positive string test was inferred if the colony stretched for more than 5mm before breaking.

4.1.2 Classical *K. pneumoniae* (C*Kp* \ non-hv*Kp*)

K. pneumoniae which do not express the hypervirulent phenotype, are broadly referred to as classical *Kp*, or non-hv*Kp.* non-hv*Kp* are defined based on a negative string test, and on the absence of key virulence genes such as those encoding siderophores [431]. Non-hv*Kp* are a major cause of nosocomial infections predominantly in immunocompromised individuals [432]. They present their own unique clinical problem, as many lineages have acquired a number of resistance mechanisms to clinically relevant antibiotics, rendering them multi, or even pan drug resistant (MDR, and XDR respectively) [433]. While non-hv*Kp,* MDR lineages typically do not express the hypermucoviscous phenotype, strains with convergence of both phenotypes are being increasingly reported [434]. Classical *Kp* tend to be less virulent than their hv*Kp* counterparts, as evidenced by less severe clinical presentations in humans [435], and by infectious dose 50s in mice which are several orders of magnitude lower [436].

Kp are intrinsically highly resistant to antibiotics, mediated in part by expression of outer membrane porins [437], and through expression of tripartite efflux pumps of the RND family [438], which export a number of substrates including antibiotics, conferring resistance. Perhaps the most worrisome of acquired resistances in *Kp* are found in carbapenemase producing strains (CR*Kp*) [439]. Carbapenems are a class of b-lactam antibiotics, and the first line treatment for severe systemic infections (such as sepsis), in UK hospitals [440] and for treatment of MDR strain infections [441]. Carbapenemases catalyse the degradation of carbapenem antibiotics, rendering the strain resistant to these drugs. In cases where strains are resistance to carbapenems, colistin remains in most cases the last resort antibiotic therapy [442]. Colistin resistance has arisen in *Kp* mediated by horizontal transmission of the *mcr-1* gene [443], rendering many strains resistant to even this last resort drug. Resistance to colistin can also be mediated by modifications to the bacterial LPS [444], mediated by mutations in other genes such as *mgrB* [445] or *phoQ* of the PhoPQ 2-component regulatory system [243].

4.1.3 Epidemiology of *K. pneumoniae* infections: case of Europe and south east Asia

In recent years, *K. pneumoniae* has emerged as a major human pathogen from its original prevalence in low income countries [425], to becoming a major pathogen in Europe [446], America, and Australia. In Europe, *Kp* blood stream infections are predominantly caused by non-hv*Kp* in nosocomial settings, and are associated with carriage of extended spectrum beta-lactamase (ESBL) and carbapenemase genes. Recent work has demonstrated that spread of *Kp* across Europe is driven by nosocomial spread, and is likely mediated by antibiotic selection for and propagation of resistant strains [446]. Furthermore, Europe is dominated by an epidemic of ST258 non-hv*Kp* and the closely related ST512 clone which both have high carriage rates of carbapenemase genes, and are frequently associated with nosocomial outbreaks. Whilst a comparatively minor cause of the total *Kp* infection burden, hv*Kp* have now arisen as the major cause of hepatic abscesses in Europe [447].

hv*Kp* previously dominated the clinical setting in lower income countries in south east Asia such as Vietnam, and Taiwan. In these countries, hv*Kp* of sequence types 23, 25, and 65 are major causes of pyogenic liver abscesses [447]. A recent genomic survey of hypervirulence and drug resistance *Kp* blood stream infection isolates in Asia indicated ~50% carriage of carbapenemase genes, and ~30% carriage of the aerobactin synthesis locus – a gene strongly linked with the hypervirulent phenotype. Furthermore, in these settings the dominant clone was derived from a K24 ST15 with high carriage rates of carbapenemase [448]. Although in many countries the number of genomes analysed was small, there appeared to be a distinct geographic shift in sequence type aetiology for example with infections in India being dominated by ST14 strains [448].

The relative epidemic success of carbapenemase producing non-hv*Kp* when compared to hypermucoid hv*Kp* likely arises from their enhanced ability to undergo horizontal gene transfer and incorporate traits which provide a fitness advantaged. Wyres *et al* (2019) [449] demonstrated using a large collection of genome sequence data comprising multiple clones displaying either the MDR or hypervirulent

phenotype, that recombination events were far less common in the latter. This led to the generation of more genetic diversity in the former group, which may explain their evolutionary success. Further, they postulated that this may be due to an impediment of the mucoid capsule in uptake of foreign DNA. Following this line of thinking, there is a greater threat of carbapenemase-producing non-hv*Kp* – which are already endemic in many areas of Europe and Asia – acquiring hypervirulence genes, than the reverse [430].

4.1.4 **Treatment**

4.1.4.1 **Chemotherapuetic**

In the case of MDR*Kp*, there are very few treatment options in the therapeutic arsenal. The last resort drug of choice for treatment of these infections in colistin [450]. Tigecycline is also a viable treatment option [451], although resistance to both of these drugs arise readily [243, 452]. Successful treatment of CR*Kp* can in some cases be achieved by the combination of Ceftazidime (a cephalosporin) and Avibactam (a beta-lactamase inhibitor which nullifies resistance) [453]. Conversely, the majority of HV*Kp* remain sensitive to major antibiotic classes. Optimised treatment of HV*Kp* is difficult, as many clinical microbiology labs struggle to initially differentiate them from classical *Klebsiella*, which hampers the progression of clinical trials [431]. Given the ability of HV*Kp* to infect multiple organ sites with severe clinical complications, and the difficulty in conducting clinical trials on these infections, optimisation of antibiotic therapy desperately requires an enhanced understanding of the pathogenesis of HV*Kp* infection.

4.1.4.2 **Surgical**

Pyogenic tissue abscesses are a surgical as well as a microbiological problem, and require drainage in addition to antimicrobial chemotherapy [454]. Large abscesses in sites of low systemic importance can be drained percutaneously, which can then be escalated to a full-scale surgical drainage if this approach fails [455]. Smaller abscesses in many cases can be cured without surgical intervention, by antimicrobial therapy alone, leaving clearance of the abscess to the host immune response.

4.1.4.3 **Vaccination and passive immunisation**

There are currently no licenced vaccines available for protection against *K. pneumoniae* infection in humans. A broadly protective vaccine against multiple *Kp* serotypes – especially against K1 and K2 capsule types – would dramatically reduce the burden currently placed on antimicrobial chemotherapy. Furthermore, a better understanding of the pathogenesis and immune response to *Kp* infection would drastically aid the development of novel vaccines. Feldman *et al*. (2019) [456] recently developed a promising bi-conjugate vaccine which elicits a promising IgG antibody titre, and was protective against K1 and K2 *Kp* infection in a mouse model of sepsis, although this vaccine is still in pre-clinical development. Malachowa *et al.* (2018) [457] demonstrated the efficacy of a capsule-based vaccine against *Kp* ST258 in a non-human primate model of pneumonia, which induced production of antibodies which confered bacticidal activity in a neutrophil killing assay. In veterinary medicine, the use of autologous vaccines have found some success in controlling outbreaks, and a 23-valent capsular polysaccharide vaccine (KLEBVax SRP)[458] is available to prevent mastitis in cattle [459]. Passive immunisation, by the administration of monoclonal antibodies represent another treatment avenue. In experimental infection, antibodies which target the capsule, and also the O-antigen (discussed below) have been successful at treating *Kp* infection, by targeting cells for complement deposition, or efficient uptake by macrophages [460, 461]. The downsides of passive immunisation come in the enormous heterogeneity in surface structures which represent targets, and the massive expense of manufacturing large quantities of antibody.

4.1.5 **Virulence factors of *K. pneumoniae***

4.1.5.1 **Capsule**

As described above, the *Kp* capsule is a major virulence determinant, and its overexpression is a key phenotype differentiating classical and HV*Kp.* The capsule has been demonstrated to have a number of mechanistic interactions with the host immune system which facilitate virulence. A major phenotype of the capsule – in close analogy to the pneumococcus and other typically extracellular pathogens – is facilitating resistance to phagocytosis [436, 462]. The physical barrier and charge of the capsule prevents phagocyte, receptor-mediated clearance of bacteria from systemic sites, allowing them to proliferate extracellularly and cause disease.

Furthermore, in *Kp*, shed capsule has also been demonstrated as a decoy for host antimicrobial peptides [463]. The release of capsule therefore, sequesters anti-microbial immune effectors allowing bacteria to escape killing. Lastly, of particular interest to this thesis, in addition to the indirect roles of capsule in mediating immune killing, studies have indicated that it may be a direct immune evasion by modulating macrophage cell biology. Dumigan *et al.* (2019) [464] demonstrated that capsule is capable of polarising porcine bone marrow-derived macrophages to an M2-like state, which is predicted to be less microbiocidal and may facilitate persistence of *Kp* intracellularly. Lastly, the capsule of *Kp* has been demonstrated to be involved in resistance to complement-mediated killing [465].

4.1.5.2 **Iron acquisition by siderophores**

Iron is a critical metal for bacterial metabolism, subsequent growth and virulence of a number of bacterial pathogens. In many cases, iron is a critical regulator of virulence gene expression, by modulating the *fur* regulon, encoding an iron-responsive transcription factor. The majority of iron in the human body is sequestered with carrier proteins such as haemoglobin, meaning bacteria require high affinity mechanisms to compete with the host for iron. Bacteria have evolved a number of mechanisms for acquisition of iron from the host, and indeed iron acquisition systems in *Kp* have been shown to be essential for virulence [466]. Siderophores are a common mechanism of iron acquisition in bacteria. Siderophores are high affinity iron chelating molecules secreted by bacteria which compete with the host for iron. Bacteria then encode siderophore-specific receptors to mediate uptake of the protein bound iron. Intake of siderophore-iron complexes are often mediated by the periplasmic adaptor protein TonB. *Kp* are known to encode up to 4 siderophores in their genome; yersiniabactin [467], aerobactin [468], colibactin [469], and salmochelin [470]. These loci are overrepresented in invasive isolates of *Kp* [447], and studies have indicated their expression *in vivo*, and in host mimicking conditions [471]. Furthermore, murine studies with knockouts have indicated redundant roles for these systems in virulence, indicating a complex interaction with the host [466]. It should be noted that other iron acquisition systems are encoded by *Kp*, but the relative contributions of these individual loci to virulence are yet to be determined.

4.1.5.3 **LPS and the O-antigen**

Kp lipopolysaccharide (LPS) consists of three structural components. These are the lipid A, the core oligosaccharide, and the repetitive O-polysaccharide (termed the O-antigen). O antigen displays variation among *Kp* strains, which is likely due to immune selection in analogy to the capsule. The O antigen of *Kp* was demonstrated in early studies to be a factor associated with colonisation of the nasopharynx, and also a major virulence determinant during systemic infection [472]. Additional work has delineated a number of interactions of O-antigen with the host which may explain this virulence contribution. Studies have indicated that LPS plays a role in resistance to phagocytic killing [473], but also that it is a key player in dendritic cell activation which may facilitate their clearance [474]. As the outermost layer of the bacterial surface, LPS forms a major target of the host complement system, which efficiently kills non-HV*Kp* [475]. *Kp* are known to secrete outer membrane vesicles which contain LPS, which sequesters complement rendering the associated bacteria un-killed [476, 477]. Furthermore, serum resistant strains of *Kp* encode LPS types with an extended O-antigen. Extension of this variable domain is likely to prevent either the efficient binding of antibody to surface proteins, or will interfere with either deposition of complement, or initiation of the membrane attack complex (MAC). Lastly, Llobet *et al.* (2015) demonstrated that *Kp* actively remodels its LPS *in vivo* to dampen the inflammatory response to infection, mediating persistence [478], and also to reduce susceptibility to the LPS-active antibiotic colistin.

4.1.6 **Evidence for macrophage manipulation by *K. pneumoniae***

K. pneumoniae are traditionally considered to be extracellular pathogens. A number of recent studies however have used *in vitro* cell culture models to demonstrate that *K. pneumoniae* may be able to persist within macrophages.

Cano and colleagues (2015) [73] analysed in detail, the fate of a *K. pneumoniae* serotype K2 strain following internalisation within a human monocyte cell line (THP-1), a murine alveolar macrophage cell line (MH-S), and primary murine alveolar macrophages. They demonstrated that following internalisation, *K. pneumoniae* resided in a non-canonical lysosomal compartment (the Klebsiella-containing vacuole) which did not display cellular markers of a lysosome (acidic pH and LAMP-1 co-localisation were two examples). This was shown to be an active manipulation of the

lysosomal trafficking pathway, as heat killed *Kp* appeared to progress normally through this pathway. Furthermore, they demonstrated that *Kp* infection of macrophages triggered a cell death with the hallmarks of apoptosis. Further, a later publication of this group [464] demonstrated that *Kp* and particularly its capsular polysaccharide polarised macrophages into the less microbiocidal, M2-like state.

Fodah and colleagues [479] performed a microbiological investigation of whether three strains (a K1, K2, and K52 isolate respectively) could replicate within a the two murine derived, macrophage cell lines RAW264.7, and J774a.1. They observed that all three strains were capable of growth within these cell types, but that a non-logarithmic growth was observed, with periodic peaks and troughs of CFU recover from cells across a 24h period, indicating more complex ongoing infection dynamics.

More recently, Hoh et al (2019) [421] demonstrated the ability of Kupffer cells and to a lesser extent pooled splenic macrophages to efficiently kill HV*Kp in vitro*. Further, they demonstrated a protective role of these cells *in vivo* in protection of *Kp* infection, by showing that mice had shorter survival times when they were depleted of macrophages by clodronate liposomes. This study however, provided no details on the dynamics of infection *in vivo*, or at the single cell level *in vitro*.

In this chapter, my aim was to analyse the tissue tropism of a diverse set of *Kp* clinical isolates representative of five capsule types, multiple sequence types and both the classical and hypervirulent phenotype, in a number of experimental models of infection (see methods; Table 3). In addition, I aimed to test the hypothesis that replication of *Kp* within tissue-resident phagocytes precedes the formation of hepatic and splenic tissue abscesses, which characterise the severe disease causes by hypervirulent *Kp*.

4.2 Results

4.2.1 Growth kinetics of clinical *Kp* isolates in host-mimicking media

I first aimed to characterise the growth kinetics of our collection of clinical *K. pneumoniae* isolates. Growth kinetics are often investigated in rich, and nutrient limited media, but we aimed to extend this analysis to growth media that specifically mimicked different host niches encountered by the bacterium during systemic infection. As such

growth curves were performed for all strains in rich (Brain heart infusion, BHI) broth, *ex vivo* mouse serum, *ex vivo* mouse whole blood, and Low Phosphate and Magnesium (LPM) medium at either pH 7 or 5.8. LPM medium replicates the growth conditions present in cytosolic, and acidic vacuolar intracellular compartments and is known to induce the same virulence factors expressed by *Salmonella ssp*. in the intracellular niche [249], indicating that there are common nutritional aspects to this medium and these environments. Both *Kp* and *Salmonella* are members of the Enterobacteriaceae family, and as such may respond similarly to these growth conditions.

All strains displayed comparable growth kinetics in BHI (Figure 28a), with exponential doubling times ranging between 30-40 minutes respectively. Strains grew with comparable growth kinetics in LPM pH7 (cytosolic conditions; Figure 28b), with both groups having statistically different doubling times (Figure 28c), insignificant lag times (Figure 28e), but with the hypervirulent strains growing to significantly higher maximum optical densities (Figure 28f). This phenotype was enhanced, when grown in LPM pH 5.8 (phagosomal conditions; Figure 28), with hypervirulence strains having longer exponential growth phases, and reaching higher maximum optical densities than their classical counterparts (Figure 28b). To confirm these phenotypes, future work should include measurement of the CFU:OD_{600} ratio for each individual strain to determine whether heightened OD values are a result of the thick capsule expressed by HV strains. Furthermore, as capsule is a major virulence factor during infection, additional experiments should investigate capsule production in these media to see if they can accurately model the *in vivo* transcriptome. Together, these data indicate that hypervirulent strains may have a modest advantage resisting the nutrient limited, and acidic pH conditions which are reminiscent of the intracellular, lysosomal compartment.

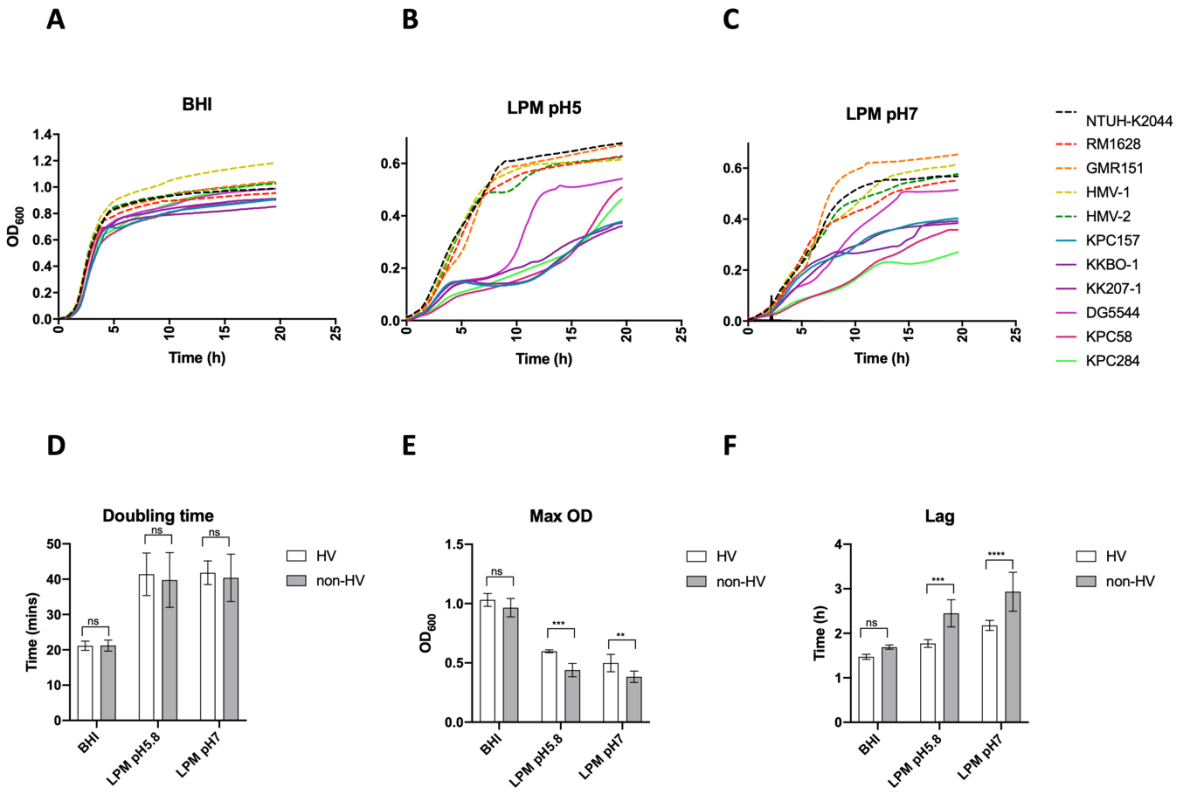

Figure 28 - *Growth kinetics of Kp clinical isolates*. Growth kinetics of *Kp* strains following inoculation of rich medium BHI (A), LPM medium buffered to pH 5 (B), and LPM medium buffers to pH 5 (C). Growth curves were prepared as described in the methods, with an approximate starting OD of 0.002. hv*Kp* strains are shown by dotted lines, whereas non-hv*Kp* strains are shown by solid lines. Strain names corresponding to the colour of each strain are shown to the right of the graph. (D) From the growth curves, doubling times were calculated using the equation outlined in the methods. Maximum OD_{600} (E) values after 20h of growth and the lag times (E) were calculated in Microsoft Excel. For panels D-F, hv*Kp* strains are shown by white bars, whereas non-hv*Kp* strains are shown by grey bars. Statistical significance were determined by a t-test. **; P<0.005, ***; P<0.0005, ****; P<0.00005.

4.2.2 Intracellular persistence and replication of hv*Kp* in the murine macrophage cell like J774a.1

To determine whether our strains were replication competent within murine macrophages, I utilised the J774a cell line, with a modified phagocytosis assay. Phagocytosis assays rely on the ability of antibiotics with in-efficient intracellular penetration to kill extracellular bacteria, allowing enumeration of only phagocytosed

organisms. As many of our clinical isolates are highly antibiotic resistant, I first aimed to determine optimum antibiotic concentrations for killing in a phagocytosis assay. For both hv*Kp* and non-hv*Kp*, two conditions were tested for all strains; (1) 20 µg/mL gentamicin (Figure 29a), and (2) 300 µg/mL polymyxin B and 15 µg/mL gentamicin (Figure 29b). Approximately 10^7 CFU of each strain were added to complete cell culture medium containing the respective antibiotics, and incubated for 60 or 90 minutes. Figure 29 shows that for both the K1 and K2 isolates, a treatment of 20 µg/mL gentamicin for either 1h, or 1.5h, was sufficient to reduce bacterial counts by ~5 logs, whereas the K17 and K107 strain showed only a modest reduction. To reduce bacterial counts for these latter two strains, 300 ug/mL gentamicin + 15 µg/mL polymyxin B treatment for 1h was required. In the subsequent assays, HV strains were treated with the former condition, whilst MDR strains were treated with the latter.

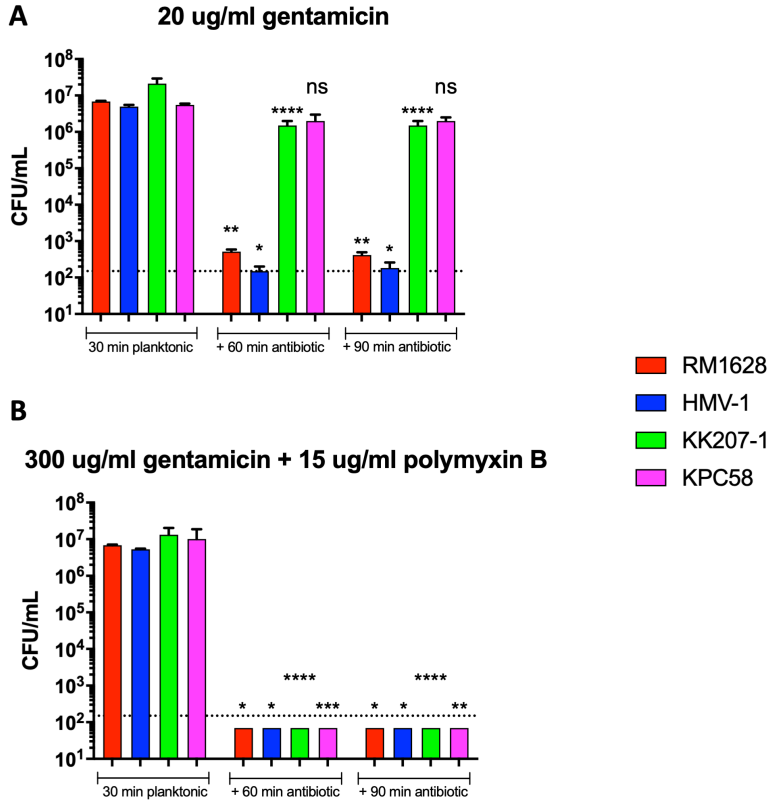

Figure 29 *- Optimization of conditions for killing of extracellular bacteria in phagocytosis assays.* Treatment of representative serotype K1 (blue), K2 (red), K107 (green), and K17 (purple) with 20 µg/ml gentamicin alone (A), or 300 µg/ml gentamicin + 15 µg/mL polymyxin B (B). Bacteria were inoculated from frozen stocks into cell culture medium, at a concentration of ~ 10^7 CFU/mL as this is the starting extracellular inocula for a cell culture experiment with an MOI of 10, and were

incubated for 60 minutes, and 90 minutes in a 37°C incubator with 5% CO_2. A 2-way ANOVA with Dunnett's multiple comparison test was performed comparing antibiotic treated strains with the relative planktonic culture. *; P<0.05, **; P<0.005, ***; P<0.0005, ****; P<0.00005. The limit of detection is indicated by a dotted line.

For phagocytosis assays, cells were infected at an MOI of 50 for each strain, and infections were synchronised by centrifugation of the tissue culture plate. After 30 minutes adhesion, strains were treated with antibiotic as described above. Cells were then washed, and exposed to media containing the respective gentamicin MICs for each strain for the remainder of the experiment to prevent bacterial outgrowth. A diagrammatic representation of the phagocytosis assay method is shown in Figure 30a.

The data indicate that K1 strains were highly resistant to phagocytosis, as approximately 1 log lower bacterial counts were obtained at the 'adhesion' step for these strains than all others (Figure 30b). K2 strains showed a lesser resistance to phagocytosis, comparable to both K17 and K107 isolates, for which approximately 20% of the inoculum were recovered (Figure 30b).

At this early stage of infection (30 minutes adhesion, plus 1h antibiotic treatment), K1 isolates, despite having a lower number of total adhesive bacteria, have a greater fraction of live intracellular bacteria than K2, K17, and K107 isolates, possibly indicating greater resistance to the initial innate macrophage response (Figure 30c) .

For time course experiments, I analysed time points of 0h, 2h, and 5h post infection. This is because *Kp* are known to induce apoptosis in macrophages by 24h post infection, and inspection of 24h infected cells in our model confirm a reduced confluence of cell monolayers. K1 and K2 counts remained stable from 0-2h post infection, but all 4 strains increased in counts by 5h hours post infection (Figure 30di-ii). 4 of 6 K107 and K17 isolates assayed reduced in numbers over the time course indicating intracellular clearance, whilst the remaining 2 appeared able to increase in numbers (Figure 30iii-iv). Estimated doubling times, and clearance half-lives for each strain in this model, and the statistical comparison of intracellular bacterial counts are shown in Table 9.

Together, these data indicate serotype-dependent resistance to phagocytosis, and a propensity of hypervirulent strains, and some classical strains to replicate within murine macrophages *in vitro*.

Table 9 - *Statistical comparison of intracellular growth in J774a macrophages*

	K1		K2		K107			K17		
	NTUH	**RM1628**	**GMR151**	**HMV-1**	**KK207-1**	**KKBO-1**	**KPC157**	**KPC58**	**KPC284**	**DG5544**
P value	0.038	0.017	0.047	0.026	0.002	0.048	<0.00005	<0.00005	0.009	<0.00005
D (mins)	202	169	108	120	-300	73	-172	-58	83	-33

D; doubling time, P value; arising from a 1-tailed t test comparing time 0, to 5h post infection. –; indicates the rate at which bacterial numbers decreased.

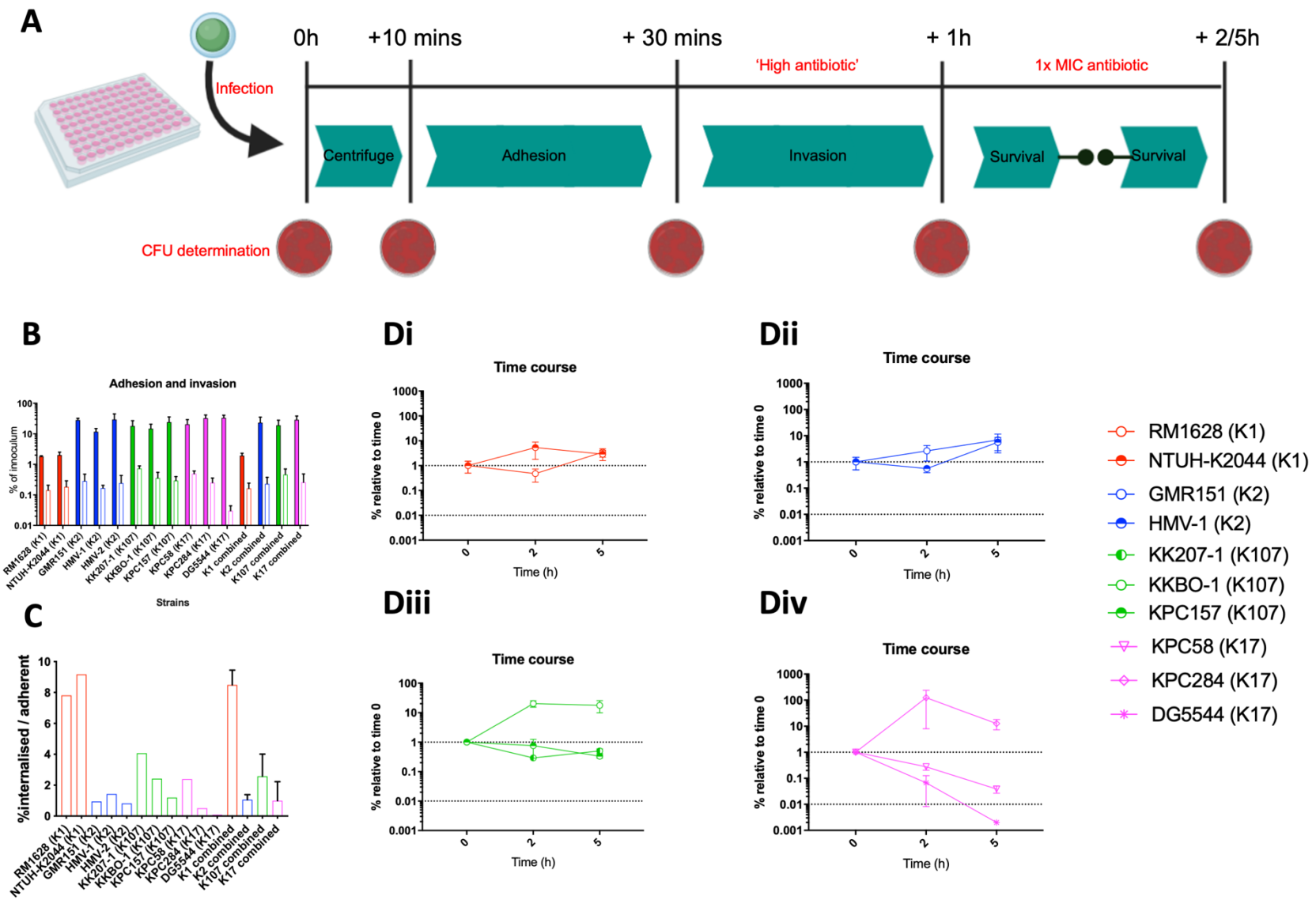
A
Infection
0h
+10 mins
+ 30 mins
+ 1h
+ 2/5h
'High antibiotic'
1x MIC antibiotic
Centrifuge
Adhesion
Invasion
Survival
Survival
CFU determination
B
Adhesion and invasion
% of innoculum
RM1628 (K1)
NTUH-K2044 (K1)
GMR151 (K2)
HMV-1 (K2)
HMV-2 (K2)
KK207-1 (K107)
KKBO-1 (K107)
KPC157 (K107)
KPC58 (K17)
KPC284 (K17)
DG5544 (K17)
K1 combined
K2 combined
K107 combined
K17 combined
Strains
C
%internalised / adherent
Di
Time course
% relative to time 0
Time (h)
Dii
Time course
% relative to time 0
Time (h)
Diii
Time course
% relative to time 0
Time (h)
Div
Time course
% relative to time 0
Time (h)
RM1628 (K1)
NTUH-K2044 (K1)
GMR151 (K2)
HMV-1 (K2)
HMV-2 (K2)
KK207-1 (K107)
KKBO-1 (K107)
KPC157 (K107)
KPC58 (K17)
KPC284 (K17)
DG5544 (K17)

Figure 30 - *Phagocytosis assays with clinical isolates of K. pneumoniae and the murine macrophage cell line J774a.1.* (A) shows a schematic representation of the phagocytosis assay protocol. High antibiotic concentrations were determined in section 4.2.2, whilst 'MIC antibiotic' concentrations were determined by the microbroth dilution technique. (B) shows the adhesion (filled bars) and invasion (empty bars) of 2 K1 (red), 3 K2 (blue), 3 K107 (green), and 3 K17 (pink) clinical isolates of *Kp* within J774a.1 macrophages. (C) expresses the percentage of internalised organisms from panel B against the total adhesive bacteria. (D) shows a time course analysis of *Kp* survival following 'high antibiotic' treatment for K1 (i), K2 (ii), K107 (iii), and K17 (iv) strains normalised to the intracellular CFU following initial treatment. In all panels, error bars show the standard deviation of the mean of 3 biological replicates.

4.2.3 Screening the tropism and replication competence of *Kp* strains in a murine infection model

To test if a mouse model of infection could replicate both the observed *in vitro* replication of *Kp* in macrophages, and the clearly distinct lineage/serotype-specific disease phenotypes observed for hv*Kp* and non-hv*Kp*, I challenged individual mice intravenously with a panel of five hv*Kp* and six non-hv*Kp* isolates (Table 3). The scope of this screening experiment, was to determine the cellular tropism of *Kp* clinical isolates in both the liver and spleen (two sites of *Kp* infection), and to see if my observation that hv*Kp* were replication competent in murine macrophages *in vitro*, translated to tissue macrophages *in vivo*. I therefore monitored the fate of bacteria in the liver and spleen, at 6h post intravenous infection in mice. I used high throughput scanning fluorescence microscopy and semi-automated image analysis to determine the distribution of bacteria and to evaluate their association to tissue macrophages. Furthermore, I used confocal microscopy to identify the subcellular localisation of *Kp* in macrophages and the bacterial load per macrophage.

4.2.4 Diverse phylogroups of hv*Kp* but not non-hv*Kp* replicate in hepatic Kupffer cells

In the liver, both the hv*Kp* and non-hv*Kp* group of isolates, significantly localized to the only hepatic macrophage population, the F4/80-positive Kupffer cells (Figure 31a).

Exemplar co-localisation images are shown for K1 (Figure 31di), K2 (Figure 31e), K17 (Figure 31fi) and KL107 (Figure 31g). Images of liver sections from which these images were derived are shown in 32a-d). Higher resolution confocal microscopy allowed quantification of the number of bacteria associated with each Kupffer cell. These data showed that the number of bacteria associated to a single Kupffer cell was significantly larger for hv*Kp* with respect to non-hv*Kp* isolates (Figure 31b). In the case of hv*Kp* isolates, irrespective of the strain or capsule type, the average number of bacteria forming a focus of infection was six to eight bacteria, while in contrast all non-hv*Kp* isolates colocalised with macrophages on average as single bacteria. When comparing focus size within the two groups, the size of foci was consistent within both the hv*Kp* and the non-hv*Kp* groups. When testing the bacterial organ loads following intravenous infection, K2 strains demonstrated very high bacteraemia levels, whilst K1 and non-hv*Kp* strains had low or absent bacteraemia (Figure 31c). Spleen and liver counts reflected blood counts with K2 strains showing higher counts than both K1 and non-hv*Kp* strains. As an additional reference To define the spatial localisation of bacteria with macrophages I reconstructed multiple confocal microscopy stacks into 3D images using Imaris. Z-stack images used to make the reconstruction are shown in supplementary Figures 32e-f. For all eleven isolates tested confocal images showed unequivocally that the hv*Kp* and the non-hv*Kp* isolates were localised within the Kupffer cells (Figure 31diii and fiii). To confirm that clusters of intracellular hv*kp* were caused by intracellular replication of the organism, and not continual phagocytic events, I performed a co-infection of mice with the K1 strain RM1628, and the K2 strain GMR151, both of which could be distinguished by specific staining with purified anti-capsule IgG conjugated to different fluorophores (see methods). In the liver, I observed that clusters of bacteria were formed by entirely monochrome cells indicating that clusters were formed by a single founder bacterium (Figure 31h).

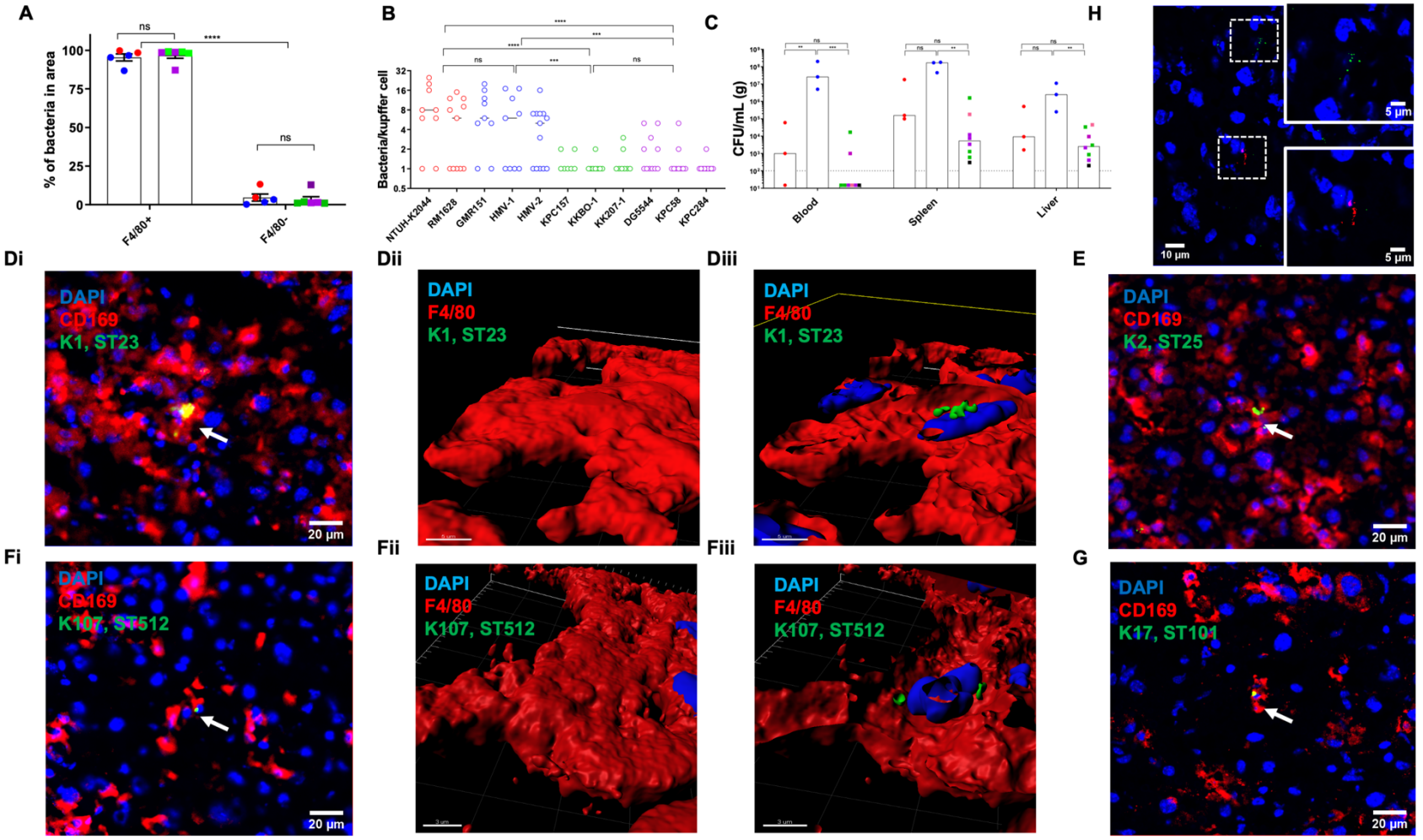
A
% of bacteria in area
F4/80+
F4/80-
B
Bacteria/kupffer cell
NTUH-K2044
RM1628
GMR151
HMV-1
HMV-2
KPC157
KKBO-1
KK207-1
DG5544
KPC58
KPC284
C
CFU/mL (g)
Blood
Spleen
Liver
H
5 µm
10 µm
Di
DAPI
CD169
K1, ST23
20 µm
Dii
DAPI
F4/80
K1, ST23
Diii
DAPI
F4/80
K1, ST23
E
DAPI
CD169
K2, ST25
20 µm
Fi
DAPI
CD169
K107, ST512
20 µm
Fii
DAPI
F4/80
K107, ST512
Fiii
DAPI
F4/80
K107, ST512
G
DAPI
CD169
K17, ST101
20 µm

Figure 31 - *Tissue tropism and intracellular localisation of Kp in mouse livers following intravenous infection.* (A) Quantitative distribution of *Kp* in F4/80+ and F4/80- cells in the murine liver. Hypervirulent strains are shown as circles (K1 red, K2 blue) and non-hv*Kp* strains as squares (KL107 green, KL17 purple). (B) Size of bacterial clusters associated with Kupffer cells at 6h post infection (same colour scheme as in 1A). Statistical significance was determined by 1-way ANOVA. ****, $p<0.0005$; ***, $p<0.005$, NS; $P>0.05$ (C) CFU/mL or CFU/g of blood, liver and spleen from individual mice infected with the same panel of *Kp* isolates (same colour scheme as in A). Statistical significance was determined using multiple t tests. *, $p<0.05$; **, $p<0.005$. The limit of detection is indicated by the dotted black line. The bars indicate the median value. (Di) representative scanning microscopy image of K1 (green) co-localization with Kupffer cells (red). (Dii-iii) 3D reconstruction using Imaris of a K1 foci of infection Z stack acquired on the confocal microscope showing the top of the cell layer, and a single cut into the cell. (E) Representative scanning microscopy image of K2 *Kp* (green) with Kupffer cells (red). (FI) Representative scanning microscopy image of K17 *Kp* (green) localization with Kupffer cells (red) with 3D reconstruction (F2-3) (G) Representative scanning microscopy image of KL107 *Kp* (green) with Kupffer cells (red). (H) K1:K2 co-infected tissue section stained with purified IgG raised against K1 (green) capsule, or K2 (red) indicating two monochrome bacterial foci. A higher magnification of each monochrome foci is shown in insets. Lower magnification images for Di, E, Fi, and G are in Figure 32A-D, confocal Z-stacks for Di-ii and Fi-ii are in 31E and F. Murine infection experiments were performed with the help of Dr David Carreno, and Miss Zydrune Jasiunaite.

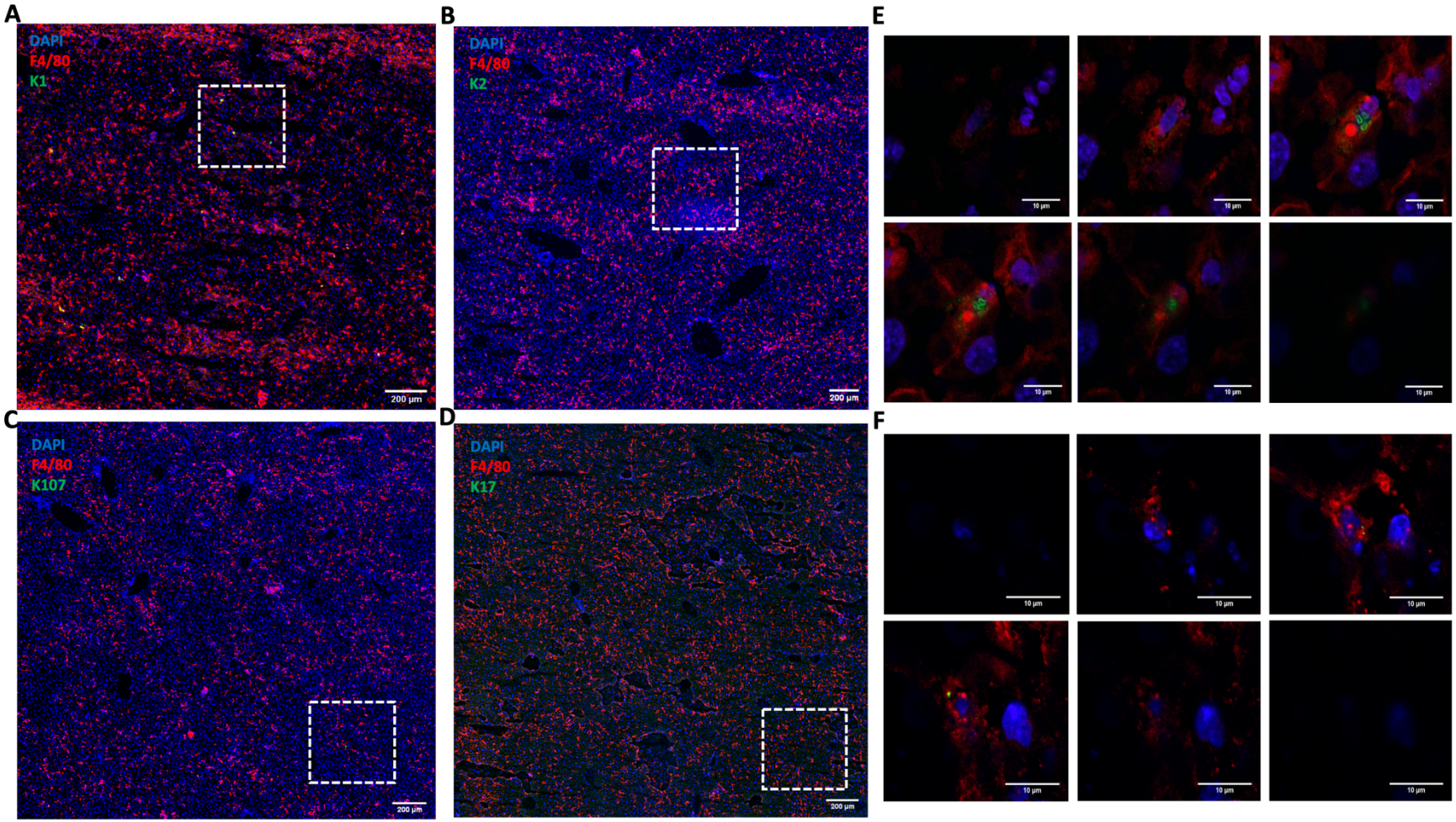
A
DAPI
F4/80
K1
200 µm
B
DAPI
F4/80
K2
200 µm
C
DAPI
F4/80
K107
200 µm
D
DAPI
F4/80
K17
200 µm
E
10 µm
F
10 µm

Figure 32 *- Scanning microscopy regions of interest, and Z stack images used for 3D reconstruction in the liver.* Low magnification image of multispectral images of liver section, stitched together from images acquired with a 40x objective. Samples are stained with DAPI, shown in blue, F4/80 in red, and antibodies targeted against *Kp* K1 (A), K2 (B), KL107 (C), and K17 (D) shown in green in each case. In each image the scale bar is 200 um in width. The areas presented in Figure 31 in the main text are outlined by dotted white lines. Z-stack images of K1 (E) and K17 (F) infected F4/80+ (red) macrophages. Sections are shown at 2um optical plane intervals from the top of the tissue section (top left) to the bottom of the tissue section (bottom right). These Z stacks were used to produce the 3D reconstructions shown in Figure 31. The scale bars for these images are 10um in width.

4.2.5 hv*Kp* replicate within multiple subsets of splenic macrophages

In the spleen where multiple macrophage subtypes are present and both an open and closed circulation work in tandem, the situation was more complex. Here, the majority of bacteria were found to be associated to F4/80+ red pulp macrophages. After normalization for the number of macrophages, the CD169+ metallophilic macrophages lining the while pulp (Figure 33a) were found to be the cell type most likely associated to bacteria. Exemplar co-localisation images are shown for K1 (Figure 33ci), K2 (Figure 33d), K17 (Figure 33ei) and KL107 (Figure 33f). Images of spleen sections from which these images were derived are shown in Figure 34a-d) No statistically significant difference in macrophage tropism was observed between hv*Kp* and non-hv*Kp* isolates. Quantification of the number of bacteria associated with single splenic macrophages showed that foci of hv*Kp* K1 isolates were of a significantly larger size than those formed by non-hv*Kp* isolates (Figure 33b). As in the liver, these foci of infection in splenic macrophages consisted of seven to eight bacteria for hv*Kp* isolates and of one bacterium for non-hv*Kp* isolates. In the spleen we excluded K2 strains from the analysis due to the high counts in the red pulp resulting from severe bacteraemia (Figure 31c). Confocal microscopy also confirmed in the spleen that the foci of infection of all hv*Kp* and non-hv*Kp* isolates were localised inside macrophages (Figure 33cii-iii and Figure 33eii-iii). Analysis of splenic sections from K1:K2 co-infected infected mice revealed also the prevalence of monochrome bacteria clusters, indicating intracellular replication rather than continual phagocytic events (Figure 33g).

I performed an infection with the ATCC 700603 reference strain for susceptibility testing, recently reclassified as *K. quasipneumoniae* [480], which showed comparable organ loads to the non-hv*Kp* strains (Figure 35a). Lastly, control growth curves in both *ex vivo* CD1 mouse serum and whole blood indicate that all strains not only survived, but replicated with indistinguishable growth dynamics (Figure 35b-d). These data using five independent hv*Kp* and six non-hv*Kp* strains demonstrated that there was a specific signature in the early stages of infection - the within macrophage growth behaviour - in which the mouse model clearly distinguished hv*Kp* and non-hv*Kp* strains, validating the use of the model for the study of tissue macrophage infection.

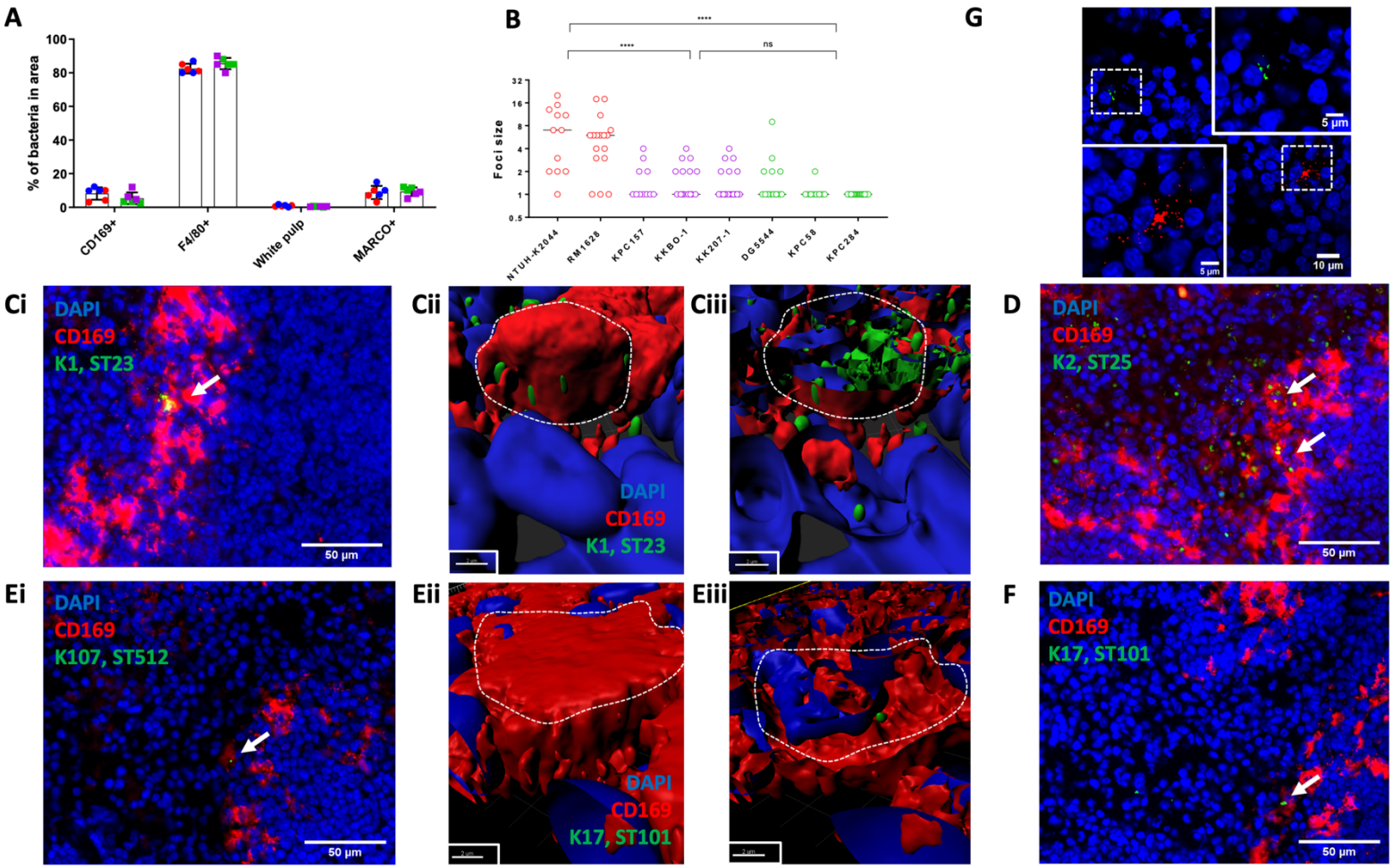
A
% of bacteria in area
100
80
60
40
20
0
CD169+
F4/80+
White pulp
MARCO+
B
****
****
ns
Foci size
32
16
8
4
2
1
0.5
NTUH-K2044
RM1628
KPC157
KKBO-1
KK207-1
DG5544
KPC58
KPC284
G
5 µm
5 µm
10 µm
Ci
DAPI
CD169
K1, ST23
50 µm
Cii
DAPI
CD169
K1, ST23
Ciii
D
DAPI
CD169
K2, ST25
50 µm
Ei
DAPI
CD169
K107, ST512
50 µm
Eii
DAPI
CD169
K17, ST101
Eiii
F
DAPI
CD169
K17, ST101
50 µm

Figure 33 - *Tissue tropism and intracellular localisation of Kp in mouse spleens following intravenous infection.* (A) Quantitative distribution of *Kp* between CD169+, F4/80+, and SIGN-R1+ macrophages in the murine spleen. hv-*Kp* are shown as circles (K1 red, K2 blue) and non-hv*Kp* strains as squares (KL107 green, KL17 purple). (B) Size of bacterial clusters associated with host cells at 6h post infection. Strains names are shown on the x-axis and follow the same colour scheme as above. K2 strains were excluded due to the high contaminating blood counts. Statistical significance was determined by 1-way ANOVA. ****, $p<0.0005$; ***, $p<0.005$, NS; $P<0.05$. (Ci) representative scanning microscopy image of K1 (green) localization with CD169+ macrophages (red). (Cii-iii) 3D reconstruction of a K1 focus of infection Z stack acquired by confocal microscopy showing the top of the cell layer, and a single cut into the cell. (D) Image of K2 (green) localization with CD169+ macrophages (red). (Ei) Image of K17 (green) localization with CD169+ macrophages (red). (Eii-iii) 3D reconstruction of K17 foci (F) Image of KL107 (green) localization with CD169+ macrophages (red). (G) K1:K2 co-infected tissue section stained with purified IgG raised against K1 (green) capsule, or K2 (red). Lower magnification images for Ci, D, Ei, and F, area is shown in Figure 34a-d, the Z-stacks for Cii-iii and Eii-iii are in Figure 34e-f. Murine infection experiments were performed with the help of Dr David Carreno, and Miss Zydrune Jasiunaite

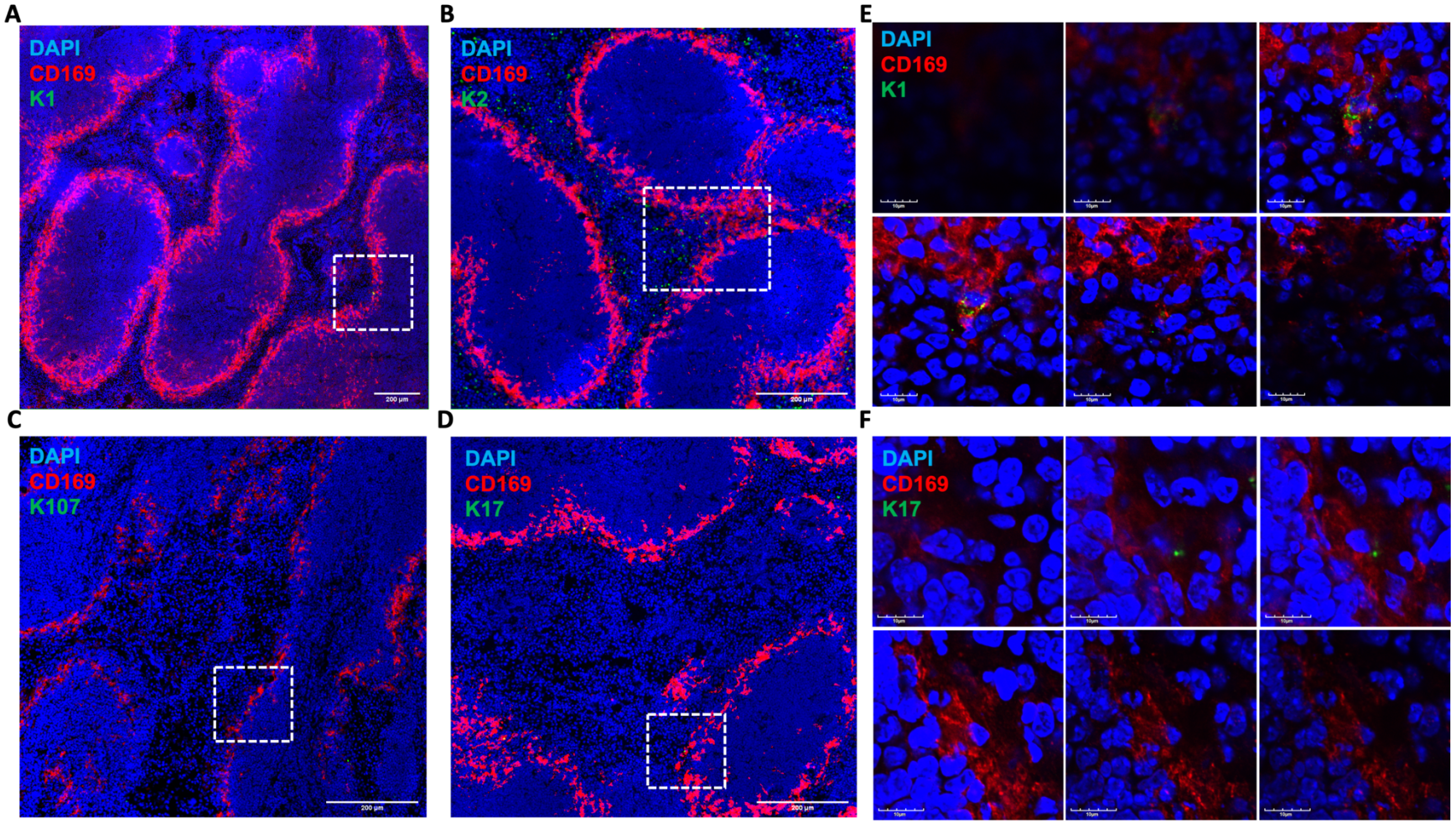
A
DAPI
CD169
K1
200 µm
B
DAPI
CD169
K2
200 µm
E
DAPI
CD169
K1
C
DAPI
CD169
K107
200 µm
D
DAPI
CD169
K17
200 µm
F
DAPI
CD169
K17

Figure 34 *- Scanning microscopy regions of interest, and Z stack images used for 3D reconstruction in the spleen.* Low magnification image of multispectral images of spleen sections, stitched together from images acquired with a 40x objective. Samples are stained with DAPI, shown in blue, CD169 in red, and antibodies targeted against *Kp* K1 (A), K2 (B), KL107 (C), and K17 (D) shown in green in each case. In each image the scale bar is 200 um in width. The areas presented in Figure 33 in the main text are outlined by dotted white lines. Z-stack images of K1 (E) and K17 (F) infected CD169+ (red) macrophages. Sections are shown at 2μm optical plane intervals from the top of the tissue section (top left) to the bottom of the tissue section (bottom right). These Z stacks were used to produce the 3D reconstructions shown in Figure 33. The scale bars for these images are 10μm in width.

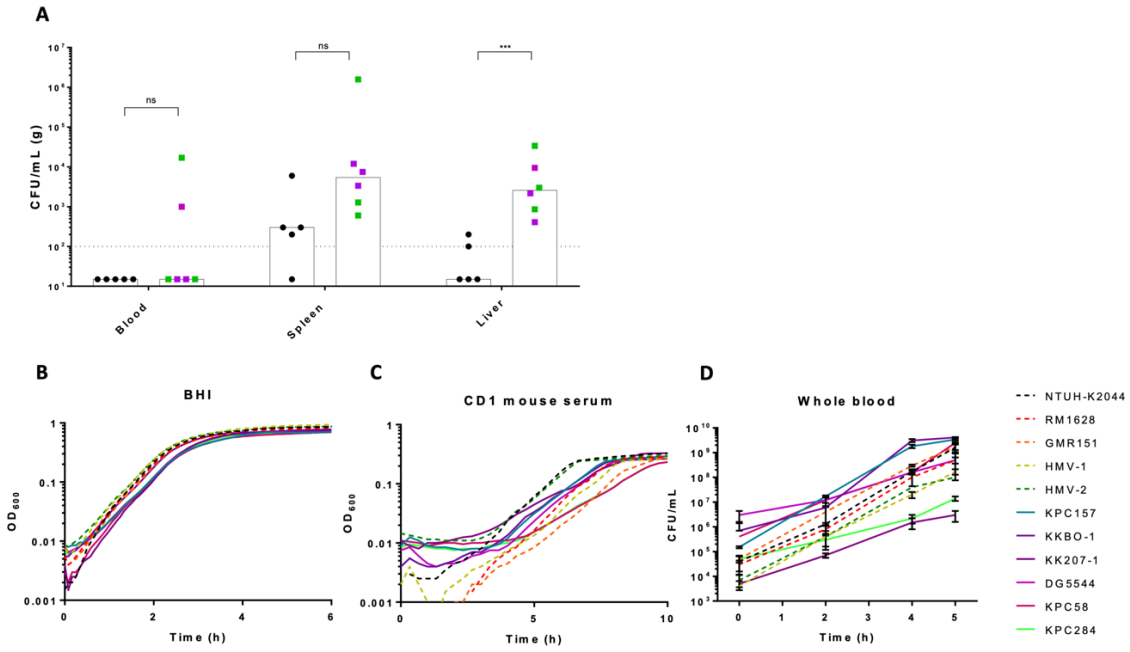

Figure 35 *- Comparison of organ loads in mice infected with non-hvKp or the K6 type strain ATCC 700603.* (A) Comparison of bacterial organ loads between 5 mice infected intravenously with the *K. quasipneumoniae* K6 type strain ATCC 700603, and 6 mice each infected with a different non-hv*Kp* clinical isolate. Mice infected with the type strain are shown as black circles, KL107 non-hv*Kp* strains are shown as green squares, and K17 non-hv*Kp* strains are shown as purple squares. The limit of detection is indicated by a black dotted line. Statistical significance was determined

by a student's t-test. NS; non-significant, ****; P<0.0005. Growth of *Kp* strains was also determined in BHI (B), *ex vivo* CD1 mouse serum (C) and whole blood (D) following inoculation of approximately 10^5 CFU of each strain. For BHI and serum growth curves, optical density was monitored, whereas for whole blood, growth was determined by CFU counting. The colour and line representing each strain is shown in the legend.

4.2.6 Initial growth of hv*Kp* in the tissue is followed by a period of within-cell persistence

From the strains used for screening, I selected one hv*Kp* strain (K1 NTUH-K2044) and one non-hv*Kp* strain (K17 KPC58) to conduct a time course analysis and to tie my observations to a role in the pathogenesis of abscess formation. I observed that following IV infection with 10^6 CFU of bacteria, the hv*Kp* K1 strain was cleared slowly from the blood over the first 24h, while the non-hv*Kp* K17 strain was completely cleared from the blood as early as 30 minutes post infection (Figures 36a). Furthermore, the K1 strain had significantly higher spleen and liver counts compared to the K17 strain at all time points (Figure 36 b-c). In the case of the K1 strain, bacterial intracellular foci sizes increased significantly up to 6h post infection, but then plateaued in both the spleen (Figure 36 di, exemplified in Figures dii-iii), and liver (Figure 36 ei, exemplified in Figures eii-iii) indicating that intracellular replication was limited to the first few hours after invasion. As expected, at all stages of infection the K17 strain was found generally as single bacteria associated with the phagocytes in both the spleen (Figure 36 di, exemplified in Figures div-v), and liver (Figure 36 ei, exemplified in eiv-v). These data indicate that both in liver and spleen, hv*Kp* were able to replicate in macrophages as opposed to non-hv*Kp* which were unable to replicate, irrespective of the fact that both groups of strains co-localised with the same type of macrophages and were detected within these macrophages. Further experiments with capsule deficient mutants in each strain background will be required to demonstrate the role of the HMV phenotype in within-macrophage survival.

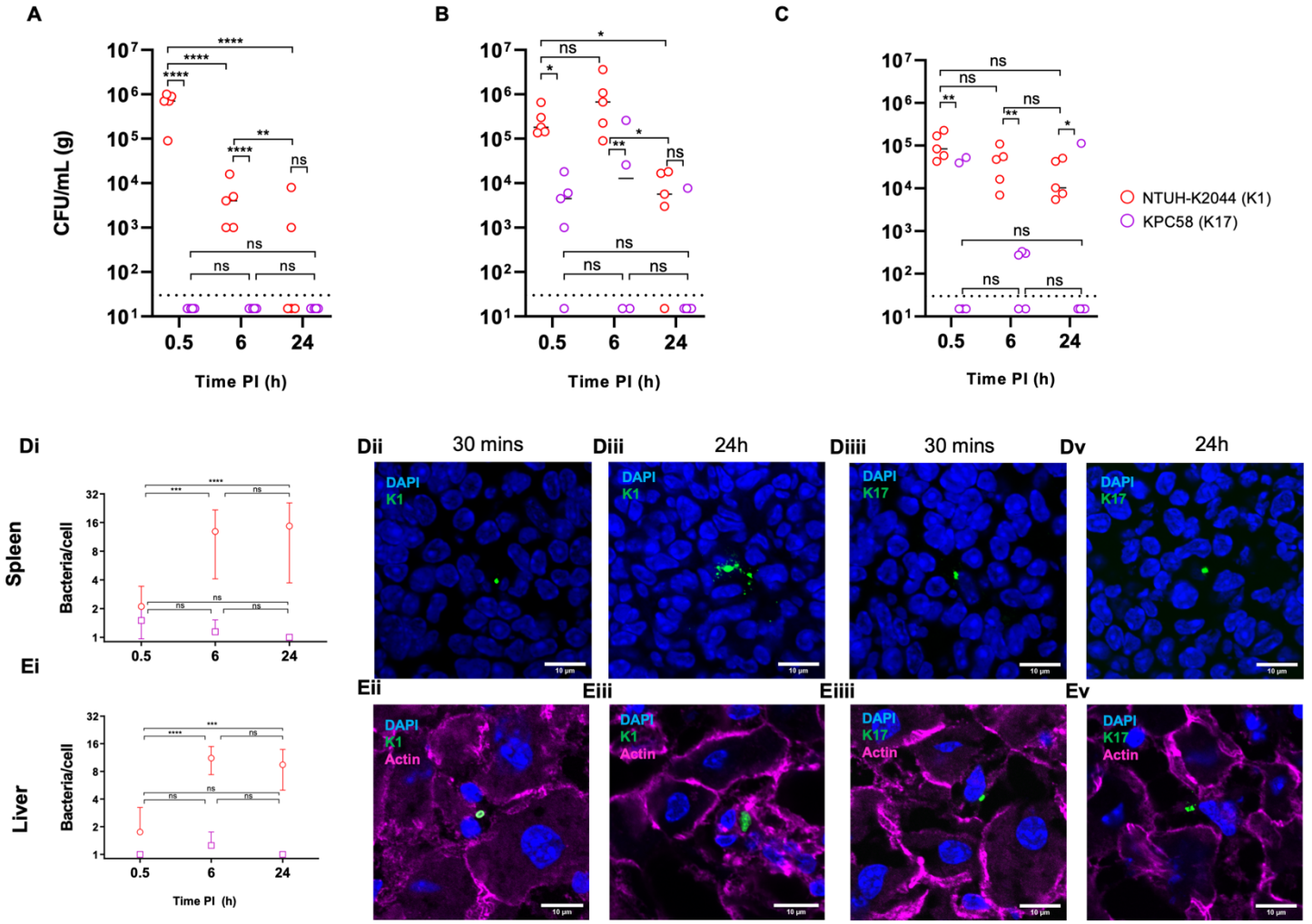
A
B
C
CFU/mL (g)
Time PI (h)
NTUH-K2044 (K1)
KPC58 (K17)
Di
Ei
Spleen
Liver
Bacteria/cell
Dii 30 mins
Diii 24h
Diiii 30 mins
Dv 24h
Eii
Eiii
Eiiii
Ev
DAPI
K1
K17
Actin

Figure 36 - *Time course analysis of K1 hvKp and K17 non-hvKp growth and tissue distribution.* Mice were infected iv with 10^6 CFU of either Kp K1 or K17. Blood (A), liver (B) and spleen (C) bacterial counts are shown at 30 minutes, 6h and 24h post-infection. The limit of detection is shown as a dotted black line (K1 red circles, K17 purple circles). Statistical significance was determined by ANOVA. ****; p<0.00005, ***; p<0.0005, **; p<0.005, *; p<0.05, NS; p>0.05. The median values are indicated by horizontal bars. (Di) Size of host cell-associated bacterial clusters, of K1 and K17 *Kp* throughout the infection in the spleen as determined from confocal microscopy. Data are representative of 3 mice per time point, per organ. Statistical significance was determined using a 1-way ANOVA. ****, p<0.0005; ***, p<0.005, NS; P<0.05. Error bars indicate the standard deviation. Exemplar images of the spleen after infection with K1 and K17 *Kp* are shown for the 30 minute (Dii and Diiii respectively) and the 24h time point (Diii and Dv respectively). (Ei) Foci sizes of K1 and K17 *Kp* during the infection in the liver are as determined for panel Di. Exemplar images of the liver after infection with K1 and K17 *Kp* are shown from the 30 minute (Eii and Eiiii) and the 24h time point (Eiii and Ev). For microscopy images, 10μm tissue sections were stained with antibodies/reagents against *Kp* (green), nuclei (blue) and actin (magenta). Murine infection experiments were performed with the help of Dr David Carreno, and Miss Zydrune Jasiunaite.

4.2.7 hvKp infection promotes neutrophil infiltration, leading to hepatic abscesses formation

As localised neutrophil infiltration is a key hallmark of abscesses, I stained both liver and spleen sections with antibodies against neutrophils and analysed their co-localisation with bacterial foci. As K17-infected mice had negative organ counts as early as 6h post infection, I excluded these early time points from the analysis. I observed gradual recruitment of neutrophils to K1 infected foci over time (Figure 37a; exemplified in Figure 37b), with bacteria with intact capsule still observable even at the late time point. At the later 48h post-challenge time point, around many of the hepatic foci, inflammatory cells formed clusters of approximately 30 cells (Figure 37c), centred around infectious foci which derived from Kupffer cells, clearly indicative of the formation of micro-abscess. Higher magnification (100x) imaging of haematoxylin and eosin stain sections indicated the presence of a clustered inflammatory infiltrate,

histologically in keeping with neutrophils. Inflammatory cells were confirmed as neutrophils by staining tissue sections with the neutrophil-specific anti-Ly6G antibody, which showed aggregate structures reminiscent of the H&E stain. H&E stains of the late time point of K17 revealed far more diffuse inflammatory infiltrate, resembling an uninflamed liver (Figure 37d). In each case, IHC staining of tissue sections with the neutrophil-specific antibody confirmed the identity of the inflammatory infiltrate. Interestingly, staining of F4/80 (Kupffer cell specific) in these later time point livers indicated that *Kp* at the centre of abscesses were F4/80 negative (Figure 37e). This implies that despite earlier persistence within Kupffer cells, bacteria at the later stage may become extracellular through host cell lysis. These data show clearly how neutrophil influx generated abscesses around the infectious foci which had arisen from intracellular replication of the hv*Kp* strain in permissive tissue macrophages.

To test the hypothesis that abscess formation derived from an inability of neutrophils to kill hv*Kp*, Dr David Carreno kindly performed an *in vitro* killing assay with single representative strains from each serotype of both non-hv*Kp* (KL107, and K17) and hv*Kp* (K1 and K2) and murine primary neutrophils (Figure 37f). These data indicated that in the absence of neutrophils in the assay buffer, all strains had a comparable number of CFU/mL in the tube. Following incubation with neutrophils isolated from murine whole blood, K1 and K2 isolates were killed only modestly, whereas both the KL107 and K17 strains showed a significant reduction in bacterial counts following incubation with neutrophils. These data show that in the tissue, and in vitro, K1 and K2 strains were less susceptible to neutrophil mediated clearance than their non-hv*Kp* counterparts.

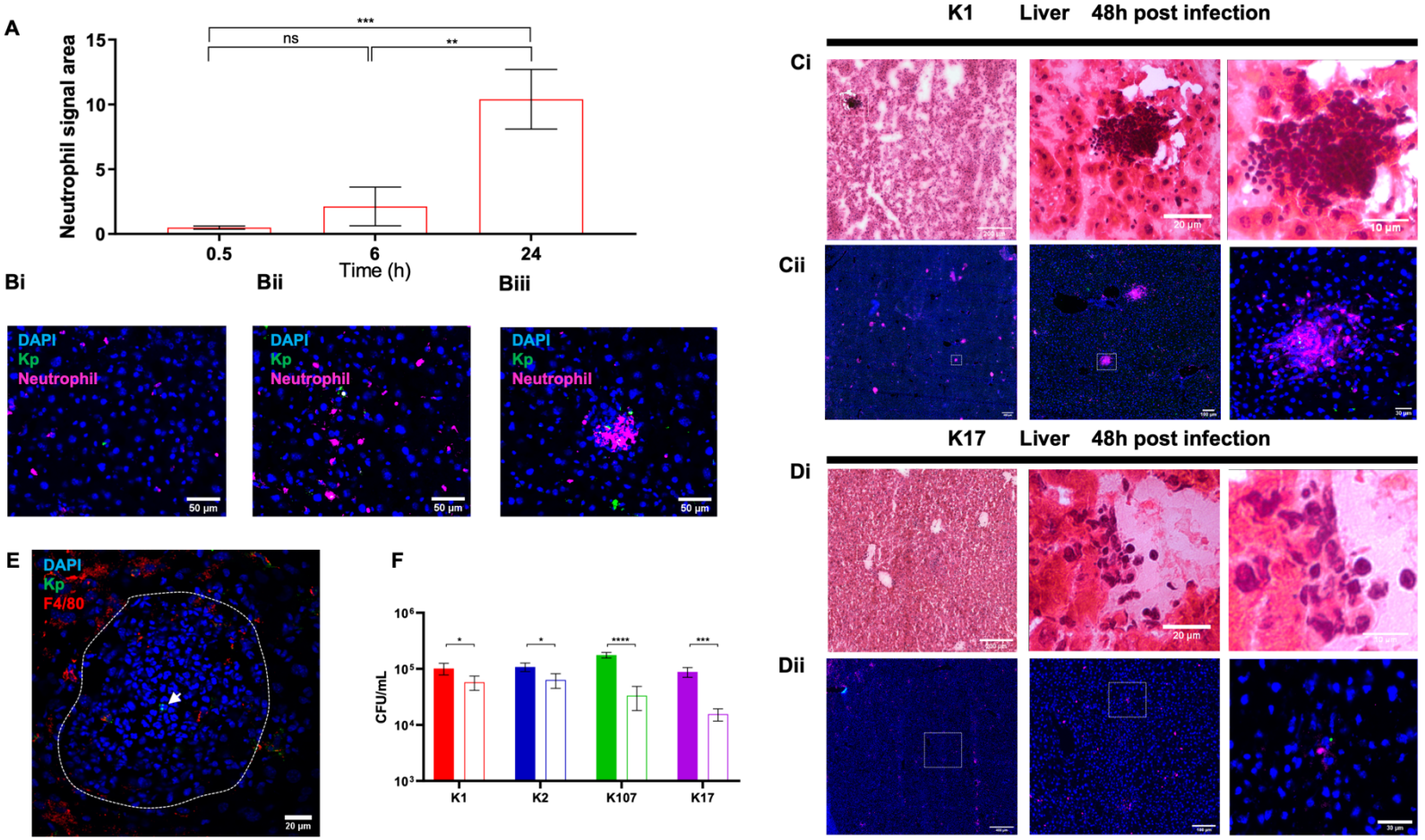
A
Neutrophil signal area
15
10
5
0
ns
**
***
0.5
6
24
Time (h)
Bi
Bii
Biii
DAPI
Kp
Neutrophil
50 µm
E
DAPI
Kp
F4/80
20 µm
F
CFU/mL
10^6
10^5
10^4
10^3
*
*
****
***
K1
K2
K107
K17
K1 Liver 48h post infection
Ci
Cii
20 µm
10 µm
K17 Liver 48h post infection
Di
Dii
20 µm

Figure 37 - *Neutrophil recruitment to bacterial foci in the liver leads to the formation of microabsesses.* (A) Quantification of neutrophil recruitment to infectious foci. Immunostained liver sections from 3 K1 *Kp* infected mice were quantified for neutrophil-associated fluorescence (RFU; relative fluorescence units) in a 25μm radius around bacteria at 30 min, 6h, and 24h post-infection. Statistical significance was determined by 1-way ANOVA. ****; p<0.00005, ***; p<0.0005, **; p<0.005, *; p<0.05, NS; p>0.05. Error bars indicate the standard deviation. (B) Representative image showing neutrophil recruitment to K1 foci at 30 min (Bi), 6h (Bii), and 24h (Biii) post-infection. The scale bar in each image is 50μm. (Ci) Representative H&E stain of mouse liver 48h post-infection with K1 *Kp*, at three increasing magnifications from left to right, with scale bars of 200, 20, and 10 um width respectively. (Cii) Mouse liver sections 48h post-infection with K1, immunostained for neutrophils (magenta), bacteria (green), and nuclei (blue). From left to right, three increasing magnifications are shown, with scale bars of 400, 100, and 30μm respectively. (Di and Dii) Representative H&E and immunostain of mouse liver 48h post infection with K17 *Kp* (details as in panel Ci and Cii). (E) F4/80 stain of a cluster of PMN cells forming visible microabscess in the liver. The border of the cluster of PMN cells are indicated by a dotted white line, and the foci of infection at the centre is indicated by a white arrow. (F) Neutrophil bactericidal assay of hv*Kp* (K1 red, K2 blue) and non-hv*Kp* (K107 green, K17 purple) showing bacterial counts before (filled bars) and after (open bars) 2h incubation with the neutrophils at an MOI of 10.N. Statistical comparison were determined by 1-way ANOVA. ****, p<0.0005, NS; P<0.05. Error bars indicate the standard deviation. Murine infections and neutrophil assays were performed with the help of Dr D. Carreno, and Miss Z. Jasiunaite.

4.2.8 **Histological observations in the spleen**

Compared with the liver, in the spleen a less pronounced neutrophil influx was observed. In mice infected for 48h with both the K1 (Figure 38a), and K107 (Figure 38d) strain, H&E stains were indistinguishable , with identically pronounced marginal zones, and no evidence of dense inflammatory infiltrate. Staining of these sections with a neutrophil specific antibody indicated the presence of some neutrophil clustering in mice infected with the K1 strain (Figure 38b), with this being less pronounced in K107 infected mice (Figure 38c). Importantly, these sections did not show any

inflammatory cell aggregation consistent with abscess formation, which may explain why splenic abscesses are clinically far rarer than hepatic abscesses.

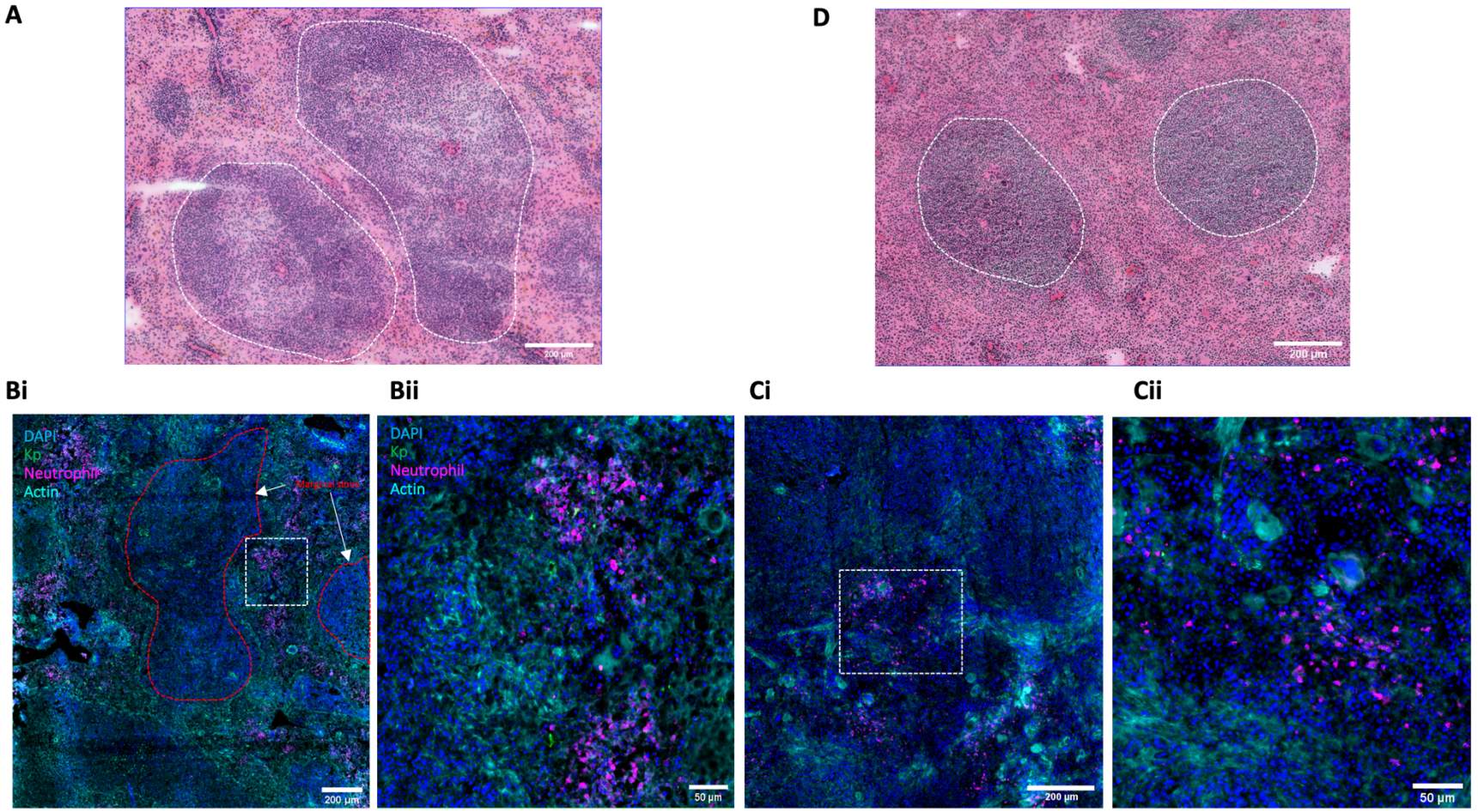
A
D
Bi
Bii
Ci
Cii
DAPI
Kp
Neutrophil
Actin
Marginal sinus
200 µm
50 µm

Figure 38 *- Histological features of Kp infected mouse spleens.* H&E stain of a mouse spleen infected for 48h with hv*Kp* strain NTUH-K2044 (A) or with the non-hv*Kp* strain KPC58 (B). In both images the border between the splenic white pulp and red pulp are shown by a dotted white line. For both images, the scale bar is 200 μm in width. (Bi) Fluorescence image of the murine spleen infected for 48h with hv*Kp*. The border of the splenic white pulp is shown by a dotted red line. A dotted white line indicates an infected area, which is shown at higher magnification in Bii. (Ci) Fluorescence image of the murine spleen infected for 48h with non-hv*Kp*. A dotted white line indicates an infected area, which is shown at higher magnification in Cii. For Bi and Ci, the scale bar is 200 μm in width. For Bii and Cii, the scale bar is 50 μm in width. All samples are stained for nuclei (blue), bacteria (green), neutrophils (magenta) and actin (cyan).

4.2.9 Manipulation of splenic macrophage uptake by monoclonal antibiotic treatment

To test if this phase of pre-abscess intracellular replication could be functionally manipulated, I treated mice with anti-CD169 antibodies that in our *Streptococcus pneumoniae* model blocked uptake and consequent intracellular replication in splenic CD169+ macrophages [253]. I performed an infection experiment with the hv*Kp* strain K1 NTUH-K2044 by treating mice 30 minutes prior to intravenous challenge with an intravenous injection of anti-CD169 antibody. Results at 6h post challenge show that anti-CD169 treated mice had significantly less bacteria in the spleen (Figure 39a). There was no difference in bacterial counts in the liver between blocking antibody and control mice. As expected, splenic MMMs expressed high amounts of CD169, but Kupffer cells did not (Figure 39b). Following infection, there was no up-regulation of CD169 expression in either the spleen, or on the Kupffer cells of the liver (Figure 39b; exemplified in c and d respectively). Lastly, administration of the blocking antibody was found to significantly reduce co-localisation of *Kp* with MMMs in the spleen, confirming the inhibitory effect and specificity of antibody treatment (Figure 39e).

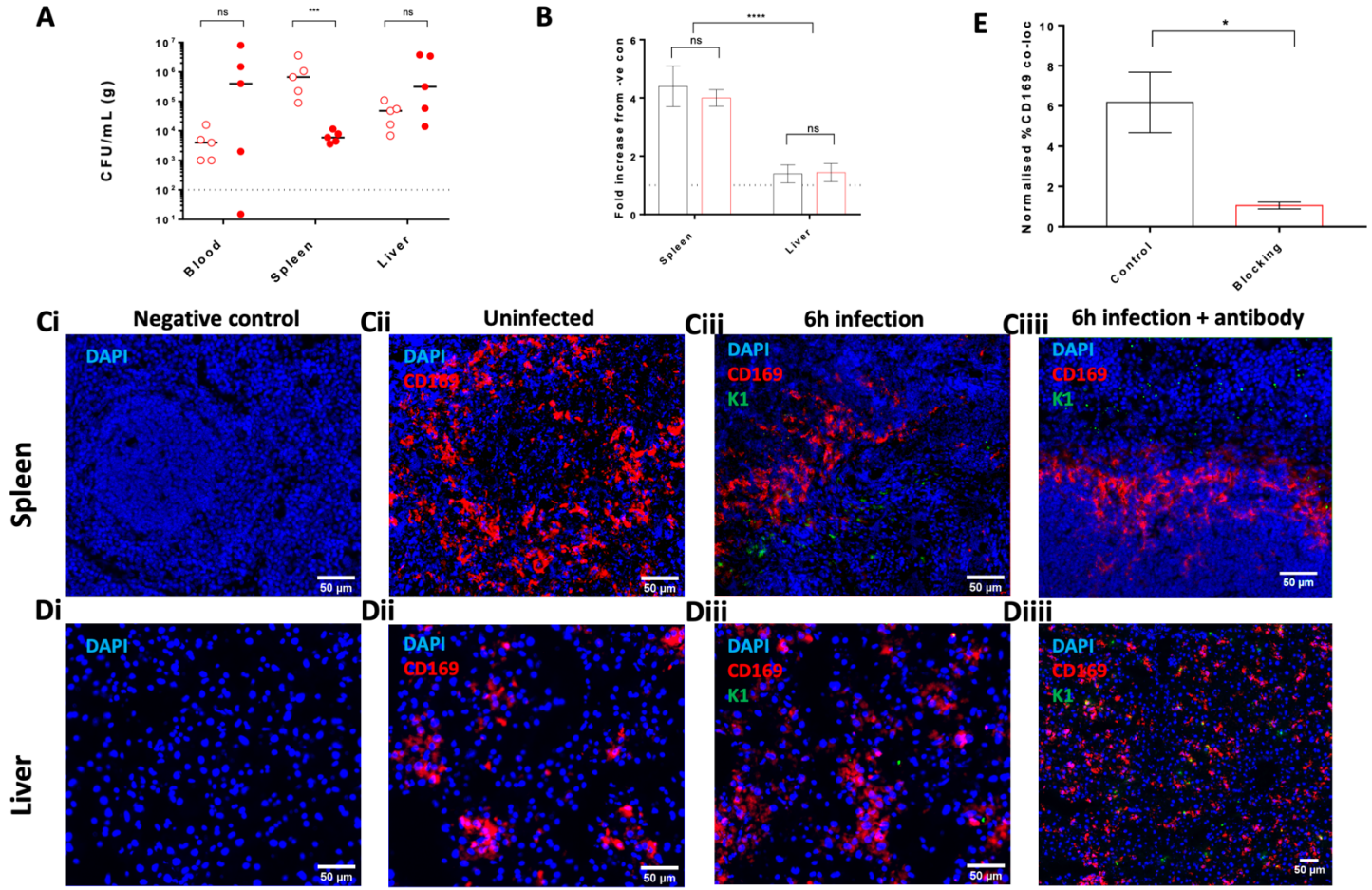
A
ns
***
ns
CFU/mL (g)
Blood
Spleen
Liver
B
****
ns
ns
Fold increase from -ve con
Spleen
Liver
E
*
Normalised %CD169 co-loc
Control
Blocking
Ci
Negative control
Cii
Uninfected
Ciii
6h infection
Ciiii
6h infection + antibody
Spleen
Liver
DAPI
CD169
K1
50 µm
Di
Dii
Diii
Diiii

Figure 39 *- CD169 antibody treatment reduces bacterial counts in the spleen but not the liver.* (A) Mice were pre-treated IV with 10μg anti-CD169 antibody (see methods) 30 minutes prior to IV infection with hv*Kp* K1 strain NTUH-K2044, and samples were taken at 6h post-infection for CFU enumeration and microscopy analysis. Control infected mice are shown by red open circles, whereas antibody treated mice are shown by red closed circles. Statistical significance were determined by ANOVA. ***, $p<0.0005$, NS; $p>0.05$. The limit of detection is shown by a dotted line. The median is indicated by a horizontal full line. (B) Expression of CD169 in splenic peri-follicular areas (which were determined visually by density of nuclei which is indicative of B-cell follicles) in the spleen, or sinusoids in the liver pre, and post K1 infection, relative to a negative control with no primary antibody. Statistical significance were determined by ANOVA. ****, $p<0.00005$, NS; $p>0.05$. The negative control fluorescence is indicated by a dotted line. Exemplar images for negative control, uninfected, infected, and infected + blocking antibody tissue sections are shown for the spleen (Ci-iiii) and liver (Di-iiii) respectively. (E) Analysis of bacterial co-localisation to CD169+ cells 6h after IV infection, with or without pre-treatment of mice with the anti-CD169 blocking antibody. The values are normalised to the area of CD169 signal in each tissue. The data are representative of 3 independent mice from each group. Statistical significance were determined by a student's t-test. *; $p<0.05$. Error bars indicate the standard deviation.

4.2.10 Evidence for release of bacteria from Kupffer cells

Following from my observation in section 4.2.7 that at the later time points, bacteria at the centre of abscesses were F4/80 negative, I attempted to find evidence of cell lysis prior to the onset of full blown disease. I found evidence, even as early as 6h post infection for macrophage membrane disruption (Figure 40a), in which bacteria could be seen spreading across macrophage membrane stains which may indicate a lysis, or bacterial egress event. Next I analysed 24h infected livers, and identified microabscesses based on the present of large clusters of PMN cells (Figure 40b). Within these inflammatory cell clusters I observed bacteria distributed across multiple cells at the centre of the abscess, in quantities far exceeding that observed at the early stages of infection. This may indicate release of the intracellular microcolonies observed at early stages of infection, and their distribution across the maturing

abscess. Future work employing live imaging of infected primary cell cultures will be required to definitively demonstrate the lysis of host cells mediated by intracellular replication.

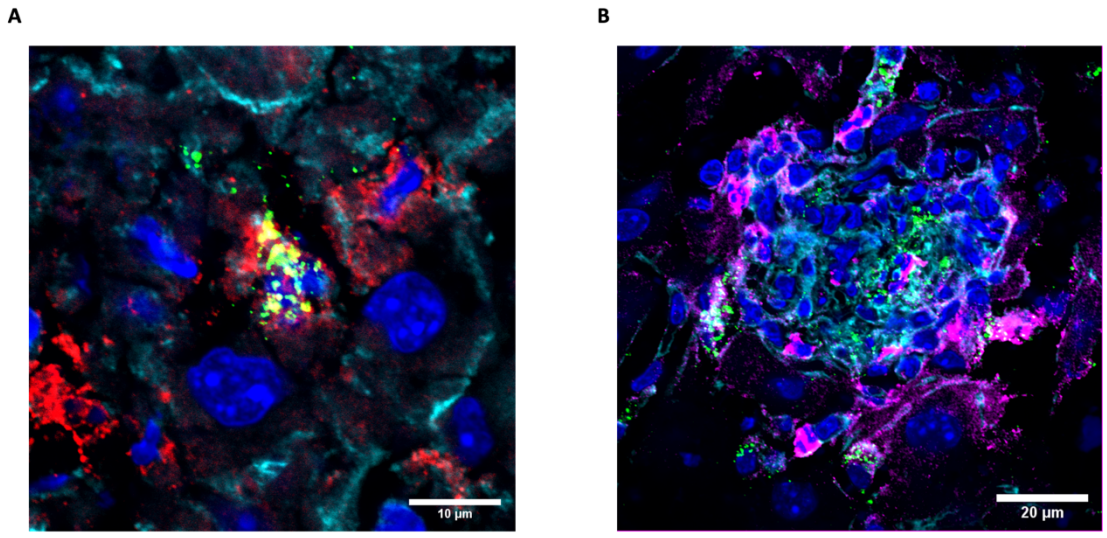

Figure 40 *- Evidence of Kupffer cell lysis following infection.* Mice were infected for 24h with 10^6 CFU of *Kp* strain NTUH-K2044, and their livers were analysed by confocal microscopy followed by staining with different antibodies. (A) Shows a Kupffer cell which is heavily infected with *Kp*, such that the bacteria extend across the cell into the neighbouring area. Nuclei; blue, *Kp*; green, CD169; red, Actin; cyan. (B) Shows a maturing abscess with *Kp* spread across multiple cells in many cases co-localising with neutrophils. Nuclei; blue, *Kp*; green, Ly-6G; magenta.

4.2.11 Establishment of *ex vivo* liver-spleen perfusions as a translational infection model

During our studies of pneumococcal infection, we used perfusions of abattoir sourced pig spleens as a translational model of infection. Owing to the major role of the liver in the pathogenesis of *Kp* infection, I aimed to determine if we could establish a model of liver-spleen co-perfusion which could serve as a model of systemic *kp* infection. Details of the perfusion set up can be found in the materials and methods section.

Briefly, I cannulated the portal vein and hepatic artery of the liver, in addition to the splenic artery, post mortem. All other vessels were ligated. I then flushed both organs with Soltran solution, to preserve the tissue, and to remove any clots, for transport to the lab. Transport of the organs to the lab was performed within 40 minutes of retrieval at the abattoir, where samples were then washed an additional time with 500mL of saline solution. Vessels were then plugged into the perfusion circuit. The experimental setup is demonstrated diagrammatically in Figure 41a. Throughout the perfusion, I observed a steady flow rate through the splenic artery and the portal vein of between 0.10 – 0.12 L/min (Figure 41b). I also monitored blood-gas parameters throughout the perfusion time course to confirm maintenance of physiological conditions. I observe that blood pH gradually decreases across the time course to a minimum of 7 at 3h post infection (Figure 41c), although pH 7 is still physiologically relevant. It is well reported that the spleen is especially fragile, hence prolonged perfusion of the liver may be possible without inclusion of the spleen [481]. Blood concentration of hemoglobin (ctHb) decreased from ~110 g/L to ~95 g/L at 3h after infection (Figure 42d). The functional saturation of hemoglobin by oxygen (FO2Hb) only marginally decreased from 99.5% to 99% after 3h of perfusion indicating efficient oxygenation by the circuit (Figure 42g). Lastly, the blood concentration of glucose remained stable at around 30 nmol/L throughout the perfusion, even in the absence of exogenous glucose, indicating functional gluconeogenesis of the liver (Figure 42q).Establishment of the perfusion model, and running of the subsequent experiments was performed with the kind help of Dr David Carreno, Mr Ryan Hames, Miss Zydrune Jasiunaite, Dr Wen Chung, and Professor Ashley Dennison.

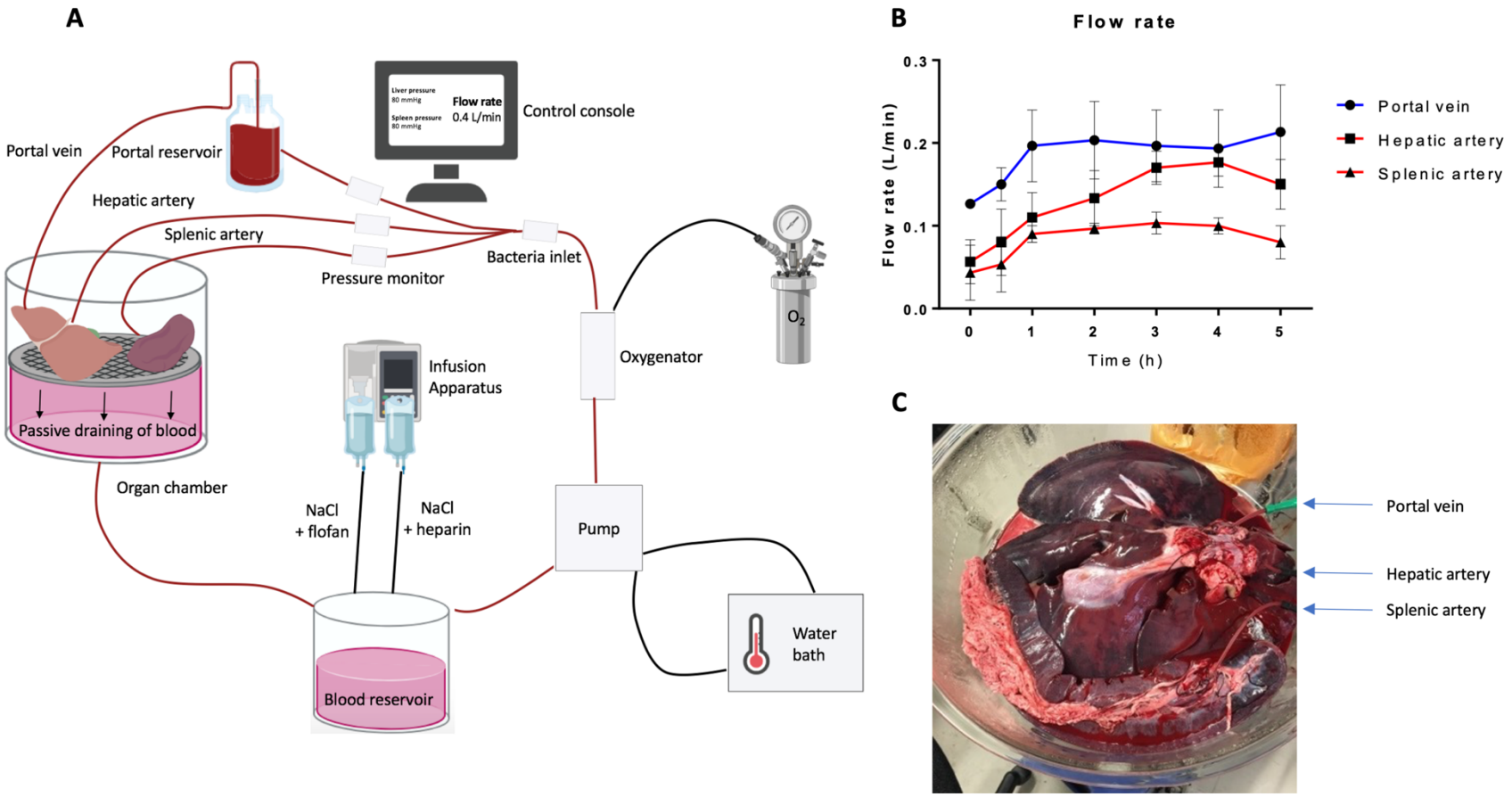
A
Portal vein
Portal reservoir
Hepatic artery
Splenic artery
Pressure monitor
Liver pressure
80 mmHg
Spleen pressure
80 mmHg
Flow rate
0.4 L/min
Control console
Bacteria inlet
Oxygenator
O_2
Infusion
Apparatus
Passive draining of blood
Organ chamber
NaCl
+ flofan
NaCl
+ heparin
Pump
Water
bath
Blood reservoir
B
Flow rate
Flow rate (L/min)
0.3
0.2
0.1
0.0
0
1
2
3
4
5
Time (h)
Portal vein
Hepatic artery
Splenic artery
C
Portal vein
Hepatic artery
Splenic artery

Figure 41 - *A normothermic model of liver-spleen co-perfusion for studies of Kp-host interactions.* (A) The circuit consists of a chamber which holds both spleen (cannulated via the splenic artery) and liver (cannulated by the hepatic artery and portal vein). Blood drains from this chamber into a blood reservoir which is fed with Flofan (vasodilator) and Heparin (anticoagulant) solutions. From here, blood is pumped through a water bath which maintains a stead 37°C temperature, and then through an oxygenator. At this point, there is an inlet for bacterial inoculation, before the circuit splits into 3 vessels; the splenic artery, the hepatic artery, and the portal vein via an additional blood reservoir. Each of these vessels is monitored for pressure, which is relayed on the control console. (B) Flow rate is monitored for each vessel at regular time points. The portal vein is shown by black circles with a blue line, the hepatic artery is shown by black squares with a red line, and the splenic artery is shown by black triangles with a red line. (C) Shows a photograph of the organs in situ, with the cannulated portal vein, splenic artery, and hepatic artery indicated by blue arrows.

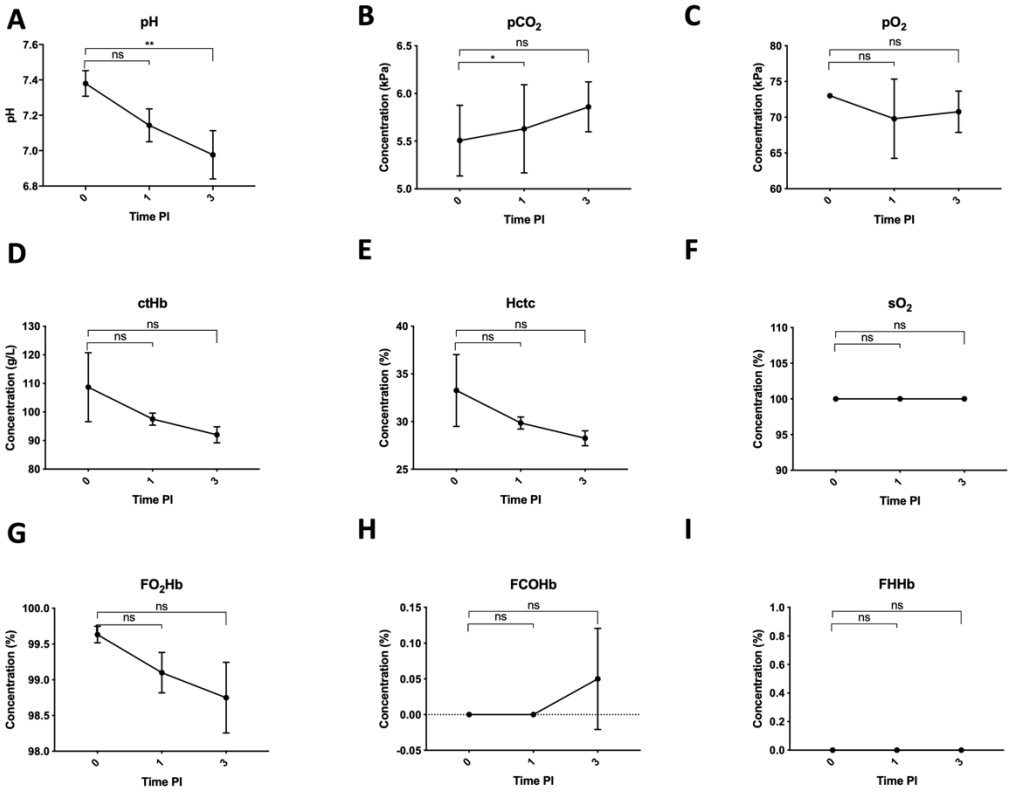

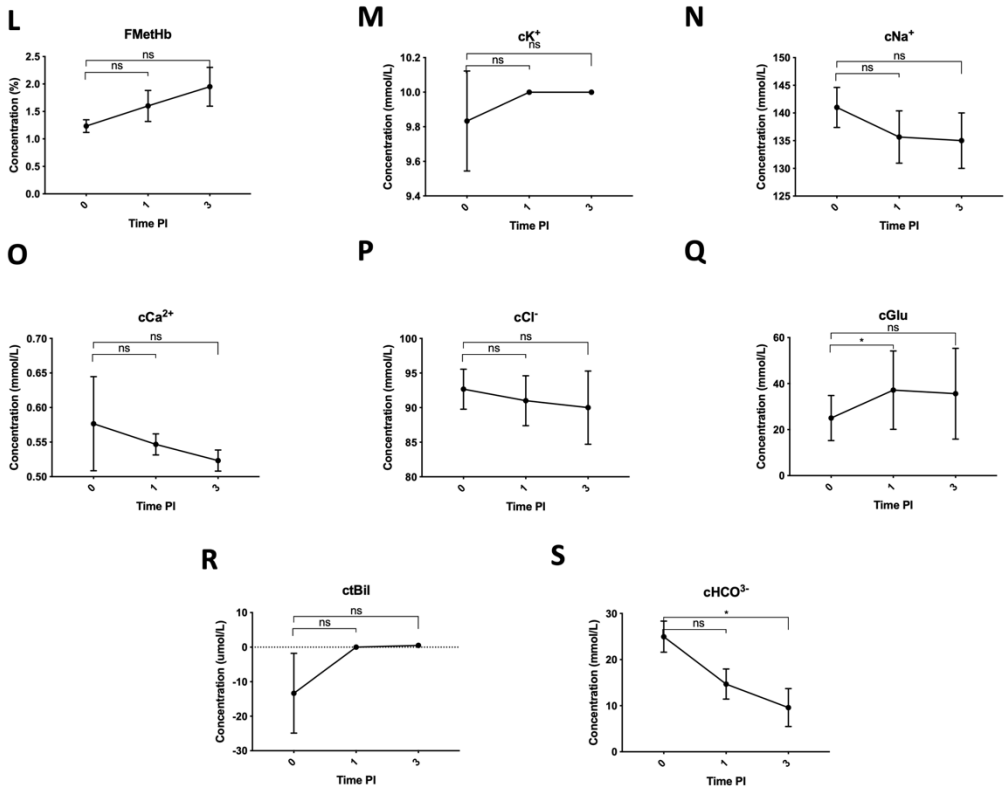

Figure 42 *- Blood gas analysis of porcine blood following ex vivo perfusion.* Blood was taken and analysed with the Radiometer ABL90 series system in the ICU at the University of Leicester for pH (A), partial pressure of carbon dioxide (pCO2; B), partial pressure of oxygen (PO_2; C), total hemoglobin (ctHb; D), ratio of erythrocytes to blood volume (hctc: E), saturation of hemoglobin with oxygen (sO_2; F), fractional oxyhemoglobin (FO_2Hb; H), fractional carboxyhemoglobin (FCOHb; I), fractional deoxyhemoglobin (FHHB; G), methemaglobin concentration (FMetHb; L), potassium concentration (cK^+; M), sodium concentration (cNa^+; N), calcium concentration (cCa^{2+}; O), chloride concentration (cCl^-: P), glucose concentration (cGlu; Q), bilirubin concentration (ctBil; R), bicarbonate concentration ($cHCO_3$-; S). PI; post infection. Statistical comparison between 1, and 3h PI was compared to the time 0 value by 1-way ANOVA. *; P<0.05, NS; non-significant.

4.2.12 Scanning microscopy enables detailed interrogation of porcine organ microarchitecture

Detailed interrogation of organ microarchitecture in animals other than mice and humans are hampered by the resolution of low magnification microscopy systems, the lack of tissue context in high magnification systems, and the lack of availability of

antibodies for these species. I aimed to used the novel scanning fluorescence microscope (the Vectra Polaris) in conjunction with staining of macrophage populations of interest (CD163+, and CD169+) in the porcine spleen and liver to delineate porcine liver and spleen microarchitecture. I also stained with Phalloidin (actin-specific) to provide indication of the location of vasculature. In the liver, actin staining allowed for the identification of central vessels (Figure 43ai) with unstained (presumable endothelial) cells separating these structures from the Kupffer cell-rich sinusoidal system. CD169+ Kupffer cells (Figure 43aii) were found distributed across the hepatic lobuli. In the spleen, staining of CD169 allowed for the visualization of peri-arteriolar lymphoid sheathes which lined the follicles surrounding central vessels (Figure 43bi). Instead, staining of CD163 (Figure 43bii) allowed for the visualization of red pulp macrophages which were present in the tissue outside of follicular structures. Together, these observations provided the tools for analysis of bacterial co-localisation in the subsequent sections.

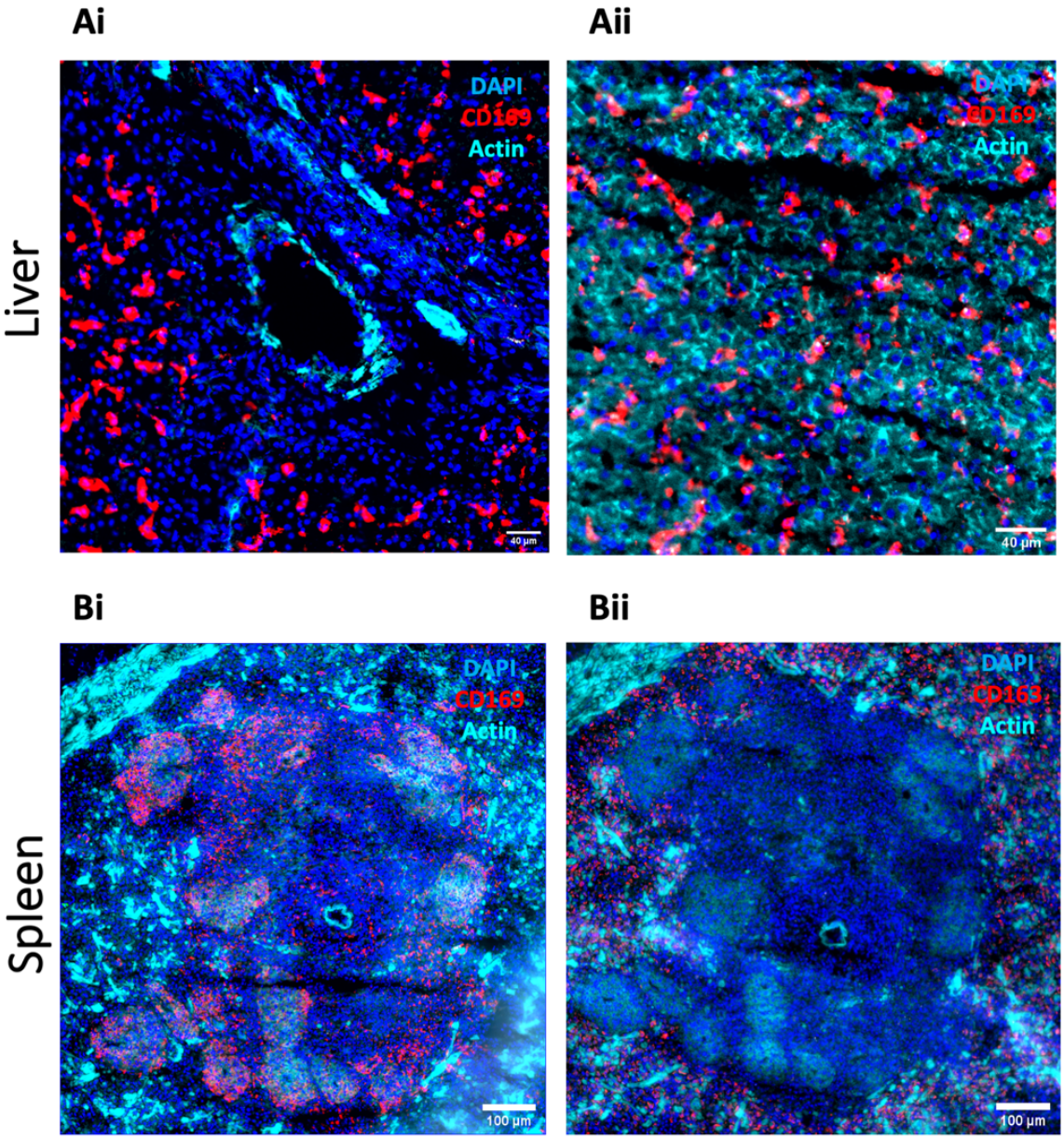

Figure 43 - *Microarchitecture of the porcine liver and spleen visible through multispectral imaging.* (Ai) Image of a hepatic vessel at the intersection of 3 porcine liver lobuli, and (Aii) image of Kupffer cell distribution in the parenchyma of the porcine liver. Both sections are stained for nuclei (blue), CD169 (red), and actin (cyan). In both AI-2, the scale bar is 40 µm in width. (B) Low magnification image of a porcine splenic follicle, with the major artery in the centre of the image, stained for nuclei (blue), actin (cyan), and either CD169 (red) which identifies the peri-arteriolar lymphoid sheathe macrophages (Bi), or CD163 (red) which delineated the splenic red pulp macrophages (Bii).

4.2.13 Replication of hv*Kp* within macrophages in a natural host during *ex vivo* organ perfusion

I next aimed to determine if our observations that hv*Kp* replicate within macrophages in the early stages of infection in the mouse, could be translated using the liver-spleen co-perfusion model. As K2 ST25 isolates have been reported as an emerging cause of sepsis in piglets [482, 483], I used this strain for infections of the *ex vivo* circuit. Three independent abattoir-sourced paired spleens and livers were co-perfused with autologous blood and serial biopsies, and blood samples were taken, and analysed by plating of the CFU, and microscopy. Following infection of the circuit with the hv*Kp* K2 ST25 strain GMR151, bacteria were rapidly cleared from the circuit (Figure 44a). At the 30-minute time point, both organs contained ~3 x 10^3 CFU/g of tissue . For the remaining time points, I saw a gradual increase in the number of CFU detected in both spleen and liver biopsies, with an estimated doubling time of 100 minutes, and throughout this period the blood remained clear. In contrast to the mouse model – where hv*Kp* were not cleared efficiently from the blood – bacteria were rapidly eliminated in the *ex vivo* porcine system. I hypothesised this may be due to serum-bactericidal activity present in the porcine sera, as these animals were sourced from abattoirs and were not raised in pathogen free conditions. A killing assay in blood and plasma from blood used to perfuse the organ demonstrated that blood and serum, from each organ donor pig had bactericidal activity against GMR151, with approximate clearance half-lives of 20 minutes (Figure 44b).

To evaluate the organ distribution and possible growth dynamics of the hv*Kp* K2 ST25 strain, I analysed, over time, biopsies from the *ex vivo* organs by confocal and high-throughput scanning microscopy, following staining of bacteria and cellular markers. In both the liver and the spleen, at 30 minute post-infection the hv*Kp* were present as single cells, or as pairs (Figure 44c, example images in di and ei). At 5h post-infection, significantly larger (P=0.048 for liver, and P=0.038 for spleen) clusters of bacteria were observed (Figure 44c, example images in dii and eii). In contrast to the mouse data, no bacteria were found in the circulating pig blood at 1h post-infection, consistent with the conclusion that the increase in intracellular bacteria over the first 5h post-infection originated from bacterial replication, rather than continuing uptake of bacteria. To identify with which cells hv*Kp* K2 ST25 was associated, the distribution of *Kp* was

determined among macrophage subsets in the porcine liver and spleen – namely, the CD169+ Kupffer cells, the splenic CD163+ red pulp macrophages and CD169+ periarteriolar sheath macrophages. Within the spleen, at 30 minutes post-infection, *hvKp* were most abundant in CD163+ macrophages but by 5h post-infection, they were mainly within the CD169+ macrophages (Figure 44fi). In the liver, CD169+ Kupffer cells remained the majority hv*Kp* infected cell population throughout the infection time course (Figure 44fii). Similarly to the murine data, confocal microscopy and 3D reconstruction demonstrated that hv*Kp* were present in the intracellular environment, as evidenced by the presence of the bacteria within the CD169 surface marker stain, in both the liver (Figure 44g), and the spleen (Figure 44h).

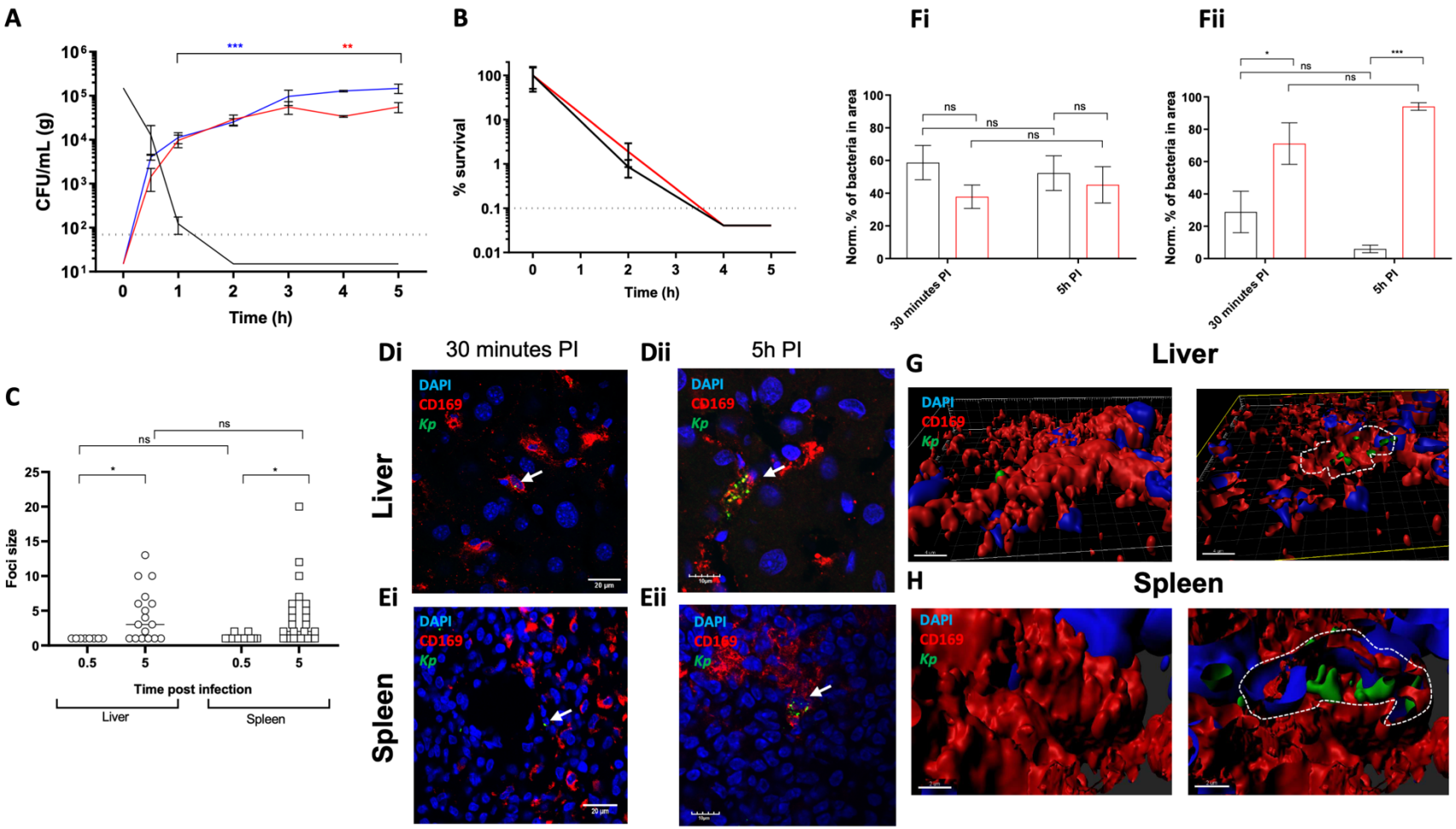
A
CFU/mL (g)
Time (h)
***
**
B
% survival
Time (h)
Fi
Norm. % of bacteria in area
ns
30 minutes PI
5h PI
Fii
Norm. % of bacteria in area
*
ns
***
C
Foci size
Time post infection
0.5
5
Liver
Spleen
Di
30 minutes PI
Dii
5h PI
Liver
Ei
Eii
Spleen
DAPI
CD169
Kp
G
Liver
H
Spleen

Figure 44 - *Ex vivo infection of perfused porcine liver and spleen.* (A) Bacterial concentrations in porcine blood (CFU/mL; black line), liver biopsies (CFU/g; red line) and spleen biopsies (CFU/g; blue line) after infection of the perfusion circuit with 6.5 x 10^7 CFU of *Kp* GMR151 K2-ST25. Data are representative of 3 independent perfusion experiments. Statistical significance was determined using a t-test. (B) Whole blood (black line) and plasma (red line) bactericidal assay of strain GMR151. Data are representative of three independent experiments. (C) Size of infectious foci (number of bacteria/macrophage) at 30 minute and 5h post-infection in the porcine liver and spleen. Data were counted from confocal images of at least 20 macrophages per group. Representative images of foci associated with CD169+ cells in the porcine liver (D) and spleen (E) at 30 minutes (i) and 5h (ii) post-infection. Nuclei are stained with DAPI (blue), CD169 is shown in red, and *Kp* are shown in green. (Fi) Normalised distribution of bacteria in splenic CD163 (black) and CD169 (red) macrophages at 30 minutes and 5h post-infection. (Fii) Distribution of bacteria in Kupffer cells (black) and unstained area (red) at 30 minutes and 5h post infection. Data were normalised per unit area. (G-H) 3D reconstruction of confocal Z-stacks, demonstrating that *Kp* are intracellular in CD169+ cells, within liver and spleen respectively. Nuclei are shown in blue, bacteria in green, and CD169 in red. The cell borders are indicated by dotted white lines. Imaging of *Kp* foci in the porcine organs was kindly provided by Miss Zydrune Jasiunaite.

4.2.14 **Neutrophil recruitment in the porcine organs**

To evaluate events leading to abscess formation in the porcine organs, I determined if neutrophils were recruited to sites of infection. The neutrophils in our *ex vivo* model derive from one litre of autologous heparinised blood used for the organ perfusion. Using high resolution scanning images followed by image analysis, I selected 10 random, circular tissue areas (radius 50μm) which both had bacteria present, or bacteria absent and analysed the total neutrophil fluorescence in these areas. These data indicated that between 30 minutes and 5h post infection, the amount of neutrophil signal significantly increased around infectious foci in the liver, indicating that neutrophils were recruited to the site of infection in this *ex vivo* model (Figure 45a). Furthermore, the amount of neutrophil signal in non-infected areas remained static, indicating that this neutrophil influx was an infection-specific signature. In the spleen,

no significant neutrophil recruitment was observed in infected compared to uninfected areas (Figure 45b). When considering the whole tissue section, total neutrophil fluorescence increased significantly over time in the spleen and liver (Figure 45c). Microscopy demonstrated that in early biopsies neutrophils were scattered throughout the liver tissue, with a strong preponderance for the vascular spaces separating hepatic lobuli, while at the later time point neutrophils clearly showed clustering around infectious foci (Figure 45d). In the spleen, a significant increase of neutrophils could be detected over time, but localisation remained localised to the red pulp surrounding the follicle (Figure 45e).

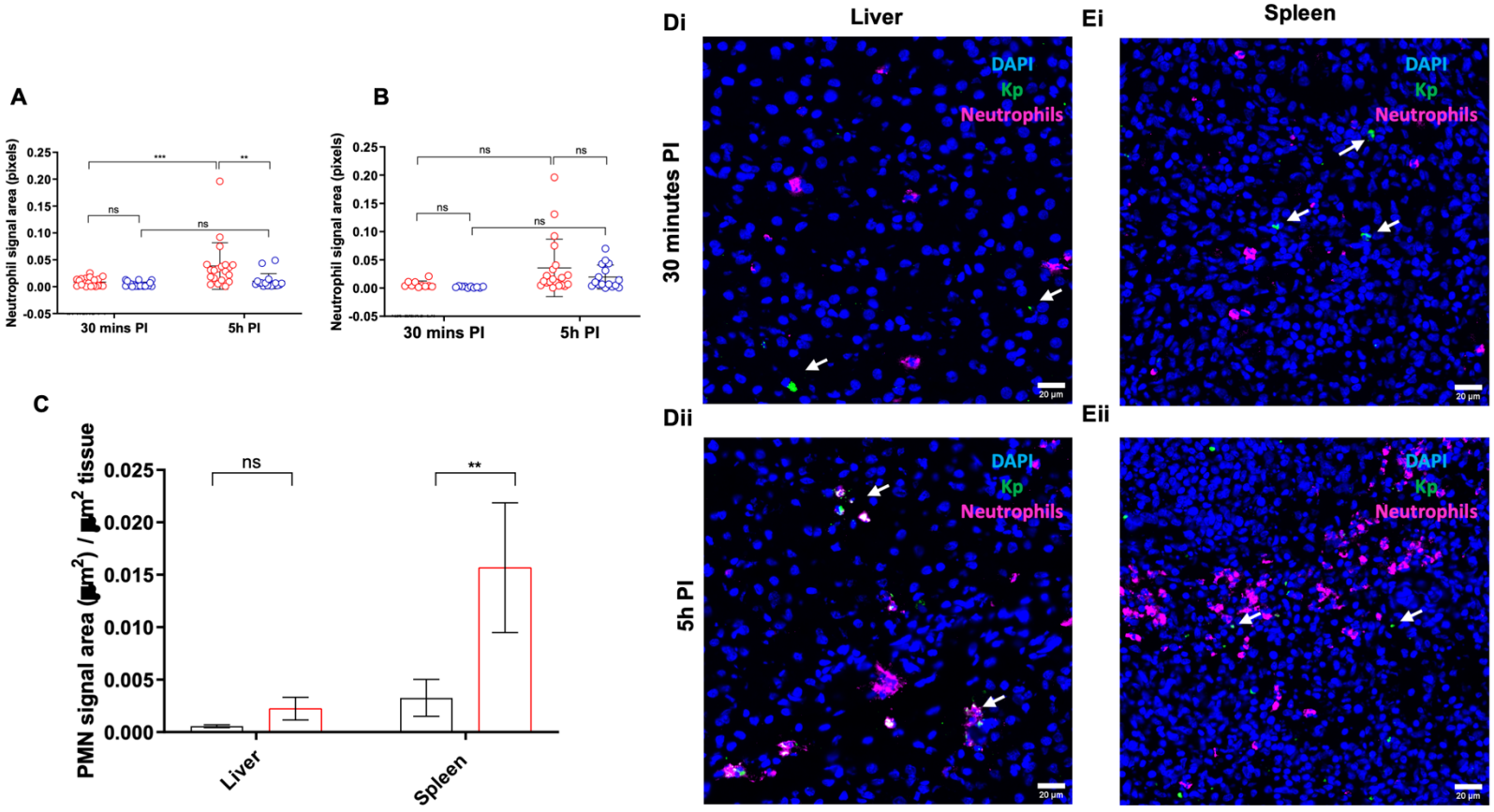
A
B
Neutrophil signal area (pixels)
0.25
0.20
0.15
0.10
0.05
0.00
-0.05
***
**
ns
ns
30 mins PI
5h PI
C
PMN signal area (μm²) / μm² tissue
0.025
0.020
0.015
0.010
0.005
0.000
ns
**
Liver
Spleen
Di
Liver
Ei
Spleen
30 minutes PI
5h PI
Dii
Eii
DAPI
Kp
Neutrophils
20 μm

Figure 45 *- Neutrophil recruitment in in the ex vivo porcine system.* (A) Neutrophil signal area within a 50 μm radius of infected (red circles) or random non-infected (blue circles) macrophages, at 30 minutes and 5h post-infection of the porcine liver. (B) Comparable analysis of neutrophil association to macrophages in the spleen. Data are representative of entire tissue sections (~2cm^2) from 3 replicate organs. Statistical significance were determined using a 1-way ANOVA. . ***; $p<0.0005$, **; $p<0.005$, *, NS; $p>0.05$. (C) Neutrophil influx to the entire tissue section (30 min black, 5h red). Whole tissue sections from 3 replicate organs were analysed. Data are expressed as neutrophil fluorescence signal area per unit whole tissue area . Representative neutrophil immunostained sections of liver (D), and spleen (E) at the 30 minute (i) and 5h (ii) time point.

4.2.15 Investigation of antibody titres in pig sera

I was interested to identify whether the serum from pigs used for perfusion experiments contained anti-*Kp* antibodies because (1) porcine sera and whole blood were bactericidal, which may be caused by IgG-mediated deposition of complement, and (2) Fc-receptor mediated phagocytosis may pre-dispose bacteria in this model to a different fate of those in the mouse model. To achieve this, I utilised a whole cell ELISA probing strain GMR151 and the unrelated K6 type strain ATCC 700603 with dilutions of each serum, using BSA as a control antigen. In addition, I utilised sera from gnotobiotic pigs which were removed by caesarean section from sows prior to weaning as a negative IgG control (kind gift of Professor Andrew Rycroft), and sera from 5 adult pigs administered with an autologous *Kp* ST25 whole cell vaccine as a positive control (kind gift of the Animal and Plant Health Protection Agency). An example titration is shown in Figure 46a, and demonstrates that vaccinated sera titrate out far later than their non-vaccinated, and germ free counterparts. Analysis of titres against GMR151 (defined as the reciprocal of the first dilution where a signal greater than the negative control was detected) indicated values ranging between 512-2048 for unvaccinated sera, whereas vaccinated sera had titres ranging between 2048 and 8192 (Figure 46b). Interestingly, the same pattern was observed when probing the unrelated K6 strain (Figure 46c) indicating that sera used in our perfusion experiment contained cross reactive antibodies, and that autologous vaccination with K2 ST25 also induces a cross-reactive immune response. I therefore conclude that the porcine

system differs from that of the mouse in that the former is immunologically naïve, and the latter contains *Kp*-specific antibodies.

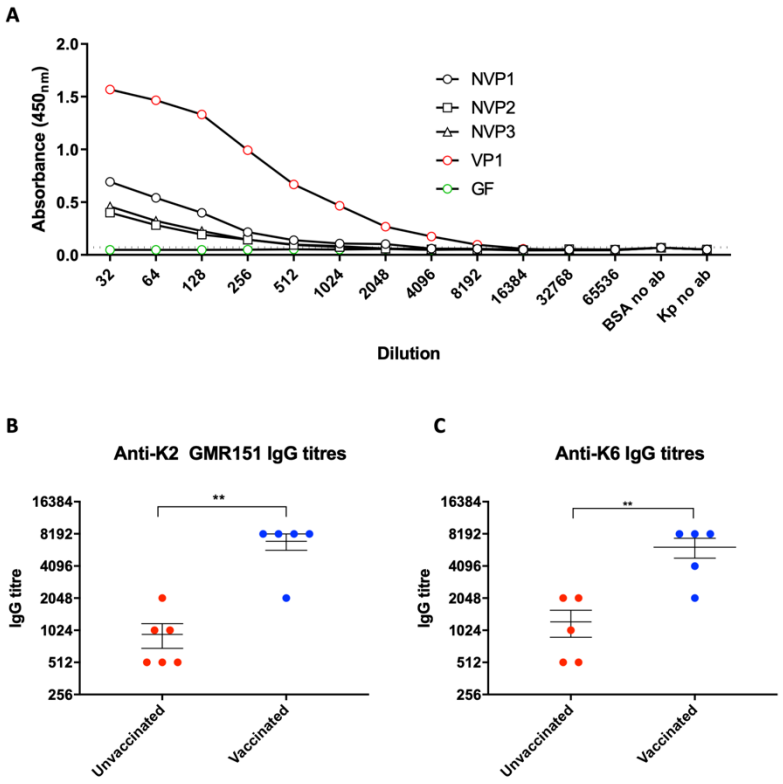

Figure 46 *- Detection of IgG binding to whole Kp cells by ELISA.* (A) Whole cells of *Kp* GMR151 were coated onto ELISA plates as described in the methods section. Serial dilution were prepared of non vaccinated pigs (NVP) used in perfusion experiments 1 (open circles), 2 (open squares), and 3 (open triangles) in ELISA blocking buffer. As a positive control, sera from pigs given an autologous ST25 *Kp* vaccine provided by the Animal and Plant Health Protection Agency was used (red open circles). As negative control, germ-free pig sera (open green circles) provided by Professor Andrew Rycroft was used. As addition controls wells coated with bovine serum albumin (BSA), and *Kp*, were probed with only blocking buffer. Serial dilutions were probed against coated ELISA plates, followed by detection using an anti-porcine IgG secondary antibody conjugated to horse raddish peroxidase, and colorimetric detection using TMB. Absorbance was detected at a wavelength of 450 nanometers (nm). Titrations were performed in duplicate on at least two independent experiments. Titres were defined as the reciprocal of the final dilution where signal greater than the background could be detected. Titres for the K2 isolate GMR151 (B) and the unrelated K6 isolate ATCC 700 603 (C) are shown in the figure.

4.3 Discussion of chapter

Klebsiella pneumoniae invasive tissue abscess caused by serotype K1 and K2 isolates is an emerging condition of immense clinical concern [484]. The recent description in Asia of ST11 carbapenem-resistant strains acquiring the virulence plasmid conferring hypervirulent phenotypes pose a substantial threat to human health (Gu et al., 2018). Not only are these infections exceptionally difficult to treat, but there is a fundamental lack of understanding of the microbial and host factors which contribute to the pathogenesis of tissue abscess, which hampers the development of novel therapies. In this chapter, I have demonstrated in a number of basic (murine, and *in vitro*) and translational (porcine organ perfusion) models that diverse phylogroups of *Kp* can be distinguished in their pathogenesis by their interaction with tissue-resident macrophages and neutrophils.

4.3.1 Insights into mechanisms of abscess formation

The pathogenesis of K1 and K2 *Kp* infection are characterised by the onset of splenic and hepatic abscess formation [241, 484, 485]. Tissue abscesses consist of a massive influx of white immune cells including neutrophils and tissue necrosis [486]. It is known that in the pathogenesis of *S. aureus* kidney abscess formation neutrophils are recruited to infectious foci, and that bacterial factors subvert neutrophil killing mechanisms mediated by neutrophil traps, which subsequently exclude macrophages from the encapsulated structure that results [487]. Neutrophils are known to kill by both intracellular, phagocytic mechanisms, and by the extracellular NETosis mechanism in which extracellular traps are released to capture pathogens, in addition to the contents of anti-microbial and cytotoxic granules [488]. Furthermore, it is known that intracellular infection of macrophages with *Kp* promotes both apoptosis and pyronecrosis; the latter of which is known to promote neutrophil migration to inflammatory sites [489, 490]. Published literature are available to demonstrate that lineages of non-hv*Kp* are effectively killed by human neutrophils, but that hv*Kp* are resistant to both extra, and intracellular neutrophil killing mechanisms [491, 492]. Our data indicate hv*Kp* are able to replicate and persist in the murine spleen and liver for many days, and that this persistence promotes ongoing neutrophil recruitment to the sites of infection. Examining previous observations together with our own, we propose

a model in which neutrophils recruited to the spleen and liver, can effectively kill non-hv*Kp* synergistically with macrophages, but not hv*Kp* [493–495]. Resistance to killing then promotes continual neutrophil recruitment and the continued release of anti-microbial granular agents promote tissue cytotoxicity at the infection focus, which after sustained infection results in abscess formation in the liver, but less clearly in the spleen. The liver and spleen are highly divergent in their microarchitecture, physiological function, and importantly in their macrophage heterogeneity. In this study we identified only diffuse influx of neutrophils into the spleen compared with the liver, and the immunological mechanisms underpinning this observation require further investigation.

4.3.2 Importance of considering clinical epidemiology in pathogenesis studies

A large number of studies examining pathogenesis utilise single, laboratory-adapted strains of pathogens to study infection, despite these isolates often not reflecting current clinical epidemiology. This approach allows for detailed characterisation of specific bacterial factors contributing to disease pathogenesis but is unlikely to capture the full complexity of pathogenic mechanisms across related strains. *Kp* is an excellent example of a pathogen where strains of diverse sequence types and phylogenetic relatedness, can cause diseases with similar clinical presentation [496–498]. In the case of hv*Kp*, the propensity to cause tissue abscess in the immunocompetent host, and in the case of non-hv*Kp*, a predominate association with nosocomial bacteraemic infections. In this chapter, I confirm propensity of hv*Kp* strains to cause massive localised inflammation consistent with abscess formations in the mouse model, whereas non-hv*Kp* strains do not. Our strain screening analysis indicates that despite their being divergent lineages even within hv*Kp* and non-hv*Kp*, that that these two general groups can be differentiated by their ability to persist within murine macrophages, an observation which may have profound implications for the management of infections caused by these groups of strains. The most likely phenotype conferring this within host fitness is the hyper-viscous phenotype which is common to both K1 and K2 isolates. In our model, this a major contributor in respect of the ability to survive within the cell, but does not determine tissue tropism, as bacteria from both groups localise to the same compartments but have different

numbers of bacteria per phagocyte – an observation consistent with the within-cell replication of the former group, but not the latter. This raises the point, in contrast to what is reported by Cano et al. [499] in lung derived macrophages, that *Kp* capsule may be a major determinant of intracellular fate in the spleen and liver. It is well known that K1 and K2 capsule types are highly resistant to phagocytosis compared with other capsule types [500], but their contribution to within cell survival requires further exploration. Hoh and others (2019) [501] recently demonstrated the critical role of Kupffer cells in control of hv*Kp* infection. My data extends these observations, by highlighting a "double edge sword scenario", in that while Kupffer cells (and indeed other tissue macrophages) can efficiently sequester systemic *Kp*, they also form a replicative niche which plays a critical role in the pathology of tissue abscess formation. These data provide a logical framework, for the study of pathogenesis in single, representative isolates of *Kp* to which bacterial factors can be attributed to pathogenic mechanisms.

4.3.3 ***Kp* as an intracellular pathogens**

In recent years, our group and others have challenged the binary definition of intra, and extracellular pathogens. Our work on *Streptococcus pneumoniae* demonstrated a critical role for permissive, intracellular replication of organisms in the spleen in overcoming host clearance mechanisms, eventually resulting in a monoclonal bacteremia [253]. *K. pneumoniae* is another organism, traditionally considered to be extracellular during its pathogenesis. Despite this, studies have alluded to the ability of *Kp* to persist within macrophages [499, 502]. Cano et al. demonstrated that *Kp* strain ATCC®43816 (K2) was able to persist within murine and human derived, immortalized macrophage cell cultures, by avoiding delivery to host lysosomes. This study is the first to document the tissue distribution and growth dynamics of *Kp* in systemic host compartments *in vivo*.

4.3.4 **Implications for therapy**

Clinical management of non-hv*Kp* is extremely difficult due to extremely high levels of drug resistance [503], which in many cases leaves only colistin as a last resort antimicrobial therapy, although colistin resistance and pan-drug resistance in *Kp* are now reported [243, 504]. Even more concerning is the emergence of both

hypervirulent, and MDR strains of *Kp* [505]. hv*Kp* provide their own unique clinical management problems, due the difficulties in drainage of tissue abscesses, and the opportunity of relapsing infection due to extravascular reservoirs of infectious organisms within the abscess. The recommended treatment for hv*Kp* infection is adequate drainage of metastatic tissue abscess, followed by treatment with either a third generation cephalosporin, or in the case of ESBL-negative strains, the combination of ampicillin-sulbactam and a quinolone [506]. This chapter highlights a critical intracellular phase of the pathogenesis of *Kp* infection, a key consideration when selecting therapeutic drugs for an optimum pharmacological effect. Cephalosporins and quinolones both have modest accumulation within macrophages [507, 508], when compared to drugs such as macrolides which have excellent intracellular accumulation [253, 509]. These data may provide reason to re-examine the antibiotic therapy of hv*Kp* induced tissue abscess, with a focus on the use of intracellularly active drugs.

4.3.5 **Translation to humans**

Humans and mice vary considerably in their immunology and of particular importance for this work, mice have considerably lower circulating neutrophil counts, and different organisation of their splenic and liver macrophages [256, 510, 511]. These immunological differences have been described in detail elsewhere [511]. Porcine immunology far more closely resembles the situation in man, with comparable splenic and hepatic tissue macrophage architecture, and neutrophil counts. We have recently published details of a normothermic, ex vivo porcine spleen perfusion model to study aspects of innate immunity and bacterial infection [256]. In this present study, I have extended the model to include the porcine liver. These experiments, owing to the sensitivity of *Kp* to porcine serum, allowed me to accurately document the replication of *Kp* within tissue, a phenomenon that was difficult in the murine model. Further, I demonstrate in a translatable model, the significance of which is enhanced by the prevalence of K2 *Kp* infection of pigs in the UK and Australia [482, 483], that replication occurs in an intracellular niche in tissue-resident macrophages, in both spleen and liver. This allows me to speculate that the same phenomenon may occur in humans.

4.4 Conclusions

In conclusion, I demonstrate that pyogenic liver abscesses start from a phase of replication of hypermucoid/hypervirulent *K. pneumoniae* within permissive tissue macrophages which generated microcolony like foci of bacteria which are resistant to neutrophil clearance. These data while describing the fundamental mechanism of the initial stages of the pathogenesis of a disease process, highlight that antimicrobial drugs with high or low intracellular concentration and thus potentially low or high capacity to clear intracellular bacterial replication could have different efficacy in preventing the increasing prevalence of this serious invasive disease complication.

4.5 Future work

I am interested to know what inflammatory responses pre-dispose infected Kupffer cells to become a focal point for abscess formation, and the Kupffer cell-neutrophil interactions which determine the outcome of infection. Protocols for primary Kupffer cell and neutrophil isolation are validated, as are immune cell co-culture models. Understanding the production (or not) of inflammatory mediators in the context of bacterial fate may provide avenues for therapeutic intervention to prevent abscess formation.

Chapter 5

General Discussion of Thesis

5 General discussion of thesis

5.1 Challenging the Intracellular Pathogen Paradigm

Historically, bacterial pathogens have been divided into two binary categories based on their mechanisms of pathogenesis. Those which survive and replicate outside of cells (extracellular pathogens), and those which are able to evade intracellular host killing mechanisms to proliferate, or even hijack the host cellular machinery (intracellular pathogens). This classification has led to distinct research efforts on these two classes of pathogens, with for example large amounts of research going into cell biology with respect to intracellular pathogens, but less so with their extracellular counterparts [512].

5.1.1 Emerging evidence of transiently intracellular pathogens

Increasing evidence from a number of bacterial taxa is blurring the lines between extra, and intracellular pathogens. Garai *et al.* (2019) [513] demonstrated that the extracellular pathogen *Pseudomonas aeruginosa*, was able to resist killing of J774a macrophages, and that this was in part mediated by its Type 3 Secretion System, and the protein product of the *mgtC* gene. Both, the T3SS and *mgtC* gene of *S. enterica* have a known role in within-macrophage persistence [514, 515]. T3SSs and the *mgtC* are widely distributed across Gram-negative pathogens [516], including *K. pneumoniae,* and the Gram-negative pathogens *E. coli* and *Yersinia pestis,* two additional typically extracellular pathogen, which also have emerging evidence of transient “colonisation” of the intracellular niche [517, 518]. In addition to survival within macrophages, there is evidence for persistence of Gram-negative pathogens within non-phagocytic cells. *Neisseria meningitidis* – a major cause of bacterial meningitis – has been shown to invade, survive, and replicate within microvascular brain endothelial cells [519]. Beyond Gram-negative pathogens, there are examples of Gram-positive pathogens which can replicate within macrophages. For example, *S. aureus* has been shown to replicate within Kupffer cells in the liver [520, 521], and group A *Streptococci* have been shown to replicate in the cytosol of human macrophages [522]. The data reported in this thesis add to the growing volume of literature that indicates appreciation must be given to intracellular phases for all pathogens.

5.1.2 **Potential factors governing infection outcome**

Gerlini and colleagues [235] demonstrated at the LD_{50}, pneumococcal bacteraemia was initiated by a single bacterial cell. This work follows long standing evidence for the independent action hypothesis, which proposes that invasive disease is initiated by a single bacterium [223]. The work in this thesis indicated that in the case of the pneumococcus, this bacteraemic population most likely originated from a single CD169+ cell in the spleen [362]. The question which remains is why, despite the fact that multiple CD169+ cells are associated with intracellular pneumococci, do only one of these infection events initiate disease? The lack of a single set of adaptive mutations selected for by the bottleneck observed by Gerlini *et al* indicate that this event is likely random, and that there are in fact multiple ways for pathogens to overcome the bottleneck. This is closely analogous to cancer whereby multiple mutational routes can lead to the development of cancers which allow seeding of metastasis. Below I speculate both host and bacterial factors which may facilitate pathogens overcoming the bottleneck to cause disease.

5.1.2.1 **Heterogeneity in macrophage polarisation**

In the introduction to this thesis I described the spectrum of macrophage polarisation ranging from highly microbiocidal and inflammatory (M1) to alternatively activated which is associated with reduced microbiocidal activity (M2) [90]. In a variety of tissues, macrophages are positioned across this spectrum even in the steady state [523]. Studies have demonstrated that for the intracellular pathogens *Francisella* [524], *Coxiella* [525], and *Salmonella* [526], that polarisation of macrophages to the M2-like state was a mechanism for intracellular persistence. This line of thought could be applied to this thesis, whereby the small fraction of invading organisms which survive killing may be due to an innate susceptibility of macrophages polarised into a non-microbiocidal state. Indeed for *K. pneumoniae,* Dumigan *et al* [464] have demonstrated this pathogen is capable of macrophage polarisation. This line of thinking is further supported when considering the co-morbidities of infection, and their influence on macrophage polarisation. For example, alcoholism is highly correlated with incidence of *K. pneumoniae* liver abscess [527]. Tsuchimoto and colleagues [528] also demonstrated that alcoholism leads to an increased number of M2 macrophages in the tissue. It is tempting to correlate these observations and hypothesise that this

increased incidence is due to the higher proportions of innately replication permissive macrophages in these patients.

5.1.2.2 Phase variable bacterial gene expression

Myriad bacterial pathogens have evolved the ability to rapidly vary their gene expression and subsequently the phenotypic heterogeneity of the populations [529–531]. For some bacteria this occurs at individual loci [225, 532] whilst in others it occurs at a global scale across the genome [533]. Variations in phenotype across a population may be another candidate factor governing the ability of only a few bacteria to initiate infection within the host. For example, *S. pneumoniae* is known to encode a number of virulence determinants which may be involved in resistance to phagocytic killing (e.g. PspA, capsule, pneumolysin) [181, 300, 534]. It is tempting to speculate that in only a few bacteria in the population, the transcriptional landscape is optimum to survive within single macrophages, and that these 'lucky' pathogens are those which proliferate to cause disease. Indeed, Surve *et al.* [535] demonstrated that heterogeneity in expression of pneumolysin determines bacterial fate following translocation across the BBB. It is therefore tempting to speculate that similar mechanisms for generating phenotypic heterogeneity may influence survival within macrophages.

5.2 Implications of the Intracellular Niche for Antibiotic and Host-Directed Therapeutics

With the inescapable rise of mortality due to antimicrobial resistance infections, investigation of novel therapeutic strategies is required. Below I will discuss how strategies which enhance the immune response to infection are candidate therapeutic strategies, and also how repurposing antibiotics with different penetrations to host cells could target transiently intracellular pathogens.

5.2.1 Macrophage directed therapeutics

This thesis and an enormous body of previous literature have demonstrated the critical role of macrophages in providing a safe haven for microbial persistence [536]. My data which demonstrate that inhibition of bacterial uptake by a single macrophage population can prevent disease in a pre-clinical model of infection indicates

macrophage directed therapeutics may be a viable therapeutic strategy in the future. Therapies based on work with single organisms, and single cell types may prove costly for minimal patient benefit, therefore careful economic consideration should be paid to development of these [537]. A number of compounds such as cytokines which globally target host cells to enhance bacterial killing are in development [538]. The macrophage activating cytokine IFNγ has been investigated pre-clinically for enhancing treatment of COPD and infectious complications of granulomatous disease by enhancing intracellular killing of pathogens in these conditions [539, 540]. Further, Nalos *et al.* (2012) [541] reported adjunct therapy of a *S. aureus* bacteraemic infection with interferon which resulted in improved clinical condition and discharge from the intensive care unit. An issue with this is the potential off target effects of IFNγ, which produce inflammatory responses in diverse tissues which may mediate host cell damage [542]. Statins are an additional class of compounds which are being considered to as an adjunctive therapy in *S. aureus* bacteraemia, as they enhance the oxidative burst in macrophages and promote bacterial killing [543].

5.2.2 **Intracellular accumulating antibiotics**

When optimising antimicrobial treatment regimens for bacterial infections, it is critical to consider both the tissue reservoirs, and also the pharmacology of candidate antimicrobial therapies [544]. As a result, a large body of research has aimed to address the activity of different antibiotic classes on the clearance of intracellular bacterial pathogens – primarily *L. monocytogenes* and *Salmonella* [545–547]. With a refined understanding of the pathogenesis of infection caused by *S. pneumoniae* and *K. pneumoniae* – which we now know to contain a transient phase of intracellular replication – it is critical to re-evaluate the therapeutic efficacy of current antimicrobials. Two examples at opposite ends of the spectrum are beta-lactams and macrolides. Beta-lactams have been shown to accumulate only 0.1x within macrophages [548], contrasting with macrolides which concentrate between 30 and 300x within host cells [549, 550]. The macrolide azithromycin is added to ceftriaxone in the case of high vs low severity pneumonia [551, 552]. Clinical and murine studies indicate this combination leads to greater treatment efficacy [553, 554], although the basis for this is unknown as these drugs show limited synergy *in vitro* against planktonic bacteria [555]. This raises the question that the use of azithromycin – which accumulates ~300x

within macrophage [556] – may enhance infection outcome by clearing an intracellular pneumococcal reservoir. I propose consideration of the intracellular accumulation of drugs should be given in the case of *Sp* and *Kp* therapy.

5.3 **Translational *ex vivo* Models in Drug Development**

No new treatments for bacteria-induced sepsis have been licenced in the last two decades, which is reflected by the failure of a number of clinical trials [220]. Furthermore, whilst a relatively new syndrome, treatment of *Kp*-induced tissue abscess remain restricted to antimicrobial therapy and surgical drainage – generic strategies employed for multiple infectious agents [426]. The development of translational models would greatly aid in the development of drugs. This thesis reports the use of an *ex vivo* human spleen perfusion model, and the development of a novel liver-spleen co-perfusion model using organs from pigs, an animal closely related to humans [158]. Now these models have been validated for use in pathogenesis studies by our lab, their use in the pre-clinical development of therapies should be considered. With reference to antimicrobial therapy, our model reliably recapitulates tissue infection, and incorporates the natural flow of blood through the vasculature – a feature missing from *in vitro* systems [557], even those which display tissue structure such as organoids [558]. Studies of antibiotic accumulation in splenic and hepatic tissue may benefit the pre-clinical development of novel intracellularly accumulating drugs. Further, I have demonstrated that our model maintains physiological parameters and host immune cell function, opening the door to the trial of host-directed therapeutics.

5.4 **Conclusions**

This thesis defines novel intracellular phases of pathogenesis caused by two phylogenetically distinct pathogens; *S. pneumoniae*, and *K. pneumoniae.* I demonstrate that these two pathogens previously considered extracellular can replicate within tissue macrophages in the spleen and liver. I elude to immunological mechanisms which may facilitate within host persistence, such as the resistance to neutrophil-mediated killing. Lastly, these findings have been extended to two novel, translational *ex vivo* organ perfusion infection models, which will aid the pre-clinical development of novel antimicrobials.

5.5 References

1. **Peschel A, Sahl HG**. The co-evolution of host cationic antimicrobial peptides and microbial resistance. *Nature Reviews Microbiology*. Epub ahead of print 2006. DOI: 10.1038/nrmicro1441.
2. **Gomez Perdiguero E, Klapproth K, Schulz C, Busch K, Azzoni E, *et al.*** Tissue-resident macrophages originate from yolk-sac-derived erythro-myeloid progenitors. *Nature*. Epub ahead of print 2015. DOI: 10.1038/nature13989.
3. **van de Laar L, Saelens W, De Prijck S, Martens L, Scott CL, *et al.*** Yolk Sac Macrophages, Fetal Liver, and Adult Monocytes Can Colonize an Empty Niche and Develop into Functional Tissue-Resident Macrophages. *Immunity*. Epub ahead of print 2016. DOI: 10.1016/j.immuni.2016.02.017.
4. **Scott CL, Zheng F, De Baetselier P, Martens L, Saeys Y, *et al.*** Bone marrow-derived monocytes give rise to self-renewing and fully differentiated Kupffer cells. *Nat Commun*. Epub ahead of print 2016. DOI: 10.1038/ncomms10321.
5. **Varol C, Mildner A, Jung S**. Macrophages: Development and Tissue Specialization. *Annu Rev Immunol*. Epub ahead of print 2015. DOI: 10.1146/annurev-immunol-032414-112220.
6. **Krenkel O, Tacke F**. Liver macrophages in tissue homeostasis and disease. *Nature Reviews Immunology*. Epub ahead of print 2017. DOI: 10.1038/nri.2017.11.
7. **Herbst S, Schaible UE, Schneider BE**. Interferon gamma activated macrophages kill mycobacteria by nitric oxide induced apoptosis. *PLoS One*. Epub ahead of print 2011. DOI: 10.1371/journal.pone.0019105.
8. **Ziegler K, Unanue ER**. Identification of a macrophage antigen-processing event required for I-region-restricted antigen presentation to T lymphocytes. *J Immunol*.
9. **Mirza R, DiPietro LA, Koh TJ**. Selective and specific macrophage ablation is detrimental to wound healing in mice. *Am J Pathol*. Epub ahead of print 2009.

DOI: 10.2353/ajpath.2009.090248.

10. **Gordon S, Plüddemann A**. Tissue macrophages: Heterogeneity and functions. *BMC Biology*. Epub ahead of print 2017. DOI: 10.1186/s12915-017-0392-4.
11. **Raoust E, Balloy V, Garcia-Verdugo I, Touqui L, Ramphal R, *et al.*** Pseudomonas aeruginosa LPS or flagellin are sufficient to activate TLR-dependent signaling in murine alveolar macrophages and airway epithelial cells. *PLoS One*. Epub ahead of print 2009. DOI: 10.1371/journal.pone.0007259.
12. **Devitt A, Moffatt OD, Raykundalia C, Capra JD, Simmons DL, *et al.*** Human CD14 mediates recognition and phagocytosis of apoptotic cells. *Nature*. Epub ahead of print 1998. DOI: 10.1038/33169.
13. **Meesmann HM, Fehr EM, Kierschke S, Herrmann M, Bilyy R, *et al.*** Decrease of sialic acid residues as an eat-mesignal on the surface of apoptotic lymphocytes. *J Cell Sci*. Epub ahead of print 2010. DOI: 10.1242/jcs.066696.
14. **Hajjar AM, Tsai JH, Wilson CB, Miller SI**. Human Toll-like receptor 4 recognizes host-specific LPS modifications. *Nat Immunol*. Epub ahead of print 2002. DOI: 10.1038/ni777.
15. **Yoshimura A, Lien E, Ingalls RR, Tuomanen E, Dziarski R, *et al.*** Cutting edge: recognition of Gram-positive bacterial cell wall components by the innate immune system occurs via Toll-like receptor 2. *J Immunol*.
16. **Mellman IS, Plutner H, Steinman RM, Unkeless JC, Cohn ZA**. Internalization and degradation of macrophage Fc receptors during receptor-mediated phagocytosis. *J Cell Biol*. Epub ahead of print 1983. DOI: 10.1083/jcb.96.3.887.
17. **Griffin FM, Bianco C, Silverstein SC**. Characterization of the macrophage receptor for complement and demonstration of its functional independence from the receptor for the Fc portion of immunoglobulin G. *J Exp Med*. Epub ahead of print 1975. DOI: 10.1084/jem.141.6.1269.
18. **Viegas MS, Estronca LMBB, Vieira O V.** Comparison of the Kinetics of Maturation of Phagosomes Containing Apoptotic Cells and IgG-Opsonized Particles. *PLoS One*. Epub ahead of print 2012. DOI: 10.1371/journal.pone.0048391.
19. **Petersen M, Fessner WD, Frosch M, Lüneberg E**. The siaA gene involved in

capsule polysaccharide biosynthesis of Neisseria meningitidis B codes for N-acylglucosamine-6-phosphate 2-epimerase activity. *FEMS Microbiol Lett*. Epub ahead of print 2000. DOI: 10.1016/S0378-1097(00)00037-9.

20. **Bayliss CD, Hoe JC, Makepeace K, Martin P, Hood DW, *et al.*** Neisseria meningitidis escape from the bactericidal activity of a monoclonal antibody is mediated by phase variation of lgtG and enhanced by a mutator phenotype. *Infect Immun* 2008;76:5038–5048.
21. **Mao Y, Finnemann SC**. Regulation of phagocytosis by Rho GTPases. *Small GTPases*. Epub ahead of print 2015. DOI: 10.4161/21541248.2014.989785.
22. **Leung DW, Otomo C, Chory J, Rosen MK**. Genetically encoded photoswitching of actin assembly through the Cdc42-WASP-Arp2/3 complex pathway. *Proc Natl Acad Sci U S A*. Epub ahead of print 2008. DOI: 10.1073/pnas.0801232105.
23. **Tsuboi S, Meerloo J**. Wiskott-Aldrich syndrome protein is a key regulator of the phagocytic cup formation in macrophages. *J Biol Chem*. Epub ahead of print 2007. DOI: 10.1074/jbc.M705999200.
24. **Garin J, Diez R, Kieffer S, Dermine JF, Duclos S, *et al.*** The phagosome proteome: Insight into phagosome functions. *J Cell Biol*. Epub ahead of print 2001. DOI: 10.1083/jcb.152.1.165.
25. **Christoforidis S, McBride HM, Burgoyne RD, Zerial M**. The rab5 effector EEA1 is a core component of endosome docking. *Nature*. Epub ahead of print 1999. DOI: 10.1038/17618.
26. **Law F, Seo JH, Wang Z, DeLeon JL, Bolis Y, *et al.*** The VPS34 PI3K negatively regulates RAB-5 during endosome maturation. *J Cell Sci*. Epub ahead of print 2017. DOI: 10.1242/jcs.194746.
27. **Scott CC, Cuellar-Mata P, Matsuo T, Davidson HW, Grinstein S**. Role of 3-phosphoinositides in the maturation of Salmonella-containing vacuoles within host cells. *J Biol Chem*. Epub ahead of print 2002. DOI: 10.1074/jbc.M110399200.
28. **Kinchen JM, Doukoumetzidis K, Almendinger J, Stergiou L, Tosello-Trampont A, *et al.*** A pathway for phagosome maturation during engulfment of apoptotic cells. *Nat Cell Biol*. Epub ahead of print 2008. DOI: 10.1038/ncb1718.
29. **Harrison RE, Bucci C, Vieira O V., Schroer TA, Grinstein S**. Phagosomes

Fuse with Late Endosomes and/or Lysosomes by Extension of Membrane Protrusions along Microtubules: Role of Rab7 and RILP. *Mol Cell Biol*. Epub ahead of print 2003. DOI: 10.1128/mcb.23.18.6494-6506.2003.

30. **Tsang AW, Oestergaard K, Myers JT, Swanson JA**. Altered membrane trafficking in activated bone marrow-derived macrophages. *J Leukoc Biol*. Epub ahead of print 2000. DOI: 10.1189/jlb.68.4.487.
31. **Shiratsuchi A, Watanabe I, Takeuchi O, Akira S, Nakanishi Y**. Inhibitory Effect of Toll-Like Receptor 4 on Fusion between Phagosomes and Endosomes/Lysosomes in Macrophages. *J Immunol*. Epub ahead of print 2004. DOI: 10.4049/jimmunol.172.4.2039.
32. **Smith LM, May RC**. Mechanisms of microbial escape from phagocyte killing. *Biochemical Society Transactions*. Epub ahead of print 2013. DOI: 10.1042/BST20130014.
33. **Runyen-Janecky LJ**. Role and regulation of heme iron acquisition in gram-negative pathogens. *Frontiers in Cellular and Infection Microbiology*. Epub ahead of print 2013. DOI: 10.3389/fcimb.2013.00055.
34. **Gruenheid S, Pinner E, Desjardins M, Gros P**. Natural resistance to infection with intracellular pathogens: The Nramp1 protein is recruited to the membrane of the phagosome. *J Exp Med*. Epub ahead of print 1997. DOI: 10.1084/jem.185.4.717.
35. **Cellier MF, Courville P, Campion C**. Nramp1 phagocyte intracellular metal withdrawal defense. *Microbes Infect*. Epub ahead of print 2007. DOI: 10.1016/j.micinf.2007.09.006.
36. **Fritsche G, Nairz M, Theurl I, Mair S, Bellmann-Weiler R, *et al.*** Modulation of macrophage iron transport by Nramp1 (Slc11a1). *Immunobiology*. Epub ahead of print 2008. DOI: 10.1016/j.imbio.2007.09.014.
37. **Donovan A, Lima CA, Pinkus JL, Pinkus GS, Zon LI, *et al.*** The iron exporter ferroportin/Slc40a1 is essential for iron homeostasis. *Cell Metab*. Epub ahead of print 2005. DOI: 10.1016/j.cmet.2005.01.003.
38. **De Domenico I, Ward DMV, Langelier C, Vaughn MB, Nemeth E, *et al.*** The molecular mechanism of hepcidin-mediated ferroportin down-regulation. *Mol Biol Cell*. Epub ahead of print 2007. DOI: 10.1091/mbc.E07-01-0060.
39. **Alpuche Aranda CM, Swanson JA, Loomis WP, Miller SI**. Salmonella typhimurium activates virulence gene transcription within acidified macrophage

phagosomes. *Proc Natl Acad Sci U S A*. Epub ahead of print 1992. DOI: 10.1073/pnas.89.21.10079.

40. **Lou L, Zhang P, Piao R, Wang Y**. Salmonella Pathogenicity Island 1 (SPI-1) and Its Complex Regulatory Network. *Frontiers in Cellular and Infection Microbiology*. Epub ahead of print 2019. DOI: 10.3389/fcimb.2019.00270.
41. **Helaine S, Cheverton AM, Watson KG, Faure LM, Matthews SA, *et al.*** Internalization of salmonella by macrophages induces formation of nonreplicating persisters. *Science (80-)*. Epub ahead of print 2014. DOI: 10.1126/science.1244705.
42. **Levin BR, Rozen DE**. Non-inherited antibiotic resistance. *Nature Reviews Microbiology*. Epub ahead of print 2006. DOI: 10.1038/nrmicro1445.
43. **Rossi O, Dybowski R, Maskell DJ, Grant AJ, Restif O, *et al.*** Within-host spatiotemporal dynamics of systemic Salmonella infection during and after antimicrobial treatment. *J Antimicrob Chemother*. Epub ahead of print 2017. DOI: 10.1093/jac/dkx294.
44. **Rathman M, Sjaastad MD, Falkow S**. Acidification of phagosomes containing Salmonella typhimurium in murine macrophages. *Infect Immun*.
45. **Lukacs GL, Rotstein OD, Grinstein S**. Phagosomal acidification is mediated by a vacuolar-type H+-ATPase in murine macrophages. *J Biol Chem*.
46. **McGhie EJ, Brawn LC, Hume PJ, Humphreys D, Koronakis V**. Salmonella takes control: effector-driven manipulation of the host. *Current Opinion in Microbiology*. Epub ahead of print 2009. DOI: 10.1016/j.mib.2008.12.001.
47. **Steele-Mortimer O**. The Salmonella-containing vacuole-Moving with the times. *Current Opinion in Microbiology*. Epub ahead of print 2008. DOI: 10.1016/j.mib.2008.01.002.
48. **Small P, Blankenhorn D, Welty D, Zinser E, Slonczewski JL**. Acid and base resistance in Escherichia coli and Shigella flexneri: Role of rpoS and growth pH. *J Bacteriol*. Epub ahead of print 1994. DOI: 10.1128/jb.176.6.1729-1737.1994.
49. **Lin J, In Soo Lee, Frey J, Slonczewski JL, Foster JW**. Comparative analysis of extreme acid survival in Salmonella typhimurium, Shigella flexneri, and Escherichia coli. *J Bacteriol*. Epub ahead of print 1995. DOI: 10.1128/jb.177.14.4097-4104.1995.
50. **Lu P, Ma D, Chen Y, Guo Y, Chen GQ, *et al.*** L-glutamine provides acid

resistance for Escherichia coli through enzymatic release of ammonia. *Cell Res*. Epub ahead of print 2013. DOI: 10.1038/cr.2013.13.

51. **Piñas GE, Cortes PR, Albarracín Orio AG, Echenique J**. Acidic stress induces autolysis by a CSP- independent ComE pathway in Streptococcus pneumoniae. *Microbiology*. Epub ahead of print 2008. DOI: 10.1099/mic.0.2007/015925-0.
52. **White C, Lee J, Kambe T, Fritsche K, Petris MJ**. A role for the ATP7A copper-transporting ATPase in macrophage bactericidal activity. *J Biol Chem*. Epub ahead of print 2009. DOI: 10.1074/jbc.M109.070201.
53. **Lichten LA, Cousins RJ**. Mammalian Zinc Transporters: Nutritional and Physiologic Regulation. *Annu Rev Nutr*. Epub ahead of print 2009. DOI: 10.1146/annurev-nutr-033009-083312.
54. **Ammendola S, Pasquali P, Pistoia C, Petrucci P, Petrarca P, *et al.*** High-affinity Zn2+ uptake system ZnuABC is required for bacterial zinc homeostasis in intracellular environments and contributes to the virulence of Salmonella enterica. *Infect Immun*. Epub ahead of print 2007. DOI: 10.1128/IAI.00559-07.
55. **Alquethamy SF, Khorvash M, Pederick VG, Whittall JJ, Paton JC, *et al.*** The role of the copA copper efflux system in acinetobacter baumannii virulence. *Int J Mol Sci*. Epub ahead of print 2019. DOI: 10.3390/ijms20030575.
56. **Purves J, Thomas J, Riboldi GP, Zapotoczna M, Tarrant E, *et al.*** A horizontally gene transferred copper resistance locus confers hyper-resistance to antibacterial copper toxicity and enables survival of community acquired methicillin resistant Staphylococcus aureus USA300 in macrophages. *Environ Microbiol*. Epub ahead of print 2018. DOI: 10.1111/1462-2920.14088.
57. **Wolschendorf F, Ackart D, Shrestha TB, Hascall-Dove L, Nolan S, *et al.*** Copper resistance is essential for virulence of Mycobacterium tuberculosis. *Proc Natl Acad Sci U S A*. Epub ahead of print 2011. DOI: 10.1073/pnas.1009261108.
58. **Fang FC**. Antimicrobial reactive oxygen and nitrogen species: Concepts and controversies. *Nature Reviews Microbiology*. Epub ahead of print 2004. DOI: 10.1038/nrmicro1004.
59. **Rybicka JM, Balce DR, Khan MF, Krohn RM, Yates RM**. NADPH oxidase activity controls phagosomal proteolysis in macrophages through modulation

of the lumenal redox environment of phagosomes. *Proc Natl Acad Sci U S A*. Epub ahead of print 2010. DOI: 10.1073/pnas.0914867107.

60. **Moore SF, MacKenzie AB**. NADPH Oxidase NOX2 Mediates Rapid Cellular Oxidation following ATP Stimulation of Endotoxin-Primed Macrophages. *J Immunol*. Epub ahead of print 2009. DOI: 10.4049/jimmunol.0900394.
61. **Guo Dong Mao, Thomas PD, Lopaschuk GD, Poznansky MJ**. Superoxide dismutase (SOD)-catalase conjugates. Role of hydrogen peroxide and the Fenton reaction in SOD toxicity. *J Biol Chem*.
62. **Zhou R, Yazdi AS, Menu P, Tschopp J**. A role for mitochondria in NLRP3 inflammasome activation. *Nature*. Epub ahead of print 2011. DOI: 10.1038/nature09663.
63. **Aktan F**. iNOS-mediated nitric oxide production and its regulation. *Life Sciences*. Epub ahead of print 2004. DOI: 10.1016/j.lfs.2003.10.042.
64. **Slauch JM**. How does the oxidative burst of macrophages kill bacteria? Still an open question. *Mol Microbiol*. Epub ahead of print 2011. DOI: 10.1111/j.1365-2958.2011.07612.x.
65. **Cabiscol E, Tamarit J, Ros J**. Oxidative stress in bacteria and protein damage by reactive oxygen species. *Int Microbiol*. Epub ahead of print 2000. DOI: 10.2436/im.v3i1.9235.
66. **Cadet J, Delatour T, Douki T, Gasparutto D, Pouget JP, *et al.*** Hydroxyl radicals and DNA base damage. *Mutat Res - Fundam Mol Mech Mutagen*. Epub ahead of print 1999. DOI: 10.1016/S0027-5107(99)00004-4.
67. **El Chemaly A, Nunes P, Jimaja W, Castelbou C, Demaurex N**. Hv1 proton channels differentially regulate the pH of neutrophil and macrophage phagosomes by sustaining the production of phagosomal ROS that inhibit the delivery of vacuolar ATPases. *J Leukoc Biol*. Epub ahead of print 2014. DOI: 10.1189/jlb.0513251.
68. **Gallois A, Klein JR, Allen L-AH, Jones BD, Nauseef WM**. Salmonella Pathogenicity Island 2-Encoded Type III Secretion System Mediates Exclusion of NADPH Oxidase Assembly from the Phagosomal Membrane . *J Immunol*. Epub ahead of print 2001. DOI: 10.4049/jimmunol.166.9.5741.
69. **Hébrard M, Viala JPM, Méresse S, Barras F, Aussel L**. Redundant hydrogen peroxide scavengers contribute to Salmonella virulence and oxidative stress resistance. *J Bacteriol*. Epub ahead of print 2009. DOI: 10.1128/JB.00144-09.

70. **Mantena RKR, Wijburg OLC, Vindurampulle C, Bennett-Wood VR, Walduck A, *et al.*** Reactive oxygen species are the major antibacterials against Salmonella Typhimurium purine auxotrophs in the phagosome of RAW 264.7 cells. *Cell Microbiol*. Epub ahead of print 2008. DOI: 10.1111/j.1462-5822.2007.01105.x.
71. **Chen Y, Smith MR, Thirumalai K, Zychlinsky A**. A bacterial invasin induces macrophage apoptosis by binding directly to ICE. *EMBO J*. Epub ahead of print 1996. DOI: 10.1002/j.1460-2075.1996.tb00759.x.
72. **Gobert AP, Cheng Y, Wang J-Y, Boucher J-L, Iyer RK, *et al.*** Helicobacter pylori Induces Macrophage Apoptosis by Activation of Arginase II . *J Immunol*. Epub ahead of print 2002. DOI: 10.4049/jimmunol.168.9.4692.
73. **Cano V, March C, Insua JL, Aguiló N, Llobet E, *et al.*** Klebsiella pneumoniae survives within macrophages by avoiding delivery to lysosomes. *Cell Microbiol*. Epub ahead of print 2015. DOI: 10.1111/cmi.12466.
74. **Hersh D, Monack DM, Smith MR, Ghori N, Falkow S, *et al.*** The Salmonella invasin SipB induces macrophage apoptosis by binding to caspase-1. *Proc Natl Acad Sci U S A*. Epub ahead of print 1999. DOI: 10.1073/pnas.96.5.2396.
75. **Aberdein JD, Cole J, Bewley MA, Marriott HM, Dockrell DH**. Alveolar macrophages in pulmonary host defence-the unrecognized role of apoptosis as a mechanism of intracellular bacterial killing. *Clinical and Experimental Immunology*. Epub ahead of print 2013. DOI: 10.1111/cei.12170.
76. **Chen CJ, Kono H, Golenbock D, Reed G, Akira S, *et al.*** Identification of a key pathway required for the sterile inflammatory response triggered by dying cells. *Nat Med*. Epub ahead of print 2007. DOI: 10.1038/nm1603.
77. **Dockrell DH, Lee M, Lynch DH, Read RC**. Immune-Mediated Phagocytosis and Killing of Streptococcus pneumoniae Are Associated with Direct and Bystander Macrophage Apoptosis . *J Infect Dis*. Epub ahead of print 2001. DOI: 10.1086/323084.
78. **Dockrell DH, Marriott HM, Prince LR, Ridger VC, Ince PG, *et al.*** Alveolar Macrophage Apoptosis Contributes to Pneumococcal Clearance in a Resolving Model of Pulmonary Infection. *J Immunol*. Epub ahead of print 2003. DOI: 10.4049/jimmunol.171.10.5380.
79. **Marriott HM, Hellewell PG, Cross SS, Ince PG, Whyte MKB, *et al.*** Decreased Alveolar Macrophage Apoptosis Is Associated with Increased

Pulmonary Inflammation in a Murine Model of Pneumococcal Pneumonia. *J Immunol*. Epub ahead of print 2006. DOI: 10.4049/jimmunol.177.9.6480.

80. **Cole J, Aberdein J, Jubrail J, Dockrell DH**. The Role of Macrophages in the Innate Immune Response to Streptococcus pneumoniae and Staphylococcus aureus. Mechanisms and Contrasts. In: *Advances in Microbial Physiology*. 2014. Epub ahead of print 2014. DOI: 10.1016/bs.ampbs.2014.08.004.
81. **Guo H, Callaway JB, Ting JPY**. Inflammasomes: Mechanism of action, role in disease, and therapeutics. *Nature Medicine*. Epub ahead of print 2015. DOI: 10.1038/nm.3893.
82. **Swanson K V., Deng M, Ting JPY**. The NLRP3 inflammasome: molecular activation and regulation to therapeutics. *Nature Reviews Immunology*. Epub ahead of print 2019. DOI: 10.1038/s41577-019-0165-0.
83. **Witzenrath M, Pache F, Lorenz D, Koppe U, Gutbier B, *et al.*** The NLRP3 inflammasome is differentially activated by pneumolysin variants and contributes to host defense in pneumococcal pneumonia1. *Pneumologie*. Epub ahead of print 2011. DOI: 10.1055/s-0030-1270363.
84. **Miller LS, Pietras EM, Uricchio LH, Hirano K, Rao S, *et al.*** Inflammasome-mediated production of IL-1β is required for neutrophil recruitment against Staphylococcus aureus in vivo. . *J Immunol*. Epub ahead of print 2008. DOI: 10.4049/jimmunol.180.1.665.
85. **Hoegen T, Tremel N, Klein M, Angele B, Wagner H, *et al.*** The NLRP3 Inflammasome Contributes to Brain Injury in Pneumococcal Meningitis and Is Activated through ATP-Dependent Lysosomal Cathepsin B Release. *J Immunol*. Epub ahead of print 2011. DOI: 10.4049/jimmunol.1100790.
86. **Kuwar R, Rolfe A, Di L, Xu H, He L, *et al.*** A novel small molecular NLRP3 inflammasome inhibitor alleviates neuroinflammatory response following traumatic brain injury. *J Neuroinflammation*. Epub ahead of print 2019. DOI: 10.1186/s12974-019-1471-y.
87. **MACKANESS GB**. Cellular resistance to infection. *J Exp Med*. Epub ahead of print 1962. DOI: 10.1084/jem.116.3.381.
88. **Doyle AG, Herbein G, Montaner LJ, Minty AJ, Caput D, *et al.*** Interleukin-13 alters the activation state of murine macrophages in vitro: Comparison with interleukin-4 and interferon-γ. *Eur J Immunol*. Epub ahead of print 1994. DOI: 10.1002/eji.1830240630.

89. **Martinez FO, Gordon S**. The M1 and M2 paradigm of macrophage activation: Time for reassessment. *F1000Prime Rep*. Epub ahead of print 2014. DOI: 10.12703/P6-13.
90. **Benoit M, Desnues B, Mege J-L**. Macrophage Polarization in Bacterial Infections. *J Immunol*. Epub ahead of print 2008. DOI: 10.4049/jimmunol.181.6.3733.
91. **Nau GJ, Richmond JFL, Schlesinger A, Jennings EG, Lander ES, *et al.*** Human macrophage activation programs induced by bacterial pathogens. *Proc Natl Acad Sci U S A*. Epub ahead of print 2002. DOI: 10.1073/pnas.022649799.
92. **Müller E, Christopoulos PF, Halder S, Lunde A, Beraki K, *et al.*** Toll-like receptor ligands and interferon-γ synergize for induction of antitumor M1 macrophages. *Front Immunol*. Epub ahead of print 2017. DOI: 10.3389/fimmu.2017.01383.
93. **Wu X, Xu W, Feng X, He Y, Liu X, *et al.*** TNF-a mediated inflammatory macrophage polarization contributes to the pathogenesis of steroid-induced osteonecrosis in mice. *Int J Immunopathol Pharmacol*. Epub ahead of print 2015. DOI: 10.1177/0394632015593228.
94. **Garcia-Diaz A, Shin DS, Moreno BH, Saco J, Escuin-Ordinas H, *et al.*** Interferon Receptor Signaling Pathways Regulating PD-L1 and PD-L2 Expression. *Cell Rep*. Epub ahead of print 2017. DOI: 10.1016/j.celrep.2017.04.031.
95. **Jutras I, Houde M, Currier N, Boulais J, Duclos S, *et al.*** Modulation of the phagosome proteome by interferon-γ. In: *Molecular and Cellular Proteomics*. 2008. Epub ahead of print 2008. DOI: 10.1074/mcp.M700267-MCP200.
96. **Kayagaki N, Wong MT, Stowe IB, Ramani SR, Gonzalez LC, *et al.*** Noncanonical inflammasome activation by intracellular LPS independent of TLR4. *Science (80-)*. Epub ahead of print 2013. DOI: 10.1126/science.1240248.
97. **Takeda K, Yamamoto M**. Current views of toll-like receptor signaling pathways. *Gastroenterology Research and Practice*. Epub ahead of print 2010. DOI: 10.1155/2010/240365.
98. **Netea MG, Wijmenga C, O'Neill LAJ**. Genetic variation in Toll-like receptors and disease susceptibility. *Nature Immunology*. Epub ahead of print 2012.

DOI: 10.1038/ni.2284.

99. **Nathan CF, Murray HW, Wlebe lE, Rubin BY**. Identification of interferon-γ, as the lymphokine that activates human macrophage oxidative metabolism and antimicrobial activity. *J Exp Med*. Epub ahead of print 1983. DOI: 10.1084/jem.158.3.670.
100. **Ip WKE, Sokolovska A, Charriere GM, Boyer L, Dejardin S, *et al.*** Phagocytosis and Phagosome Acidification Are Required for Pathogen Processing and MyD88-Dependent Responses to Staphylococcus aureus . *J Immunol*. Epub ahead of print 2010. DOI: 10.4049/jimmunol.1000110.
101. **Murray RZ, Kay JG, Sangermani DG, Stow JL**. A Role for the Phagosome in Cytokine Secretion10.1126/science.1120225. *Science (80-)*.
102. **Muraille E, Leo O, Moser M**. Th1/Th2 paradigm extended: Macrophage polarization as an unappreciated pathogen-driven escape mechanism? *Frontiers in Immunology*. Epub ahead of print 2014. DOI: 10.3389/fimmu.2014.00603.
103. **Jablonski KA, Amici SA, Webb LM, Ruiz-Rosado JDD, Popovich PG, *et al.*** Novel markers to delineate murine M1 and M2 macrophages. *PLoS One*. Epub ahead of print 2015. DOI: 10.1371/journal.pone.0145342.
104. **Shearer JD, Richards JR, Mills CD, Caldwell MD**. Differential regulation of macrophage arginine metabolism: A proposed role in wound healing. *Am J Physiol - Endocrinol Metab*. Epub ahead of print 1997. DOI: 10.1152/ajpendo.1997.272.2.e181.
105. **Roszer T**. Understanding the mysterious M2 macrophage through activation markers and effector mechanisms. *Mediators of Inflammation*. Epub ahead of print 2015. DOI: 10.1155/2015/816460.
106. **Zhang MZ, Wang X, Wang Y, Niu A, Wang S, *et al.*** IL-4/IL-13–mediated polarization of renal macrophages/dendritic cells to an M2a phenotype is essential for recovery from acute kidney injury. *Kidney Int*. Epub ahead of print 2017. DOI: 10.1016/j.kint.2016.08.020.
107. **Oeser K, Maxeiner J, Symowski C, Stassen M, Voehringer D**. T cells are the critical source of IL-4/IL-13 in a mouse model of allergic asthma. *Allergy Eur J Allergy Clin Immunol*. Epub ahead of print 2015. DOI: 10.1111/all.12705.
108. **Lu J, Cao Q, Zheng D, Sun Y, Wang C, *et al.*** Discrete functions of M2a and M2c macrophage subsets determine their relative efficacy in treating chronic

kidney disease. *Kidney Int*. Epub ahead of print 2013. DOI: 10.1038/ki.2013.135.

109. **Alvarado-Vazquez PA, Bernal L, Paige CA, Grosick RL, Moracho Vilrriales C, *et al.*** Macrophage-specific nanotechnology-driven CD163 overexpression in human macrophages results in an M2 phenotype under inflammatory conditions. *Immunobiology*. Epub ahead of print 2017. DOI: 10.1016/j.imbio.2017.05.011.
110. **Mantovani A, Sica A, Sozzani S, Allavena P, Vecchi A, *et al.*** The chemokine system in diverse forms of macrophage activation and polarization. *Trends in Immunology*. Epub ahead of print 2004. DOI: 10.1016/j.it.2004.09.015.
111. **Wang L xun, Zhang S xi, Wu H juan, Rong X lu, Guo J**. M2b macrophage polarization and its roles in diseases. *Journal of Leukocyte Biology*. Epub ahead of print 2019. DOI: 10.1002/JLB.3RU1018-378RR.
112. **Ambarus CA, Santegoets KCM, van Bon L, Wenink MH, Tak PP, *et al.*** Soluble immune complexes shift the TLR-induced cytokine production of distinct polarized human macrophage subsets towards IL-10. *PLoS One*. Epub ahead of print 2012. DOI: 10.1371/journal.pone.0035994.
113. **Ortiz MC, Lefimil C, Rodas PI, Vernal R, Lopez M, *et al.*** Neisseria gonorrhoeae modulates immunity by polarizing human macrophages to a M2 profile. *PLoS One*. Epub ahead of print 2015. DOI: 10.1371/journal.pone.0130713.
114. **Sironi M**. Differential regulation of chemokine production by Fc receptor engagement in human monocytes: association of CCL1 with a distinct form of M2 monocyte activation (M2b, Type 2). *J Leukoc Biol*. Epub ahead of print 2006. DOI: 10.1189/jlb.1005586.
115. **Zizzo G, Hilliard BA, Monestier M, Cohen PL**. Efficient Clearance of Early Apoptotic Cells by Human Macrophages Requires M2c Polarization and MerTK Induction. *J Immunol*. Epub ahead of print 2012. DOI: 10.4049/jimmunol.1200662.
116. **Lurier EB, Dalton D, Dampier W, Raman P, Nassiri S, *et al.*** Transcriptome analysis of IL-10-stimulated (M2c) macrophages by next-generation sequencing. *Immunobiology*. Epub ahead of print 2017. DOI: 10.1016/j.imbio.2017.02.006.

117. **Chang MY, Tanino Y, Vidova V, Kinsella MG, Chan CK, *et al.*** A rapid increase in macrophage-derived versican and hyaluronan in infectious lung disease. *Matrix Biol*. Epub ahead of print 2014. DOI: 10.1016/j.matbio.2014.01.011.
118. **Duque GA, Descoteaux A**. Macrophage cytokines: Involvement in immunity and infectious diseases. *Frontiers in Immunology*. Epub ahead of print 2014. DOI: 10.3389/fimmu.2014.00491.
119. **Ozaki K, Leonard WJ**. Cytokine and cytokine receptor pleiotropy and redundancy. *Journal of Biological Chemistry*. Epub ahead of print 2002. DOI: 10.1074/jbc.R200003200.
120. **Dalvi PS, Chalmers JA, Luo V, Han DY, Wellhauser L, *et al.*** High fat induces acute and chronic inflammation in the hypothalamus: Effect of high-fat diet, palmitate and TNF-α on appetite-regulating NPY neurons. *Int J Obes*. Epub ahead of print 2017. DOI: 10.1038/ijo.2016.183.
121. Anti-TNF therapy inhibits fever in cerebral malaria. *QJM An Int J Med*. Epub ahead of print 1993. DOI: 10.1093/oxfordjournals.qjmed.a068783.
122. **Ferro TJ, Hocking DC, Johnson A**. Tumor necrosis factor-α alters pulmonary vasoreactivity via neutrophil- derived oxidants. *Am J Physiol - Lung Cell Mol Physiol*. Epub ahead of print 1993. DOI: 10.1152/ajplung.1993.265.5.l462.
123. **Rath PC, Aggarwal BB**. TNF-induced signaling in apoptosis. *Journal of Clinical Immunology*. Epub ahead of print 1999. DOI: 10.1023/A:1020546615229.
124. **Hsieh CS, Macatonia SE, Tripp CS, Wolf SF, O'Garra A, *et al.*** Development of T H 1 CD4 + T cells through IL-12 produced by Listeria-induced macrophages. *Science (80-)*. Epub ahead of print 1993. DOI: 10.1126/science.8097338.
125. **Yoshimoto T, Takeda K, Tanaka T, Ohkusu K, Kashiwamura S, *et al.*** IL-12 up-regulates IL-18 receptor expression on T cells, Th1 cells, and B cells: synergism with IL-18 for IFN-gamma production. *J Immunol*.
126. **Bhattacharjee A, Shukla M, Yakubenko VP, Mulya A, Kundu S, *et al.*** IL-4 and IL-13 employ discrete signaling pathways for target gene expression in alternatively activated monocytes/macrophages. *Free Radic Biol Med*. Epub ahead of print 2013. DOI: 10.1016/j.freeradbiomed.2012.10.553.
127. **Dinarello CA, van der Meer JWM**. Treating inflammation by blocking

interleukin-1 in humans. *Seminars in Immunology*. Epub ahead of print 2013. DOI: 10.1016/j.smim.2013.10.008.

128. **De Filippo K, Dudeck A, Hasenberg M, Nye E, Van Rooijen N, *et al.*** Mast cell and macrophage chemokines CXCL1/CXCL2 control the early stage of neutrophil recruitment during tissue inflammation. *Blood*. Epub ahead of print 2013. DOI: 10.1182/blood-2013-02-486217.
129. **Muntaka S, Almuhanna Y, Jackson D, Singh S, Afryie-Asante A, *et al.*** Gamma interferon and interleukin-17A differentially influence the response of human macrophages and neutrophils to pseudomonas aeruginosa infection. *Infect Immun*. Epub ahead of print 2019. DOI: 10.1128/IAI.00814-18.
130. **Honey K, Rudensky AY**. Lysosomal cysteine proteases regulate antigen presentation. *Nature Reviews Immunology*. Epub ahead of print 2003. DOI: 10.1038/nri1110.
131. **Riese RJ, Chapman HA**. Cathepsins and compartmentalization in antigen presentation. *Current Opinion in Immunology*. Epub ahead of print 2000. DOI: 10.1016/S0952-7915(99)00058-8.
132. **Kleijmeer MJ, Escola JM, Uytdehaag FGCM, Jakobson E, Griffith JM, *et al.*** Antigen loading of MHC class I molecules in the endocytic tract. *Traffic*. Epub ahead of print 2001. DOI: 10.1034/j.1600-0854.2001.020207.x.
133. **Cho KJ, Ishido S, Eisenlohr L, Roche P**. Rab11a Regulates MHC Class II Recycling and Promotes Antigenic Peptide Exchange in Recycling Endosomes of Mature Dendritic Cells. *J Immunol*.
134. **Jiang Y, Arase N, Kohyama M, Hirayasu K, Suenaga T, *et al.*** Transport of misfolded endoplasmic reticulum proteins to the cell surface by MHC class II molecules. *Int Immunol*. Epub ahead of print 2013. DOI: 10.1093/intimm/dxs155.
135. **Underhill DM, Bassetti M, Rudensky A, Aderem A**. Dynamic interactions of macrophages with T cells during antigen presentation. *J Exp Med*. Epub ahead of print 1999. DOI: 10.1084/jem.190.12.1909.
136. **Buseyne F, Gall S Le, Boccaccio C, Abastado JP, Lifson JD, *et al.*** MHC-I-restricted presentation of HIV-1 virion antigens without viral replication. *Nat Med*. Epub ahead of print 2001. DOI: 10.1038/85493.
137. **Dancey JT, Deubelbeiss KA, Harker andFinch LACA**. Neutrophil kinetics in man. *J Clin Invest*. Epub ahead of print 1976. DOI: 10.1172/JCI108517.

138. **Lin F, Nguyen CMC, Wang SJ, Saadi W, Gross SP, *et al.*** Effective neutrophil chemotaxis is strongly influenced by mean IL-8 concentration. *Biochem Biophys Res Commun*. Epub ahead of print 2004. DOI: 10.1016/j.bbrc.2004.05.029.
139. **Winterbourn CC, Kettle AJ, Hampton MB**. Reactive Oxygen Species and Neutrophil Function. *Annu Rev Biochem*. Epub ahead of print 2016. DOI: 10.1146/annurev-biochem-060815-014442.
140. **Papayannopoulos V, Metzler KD, Hakkim A, Zychlinsky A**. Neutrophil elastase and myeloperoxidase regulate the formation of neutrophil extracellular traps. *J Cell Biol*. Epub ahead of print 2010. DOI: 10.1083/jcb.201006052.
141. **Yin C, Heit B**. Armed for destruction: formation, function and trafficking of neutrophil granules. *Cell and Tissue Research*. Epub ahead of print 2018. DOI: 10.1007/s00441-017-2731-8.
142. **Yipp BG, Petri B, Salina D, Jenne CN, Scott BNV, *et al.*** Infection-induced NETosis is a dynamic process involving neutrophil multitasking in vivo. *Nat Med*. Epub ahead of print 2012. DOI: 10.1038/nm.2847.
143. **Fox S, Leitch AE, Duffin R, Haslett C, Rossi AG**. Neutrophil apoptosis: Relevance to the innate immune response and inflammatory disease. *Journal of Innate Immunity*. Epub ahead of print 2010. DOI: 10.1159/000284367.
144. **Mahadevan V**. Anatomy of the pancreas and spleen. *Surgery (United Kingdom)*. Epub ahead of print 2016. DOI: 10.1016/j.mpsur.2016.03.014.
145. **Wright HD**. Experimental pneumococcal septicaemia and anti-pneumococcal immunity. *J Pathol Bacteriol*. Epub ahead of print 1927. DOI: 10.1002/path.1700300202.
146. **Liu DL, Xia S, Xu W, Ye Q, Gao Y, *et al.*** Anatomy of vasculature of 850 spleen specimens and its application in partial splenectomy. *Surgery*. Epub ahead of print 1996. DOI: 10.1016/S0039-6060(96)80209-1.
147. **Bronte V, Pittet MJ**. The spleen in local and systemic regulation of immunity. *Immunity*. Epub ahead of print 2013. DOI: 10.1016/j.immuni.2013.10.010.
148. **Mebius RE, Kraal G**. Structure and function of the spleen. *Nature Reviews Immunology*. Epub ahead of print 2005. DOI: 10.1038/nri1669.
149. **Martin F, Kearney JF**. Marginal-zone B cells. *Nature Reviews Immunology*. Epub ahead of print 2002. DOI: 10.1038/nri799.

150. **Yang Y, Tung JW, Ghosn EEB, Herzenberg LA, Herzenberg LA**. Division and differentiation of natural antibody-producing cells in mouse spleen. *Proc Natl Acad Sci U S A*. Epub ahead of print 2007. DOI: 10.1073/pnas.0700001104.
151. **Kraal G**. Cells in the Marginal Zone of the Spleen. *Int Rev Cytol*. Epub ahead of print 1992. DOI: 10.1016/S0074-7696(08)62453-5.
152. **Martinez-Pomares L, Gordon S**. CD169 + macrophages at the crossroads of antigen presentation. *Trends in Immunology*. Epub ahead of print 2012. DOI: 10.1016/j.it.2011.11.001.
153. **Ito S, Naito M, Kobayashi Y, Takatsuka H, Jiang S, *et al.*** Roles of a macrophage receptor with collagenous structure (MARCO) in host defense and heterogeneity of splenic marginal zone macrophages. *Arch Histol Cytol*. Epub ahead of print 1999. DOI: 10.1679/aohc.62.83.
154. **Lanoue A, Clatworthy MR, Smith P, Green S, Townsend MJ, *et al.*** SIGN-R1 contributes to protection against lethal pneumococcal infection in mice. *J Exp Med*. Epub ahead of print 2004. DOI: 10.1084/jem.20040795.
155. **Kurotaki D, Uede T, Tamura T**. Functions and development of red pulp macrophages. *Microbiology and Immunology*. Epub ahead of print 2015. DOI: 10.1111/1348-0421.12228.
156. **Deniset JF, Surewaard BG, Lee WY, Kubes P**. Splenic Ly6Ghigh mature and Ly6Gint immature neutrophils contribute to eradication of S. pneumoniae. *J Exp Med*. Epub ahead of print 2017. DOI: 10.1084/jem.20161621.
157. **Steiniger BS**. Human spleen microanatomy: Why mice do not suffice. *Immunology*. Epub ahead of print 2015. DOI: 10.1111/imm.12469.
158. **Kirk AD**. Crossing the bridge: Large animal models in translational transplantation research. *Immunological Reviews*. Epub ahead of print 2003. DOI: 10.1046/j.1600-065X.2003.00081.x.
159. **Cesta MF**. Normal Structure, Function, and Histology of the Spleen. *Toxicol Pathol*. Epub ahead of print 2006. DOI: 10.1080/01926230600867743.
160. **Steiniger B, Barth P, Herbst B, Hartnell A, Crocker PR**. The species-specific structure of microanatomical compartments in the human spleen: Strongly sialoadhesin-positive macrophages occur in the perifollicular zone, but not in the marginal zone. *Immunology*. Epub ahead of print 1997. DOI: 10.1046/j.1365-2567.1997.00328.x.

161. **Kang YS, Yamazaki S, Iyoda T, Pack M, Bruening SA, *et al.*** SIGN-R1, a novel C-type lectin expressed by marginal zone macrophages in spleen, mediates uptake of the polysaccharide dextran. *Int Immunol*. Epub ahead of print 2003. DOI: 10.1093/intimm/dxg019.
162. **Park CG, Takahara K, Umemoto E, Yashima Y, Matsubara K, *et al.*** Five mouse homologues of the human dendritic cell C-type lectin, DC-SIGN. *Int Immunol*. Epub ahead of print 2001. DOI: 10.1093/intimm/13.10.1283.
163. **Hein WR, Griebel PJ**. A road less travelled: Large animal models in immunological research. *Nature Reviews Immunology*. Epub ahead of print 2003. DOI: 10.1038/nri977.
164. **Hartnell A, Steel J, Turley H, Jones M, Jackson DG, *et al.*** Characterization of human sialoadhesin, a sialic acid binding receptor expressed by resident and inflammatory macrophage populations. *Blood*. Epub ahead of print 2001. DOI: 10.1182/blood.V97.1.288.
165. **Heikema AP, Bergman MP, Richards H, Crocker PR, Gilbert M, *et al.*** Characterization of the specific interaction between sialoadhesin and sialylated Campylobacter jejuni lipooligosaccharides. *Infect Immun*. Epub ahead of print 2010. DOI: 10.1128/IAI.01273-09.
166. **Jones C, Virji M, Crocker PR**. Recognition of sialylated meningococcal lipopolysaccharide by siglecs expressed on myeloid cells leads to enhanced bacterial uptake. *Mol Microbiol*. Epub ahead of print 2003. DOI: 10.1046/j.1365-2958.2003.03634.x.
167. **Sewald X, Ladinsky MS, Uchil PD, Beloor J, Pi R, *et al.*** Retroviruses use CD169-mediated trans-infection of permissive lymphocytes to establish infection. *Science (80-)*. Epub ahead of print 2015. DOI: 10.1126/science.aab2749.
168. **Veninga H, Borg EGF, Vreeman K, Taylor PR, Kalay H, *et al.*** Antigen targeting reveals splenic CD169 + macrophages as promoters of germinal center B-cell responses. *Eur J Immunol*. Epub ahead of print 2015. DOI: 10.1002/eji.201444983.
169. **Phan TG, Green JA, Xu Y, Cyster JG**. Immune complex relay by subcapsular sinus macrophages and noncognate B cells drives antibody affinity maturation. *Nat Immunol*. Epub ahead of print 2009. DOI: 10.1038/ni.1745.
170. **Kang YS, Kim JY, Bruening SA, Pack M, Charalambous A, *et al.*** The C-

type lectin SIGN-R1 mediates uptake of the capsular polysaccharide of Streptococcus pneumoniae in the marginal zone of mouse spleen. *Proc Natl Acad Sci U S A*. Epub ahead of print 2004. DOI: 10.1073/pnas.0307124101.

171. **Delamarre L, Pack M, Chang H, Mellman I, Trombetta ES**. Differential lysosomal proteolysis in antigen-presenting cells determines antigen fate. *Science (80-)*. Epub ahead of print 2005. DOI: 10.1126/science.1108003.
172. **Kang YS, Do Y, Lee HK, Park SH, Cheong C, *et al.*** A Dominant Complement Fixation Pathway for Pneumococcal Polysaccharides Initiated by SIGN-R1 Interacting with C1q. *Cell*. Epub ahead of print 2006. DOI: 10.1016/j.cell.2006.01.046.
173. **Roomi Nusrat A, Wright SD, Aderem AA, Steinman RM, Cohn ZA**. Properties of isolated red pulp macrophages from mouse spleen. *J Exp Med*. Epub ahead of print 1988. DOI: 10.1084/jem.168.4.1505.
174. **Nagelkerke SQ, Bruggeman CW, Den Haan JMM, Mul EPJ, Van Den Berg TK, *et al.*** Red pulp macrophages in the human spleen are a distinct cell population with a unique expression of Fc-g receptors. *Blood Adv*. Epub ahead of print 2018. DOI: 10.1182/bloodadvances.2017015008.
175. **Alvarez B, Martínez P, Yuste M, Poderoso T, Alonso F, *et al.*** Phenotypic and functional heterogeneity of CD169+ and CD163+ macrophages from porcine lymph nodes and spleen. *Dev Comp Immunol*. Epub ahead of print 2014. DOI: 10.1016/j.dci.2013.11.010.
176. **Leers MPG, Björklund V, Björklund B, Jörnvall H, Nap M**. An immunohistochemical study of the clearance of apoptotic cellular fragments. *Cell Mol Life Sci*. Epub ahead of print 2002. DOI: 10.1007/s00018-002-8513-8.
177. **Roberts AW, Lee BL, Deguine J, John S, Shlomchik MJ, *et al.*** Tissue-Resident Macrophages Are Locally Programmed for Silent Clearance of Apoptotic Cells. *Immunity*. Epub ahead of print 2017. DOI: 10.1016/j.immuni.2017.10.006.
178. **Kim CC, Nelson CS, Wilson EB, Hou B, DeFranco AL, *et al.*** Splenic Red Pulp Macrophages Produce Type I Interferons as Early Sentinels of Malaria Infection but Are Dispensable for Control. *PLoS One*. Epub ahead of print 2012. DOI: 10.1371/journal.pone.0048126.
179. **Martinez-Pomares L, Hanitsch LG, Stillion R, Keshav S, Gordon S**. Expression of mannose receptor and ligands for its cysteine-rich domain in

venous sinuses of human spleen. *Lab Investig*. Epub ahead of print 2005. DOI: 10.1038/labinvest.3700327.

180. **Zamze S, Martinez-Pomares L, Jones H, Taylor PR, Stillion RJ, *et al.*** Recognition of bacterial capsular polysaccharides and lipopolysaccharides by the macrophage mannose receptor. *J Biol Chem*. Epub ahead of print 2002. DOI: 10.1074/jbc.M207057200.
181. **Subramanian K, Neill DR, Malak HA, Spelmink L, Khandaker S, *et al.*** Pneumolysin binds to the mannose receptor C type 1 (MRC-1) leading to anti-inflammatory responses and enhanced pneumococcal survival. *Nature Microbiology*. Epub ahead of print 2019. DOI: 10.1038/s41564-018-0280-x.
182. **Gordon S, Plüddemann A, Mukhopadhyay S**. Sinusoidal immunity: Macrophages at the lymphohematopoietic interface. *Cold Spring Harb Perspect Biol*. Epub ahead of print 2015. DOI: 10.1101/cshperspect.a016378.
183. **Déchanet J, Grosset C, Taupin JL, Merville P, Banchereau J, *et al.*** CD40 ligand stimulates proinflammatory cytokine production by human endothelial cells. *J Immunol*.
184. **Bismuth H**. Surgical anatomy and anatomical surgery of the liver. *World J Surg*. Epub ahead of print 1982. DOI: 10.1007/BF01656368.
185. **Michels NA**. Newer anatomy of the liver and its variant blood supply and collateral circulation. *Am J Surg*. Epub ahead of print 1966. DOI: 10.1016/0002-9610(66)90201-7.
186. Liver and biliary system. In: *Swine in the Laboratory: Surgery, Anesthesia, Imaging, and Experimental Techniques, Second Edition*. 2007. Epub ahead of print 2007. DOI: 10.5005/jp/books/12902_35.
187. **Llorente C, Schnabl B**. Fast-Track Clearance of Bacteria from the Liver. *Cell Host and Microbe*. Epub ahead of print 2016. DOI: 10.1016/j.chom.2016.06.012.
188. **Kmieć Z**. Cooperation of liver cells in health and disease. *Adv Anat Embryol Cell Biol*.
189. **Braet F, Wisse E**. Structural and functional aspects of liver sinusoidal endothelial cell fenestrae: A review. *Comparative Hepatology*. Epub ahead of print 2002. DOI: 10.1186/1476-5926-1-1.
190. **Enomoto K, Nishikawa Y, Omori Y, Tokairin T, Yoshida M, *et al.*** Cell biology and pathology of liver sinusoidal endothelial cells. In: *Medical Electron*

Microscopy. 2004. Epub ahead of print 2004. DOI: 10.1007/s00795-004-0261-4.

191. **Wake K**. Karl Wilhelm Kupffer And His Contributions To Modern Hepatology. *Comp Hepatol*. Epub ahead of print 2004. DOI: 10.1186/1476-5926-2-S1-S2.
192. **Kinoshita M, Uchida T, Sato A, Nakashima M, Nakashima H, *et al.*** Characterization of two F4/80-positive Kupffer cell subsets by their function and phenotype in mice. *J Hepatol*. Epub ahead of print 2010. DOI: 10.1016/j.jhep.2010.04.037.
193. **Terpstra V, Van Berkel TJC**. Scavenger receptors on liver Kupffer cells mediate the in vivo uptake of oxidatively damaged red blood cells in mice. *Blood*. Epub ahead of print 2000. DOI: 10.1182/blood.v95.6.2157.
194. **Deppermann C, Kratofil RM, Peiseler M, David BA, Zindel J, *et al.*** Macrophage galactose lectin is critical for Kupffer cells to clear aged platelets. *J Exp Med*. Epub ahead of print 2020. DOI: 10.1084/jem.20190723.
195. **Wong CHY, Jenne CN, Petri B, Chrobok NL, Kubes P**. Nucleation of platelets with blood-borne pathogens on Kupffer cells precedes other innate immunity and contributes to bacterial clearance. *Nat Immunol*. Epub ahead of print 2013. DOI: 10.1038/ni.2631.
196. **Gregory SH, Cousens LP, van Rooijen N, Döpp EA, Carlos TM, *et al.*** Complementary Adhesion Molecules Promote Neutrophil- Kupffer Cell Interaction and the Elimination of Bacteria Taken Up by the Liver. *J Immunol*. Epub ahead of print 2002. DOI: 10.4049/jimmunol.168.1.308.
197. **Treuting PM, Dintzis SM, Montine KS**. *Comparative Anatomy and Histology*. 2012. Epub ahead of print 2012. DOI: 10.1016/C2009-0-61166-1.
198. **MacParland SA, Liu JC, Ma XZ, Innes BT, Bartczak AM, *et al.*** Single cell RNA sequencing of human liver reveals distinct intrahepatic macrophage populations. *Nat Commun*. Epub ahead of print 2018. DOI: 10.1038/s41467-018-06318-7.
199. **Azad AK, Rajaram MVS, Schlesinger LS**. Exploitation of the Macrophage Mannose Receptor (CD206) in Infectious Disease Diagnostics and Therapeutics. *J Cytol Mol Biol*. Epub ahead of print 2014. DOI: 10.13188/2325-4653.1000003.
200. **Zeng Z, Surewaard BGJ, Wong CHY, Geoghegan JA, Jenne CN, *et al.*** CRIg Functions as a Macrophage Pattern Recognition Receptor to Directly

Bind and Capture Blood-Borne Gram-Positive Bacteria. *Cell Host Microbe*. Epub ahead of print 2016. DOI: 10.1016/j.chom.2016.06.002.

201. **Opanasopit P, Shirashi K, Nishikawa M, Yamashita F, Takakura Y, *et al.*** In vivo recognition of mannosylated proteins by hepatic mannose receptors and mannan-binding protein. *Am J Physiol - Gastrointest Liver Physiol*. Epub ahead of print 2001. DOI: 10.1152/ajpgi.2001.280.5.g879.
202. **Knolle PA, Wohlleber D**. Immunological functions of liver sinusoidal endothelial cells. *Cellular and Molecular Immunology*. Epub ahead of print 2016. DOI: 10.1038/cmi.2016.5.
203. **Malovic I, Sørensen KK, Elvevold KH, Nedredal GI, Paulsen S, *et al.*** The mannose receptor on murine liver sinusoidal endothelial cells is the main denatured collagen clearance receptor. *Hepatology*. Epub ahead of print 2007. DOI: 10.1002/hep.21639.
204. **Bashirova AA, Geijtenbeek TBH, Van Duijnhoven GCF, Van Vliet SJ, Eilering JBG, *et al.*** A dendritic cell-specific intercellular adhesion molecule 3-grabbing nonintegrin (DC-SIGN)-related protein is highly expressed on human liver sinusoidal endothelial cells and promotes HIV-1 infection. *J Exp Med*. Epub ahead of print 2001. DOI: 10.1084/jem.193.6.671.
205. **Yang H, Li N, Du Y, Tong C, Lü S, *et al.*** Neutrophil adhesion and crawling dynamics on liver sinusoidal endothelial cells under shear flow. *Exp Cell Res*. Epub ahead of print 2017. DOI: 10.1016/j.yexcr.2017.01.002.
206. **Jenne CN, Kubes P**. Immune surveillance by the liver. *Nature Immunology*. Epub ahead of print 2013. DOI: 10.1038/ni.2691.
207. **Remick DG**. Pathophysiology of sepsis. *Am J Pathol*. Epub ahead of print 2007. DOI: 10.2353/ajpath.2007.060872.
208. **Van Der Poll T, Van De Veerdonk FL, Scicluna BP, Netea MG**. The immunopathology of sepsis and potential therapeutic targets. *Nature Reviews Immunology*. Epub ahead of print 2017. DOI: 10.1038/nri.2017.36.
209. **Fleischmann C, Scherag A, Adhikari NKJ, Hartog CS, Tsaganos T, *et al.*** Assessment of global incidence and mortality of hospital-treated sepsis current estimates and limitations. *Am J Respir Crit Care Med*. Epub ahead of print 2016. DOI: 10.1164/rccm.201504-0781OC.
210. **Lever A, Mackenzie I**. Sepsis: Definition, epidemiology, and diagnosis. *British Medical Journal*. Epub ahead of print 2007. DOI:

10.1136/bmj.39346.495880.AE.

211. **Martin GS**. Sepsis, severe sepsis and septic shock: Changes in incidence, pathogens and outcomes. *Expert Review of Anti-Infective Therapy*. Epub ahead of print 2012. DOI: 10.1586/eri.12.50.
212. **Angus DC, Van Der Poll T**. Severe sepsis and septic shock. *New England Journal of Medicine*. Epub ahead of print 2013. DOI: 10.1056/NEJMra1208623.
213. **Cinel I, Opal SM**. Molecular biology of inflammation and sepsis: A primer*. *Critical Care Medicine*. Epub ahead of print 2009. DOI: 10.1097/CCM.0b013e31819267fb.
214. **Pierrakos C, Vincent JL**. Sepsis biomarkers: A review. *Crit Care*. Epub ahead of print 2010. DOI: 10.1186/cc8872.
215. **Mira JP, Cariou A, Grall F, Delclaux C, Losser MR, *et al.*** Association of TNF2, a TNF-α promoter polymorphism, with septic shock susceptibility and mortality: A multicenter study. *J Am Med Assoc*. Epub ahead of print 1999. DOI: 10.1001/jama.282.6.561.
216. **Tracey KJ, Fong Y, Hesse DG, Manogue KR, Lee AT, *et al.*** Anti-cachectin/TNF monoclonal antibodies prevent septic shock during lethal bacteraemia. *Nature*. Epub ahead of print 1987. DOI: 10.1038/330662a0.
217. **Thalayasingam N, Isaacs JD**. Anti-TNF therapy. *Best Practice and Research: Clinical Rheumatology*. Epub ahead of print 2011. DOI: 10.1016/j.berh.2011.10.004.
218. **Silfvast-Kaiser A, Paek SY, Menter A**. Anti-IL17 therapies for psoriasis. *Expert Opinion on Biological Therapy*. Epub ahead of print 2019. DOI: 10.1080/14712598.2019.1555235.
219. **van der Poll T**. Future of sepsis therapies. *Critical Care*. Epub ahead of print 2016. DOI: 10.1186/s13054-016-1274-9.
220. **Marshall JC**. Why have clinical trials in sepsis failed? *Trends in Molecular Medicine*. Epub ahead of print 2014. DOI: 10.1016/j.molmed.2014.01.007.
221. **Wahl LM, Gerrish PJ, Saika-Voivod I**. Evaluating the impact of population bottlenecks in experimental evolution. *Genetics*.
222. **France R, Rigg C**. Examination of the 'founder effect' in biodiversity research: Patterns and imbalances in the published literature. *Divers Distrib*. Epub ahead of print 1998. DOI: 10.1046/j.1472-4642.1998.00018.x.

223. **MEYNELL GG**. The applicability of the hypothesis of independent action to fatal infections in mice given Salmonella typhimurium by mouth. *J Gen Microbiol*. Epub ahead of print 1957. DOI: 10.1099/00221287-16-2-396.
224. **Moxon R, Kussell E**. The impact of bottlenecks on microbial survival, adaptation, and phenotypic switching in host–pathogen interactions. *Evolution (N Y)*. Epub ahead of print 2017. DOI: 10.1111/evo.13370.
225. **Wanford JJ, Lango-Scholey L, Nothaft H, Hu Y, Szymanski CM, *et al.*** Random sorting of campylobacter jejuni phase variants due to a narrow bottleneck during colonization of broiler chickens. *Microbiol (United Kingdom)*. Epub ahead of print 2018. DOI: 10.1099/mic.0.000669.
226. **MEYNELL GG, STOCKER BA**. Some hypotheses on the aetiology of fatal infections in partially resistant hosts and their application to mice challenged with Salmonella paratyphi-B or Salmonella typhimurium by intraperitoneal injection. *J Gen Microbiol*. Epub ahead of print 1957. DOI: 10.1099/00221287-16-1-38.
227. **Abel S, Abel zur Wiesch P, Davis BM, Waldor MK**. Analysis of Bottlenecks in Experimental Models of Infection. *PLoS Pathogens*. Epub ahead of print 2015. DOI: 10.1371/journal.ppat.1004823.
228. **Moxon ER, Murphy PA**. Haemophilus influenzae bacteremia and meningitis resulting from survival of a single organism. *Proc Natl Acad Sci U S A*. Epub ahead of print 1978. DOI: 10.1073/pnas.75.3.1534.
229. **Lim CH, Voedisch S, Wahl B, Rouf SF, Geffers R, *et al.*** Independent Bottlenecks Characterize Colonization of Systemic Compartments and Gut Lymphoid Tissue by Salmonella. *PLoS Pathog*. Epub ahead of print 2014. DOI: 10.1371/journal.ppat.1004270.
230. **Dybowski R, Restif O, Price DJ, Mastroeni P**. Inferring within-host bottleneck size: A Bayesian approach. *J Theor Biol*. Epub ahead of print 2017. DOI: 10.1016/j.jtbi.2017.09.011.
231. **Pollitt EJG, Szkuta PT, Burns N, Foster SJ**. Staphylococcus aureus infection dynamics. *PLoS Pathog*. Epub ahead of print 2018. DOI: 10.1371/journal.ppat.1007112.
232. **McVicker G, Prajsnar TK, Williams A, Wagner NL, Boots M, *et al.*** Clonal Expansion during Staphylococcus aureus Infection Dynamics Reveals the Effect of Antibiotic Intervention. *PLoS Pathog*. Epub ahead of print 2014. DOI:

10.1371/journal.ppat.1003959.

233. **Schwartz DJ, Chen SL, Hultgren SJ, Seed PC**. Population dynamics and niche distribution of uropathogenic Escherichia coli during acute and chronic urinary tract infection. *Infect Immun*. Epub ahead of print 2011. DOI: 10.1128/IAI.05339-11.
234. **Pluschke G, Mercer A, Kusecek B, Pohl A, Achtman M**. Induction of bacteremia in newborn rats by Escherichia coli K1 is correlated with only certain O (lipopolysaccharide) antigen types. *Infect Immun*. Epub ahead of print 1983. DOI: 10.1128/iai.39.2.599-608.1983.
235. **Gerlini A, Colomba L, Furi L, Braccini T, Manso AS, *et al.*** The Role of Host and Microbial Factors in the Pathogenesis of Pneumococcal Bacteraemia Arising from a Single Bacterial Cell Bottleneck. *PLoS Pathog*. Epub ahead of print 2014. DOI: 10.1371/journal.ppat.1004026.
236. **Kono M, Zafar MA, Zuniga M, Roche AM, Hamaguchi S, *et al.*** Single Cell Bottlenecks in the Pathogenesis of Streptococcus pneumoniae. *PLoS Pathog*. Epub ahead of print 2016. DOI: 10.1371/journal.ppat.1005887.
237. **Iannelli F, Pearce BJ, Pozzi G**. The type 2 capsule locus of Streptococcus pneumoniae. *J Bacteriol*. Epub ahead of print 1999. DOI: 10.1128/jb.181.8.2652-2654.1999.
238. **Guild WR, Shoemaker NB**. Mismatch correction in pneumococcal transformation: donor length and hex dependent marker efficiency. *J Bacteriol*. Epub ahead of print 1976. DOI: 10.1128/jb.125.1.125-135.1976.
239. **Tettelin H, Nelson KE, Paulsen IT, Eisen JA, Read TD, *et al.*** Complete genome sequence of a virulent isolate of Streptococcus pneumoniae. *Science (80-)*. Epub ahead of print 2001. DOI: 10.1126/science.1061217.
240. **Fang CT, Chuang YP, Shun CT, Chang SC, Wang JT**. A Novel Virulence Gene in Klebsiella pneumoniae Strains Causing Primary Liver Abscess and Septic Metastatic Complications. *J Exp Med* 2004;199:697–705.
241. **Arena F, Spanu T, De Angelis LH, Liotti FM, D'Andrea MM, *et al.*** First case of bacteremic liver abscess caused by an ST260-related (ST1861), hypervirulent Klebsiella pneumoniae. *J Infect* 2016;73:88–91.
242. **Lam MMC, Wyres KL, Duchêne S, Wick RR, Judd LM, *et al.*** Population genomics of hypervirulent Klebsiella pneumoniae clonal-group 23 reveals early emergence and rapid global dissemination. *Nat Commun*;9. Epub ahead of

print 2018. DOI: 10.1038/s41467-018-05114-7.

243. **Cannatelli A, D'Andrea MM, Giani T, Di Pilato V, Arena F, *et al.*** In vivo emergence of colistin resistance in Klebsiella pneumoniae producing KPC-type carbapenemases mediated by insertional inactivation of the PhoQ/PhoP mgrB regulator. *Antimicrob Agents Chemother* 2013;57:5521–5526.
244. **Liu P, Li P, Jiang X, Bi D, Xie Y, *et al.*** Complete genome sequence of Klebsiella pneumoniae subsp. pneumoniae HS11286, a multidrug-resistant strain isolated from human sputum. *J Bacteriol* 2012;194:1841–2.
245. **Arena F, Spanu T, De Angelis LH, Liotti FM, D'Andrea MM, *et al.*** First case of bacteremic liver abscess caused by an ST260-related (ST1861), hypervirulent Klebsiella pneumoniae. *Journal of Infection*. Epub ahead of print 2016. DOI: 10.1016/j.jinf.2016.04.006.
246. **Presta L, Bosi E, Fondi M, Maida I, Perrin E, *et al.*** Phenotypic and genomic characterization of the antimicrobial producer Rheinheimera sp. EpRS3 isolated from the medicinal plant Echinacea purpurea: insights into its biotechnological relevance. *Res Microbiol* 2017;168:293–305.
247. **Rasheed JK, Anderson GJ, Yigit H, Queenan AM, Domenech-Sanchez A, *et al.*** Characterization of the extended-spectrum β-lactamase reference strain, Klebsiella pneumoniae K6 (ATCC 700603), which produces the novel enzyme SHV-18. *Antimicrob Agents Chemother* 2000;44:2382–8.
248. **Bidossi A, Mulas L, Decorosi F, Colomba L, Ricci S, *et al.*** A functional genomics approach to establish the complement of carbohydrate transporters in Streptococcus pneumoniae. *PLoS One*. Epub ahead of print 2012. DOI: 10.1371/journal.pone.0033320.
249. **Coombes BK, Brown NF, Valdez Y, Brumell JH, Finlay BB**. Expression and secretion of Salmonella pathogenicity island-2 virulence genes in response to acidification exhibit differential requirements of a functional type III secretion apparatus and SsaL. *J Biol Chem*. Epub ahead of print 2004. DOI: 10.1074/jbc.M404299200.
250. **Kadioglu A, Cuppone AM, Trappetti C, List T, Spreafico A, *et al.*** Sex-based differences in susceptibility to respiratory and systemic pneumococcal disease in mice. *J Infect Dis* 2011;204:1971–1979.
251. **Oggioni MR, Trappetti C, Kadioglu A, Cassone M, Iannelli F, *et al.*** Switch from planktonic to sessile life: A major event in pneumococcal pathogenesis.

Mol Microbiol 2006;61:1196–210.

252. **Oetke C, Vinson MC, Jones C, Crocker PR**. Sialoadhesin-Deficient Mice Exhibit Subtle Changes in B- and T-Cell Populations and Reduced Immunoglobulin M Levels. *Mol Cell Biol*. Epub ahead of print 2006. DOI: 10.1128/mcb.26.4.1549-1557.2006.
253. **Ercoli G, Fernandes VE, Chung WY, Wanford JJ, Thomson S, *et al.*** Intracellular replication of Streptococcus pneumoniae inside splenic macrophages serves as a reservoir for septicaemia. *Nat Microbiol* 2018;3:600–610.
254. **Weiler JM, Edens RE, Linhardt RJ, Kapelanski DP**. Heparin and modified heparin inhibit complement activation in vivo. *J Immunol*.
255. **Schindelin J, Arganda-Carreras I, Frise E, Kaynig V, Longair M, *et al.*** Fiji: An open-source platform for biological-image analysis. *Nature Methods*. Epub ahead of print 2012. DOI: 10.1038/nmeth.2019.
256. **Chung WY, Wanford JJ, Kumar R, Isherwood JD, Haigh RD, *et al.*** An ex vivo porcine spleen perfusion as a model of bacterial sepsis. *ALTEX* 2019;36:29–38.
257. **Chung WY, Gravante G, Al-Leswas D, Arshad A, Sorge R, *et al.*** The Development of a Multiorgan Ex Vivo Perfused Model: Results With the Porcine Liver-Kidney Circuit Over 24 Hours. *Artif Organs* 2013;37:457–66.
258. **Chung WY, Gravante G, Al-Leswas D, Alzaraa A, Sorge R, *et al.*** Addition of a kidney to the normothermic ex vivo perfused porcine liver model does not increase cytokine response. *J Artif Organs* 2012;15:290–4.
259. **Oggioni MR, A Dennison, L Martinez-Pomares PA**. *TIssue Models for Invasive Disease (TIMID)*. 2018.
260. **Gerlini A, Colomba L, Furi L, Braccini T, Manso AS, *et al.*** The Role of Host and Microbial Factors in the Pathogenesis of Pneumococcal Bacteraemia Arising from a Single Bacterial Cell Bottleneck. *PLoS Pathog*. Epub ahead of print 2014. DOI: 10.1371/journal.ppat.1004026.
261. **Sung CK, Li H, Claverys JP, Morrison DA**. An rpsL Cassette, Janus, for Gene Replacement through Negative Selection in Streptococcus pneumoniae. *Appl Environ Microbiol*. Epub ahead of print 2001. DOI: 10.1128/aem.67.11.5190-5196.2001.
262. **Untergasser A, Nijveen H, Rao X, Bisseling T, Geurts R, *et al.*** Primer3Plus,

an enhanced web interface to Primer3. *Nucleic Acids Res*. Epub ahead of print 2007. DOI: 10.1093/nar/gkm306.

263. **M. Wayne Davis**. A plasmid Editor. *A plasmid Editor*.
264. **Hung JH, Weng Z**. Sequence alignment and homology search with BLAST and ClustalW. *Cold Spring Harb Protoc*. Epub ahead of print 2016. DOI: 10.1101/pdb.prot093088.
265. **Kawamura Y, Hou XG, Sultana F, Miura H, Ezaki T**. Determination of 16S rRNA sequences of Streptococcus mitis and Streptococcus gordonii and phylogenetic relationships among members of the genus Streptococcus. *Int J Syst Bacteriol*. Epub ahead of print 1995. DOI: 10.1099/00207713-45-2-406.
266. **Kauffmann F, Lund E, Eddy BE**. Proposal for a Change in the Nomenclature of Diplococcus Pneumoniae and a Comparison of the Danish and American Type Designations. *Int Bull Bacteriol Nomencl Taxon*. Epub ahead of print 1960. DOI: 10.1099/0096266x-10-1-31.
267. **Whatmore AM, Efstratiou A, Pickerill AP, Broughton K, Woodard G, *et al.*** Genetic relationships between clinical isolates of Streptococcus pneumoniae, Streptococcus oralis, and Streptococcus mitis: Characterization of 'atypical' pneumococci and organisms allied to S. mitis harboring S. pneumoniae virulence factor-encoding genes. *Infect Immun*. Epub ahead of print 2000. DOI: 10.1128/IAI.68.3.1374-1382.2000.
268. **Mbelle N, Huebner RE, Wasas AD, Kimura A, Chang I, *et al.*** Immunogenicity and Impact on Nasopharyngeal Carriage of a Nonavalent Pneumococcal Conjugate Vaccine. *J Infect Dis*. Epub ahead of print 1999. DOI: 10.1086/315009.
269. **van der Poll T, Opal SM**. Pathogenesis, treatment, and prevention of pneumococcal pneumonia. *The Lancet*. Epub ahead of print 2009. DOI: 10.1016/S0140-6736(09)61114-4.
270. **Yu VL, Chiou CCC, Feldman C, Ortqvist A, Rello J, *et al.*** An International Prospective Study of Pneumococcal Bacteremia: Correlation with In Vitro Resistance, Antibiotics Administered, and Clinical Outcome. *Clin Infect Dis*. Epub ahead of print 2003. DOI: 10.1086/377534.
271. **Mook-Kanamori BB, Geldhoff M, van der Poll T, van de Beek D**. Pathogenesis and pathophysiology of pneumococcal meningitis. *Clin Microbiol Rev*. Epub ahead of print 2011. DOI: 10.1128/CMR.00008-11.

272. **Wei BPC, Shepherd RK, Robins-Browne RM, Clark GM, O'Leary SJ**. Pneumococcal meningitis: Development of a new animal model. *Otol Neurotol*. Epub ahead of print 2006. DOI: 10.1097/01.mao.0000231603.25961.f1.
273. **Rello J, Luján M, Gallego M, Vallés J, Belmonte Y, *et al.*** Why mortality is increased in health-care-associated pneumonia: Lessons from pneumococcal bacteremic pneumonia. *Chest*. Epub ahead of print 2010. DOI: 10.1378/chest.09-2175.
274. **Joffe MD, Alpern ER**. Occult pneumococcal bacteremia: A review. *Pediatric Emergency Care*. Epub ahead of print 2010. DOI: 10.1097/PEC.0b013e3181e15e36.
275. **Ruiz M, Ewig S, Marcos MA, Martinez JA, Arancibia F, *et al.*** Etiology of community-acquired pneumonia: Impact of age, comorbidity, and severity. *Am J Respir Crit Care Med*. Epub ahead of print 1999. DOI: 10.1164/ajrccm.160.2.9808045.
276. **Jochems SP, Weiser JN, Malley R, Ferreira DM**. The immunological mechanisms that control pneumococcal carriage. *PLoS Pathogens*. Epub ahead of print 2017. DOI: 10.1371/journal.ppat.1006665.
277. **Hanage WP, Finkelstein JA, Huang SS, Pelton SI, Stevenson AE, *et al.*** Evidence that pneumococcal serotype replacement in Massachusetts following conjugate vaccination is now complete. *Epidemics*. Epub ahead of print 2010. DOI: 10.1016/j.epidem.2010.03.005.
278. **Murad C, Dunne EM, Sudigdoadi S, Fadlyana E, Tarigan R, *et al.*** Pneumococcal carriage, density, and co-colonization dynamics: A longitudinal study in Indonesian infants. *Int J Infect Dis*. Epub ahead of print 2019. DOI: 10.1016/j.ijid.2019.06.024.
279. **Diavatopoulos DA, Short KR, Price JT, Wilksch JJ, Brown LE, *et al.*** Influenza A virus facilitates Streptococcus pneumoniae transmission and disease . *FASEB J*. Epub ahead of print 2010. DOI: 10.1096/fj.09-146779.
280. **Siegel SJ, Roche AM, Weiser JN**. Influenza promotes pneumococcal growth during coinfection by providing host sialylated substrates as a nutrient source. *Cell Host Microbe*. Epub ahead of print 2014. DOI: 10.1016/j.chom.2014.06.005.
281. **Trappetti C, Kadioglu A, Carter M, Hayre J, Iannelli F, *et al.*** Sialic Acid: A Preventable Signal for Pneumococcal Biofilm Formation, Colonization, and

Invasion of the Host. *J Infect Dis*. Epub ahead of print 2009. DOI: 10.1086/598483.

282. **Clarke TB, Francella N, Huegel A, Weiser JN**. Invasive bacterial pathogens exploit TLR-mediated downregulation of tight junction components to facilitate translocation across the epithelium. *Cell Host Microbe*. Epub ahead of print 2011. DOI: 10.1016/j.chom.2011.04.012.
283. **Iovino F, Orihuela CJ, Moorlag HE, Molema G, Bijlsma JJE**. Interactions between Blood-Borne Streptococcus pneumoniae and the Blood-Brain Barrier Preceding Meningitis. *PLoS One*. Epub ahead of print 2013. DOI: 10.1371/journal.pone.0068408.
284. **Paterson GK, Mitchell TJ**. Innate immunity and the pneumococcus. *Microbiology*. Epub ahead of print 2006. DOI: 10.1099/mic.0.28551-0.
285. **Kadioglu A, Weiser JN, Paton JC, Andrew PW**. The role of Streptococcus pneumoniae virulence factors in host respiratory colonization and disease. *Nature Reviews Microbiology*. Epub ahead of print 2008. DOI: 10.1038/nrmicro1871.
286. **Geno KA, Gilbert GL, Song JY, Skovsted IC, Klugman KP, *et al.*** Pneumococcal capsules and their types: Past, present, and future. *Clin Microbiol Rev*. Epub ahead of print 2015. DOI: 10.1128/CMR.00024-15.
287. **Bentley SD, Aanensen DM, Mavroidi A, Saunders D, Rabbinowitsch E, *et al.*** Genetic analysis of the capsular biosynthetic locus from all 90 pneumococcal serotypes. *PLoS Genet*. Epub ahead of print 2006. DOI: 10.1371/journal.pgen.0020031.
288. **van Tonder AJ, Gladstone RA, Lo SW, Nahm MH, du Plessis M, *et al.*** Putative novel cps loci in a large global collection of pneumococci. *Microb Genomics*. Epub ahead of print 2019. DOI: 10.1099/mgen.0.000274.
289. **Cowley LA, Petersen FC, Junges R, Jimson D. Jimenez M, Morrison DA, *et al.*** Evolution via recombination: Cell-to-cell contact facilitates larger recombination events in Streptococcus pneumoniae. *PLoS Genet*. Epub ahead of print 2018. DOI: 10.1371/journal.pgen.1007410.
290. **Mostowy R, Croucher NJ, Hanage WP, Harris SR, Bentley S, *et al.*** Heterogeneity in the Frequency and Characteristics of Homologous Recombination in Pneumococcal Evolution. *PLoS Genet*. Epub ahead of print 2014. DOI: 10.1371/journal.pgen.1004300.

291. **Sørensen UBS, Henrichsen J, Chen HC, Szu SC**. Covalent linkage between the capsular polysaccharide and the cell wall peptidoglycan of Streptococcus pneumoniae revealed by immunochemical methods. *Microb Pathog*. Epub ahead of print 1990. DOI: 10.1016/0882-4010(90)90091-4.
292. **Eberhardt A, Hoyland CN, Vollmer D, Bisle S, Cleverley RM, *et al.*** Attachment of capsular polysaccharide to the cell wall in Streptococcus pneumoniae. *Microb Drug Resist*. Epub ahead of print 2012. DOI: 10.1089/mdr.2011.0232.
293. **MacLEOD CM, KRAUS MR**. Relation of virulence of pneumococcal strains for mice to the quantity of capsular polysaccharide formed in vitro. *J Exp Med*. Epub ahead of print 1950. DOI: 10.1084/jem.92.1.1.
294. **Griffith F**. The Significance of Pneumococcal Types. *J Hyg (Lond)*. Epub ahead of print 1928. DOI: 10.1017/S0022172400031879.
295. **Briles DE, Crain MJ, Gray BM, Forman C, Yother J**. Strong association between capsular type and virulence for mice among human isolates of Streptococcus pneumoniae. *Infect Immun*. Epub ahead of print 1992. DOI: 10.1128/iai.60.1.111-116.1992.
296. **Avery OT, Macleod CM, McCarty M**. Studies on the chemical nature of the substance inducing transformation of pneumococcal types: Induction of transformation by a desoxyribonucleic acid fraction isolated from pneumococcus type iii. *J Exp Med*. Epub ahead of print 1944. DOI: 10.1084/jem.79.2.137.
297. **Langereis JD, de Jonge MI**. Non-encapsulated Streptococcus pneumoniae, vaccination as a measure to interfere with horizontal gene transfer. *Virulence*. Epub ahead of print 2017. DOI: 10.1080/21505594.2017.1309492.
298. **WOOD WB, SMITH MR**. The inhibition of surface phagocytosis by the capsular slime layer of pneumococcus type III. *J Exp Med*. Epub ahead of print 1949. DOI: 10.1084/jem.90.1.85.
299. **Gupta R, Yang J, Dong Y, Swiatlo E, Zhang JR, *et al.*** Deletion of arcD in streptococcus pneumoniae D39 impairs its capsule and attenuates virulence. *Infect Immun*. Epub ahead of print 2013. DOI: 10.1128/IAI.00778-13.
300. **Hyams C, Camberlein E, Cohen JM, Bax K, Brown JS**. The Streptococcus pneumoniae capsule inhibits complement activity and neutrophil phagocytosis by multiple mechanisms. *Infect Immun*. Epub ahead of print 2010. DOI:

10.1128/IAI.00881-09.

301. **Li Y, Weinberger DM, Thompson CM, Trzciński K, Lipsitch M**. Surface charge of Streptococcus pneumoniae predicts serotype distribution. *Infect Immun*. Epub ahead of print 2013. DOI: 10.1128/IAI.00724-13.
302. **Melin M, Trzciński K, Meri S, Käyhty H, Väkeväinen M**. The capsular serotype of Streptococcus pneumoniae is more important than the genetic background for resistance to complement. *Infect Immun*. Epub ahead of print 2010. DOI: 10.1128/IAI.00740-10.
303. **Rabes A, Zimmermann S, Reppe K, Lang R, Seeberger PH, *et al.*** The C-type lectin receptor mincle binds to streptococcus pneumoniae but plays a limited role in the anti-pneumococcal innate immune response. *PLoS One*. Epub ahead of print 2015. DOI: 10.1371/journal.pone.0117022.
304. **Koppel EA, Saeland E, de Cooker DJM, van Kooyk Y, Geijtenbeek TBH**. DC-SIGN specifically recognizes Streptococcus pneumoniae serotypes 3 and 14. *Immunobiology*. Epub ahead of print 2005. DOI: 10.1016/j.imbio.2005.05.014.
305. **Yother J**. Capsules of Streptococcus pneumoniae and Other Bacteria: Paradigms for Polysaccharide Biosynthesis and Regulation . *Annu Rev Microbiol*. Epub ahead of print 2011. DOI: 10.1146/annurev.micro.62.081307.162944.
306. **Aprianto R, Slager J, Holsappel S, Veening JW**. High-resolution analysis of the pneumococcal transcriptome under a wide range of infection-relevant conditions. *Nucleic Acids Res*. Epub ahead of print 2018. DOI: 10.1093/nar/gky750.
307. **Xu H, Wang L, Huang J, Zhang Y, Ma F, *et al.*** Pneumococcal wall teichoic acid is required for the pathogenesis of Streptococcus pneumoniae in murine models. *J Microbiol*. Epub ahead of print 2015. DOI: 10.1007/s12275-015-4616-4.
308. **Mellroth P, Daniels R, Eberhardt A, Rönnlund D, Blom H, *et al.*** LytA, major autolysin of Streptococcus pneumoniae, requires access to nascent peptidoglycan. *J Biol Chem*. Epub ahead of print 2012. DOI: 10.1074/jbc.M111.318584.
309. **Mellroth P, Sandalova T, Kikhney A, Vilaplana F, Hesek D, *et al.*** Structural and functional insights into peptidoglycan access for the lytic amidase LytA of

Streptococcus pneumoniae. *MBio*. Epub ahead of print 2014. DOI: 10.1128/mBio.01120-13.

310. **Orihuela CJ, Gao G, Francis KP, Yu J, Tuomanen EI**. Tissue-Specific Contributions of Pneumococcal Virulence Factors to Pathogenesis. *J Infect Dis*. Epub ahead of print 2004. DOI: 10.1086/424596.
311. **Weiser JN, Ferreira DM, Paton JC**. Streptococcus pneumoniae: Transmission, colonization and invasion. *Nature Reviews Microbiology*. Epub ahead of print 2018. DOI: 10.1038/s41579-018-0001-8.
312. **Gámez G, Castro A, Gómez-Mejia A, Gallego M, Bedoya A, *et al.*** The variome of pneumococcal virulence factors and regulators. *BMC Genomics*. Epub ahead of print 2018. DOI: 10.1186/s12864-017-4376-0.
313. **Van Pee K, Mulvihill E, Müller DJ, Yildiz Ö**. Unraveling the Pore-Forming Steps of Pneumolysin from Streptococcus pneumoniae. *Nano Lett*. Epub ahead of print 2016. DOI: 10.1021/acs.nanolett.6b04219.
314. **Tilley SJ, Orlova E V., Gilbert RJC, Andrew PW, Saibil HR**. Structural basis of pore formation by the bacterial toxin pneumolysin. *Cell*. Epub ahead of print 2005. DOI: 10.1016/j.cell.2005.02.033.
315. **Nöllmann M, Gilbert R, Mitchell T, Sferrazza M, Byron O**. The Role of Cholesterol in the Activity of Pneumolysin, a Bacterial Protein Toxin. *Biophys J*. Epub ahead of print 2004. DOI: 10.1016/S0006-3495(04)74362-3.
316. **Gedde MM, Higgins DE, Tilney LG, Portnoy DA**. Role of listeriolysin O in cell-to-cell spread of Listeria monocytogenes. *Infect Immun*. Epub ahead of print 2000. DOI: 10.1128/IAI.68.2.999-1003.2000.
317. **Johnson MK, Boese-Marrazzo D, Pierce WA**. Effects of pneumolysin on human polymorphonuclear leukocytes and platelets. *Infect Immun*. Epub ahead of print 1981. DOI: 10.1128/iai.34.1.171-176.1981.
318. **Houldsworth S, Andrew PW, Mitchell TJ**. Pneumolysin stimulates production of tumor necrosis factor alpha and interleukin-1?? by human mononuclear phagocytes. *Infection and Immunity*. Epub ahead of print 1994. DOI: 10.1128/iai.62.4.1501-1503.1994.
319. **Srivastava A, Henneke P, Visintin A, Morse SC, Martin V, *et al.*** The apoptotic response to pneumolysin is toll-like receptor 4 dependent and protects against pneumococcal disease. *Infect Immun*. Epub ahead of print 2005. DOI: 10.1128/IAI.73.10.6479-6487.2005.

320. **Paton JC, Ferrante A**. Inhibition of human polymorphonuclear leukocyte respiratory burst, bactericidal activity, and migration by pneumolysin. *Infect Immun*. Epub ahead of print 1983. DOI: 10.1128/iai.41.3.1212-1216.1983.
321. **Baba H, Kawamura I, Kohda C, Nomura T, Ito Y, *et al.*** Induction of gamma interferon and nitric oxide by truncated pneumolysin that lacks pore-forming activity. *Infect Immun*. Epub ahead of print 2002. DOI: 10.1128/IAI.70.1.107-113.2002.
322. **Camara M, Boulnois GJ, Andrew PW, Mitchell TJ**. A neuraminidase from Streptococcus pneumoniae has the features of a surface protein. *Infect Immun*. Epub ahead of print 1994. DOI: 10.1128/iai.62.9.3688-3695.1994.
323. **King SJ, Whatmore AM, Dowson CG**. NanA, a neuraminidase from Streptococcus pneumoniae, shows high levels of sequence diversity, at least in part through recombination with Streptococcus oralis. *J Bacteriol*. Epub ahead of print 2005. DOI: 10.1128/JB.187.15.5376-5386.2005.
324. **Brittan JL, Buckeridge TJ, Finn A, Kadioglu A, Jenkinson HF**. Pneumococcal neuraminidase A: An essential upper airway colonization factor for Streptococcus pneumoniae. *Mol Oral Microbiol*. Epub ahead of print 2012. DOI: 10.1111/j.2041-1014.2012.00658.x.
325. **Pettigrew MM, Fennie KP, York MP, Daniels J, Ghaffar F**. Variation in the presence of neuraminidase genes among Streptococcus pneumoniae isolates with identical sequence types. *Infect Immun*. Epub ahead of print 2006. DOI: 10.1128/IAI.01442-05.
326. **McCombs JE, Diaz JP, Luebke KJ, Kohler JJ**. Glycan specificity of neuraminidases determined in microarray format. *Carbohydr Res*. Epub ahead of print 2016. DOI: 10.1016/j.carres.2016.04.003.
327. **Sharapova Y, Suplatov D, Švedas V**. Neuraminidase A from Streptococcus pneumoniae has a modular organization of catalytic and lectin domains separated by a flexible linker. *FEBS J*. Epub ahead of print 2018. DOI: 10.1111/febs.14486.
328. **Xu G, Kiefel MJ, Wilson JC, Andrew PW, Oggioni MR, *et al.*** Three streptococcus pneumoniae sialidases: Three different products. *J Am Chem Soc*. Epub ahead of print 2011. DOI: 10.1021/ja110733q.
329. **Manco S, Hernon F, Yesilkaya H, Paton JC, Andrew PW, *et al.*** Pneumococcal neuraminidases A and B both have essential roles during

infection of the respiratory tract and sepsis. *Infect Immun*. Epub ahead of print 2006. DOI: 10.1128/IAI.01237-05.

330. **Dalia AB, Standish AJ, Weiser JN**. Three surface exoglycosidases from Streptococcus pneumoniae, NanA, BgaA, and StrH, promote resistance to opsonophagocytic killing by human neutrophils. *Infect Immun*. Epub ahead of print 2010. DOI: 10.1128/IAI.01125-09.
331. **Uchiyama S, Carlin AF, Khosravi A, Weiman S, Banerjee A, *et al.*** The surface-anchored NanA protein promotes pneumococcal brain endothelial cell invasion. *J Exp Med*. Epub ahead of print 2009. DOI: 10.1084/jem.20090386.
332. **Friedland IR**. Comparison of the response to antimicrobial therapy of penicillin-resistant and penicillin-susceptible pneumococcal disease. *Pediatr Infect Dis J*. Epub ahead of print 1995. DOI: 10.1097/00006454-199510000-00013.
333. **McGee L, McDougal L, Zhou J, Spratt BG, Tenover FC, *et al.*** Nomenclature of major antimicrobial-resistant clones of Streptococcus pneumoniae defined by the pneumococcal molecular epidemiology network. *J Clin Microbiol*. Epub ahead of print 2001. DOI: 10.1128/JCM.39.7.2565-2571.2001.
334. **Grebe T, Hakenbeck R**. Penicillin-binding proteins 2b and 2x of Streptococcus pneumoniae are primary resistance determinants for difierent classes of β-lactam antibiotics. *Antimicrob Agents Chemother*. Epub ahead of print 1996. DOI: 10.1128/aac.40.4.829.
335. **Hu F, Zhu D, Wang F, Morrissey I, Wang J, *et al.*** Results from the Survey of Antibiotic Resistance (SOAR) 2009-11 and 2013-14 in China. *J Antimicrob Chemother*. Epub ahead of print 2016. DOI: 10.1093/jac/dkw065.
336. **Cartwright K**. Pneumococcal disease in western Europe: Burden of disease, antibiotic resistance and management. *European Journal of Pediatrics*. Epub ahead of print 2002. DOI: 10.1007/s00431-001-0907-3.
337. **McGeer D, Green AK, Low DE**. Macrolide Resistance in Bacteremic Pneumococcal Disease: Implications for Patient Management. *Clin Infect Dis*. Epub ahead of print 2006. DOI: 10.1086/505871.
338. **Santagati M, Iannelli F, Oggioni MR, Stefani S, Pozzi G**. Characterization of a genetic element carrying the macrolide efflux gene mef(A) in Streptococcus pneumoniae. *Antimicrob Agents Chemother*. Epub ahead of print 2000. DOI: 10.1128/AAC.44.9.2585-2587.2000.

339. **Farrell DJ, Jenkins SG, Brown SD, Patel M, Lavin BS, *et al.*** Emergence and spread of Streptococcus pneumoniae with erm(B) and mef(A) resistance. *Emerg Infect Dis*. Epub ahead of print 2005. DOI: 10.3201/eid1106.050222.
340. **Lim WS, Baudouin S V., George RC, Hill AT, Jamieson C, *et al.*** BTS guidelines for the management of community acquired pneumonia in adults: update 2009. *Thorax*.
341. **Dulhunty JM, Webb SAR, Paterson DL, Bellomo R, Myburgh J, *et al.*** A survey of antibiotic prescribing practices in Australian and New Zealand intensive care units. *Crit Care Resusc*.
342. Book Review The Biology of Pneumococcus: The bacteriological, biochemical and immunological characters and activities of diplococcus pneumoniae . Benjamin White. 799 pp. New York: The Commonwealth Fund, 1938. $4.50. *N Engl J Med*. Epub ahead of print 1938. DOI: 10.1056/nejm193806092182314.
343. **Butler JC, Shapiro ED, Carlone GM**. Pneumococcal vaccines: History, current status, and future directions. In: *American Journal of Medicine*. 1999. Epub ahead of print 1999. DOI: 10.1016/s0002-9343(99)00105-9.
344. **Jiang Y, Gauthier A, Keeping S, Carroll S**. Cost-effectiveness of vaccinating the elderly and at-risk adults with the 23-valent pneumococcal polysaccharide vaccine or 13-valent pneumococcal conjugate vaccine in the UK. *Expert Rev Pharmacoeconomics Outcomes Res*. Epub ahead of print 2014. DOI: 10.1586/14737167.2014.950232.
345. **Westerink MAJ, Schroeder HW, Nahm MH**. Immune responses to pneumococcal vaccines in children and adults: Rationale for age-specific vaccination. *Aging and Disease*.
346. **Lin TY, Shah NK, Brooks D, Garcia CS**. Summary of invasive pneumococcal disease burden among children in the Asia-Pacific region. *Vaccine*. Epub ahead of print 2010. DOI: 10.1016/j.vaccine.2010.07.053.
347. **Campos-Outcalt D**. Pneumococcal conjugate vaccine update. *J Fam Pract*. Epub ahead of print 2019. DOI: 10.1007/978-1-4615-1823-5_31.
348. **Adams WG, Deaver KA, Cochi SL, Plikaytis BD, Zell ER, *et al.*** Decline of Childhood Haemophilus influenzae Type b (Hib) Disease in the Hib Vaccine Era. *JAMA J Am Med Assoc*. Epub ahead of print 1993. DOI: 10.1001/jama.1993.03500020055031.
349. **Black S, Shinefield H, Fireman B, Lewis E, Ray P, *et al.*** Efficacy, safety and

immunogenicity of heptavalent pneumococcal conjugate vaccine in children. Northern California Kaiser Permanente Vaccine Study Center Group. *Pediatr Infect Dis J*.

350. **Gladstone RA, Jefferies JM, Tocheva AS, Beard KR, Garley D, *et al.*** Five winters of pneumococcal serotype replacement in UK carriage following PCV introduction. *Vaccine*. Epub ahead of print 2015. DOI: 10.1016/j.vaccine.2015.03.012.
351. **Croucher NJ, Harris SR, Fraser C, Quail MA, Burton J, *et al.*** Rapid pneumococcal evolution in response to clinical interventions. *Science (80-)*. Epub ahead of print 2011. DOI: 10.1126/science.1198545.
352. **Brueggemann AB, Pai R, Crook DW, Beall B**. Vaccine escape recombinants emerge after pneumococcal vaccination in the United States. *PLoS Pathog*. Epub ahead of print 2007. DOI: 10.1371/journal.ppat.0030168.
353. **Anderson RJ, Guru S, Weeratna R, Makinen S, Falconer DJ, *et al.*** In vivo screen of genetically conserved Streptococcus pneumoniae proteins for protective immunogenicity. *Vaccine*. Epub ahead of print 2016. DOI: 10.1016/j.vaccine.2016.10.061.
354. **Croucher NJ, Campo JJ, Le TQ, Liang X, Bentley SD, *et al.*** Diverse evolutionary patterns of pneumococcal antigens identified by pangenome-wide immunological screening. *Proc Natl Acad Sci U S A*. Epub ahead of print 2017. DOI: 10.1073/pnas.1613937114.
355. **David SC, Laan Z, Minhas V, Chen AY, Davies J, *et al.*** Enhanced safety and immunogenicity of a pneumococcal surface antigen A mutant whole-cell inactivated pneumococcal vaccine. *Immunol Cell Biol*. Epub ahead of print 2019. DOI: 10.1111/imcb.12257.
356. **Tennant SM, Levine MM**. Live attenuated vaccines for invasive Salmonella infections. *Vaccine*. Epub ahead of print 2015. DOI: 10.1016/j.vaccine.2015.04.029.
357. **Horton J, Ogden ME, Williams S, Coln D**. The importance of splenic blood flow in clearing pneumococcal organisms. *Ann Surg*. Epub ahead of print 1982. DOI: 10.1097/00000658-198202000-00009.
358. **Gopal V, Bisno AL**. Fulminant Pneumococcal Infections in 'Normal' Asplenic Hosts. *Arch Intern Med*. Epub ahead of print 1977. DOI: 10.1001/archinte.1977.03630230022009.

359. **Theilacker C, Ludewig K, Serr A, Schimpf J, Held J, *et al.*** Overwhelming postsplenectomy infection: A prospective multicenter cohort study. In: *Clinical Infectious Diseases*. 2016. Epub ahead of print 2016. DOI: 10.1093/cid/civ1195.

360. **Rosado MM, Gesualdo F, Marcellini V, Di Sabatino A, Corazza GR, *et al.*** Preserved antibody levels and loss of memory B cells against pneumococcus and tetanus after splenectomy: Tailoring better vaccination strategies. *Eur J Immunol*. Epub ahead of print 2013. DOI: 10.1002/eji.201343577.

361. **Brown EJ, Hosea SW, Frank MM**. The role of the spleen in experimental pneumococcal bacteremia. *J Clin Invest*. Epub ahead of print 1981. DOI: 10.1172/JCI110148.

362. **Ercoli G, Fernandes VE, Chung WY, Wanford JJ, Thomson S, *et al.*** Intracellular replication of Streptococcus pneumoniae inside splenic macrophages serves as a reservoir for septicaemia. *Nat Microbiol*. Epub ahead of print 2018. DOI: 10.1038/s41564-018-0147-1.

363. **McIntyre KW, Stepan GJ, Kolinsky KD, Benjamin WR, Plocinski JM, *et al.*** Inhibition of interleukin 1 (IL-1) binding and bioactivity in vitro and modulation of acute inflammation in vivo by IL-1 receptor antagonist and anti-IL-1 receptor monoclonal antibody. *J Exp Med*. Epub ahead of print 1991. DOI: 10.1084/jem.173.4.931.

364. **Nesic O, Perez-Polo R, Xu GY, McAdoo D, High KW, *et al.*** IL-1 receptor antagonist prevents apoptosis and caspase-3 activation after spinal cord injury. *J Neurotrauma*. Epub ahead of print 2001. DOI: 10.1089/089771501750451857.

365. **Iwakura Y, Ishigame H, Saijo S, Nakae S**. Functional Specialization of Interleukin-17 Family Members. *Immunity*. Epub ahead of print 2011. DOI: 10.1016/j.immuni.2011.02.012.

366. **Apostolaki M, Armaka M, Victoratos P, Kollias G**. Cellular mechanisms of TNF function in models of inflammation and autoimmunity. *Current Directions in Autoimmunity*. Epub ahead of print 2010. DOI: 10.1159/000289195.

367. **Dalton DK, Pitts-Meek S, Keshav S, Figari IS, Bradley A, *et al.*** Multiple defects of immune cell function in mice with disrupted interferon-γ genes. *Science (80-)*. Epub ahead of print 1993. DOI: 10.1126/science.8456300.

368. **Cook DN, Beck MA, Coffman TM, Kirby SL, Sheridan JF, *et al.***

Requirement of MIP-1α for an inflammatory response to viral infection. *Science (80-)*. Epub ahead of print 1995. DOI: 10.1126/science.7667639.

369. **Elyaman W, Bradshaw EM, Uyttenhove C, Dardalhon V, Awasthi A, *et al.*** IL-9 induces differentiation of TH17 cells and enhances function of FoxP3+ natural regulatory T cells. *Proc Natl Acad Sci U S A*. Epub ahead of print 2009. DOI: 10.1073/pnas.0812530106.
370. **Thornton AM, Donovan EE, Piccirillo CA, Shevach EM**. Cutting Edge: IL-2 Is Critically Required for the In Vitro Activation of CD4 + CD25 + T Cell Suppressor Function . *J Immunol*. Epub ahead of print 2004. DOI: 10.4049/jimmunol.172.11.6519.
371. **Nelms K, Keegan AD, Zamorano J, Ryan JJ, Paul WE**. THE IL-4 RECEPTOR: Signaling Mechanisms and Biologic Functions. *Annu Rev Immunol*. Epub ahead of print 1999. DOI: 10.1146/annurev.immunol.17.1.701.
372. **McKenzie ANJ, Culpepper JA, De Waal Malefyt R, Briere F, Punnonen J, *et al.*** Interleukin 13, a T-cell-derived cytokine that regulates human monocyte and B-cell function. *Proc Natl Acad Sci U S A*. Epub ahead of print 1993. DOI: 10.1073/pnas.90.8.3735.
373. **Beagley KW, Eldridge JH, Kiyono H, Everson MP, Koopman WJ, *et al.*** Recombinant murine IL-5 induces high rate IgA synthesis in cycling IgA-positive Peyer's patch B cells. *J Immunol*.
374. **Frendl G, Beller DI**. Regulation of macrophage activation by IL-3: I. IL-3 functions as a macrophage-activating factor with unique properties, inducing Ia and lymphocyte function-associated antigen-1 but not cytotoxicity. *J Immunol*.
375. **Buschmann IR, Hoefer IE, Van Royen N, Katzer E, Braun-Dulleaus R, *et al.*** GM-CSF: A strong arteriogenic factor acting by amplification of monocyte function. In: *Atherosclerosis*. 2001. Epub ahead of print 2001. DOI: 10.1016/S0021-9150(01)00637-2.
376. **Scapini P, Nardelli B, Nadali G, Calzetti F, Pizzolo G, *et al.*** G-CSF-stimulated neutrophils are a prominent source of functional BLyS. *J Exp Med*. Epub ahead of print 2003. DOI: 10.1084/jem.20021343.
377. **Stewart CA, Metheny H, Iida N, Smith L, Hanson M, *et al.*** Interferon-dependent IL-10 production by Tregs limits tumor Th17 inflammation. *J Clin Invest*. Epub ahead of print 2013. DOI: 10.1172/JCI65180.
378. **Orange JS, Biron CA**. An absolute and restricted requirement for IL-12 in

natural killer cell IFN-gamma production and antiviral defense. Studies of natural killer and T cell responses in contrasting viral infections. *J Immunol*.

379. **Khader SA, Pearl JE, Sakamoto K, Gilmartin L, Bell GK, *et al.*** IL-23 Compensates for the Absence of IL-12p70 and Is Essential for the IL-17 Response during Tuberculosis but Is Dispensable for Protection and Antigen-Specific IFN-γ Responses if IL-12p70 Is Available. *J Immunol*. Epub ahead of print 2005. DOI: 10.4049/jimmunol.175.2.788.
380. **Lampinen M, Rak S, Venge P**. The role of interleukin-5, interleukin-8 and RANTES in the chemotactic attraction of eosinophils to the allergic lung. *Clin Exp Allergy*. Epub ahead of print 1999. DOI: 10.1046/j.1365-2222.1999.00390.x.
381. **Frevert CW, Huang S, Danaee H, Paulauskis JD, Kobzik L**. Functional characterization of the rat chemokine KC and its importance in neutrophil recruitment in a rat model of pulmonary inflammation. *J Immunol*.
382. **Mattes J, Foster PS**. Regulation of eosinophil migration and Th2 cell function by IL-5 and eotaxin. *Current drug targets. Inflammation and allergy*. Epub ahead of print 2003. DOI: 10.2174/1568010033484214.
383. **Paavola CD, Hemmerich S, Grunberger D, Polsky I, Bloom A, *et al.*** Monomeric monocyte chemoattractant protein-1 (MCP-1) binds and activates the MCP-1 receptor CCR2B. *J Biol Chem*. Epub ahead of print 1998. DOI: 10.1074/jbc.273.50.33157.
384. **Forbes ML, Horsey E, Hiller NL, Buchinsky FJ, Hayes JD, *et al.*** Strain-specific virulence phenotypes of Streptococcus pneumoniae assessed using the Chinchilla laniger model of otitis media. *PLoS One*. Epub ahead of print 2008. DOI: 10.1371/journal.pone.0001969.
385. **De Baere MI, Van Gorp H, Delputte PL, Nauwynck HJ**. Interaction of the European genotype porcine reproductive and respiratory syndrome virus (PRRSV) with sialoadhesin (CD169/Siglec-1) inhibits alveolar macrophage phagocytosis. *Vet Res*. Epub ahead of print 2012. DOI: 10.1186/1297-9716-43-47.
386. **Liu Y, Li R, Qiao S, Chen X, Deng R, *et al.*** Porcine sialoadhesin suppresses type I interferon production to support porcine reproductive and respiratory syndrome virus infection. *Vet Res* 2020;1–14.
387. **Sattentau QJ, Stevenson M**. Macrophages and HIV-1: An Unhealthy

Constellation. *Cell Host and Microbe*. Epub ahead of print 2016. DOI: 10.1016/j.chom.2016.02.013.

388. **Crocker PR, Gordon S**. Mouse macrophage hemagglutinin (sheep erythrocyte receptor) with specificity for sialylated glycoconjugates characterized by a monoclonal antibody. *J Exp Med*. Epub ahead of print 1989. DOI: 10.1084/jem.169.4.1333.
389. **Vaupel P, Ruppert H, Hutten H**. Splenic blood flow and intrasplenic flow distribution in rats. *Pflügers Arch Eur J Physiol*. Epub ahead of print 1977. DOI: 10.1007/BF00582184.
390. **Gualdi L, Hayre JK, Gerlini A, Bidossi A, Colomba L, *et al.*** Regulation of neuraminidase expression in Streptococcus pneumoniae. *BMC Microbiol*. Epub ahead of print 2012. DOI: 10.1186/1471-2180-12-200.
391. **Fairbairn L, Kapetanovic R, Sester DP, Hume DA**. The mononuclear phagocyte system of the pig as a model for understanding human innate immunity and disease. *J Leukoc Biol*. Epub ahead of print 2011. DOI: 10.1189/jlb.1110607.
392. **Chung WY, Wanford JJ, Kumar R, Isherwood JD, Haigh RD, *et al.*** An ex vivo porcine spleen perfusion as a model of bacterial sepsis. *ALTEX*. Epub ahead of print 2019. DOI: 10.14573/altex.1805131.
393. **Nathan CF, Prendergast TJ, Wiebe ME, Richard Stanley E, Platzer E, *et al.*** Activation of human macrophages: Comparison of other cytokines with interferon-γ. *J Exp Med*. Epub ahead of print 1984. DOI: 10.1084/jem.160.2.600.
394. **Van Rossum AMC, Lysenko ES, Weiser JN**. Host and bacterial factors contributing to the clearance of colonization by Streptococcus pneumoniae in a murine model. *Infect Immun*. Epub ahead of print 2005. DOI: 10.1128/IAI.73.11.7718-7726.2005.
395. **Kadioglu A, Cuppone AM, Trappetti C, List T, Spreafico A, *et al.*** Sex-based differences in susceptibility to respiratory and systemic pneumococcal disease in mice. *J Infect Dis*. Epub ahead of print 2011. DOI: 10.1093/infdis/jir657.
396. **Van Der Velden AWM, Copass MK, Starnbach MN**. Salmonella inhibit T cell proliferation by a direct, contact-dependent immunosuppressive effect. *Proc Natl Acad Sci U S A*. Epub ahead of print 2005. DOI:

10.1073/pnas.0504382102.

397. **Gao LY, Kwaik YA**. The modulation of host cell apoptosis by intracellular bacterial pathogens. *Trends in Microbiology*. Epub ahead of print 2000. DOI: 10.1016/S0966-842X(00)01784-4.
398. **Jubrail J, Morris P, Bewley MA, Stoneham S, Johnston SA, *et al.*** Inability to sustain intraphagolysosomal killing of Staphylococcus aureus predisposes to bacterial persistence in macrophages. *Cell Microbiol*. Epub ahead of print 2016. DOI: 10.1111/cmi.12485.
399. **Boldock E, Surewaard BGJ, Shamarina D, Na M, Fei Y, *et al.*** Human skin commensals augment Staphylococcus aureus pathogenesis. *Nature Microbiology*. Epub ahead of print 2018. DOI: 10.1038/s41564-018-0198-3.
400. **Macher AM, Bennett JE, Gadek JE, Frank MM**. Complement depletion in cryptococcal sepsis. *J Immunol*.
401. **Ren J, Zhao Y, Yuan Y, Han G, Li W, *et al.*** Complement Depletion Deteriorates Clinical Outcomes of Severe Abdominal Sepsis: A Conspirator of Infection and Coagulopathy in Crime? *PLoS One*. Epub ahead of print 2012. DOI: 10.1371/journal.pone.0047095.
402. **Boe DM, Boule LA, Kovacs EJ**. Innate immune responses in the ageing lung. *Clinical and Experimental Immunology*. Epub ahead of print 2017. DOI: 10.1111/cei.12881.
403. **Borges da Silva H, Fonseca R, Cassado A dos A, Machado de Salles É, de Menezes MN, *et al.*** In Vivo Approaches Reveal a Key Role for DCs in CD4+ T Cell Activation and Parasite Clearance during the Acute Phase of Experimental Blood-Stage Malaria. *PLoS Pathog*. Epub ahead of print 2015. DOI: 10.1371/journal.ppat.1004598.
404. **Borges Da Silva H, Fonseca R, Pereira RM, Cassado AA, Álvarez JM, *et al.*** Splenic macrophage subsets and their function during blood-borne infections. *Frontiers in Immunology*. Epub ahead of print 2015. DOI: 10.3389/fimmu.2015.00480.
405. **Satoh T, Kambe N, Matsue H**. NLRP3 activation induces ASC-dependent programmed necrotic cell death, which leads to neutrophilic inflammation. *Cell Death Dis*. Epub ahead of print 2013. DOI: 10.1038/cddis.2013.169.
406. **Aw D, Hilliard L, Nishikawa Y, Cadman ET, Lawrence RA, *et al.*** Disorganization of the splenic microanatomy in ageing mice. *Immunology*.

Epub ahead of print 2016. DOI: 10.1111/imm.12590.

407. **Huizinga R, Easton AS, Donachie AM, Guthrie J, van Rijs W, *et al.*** Sialylation of campylobacter jejuni lipo-oligosaccharides: Impact on phagocytosis and cytokine production in mice. *PLoS One*. Epub ahead of print 2012. DOI: 10.1371/journal.pone.0034416.
408. **Perez OA, Yeung ST, Vera-Licona P, Romagnoli PA, Samji T, *et al.*** CD169+ macrophages orchestrate innate immune responses by regulating bacterial localization in the spleen. *Sci Immunol*. Epub ahead of print 2017. DOI: 10.1126/sciimmunol.aah5520.
409. **Miyake Y, Asano K, Kaise H, Uemura M, Nakayama M, *et al.*** Critical role of macrophages in the marginal zone in the suppression of immune responses to apoptotic cell-associated antigens. *J Clin Invest*. Epub ahead of print 2007. DOI: 10.1172/JCI31990.
410. **Birmingham CL, Canadien V, Kaniuk NA, Steinberg BE, Higgins DE, *et al.*** Listeriolysin O allows Listeria monocytogenes replication in macrophage vacuoles. *Nature*. Epub ahead of print 2008. DOI: 10.1038/nature06479.
411. **Takahashi K, Donovan MJ, Rogers RA, Ezekowitz RAB**. Distribution of murine mannose receptor expression from early embryogenesis through to adulthood. *Cell Tissue Res*. Epub ahead of print 1998. DOI: 10.1007/s004410051062.
412. **Casewell M, Phillips I**. Hands as route of transmission for Klebsiella species. *Br Med J*. Epub ahead of print 1977. DOI: 10.1136/bmj.2.6098.1315.
413. **Casewell M, Phillips I**. Food as a source of Klebsiella species for colonisation and infection of intensive care patients. *J Clin Pathol*. Epub ahead of print 1978. DOI: 10.1136/jcp.31.9.845.
414. **Brown C, Seidler RJ**. Potential Pathogens in the Environment: Klebsiella pneumoniae, a Taxonomic and Ecological Enigma1. *Appl Microbiol*. Epub ahead of print 1973. DOI: 10.1128/aem.25.6.900-904.1973.
415. **Iniguez AL, Dong Y, Triplett EW**. Nitrogen fixation in wheat provided by Klebsiella pneumoniae 342. *Mol Plant-Microbe Interact*. Epub ahead of print 2004. DOI: 10.1094/MPMI.2004.17.10.1078.
416. **Jun JB**. Klebsiella pneumoniae liver abscess. *Infection and Chemotherapy*. Epub ahead of print 2018. DOI: 10.3947/ic.2018.50.3.210.
417. **Ko WC, Paterson DL, Sagnimeni AJ, Hansen DS, Von Gottberg A, *et al.***

Community-acquired Klebsiella pneumoniae bacteremia: Global differences in clinical patterns. *Emerg Infect Dis*. Epub ahead of print 2002. DOI: 10.3201/eid0802.010025.

418. **Bowring BG, Fahy VA, Morris A, Collins AM**. An unusual culprit: Klebsiella pneumoniae causing septicaemia outbreaks in neonatal pigs? *Vet Microbiol*. Epub ahead of print 2017. DOI: 10.1016/j.vetmic.2017.03.018.
419. **Bidewell CA, Williamson SM, Rogers J, Tang Y, Ellis RJ, *et al.*** Emergence of Klebsiella pneumoniae subspecies pneumoniae as a cause of septicaemia in pigs in England. *PLoS One*. Epub ahead of print 2018. DOI: 10.1371/journal.pone.0191958.
420. **Lawlor MS, Hsu J, Rick PD, Miller VL**. Identification of Klebsiella pneumoniae virulence determinants using an intranasal infection model. *Mol Microbiol*. Epub ahead of print 2005. DOI: 10.1111/j.1365-2958.2005.04918.x.
421. **Hoh CH, Tan YH, Gan Y-H**. PROTECTIVE ROLE OF KUPFFER CELLS AND MACROPHAGES IN KLEBSIELLA PNEUMONIAE INDUCED LIVER ABSCESS DISEASE. *Infect Immun*. Epub ahead of print 2019. DOI: 10.1128/iai.00369-19.
422. **Shon AS, Bajwa RPS, Russo TA**. Hypervirulent (hypermucoviscous) Klebsiella pneumoniae . *Virulence*. Epub ahead of print 2013. DOI: 10.4161/viru.22718.
423. **Sánchez-López J, García-Caballero A, Navarro-San Francisco C, Quereda C, Ruiz-Garbajosa P, *et al.*** Hypermucoviscous Klebsiella pneumoniae: A challenge in community acquired infection. *IDCases*. Epub ahead of print 2019. DOI: 10.1016/j.idcr.2019.e00547.
424. **Lee CH, Leu HS, Hu TH, Liu JW**. Splenic abscess in southern Taiwan. *J Microbiol Immunol Infect*.
425. **Wang J, Liu Y, Lee SS, Yen M, Wang YC, *et al.*** Primary Liver Abscess Due to Klebsiella pneumoniae in Taiwan . *Clin Infect Dis*. Epub ahead of print 1998. DOI: 10.1086/516369.
426. **Siu LK, Yeh KM, Lin JC, Fung CP, Chang FY**. Klebsiella pneumoniae liver abscess: A new invasive syndrome. *The Lancet Infectious Diseases*. Epub ahead of print 2012. DOI: 10.1016/S1473-3099(12)70205-0.
427. **Tan TY, Ong M, Cheng Y, Ng LSY**. Hypermucoviscosity, rmpA, and aerobactin are associated with community-acquired Klebsiella pneumoniae

bacteremic isolates causing liver abscess in Singapore. *J Microbiol Immunol Infect*. Epub ahead of print 2019. DOI: 10.1016/j.jmii.2017.07.003.

428. **Lee HC, Chuang YC, Yu WL, Lee NY, Chang CM, *et al.*** Clinical implications of hypermucoviscosity phenotype in Klebsiella pneumoniae isolates: Association with invasive syndrome in patients with community-acquired bacteraemia. *J Intern Med*. Epub ahead of print 2006. DOI: 10.1111/j.1365-2796.2006.01641.x.
429. **Bialek-Davenet S, Criscuolo A, Ailloud F, Passet V, Jones L, *et al.*** Genomic definition of hypervirulent and multidrug-resistant klebsiella pneumoniae clonal groups. *Emerg Infect Dis*. Epub ahead of print 2014. DOI: 10.3201/eid2011.140206.
430. **Du P, Zhang Y, Chen C**. Emergence of carbapenem-resistant hypervirulent Klebsiella pneumoniae. *The Lancet Infectious Diseases*. Epub ahead of print 2018. DOI: 10.1016/S1473-3099(17)30625-4.
431. **Russo TA, Olson R, Fang CT, Stoesser N, Miller M, *et al.*** Identification of biomarkers for differentiation of hypervirulent klebsiella pneumoniae from classical K. pneumoniae. *J Clin Microbiol*. Epub ahead of print 2018. DOI: 10.1128/JCM.00776-18.
432. **Podschun R, Ullmann U**. Klebsiella spp. as nosocomial pathogens: Epidemiology, taxonomy, typing methods, and pathogenicity factors. *Clinical Microbiology Reviews*. Epub ahead of print 1998. DOI: 10.1128/cmr.11.4.589.
433. **Elemam A, Rahimian J, Mandell W**. Infection with Panresistant Klebsiella pneumoniae: A Report of 2 Cases and a Brief Review of the Literature . *Clin Infect Dis*. Epub ahead of print 2009. DOI: 10.1086/600042.
434. **Gu D, Dong N, Zheng Z, Lin D, Huang M, *et al.*** A fatal outbreak of ST11 carbapenem-resistant hypervirulent Klebsiella pneumoniae in a Chinese hospital: a molecular epidemiological study. *Lancet Infect Dis*. Epub ahead of print 2018. DOI: 10.1016/S1473-3099(17)30489-9.
435. **Decré D, Verdet C, Emirian A, Le Gourrierec T, Petit JC, *et al.*** Emerging severe and fatal infections due to Klebsiella pneumoniae in two university hospitals in France. *J Clin Microbiol*. Epub ahead of print 2011. DOI: 10.1128/JCM.00676-11.
436. **Kabha K, Nissimov L, Athamna A, Keisari Y, Parolis H, *et al.*** Relationships among capsular structure, phagocytosis, and mouse virulence in Klebsiella

pneumoniae. *Infect Immun*. Epub ahead of print 1995. DOI: 10.1128/iai.63.3.847-852.1995.

437. **Tsai YK, Fung CP, Lin JC, Chen JH, Chang FY, *et al.*** Klebsiella pneumoniae Outer membrane porins OmpK35 and OmpK36 play roles in both antimicrobial resistance and virulence. *Antimicrob Agents Chemother*. Epub ahead of print 2011. DOI: 10.1128/AAC.01275-10.
438. **Poole K**. Efflux pumps as antimicrobial resistance mechanisms. *Annals of Medicine*. Epub ahead of print 2007. DOI: 10.1080/07853890701195262.
439. **Nordmann P, Cuzon G, Naas T**. The real threat of Klebsiella pneumoniae carbapenemase-producing bacteria. *The Lancet Infectious Diseases*. Epub ahead of print 2009. DOI: 10.1016/S1473-3099(09)70054-4.
440. Antimicrobial Prescribing Guidelines. *(NICE) National Institute for Health and Care Excellence*. https://www.nice.org.uk/about/what-we-do/our-programmes/nice-guidance/antimicrobial-prescribing-guidelines (2019, accessed 20 February 2020).
441. **Van Duin D, Kaye KS, Neuner EA, Bonomo RA**. Carbapenem-resistant Enterobacteriaceae: A review of treatment and outcomes. *Diagnostic Microbiology and Infectious Disease*. Epub ahead of print 2013. DOI: 10.1016/j.diagmicrobio.2012.11.009.
442. **Humphries RM, Kelesidis T, Bard JD, Ward KW, Bhattacharya D, *et al.*** Successful treatment of pan-resistant Klebsiella pneumoniae pneumonia and bacteraemia with a combination of high-dose tigecycline and colistin. *J Med Microbiol*. Epub ahead of print 2010. DOI: 10.1099/jmm.0.023010-0.
443. **Tian GB, Doi Y, Shen J, Walsh TR, Wang Y, *et al.*** MCR-1-producing Klebsiella pneumoniae outbreak in China. *The Lancet Infectious Diseases*. Epub ahead of print 2017. DOI: 10.1016/S1473-3099(17)30266-9.
444. **Leung LM, Cooper VS, Rasko DA, Guo Q, Pacey MP, *et al.*** Structural modification of LPS in colistin-resistant, KPC-producing Klebsiella pneumoniae. *J Antimicrob Chemother*. Epub ahead of print 2017. DOI: 10.1093/jac/dkx234.
445. **Kidd TJ, Mills G, Sá-Pessoa J, Dumigan A, Frank CG, *et al.*** A Klebsiella pneumoniae antibiotic resistance mechanism that subdues host defences and promotes virulence . *EMBO Mol Med*. Epub ahead of print 2017. DOI: 10.15252/emmm.201607336.

446. **David S, Reuter S, Harris SR, Glasner C, Feltwell T, *et al.*** Epidemic of carbapenem-resistant Klebsiella pneumoniae in Europe is driven by nosocomial spread. *Nat Microbiol*. Epub ahead of print 2019. DOI: 10.1038/s41564-019-0492-8.
447. **Lam MMC, Wyres KL, Duchêne S, Wick RR, Judd LM, *et al.*** Population genomics of hypervirulent Klebsiella pneumoniae clonal-group 23 reveals early emergence and rapid global dissemination. *Nat Commun*. Epub ahead of print 2018. DOI: 10.1038/s41467-018-05114-7.
448. **Wyres KL, Nguyen TNT, Lam MMC, Judd LM, van Vinh Chau N, *et al.*** Genomic surveillance for hypervirulence and multi-drug resistance in invasive Klebsiella pneumoniae from South and Southeast Asia. *Genome Med*. Epub ahead of print 2020. DOI: 10.1186/s13073-019-0706-y.
449. **Wyres KL, Wick RR, Judd LM, Froumine R, Tokolyi A, *et al.*** Distinct evolutionary dynamics of horizontal gene transfer in drug resistant and virulent clones of Klebsiella pneumoniae. *PLoS Genet*. Epub ahead of print 2019. DOI: 10.1371/journal.pgen.1008114.
450. **Karabinis A, Paramythiotou E, Mylona-Petropoulou D, Kalogeromitros A, Katsarelis N, *et al.*** Colistin for Klebsiella pneumoniae –Associated Sepsis . *Clin Infect Dis*. Epub ahead of print 2004. DOI: 10.1086/380461.
451. **Mouloudi E, Massa E, Piperidou M, Papadopoulos S, Iosifidis E, *et al.*** Tigecycline for treatment of carbapenem-resistant klebsiella pneumoniae infections after liver transplantation in the intensive care unit: A 3-year study. In: *Transplantation Proceedings*. 2014. Epub ahead of print 2014. DOI: 10.1016/j.transproceed.2014.09.160.
452. **Elgendy SG, Abdel Hameed MR, El-Mokhtar MA**. Tigecycline resistance among Klebsiella pneumoniae isolated from febrile neutropenic patients. *J Med Microbiol*. Epub ahead of print 2018. DOI: 10.1099/jmm.0.000770.
453. **Van Duin D, Lok JJ, Earley M, Cober E, Richter SS, *et al.*** Colistin Versus Ceftazidime-Avibactam in the Treatment of Infections Due to Carbapenem-Resistant Enterobacteriaceae. *Clin Infect Dis*. Epub ahead of print 2018. DOI: 10.1093/cid/cix783.
454. **Oikonomou KG, Aye M**. Klebsiella pneumoniae liver abscess: A case series of six Asian patients. *Am J Case Rep*. Epub ahead of print 2017. DOI: 10.12659/AJCR.905191.

455. **Tan YM, Chung AYF, Chow PKH, Cheow PC, Wong WK, *et al.*** An appraisal of surgical and percutaneous drainage for pyogenic liver abscesses larger than 5 cm. *Ann Surg*. Epub ahead of print 2005. DOI: 10.1097/01.sla.0000154265.14006.47.
456. **Feldman MF, Mayer Bridwell AE, Scott NE, Vinogradov E, McKee SR, *et al.*** A promising bioconjugate vaccine against hypervirulent Klebsiella pneumoniae. *Proc Natl Acad Sci U S A*. Epub ahead of print 2019. DOI: 10.1073/pnas.1907833116.
457. **Malachowa N, Kobayashi SD, Porter AR, Freedman B, Hanley PW, *et al.*** Vaccine protection against multidrug-resistant klebsiella pneumoniae in a nonhuman primate model of severe lower respiratory tract infection. *MBio*. Epub ahead of print 2019. DOI: 10.1128/mBio.02994-19.
458. **Choi M, Tennant SM, Simon R, Cross AS**. Progress towards the development of Klebsiella vaccines. *Expert Review of Vaccines*. Epub ahead of print 2019. DOI: 10.1080/14760584.2019.1635460.
459. **Chen K, Fisher C, Zheng M, Weaver C, Kolls JK**. Immunization Of Heat-Killed Klebsiella Pneumoniae Promotes Strong Mucosal Th17 Responses And Protects Mice From Live Infection. 2011. Epub ahead of print 2011. DOI: 10.1164/ajrccm-conference.2011.183.1_meetingabstracts.a1400.
460. **Cryz SJ, Furer E, Germanier R**. Protection against fatal Klebsiella pneumoniae burn wound sepsis by passive transfer of anticapsular polysaccharide. *Infect Immun*. Epub ahead of print 1984. DOI: 10.1128/iai.45.1.139-142.1984.
461. **Rukavina T, Tićac B, Susa M, Jendrike N, Jonjić S, *et al.*** Protective effect of antipopolysaccharide monoclonal antibody in experimental Klebsiella infection. *Infect Immun*. Epub ahead of print 1997. DOI: 10.1128/iai.65.5.1754-1760.1997.
462. **Lin JC, Chang FY, Fung CP, Xu JZ, Cheng HP, *et al.*** High prevalence of phagocytic-resistant capsular serotypes of Klebsiella pneumoniae in liver abscess. *Microbes Infect*. Epub ahead of print 2004. DOI: 10.1016/j.micinf.2004.06.003.
463. **Llobet E, Tomás JM, Bengoechea JA**. Capsule polysaccharide is a bacterial decoy for antimicrobial peptides. *Microbiology*. Epub ahead of print 2008. DOI: 10.1099/mic.0.2008/022301-0.

464. **Dumigan A, Fitzgerald M, Santos JSPG, Hamid U, O'kane CM, *et al.*** A porcine ex vivo lung perfusion model to investigate bacterial pathogenesis. *MBio*. Epub ahead of print 2019. DOI: 10.1128/mBio.02802-19.
465. **Doorduijn DJ, Rooijakkers SHM, van Schaik W, Bardoel BW**. Complement resistance mechanisms of Klebsiella pneumoniae. *Immunobiology*. Epub ahead of print 2016. DOI: 10.1016/j.imbio.2016.06.014.
466. **Hsieh P, Lin T, Lee C, Tsai S, Wang J**. Serum-Induced Iron-Acquisition Systems and TonB Contribute to Virulence in Klebsiella pneumoniae Causing Primary Pyogenic Liver Abscess . *J Infect Dis*. Epub ahead of print 2008. DOI: 10.1086/588383.
467. **Carniel E**. The Yersinia high-pathogenicity island: An iron-uptake island. *Microbes and Infection*. Epub ahead of print 2001. DOI: 10.1016/S1286-4579(01)01412-5.
468. **Nassif X, Sansonetti PJ**. Correlation of the virulence of Klebsiella pneumoniae K1 and K2 with the presence of a plasmid encoding aerobactin. *Infect Immun*.
469. **Putze J, Hennequin C, Nougayrède JP, Zhang W, Homburg S, *et al.*** Genetic structure and distribution of the colibactin genomic island among members of the family Enterobacteriaceae. *Infect Immun*. Epub ahead of print 2009. DOI: 10.1128/IAI.00522-09.
470. **Chen YT, Chang HY, Lai YC, Pan CC, Tsai SF, *et al.*** Sequencing and analysis of the large virulence plasmid pLVPK of Klebsiella pneumoniae CG43. *Gene*. Epub ahead of print 2004. DOI: 10.1016/j.gene.2004.05.008.
471. **Holden VI, Wright MS, Houle S, Collingwood A, Dozois CM, *et al.*** Iron Acquisition and Siderophore Release by Carbapenem-Resistant Sequence Type 258 Klebsiella pneumoniae . *mSphere*. Epub ahead of print 2018. DOI: 10.1128/msphere.00125-18.
472. **Shankar-Sinha S, Valencia GA, Janes BK, Rosenberg JK, Whitfield C, *et al.*** The Klebsiella pneumoniae O Antigen Contributes to Bacteremia and Lethality during Murine Pneumonia. *Infect Immun*. Epub ahead of print 2004. DOI: 10.1128/IAI.72.3.1423-1430.2004.
473. **March C, Cano V, Moranta D, Llobet E, Pérez-Gutiérrez C, *et al.*** Role of Bacterial Surface Structures on the Interaction of Klebsiella pneumoniae with Phagocytes. *PLoS One*. Epub ahead of print 2013. DOI:

10.1371/journal.pone.0056847.

474. **Evrard B, Balestrino D, Dosgilbert A, Bouya-Gachancard JLJ, Charbonnel N, *et al.*** Roles of capsule and lipopolysaccharide O antigen in interactions of human monocyte-derived dendritic cells and Klebsiella pneumoniae. *Infect Immun*. Epub ahead of print 2010. DOI: 10.1128/IAI.00864-09.
475. **Ciurana B, Tomas JM**. Role of lipopolysaccharide and complement in susceptibility of Klebsiella pneumoniae to nonimmune serum. *Infect Immun*. Epub ahead of print 1987. DOI: 10.1128/iai.55.11.2741-2746.1987.
476. **Lee JC, Lee EJ, Lee JH, Jun SH, Choi CW, *et al.*** Klebsiella pneumoniae secretes outer membrane vesicles that induce the innate immune response. *FEMS Microbiol Lett*. Epub ahead of print 2012. DOI: 10.1111/j.1574-6968.2012.02549.x.
477. **Pettit RK, Judd RC**. Characterization of naturally elaborated blebs from serum-susceptible and serum-resistant strains of Neisseria gonorrhoeae. *Mol Microbiol*. Epub ahead of print 1992. DOI: 10.1111/j.1365-2958.1992.tb01521.x.
478. **Llobet E, Martínez-Moliner V, Moranta D, Dahlström KM, Regueiro V, *et al.*** Deciphering tissue-induced Klebsiella pneumoniae lipid a structure. *Proc Natl Acad Sci U S A*. Epub ahead of print 2015. DOI: 10.1073/pnas.1508820112.
479. **Fodah RA, Scott JB, Tam HH, Yan P, Pfeffer TL, *et al.*** Correlation of Klebsiella pneumoniae comparative genetic analyses with virulence profiles in a murine respiratory disease model. *PLoS One*. Epub ahead of print 2014. DOI: 10.1371/journal.pone.0107394.
480. **Elliott AG, Ganesamoorthy D, Coin L, Cooper MA, Cao MD**. Complete genome sequence of Klebsiella quasipneumoniae subsp. similipneumoniae strain ATCC 700603. *Genome Announc*;4. Epub ahead of print 2016. DOI: 10.1128/genomeA.00438-16.
481. **Chung WY, Gravante G, Al-Leswas D, Arshad A, Sorge R, *et al.*** The Development of a Multiorgan Ex Vivo Perfused Model: Results With the Porcine Liver-Kidney Circuit Over 24 Hours. *Artif Organs*. Epub ahead of print 2013. DOI: 10.1111/aor.12003.
482. **Bidewell CA, Williamson SM, Rogers J, Tang Y, Ellis RJ, *et al.*** Emergence of Klebsiella pneumoniae subspecies pneumoniae as a cause of septicaemia

in pigs in England. *PLoS One*;22. Epub ahead of print 2018. DOI: 10.1371/journal.pone.0191958.

483. **Bowring BG, Fahy VA, Morris A, Collins AM**. An unusual culprit: Klebsiella pneumoniae causing septicaemia outbreaks in neonatal pigs? *Vet Microbiol* 2017;203:267–270.
484. **Siu LK, Yeh KM, Lin JC, Fung CP, Chang FY**. Klebsiella pneumoniae liver abscess: A new invasive syndrome. *Lancet Infect Dis* 2012;12:881–7.
485. **Kong H, Yu F, Zhang W, Li X**. Clinical and microbiological characteristics of pyogenic liver abscess in a tertiary hospital in East China. *Med (United States)*;96. Epub ahead of print 2017. DOI: 10.1097/MD.0000000000008050.
486. **Cheng AG, DeDent AC, Schneewind O, Missiakas D**. A play in four acts: Staphylococcus aureus abscess formation. *Trends Microbiol* 2011;19:225–32.
487. **Thammavongsa V, Missiakas DM, Schneewind O**. Staphylococcus aureus degrades neutrophil extracellular traps to promote immune cell death. *Science (80-)* 2013;342:863–6.
488. **Segal AW**. HOW NEUTROPHILS KILL MICROBES. *Annu Rev Immunol* 2005;23:197–223.
489. **Willingham SB, Allen IC, Bergstralh DT, Brickey WJ, Huang MT-H, *et al.*** NLRP3 (NALP3, Cryopyrin) Facilitates In Vivo Caspase-1 Activation, Necrosis, and HMGB1 Release via Inflammasome-Dependent and -Independent Pathways. *J Immunol* 2009;183:2008–2015.
490. **Satoh T, Kambe N, Matsue H**. NLRP3 activation induces ASC-dependent programmed necrotic cell death, which leads to neutrophilic inflammation. *Cell Death Dis*;23. Epub ahead of print 2013. DOI: 10.1038/cddis.2013.169.
491. **Kobayashi SD, Porter AR, Dorward DW, Brinkworth AJ, Chen L, *et al.*** Phagocytosis and Killing of Carbapenem-Resistant ST258 Klebsiella pneumoniae by Human Neutrophils. *J Infect Dis*. Epub ahead of print 2016. DOI: 10.1093/infdis/jiw001.
492. **Wang L, Shen D, Wu H, Ma Y**. Resistance of hypervirulent Klebsiella pneumoniae to both intracellular and extracellular killing of neutrophils. *PLoS One*. Epub ahead of print 2017. DOI: 10.1371/journal.pone.0173638.
493. **Kobayashi SD, Porter AR, Dorward DW, Brinkworth AJ, Chen L, *et al.*** Phagocytosis and Killing of Carbapenem-Resistant ST258 Klebsiella pneumoniae by Human Neutrophils. *J Infect Dis* 2016;213:1615–22.

494. **Kobayashi SD, Porter AR, Freedman B, Pandey R, Chen L, *et al.*** Antibody-mediated killing of carbapenem-resistant ST258 Klebsiella pneumoniae by human neutrophils. *MBio*;9. Epub ahead of print 2018. DOI: 10.1128/mBio.00297-18.
495. **Wang L, Shen D, Wu H, Ma Y**. Resistance of hypervirulent Klebsiella pneumoniae to both intracellular and extracellular killing of neutrophils. *PLoS One*. Epub ahead of print 2017. DOI: 10.1371/journal.pone.0173638.
496. **Ko WC, Paterson DL, Sagnimeni AJ, Hansen DS, Von Gottberg A, *et al.*** Community-acquired Klebsiella pneumoniae bacteremia: Global differences in clinical patterns. *Emerg Infect Dis* 2002;8:160–166.
497. **Fazili T, Sharngoe C, Endy T, Kiska D, Javaid W, *et al.*** Klebsiella pneumoniae Liver Abscess: An Emerging Disease. *Am J Med Sci* 2016;351:297–304.
498. **Shon AS, Bajwa RPS, Russo TA**. Hypervirulent (hypermucoviscous) Klebsiella pneumoniae. *Virulence* 2013;4:107–118.
499. **Cano V, March C, Insua JL, Aguiló N, Llobet E, *et al.*** Klebsiella pneumoniae survives within macrophages by avoiding delivery to lysosomes. *Cell Microbiol* 2015;17:11.
500. **Lin JC, Chang FY, Fung CP, Xu JZ, Cheng HP, *et al.*** High prevalence of phagocytic-resistant capsular serotypes of Klebsiella pneumoniae in liver abscess. *Microbes Infect* 2004;6:1191–8.
501. **Hoh CH, Tan YH, Gan Y-H**. PROTECTIVE ROLE OF KUPFFER CELLS AND MACROPHAGES IN KLEBSIELLA PNEUMONIAE INDUCED LIVER ABSCESS DISEASE. *Infect Immun*;87. Epub ahead of print 2019. DOI: 10.1128/iai.00369-19.
502. **Fodah RA, Scott JB, Tam HH, Yan P, Pfeffer TL, *et al.*** Correlation of Klebsiella pneumoniae comparative genetic analyses with virulence profiles in a murine respiratory disease model. *PLoS One*;9. Epub ahead of print 2014. DOI: 10.1371/journal.pone.0107394.
503. **Nordmann P, Cuzon G, Naas T**. The real threat of Klebsiella pneumoniae carbapenemase-producing bacteria. *Lancet Infect Dis* 2009;9:228–36.
504. **Bathoorn E, Tsioutis C, da Silva Voorham JM, Scoulica E V., Ioannidou E, *et al.*** Emergence of pan-resistance in KPC-2 carbapenemase-producing Klebsiella pneumoniae in Crete, Greece: A close call. *J Antimicrob Chemother*

2016;71:1207–12.

505. **Dong N, Lin D, Zhang R, Chan EWC, Chen S**. Carriage of bla KPC-2 by a virulence plasmid in hypervirulent Klebsiella pneumoniae. *J Antimicrob Chemother* 2018;73:3317–3321.
506. **Jun JB**. Klebsiella pneumoniae liver abscess. *Infect Chemother* 2018;50:210–218.
507. **Seral C, Barcia-Macay M, Mingeot-Leclercq MP, Tulkens PM, Van Bambeke F**. Comparative activity of quinolones (ciprofloxacin, levofloxacin, moxifloxacin and garenoxacin) against extracellular and intracellular infection by Listeria monocytogenes and Staphylococcus aureus in J774 macrophages. *J Antimicrob Chemother* 2005;55:511–7.
508. **Matsumoto SI, Saito H, Inui KI**. Transcellular transport of oral cephalosporins in human intestinal epithelial cells, Caco-2: Interaction with dipeptide transport systems in apical and basolateral membranes. *J Pharmacol Exp Ther* 1994;270:498-504.
509. **Rodvold KA**. Clinical pharmacokinetics of clarithromycin. *Clin Pharmacokinet* 1999;37:385–98.
510. **Fairbairn L, Kapetanovic R, Sester DP, Hume DA**. The mononuclear phagocyte system of the pig as a model for understanding human innate immunity and disease. *J Leukoc Biol* 2011;89:855–71.
511. **Steiniger BS**. Human spleen microanatomy: Why mice do not suffice. *Immunology* 2015;145:334–46.
512. **Casadevall A, Fang FC**. The intracellular pathogen concept. *Molecular Microbiology*. Epub ahead of print 2019. DOI: 10.1111/mmi.14421.
513. **Garai P, Berry L, Moussouni M, Bleves S, Blanc-Potard AB**. Killing from the inside: Intracellular role of T3SS in the fate of pseudomonas aeruginosa within macrophages revealed by mgtC and oprF mutants. *PLoS Pathog*. Epub ahead of print 2019. DOI: 10.1371/journal.ppat.1007812.
514. **Günzel D, Kucharski LM, Kehres DG, Romero MF, Maguire ME**. The MgtC virulence factor of salmonella enterica serovar typhimurium activates Na+,K+-ATPase. *J Bacteriol*. Epub ahead of print 2006. DOI: 10.1128/JB.00296-06.
515. **Silva-Herzog E, Detweiler CS**. Salmonella enterica replication in hemophagocytic macrophages requires two type three secretion systems. *Infect Immun*. Epub ahead of print 2010. DOI: 10.1128/IAI.00292-10.

516. **Blanc-Potard AB, Lafay B**. MgtC as a Horizontally-Acquired Virulence Factor of Intracellular Bacterial Pathogens: Evidence from Molecular Phylogeny and Comparative Genomics. *J Mol Evol*. Epub ahead of print 2003. DOI: 10.1007/s00239-003-2496-4.
517. **Subramanian S, Roberts CL, Hart CA, Martin HM, Edwards SW, *et al.*** Replication of colonic crohn's disease mucosal Escherichia coli isolates within macrophages and their susceptibility to antibiotics. *Antimicrob Agents Chemother*. Epub ahead of print 2008. DOI: 10.1128/AAC.00375-07.
518. **Pujol C, Bliska JB**. The ability to replicate in macrophages is conserved between Yersinia pestis and Yersinia pseudotuberculosis. *Infect Immun*. Epub ahead of print 2003. DOI: 10.1128/IAI.71.10.5892-5899.2003.
519. **Nikulin J, Panzner U, Frosch M, Schubert-Unkmeir A**. Intracellular survival and replication of Neisseria meningitidis in human brain microvascular endothelial cells. *Int J Med Microbiol*. Epub ahead of print 2006. DOI: 10.1016/j.ijmm.2006.06.006.
520. **Surewaard BGJ, Deniset JF, Zemp FJ, Amrein M, Otto M, *et al.*** Identification and treatment of the Staphylococcus aureus reservoir in vivo. *J Exp Med*. Epub ahead of print 2016. DOI: 10.1084/jem.20160334.
521. **Horn J, Stelzner K, Rudel T, Fraunholz M**. Inside job: Staphylococcus aureus host-pathogen interactions. *International Journal of Medical Microbiology*. Epub ahead of print 2018. DOI: 10.1016/j.ijmm.2017.11.009.
522. **O'Neill AM, Thurston TLM, Holden DW**. Cytosolic replication of group a Streptococcus in human macrophages. *MBio*. Epub ahead of print 2016. DOI: 10.1128/mBio.00020-16.
523. **Mitsi E, Kamng'ona R, Rylance J, Solórzano C, Jesus Reiné J, *et al.*** Human alveolar macrophages predominately express combined classical M1 and M2 surface markers in steady state. *Respiratory Research*. Epub ahead of print 2018. DOI: 10.1186/s12931-018-0777-0.
524. **Desnues B, Lepidi H, Raoult D, Mege J**. Whipple Disease: Intestinal Infiltrating Cells Exhibit a Transcriptional Pattern of M2/Alternatively Activated Macrophages. *J Infect Dis*. Epub ahead of print 2005. DOI: 10.1086/491745.
525. **Benoit M, Barbarat B, Bernard A, Olive D, Mege JL**. Coxiella burnetii, the agent of Q fever, stimulates an atypical M2 activation program in human macrophages. *Eur J Immunol*. Epub ahead of print 2008. DOI:

10.1002/eji.200738067.

526. **Eisele NA, Ruby T, Jacobson A, Manzanillo PS, Cox JS, *et al.*** Salmonella require the fatty acid regulator PPARδ for the establishment of a metabolic environment essential for long-term persistence. *Cell Host Microbe*. Epub ahead of print 2013. DOI: 10.1016/j.chom.2013.07.010.
527. **Lee IR, Molton JS, Wyres KL, Gorrie C, Wong J, *et al.*** Differential host susceptibility and bacterial virulence factors driving Klebsiella liver abscess in an ethnically diverse population. *Sci Rep*. Epub ahead of print 2016. DOI: 10.1038/srep29316.
528. **Tsuchimoto Y, Asai A, Tsuda Y, Ito I, Nishiguchi T, *et al.*** M2b Monocytes Provoke Bacterial Pneumonia and Gut Bacteria-Associated Sepsis in Alcoholics. *J Immunol*. Epub ahead of print 2015. DOI: 10.4049/jimmunol.1501369.
529. **Srikhanta YN, Maguire TL, Stacey KJ, Grimmond SM, Jennings MP**. The phasevarion: a genetic system controlling coordinated, random switching of expression of multiple genes. *Proc Natl Acad Sci U S A* 2005;102:5547–51.
530. **Bayliss CD**. Determinants of phase variation rate and the fitness implications of differing rates for bacterial pathogens and commensals. *FEMS Microbiol Rev* 2009;33:504–520.
531. **De Ste Croix M, Vacca I, Kwun MJ, Ralph JD, Bentley SD, *et al.*** Phase-variable methylation and epigenetic regulation by type I restriction-modification systems. *FEMS microbiology reviews*. Epub ahead of print 2017. DOI: 10.1093/femsre/fux025.
532. **Wanford JJ, Green LR, Aidley J, Bayliss CD**. Phasome analysis of pathogenic and commensal Neisseria species expands the known repertoire of phase variable genes, and highlights common adaptive strategies. *PLoS One*. Epub ahead of print 2018. DOI: 10.1371/journal.pone.0196675.
533. **Manso AS, Chai MH, Atack JM, Furi L, De Ste Croix M, *et al.*** A random six-phase switch regulates pneumococcal virulence via global epigenetic changes. *Nat Commun*. Epub ahead of print 2014. DOI: 10.1038/ncomms6055.
534. **Berry AM, Paton JC**. Additive attenuation of virulence of Streptococcus pneumoniae by mutation of the genes encoding pneumolysin and other putative pneumococcal virulence proteins. *Infect Immun*. Epub ahead of print 2000. DOI: 10.1128/IAI.68.1.133-140.2000.

535. **Surve MV, Bhutda S, Datey A, Anil A, Rawat S, *et al.*** Heterogeneity in pneumolysin expression governs the fate of Streptococcus pneumoniae during blood-brain barrier trafficking. *PLoS Pathog*. Epub ahead of print 2018. DOI: 10.1371/journal.ppat.1007168.
536. **Lee SH, Sacks DL**. Tissue-resident macrophages as replicative niches for intracellular pathogens. *Emerg Top Life Sci*. Epub ahead of print 2017. DOI: 10.1042/etls20170110.
537. **Saylor C, Dadachova E, Casadevall A**. Monoclonal antibody-based therapies for microbial diseases. *Vaccine*. Epub ahead of print 2009. DOI: 10.1016/j.vaccine.2009.09.105.
538. **Collier MA, Gallovic MD, Peine KJ, Duong AD, Bachelder EM, *et al.*** Delivery of host cell-directed therapeutics for intracellular pathogen clearance. *Expert Review of Anti-Infective Therapy*. Epub ahead of print 2013. DOI: 10.1586/14787210.2013.845524.
539. **Assani K, Tazi MF, Amer AO, Kopp BT**. IFN-γ stimulates autophagy-mediated clearance of Burkholderia cenocepacia in human cystic fibrosis macrophages. *PLoS One*. Epub ahead of print 2014. DOI: 10.1371/journal.pone.0096681.
540. **Gallin JI, Malech HL, Weening RS, Curnutte JT, Quite PG, *et al.*** A controlled trial of interferon gamma to prevent infection in chronic granulomatous disease: The international chronic granulomatous disease cooperative study group. *N Engl J Med*. Epub ahead of print 1991. DOI: 10.1056/NEJM199102213240801.
541. **Nalos M, Santner-Nanan B, Parnell G, Tang B, McLean AS, *et al.*** Immune effects of interferon gamma in persistent staphylococcal sepsis. *American Journal of Respiratory and Critical Care Medicine*. Epub ahead of print 2012. DOI: 10.1164/ajrccm.185.1.110.
542. **Lee AJ, Ashkar AA**. The dual nature of type I and type II interferons. *Frontiers in Immunology*. Epub ahead of print 2018. DOI: 10.3389/fimmu.2018.02061.
543. **Chow OA, Von Köckritz-Blickwede M, Bright AT, Hensler ME, Zinkernagel AS, *et al.*** Statins enhance formation of phagocyte extracellular traps. *Cell Host Microbe*. Epub ahead of print 2010. DOI: 10.1016/j.chom.2010.10.005.
544. **Van Bambeke F, Barcia-Macay M, Lemaire S, Tulkens PM**. Cellular pharmacodynamics and pharmacokinetics of antibiotics: Current views and

perspectives. *Current Opinion in Drug Discovery and Development*.

545. **Carryn S, Van Bambeke F, Mingeot-Leclercq MP, Tulkens PM**. Comparative intracellular (THP-1 macrophage) and extracellular activities of β-lactams, azithromycin, gentamicin, and fluoroquinolones against Listeria monocytogenes at clinically relevant concentrations. *Antimicrob Agents Chemother*. Epub ahead of print 2002. DOI: 10.1128/AAC.46.7.2095-2103.2002.
546. **Hartog E, Menashe O, Kler E, Yaron S**. Salicylate reduces the antimicrobial activity of ciprofloxacin against extracellular Salmonella enterica serovar Typhimurium, but not against Salmonella in macrophages. *J Antimicrob Chemother*. Epub ahead of print 2010. DOI: 10.1093/jac/dkq077.
547. **Cartier MB, Scorneaux B, Zenebergh A, Desnottes JF, Talkers PM**. Cellular uptake, localization and activity of fluoroquinolones in uninfected and infected macrophages. *J Antimicrob Chemother*. Epub ahead of print 1990. DOI: 10.1093/jac/26.suppl_B.27.
548. **Grayo S, Join-Lambert O, Desroches MC, Le Monnier A**. Comparison of the in vitro efficacies of moxifloxacin and amoxicillin against Listeria monocytogenes. *Antimicrob Agents Chemother*. Epub ahead of print 2008. DOI: 10.1128/AAC.01211-07.
549. **Blais J, Beauchamp D, Chamberland S**. Azithromycin uptake and intracellular accumulation by toxoplasma gondii-infected macrophages. *J Antimicrob Chemother*. Epub ahead of print 1994. DOI: 10.1093/jac/34.3.371.
550. **Seral C, Michot JM, Chanteux H, Mingeot-Leclercq MP, Tulkens PM, *et al.*** Influence of p-glycoprotein inhibitors on accumulation of macrolides in J774 murine macrophages. *Antimicrob Agents Chemother*. Epub ahead of print 2003. DOI: 10.1128/AAC.47.3.1047-1051.2003.
551. **Restrepo MI, Sole-Violan J, Martin-Loeches I**. Macrolide therapy of pneumonia: Is it necessary, and how does it help? *Current Opinion in Infectious Diseases*. Epub ahead of print 2016. DOI: 10.1097/QCO.0000000000000250.
552. **Ito A, Ishida T, Tachibana H, Tokumasu H, Yamazaki A, *et al.*** Azithromycin combination therapy for community-acquired pneumonia: propensity score analysis. *Sci Rep*. Epub ahead of print 2019. DOI: 10.1038/s41598-019-54922-4.

553. **Yoshioka D, Kajiwara C, Ishii Y, Umeki K, Hiramatsu K, *et al.*** Efficacy of β-lactam-plus-macrolide combination therapy in a mouse model of lethal pneumococcal pneumonia. *Antimicrob Agents Chemother*. Epub ahead of print 2016. DOI: 10.1128/AAC.01024-16.
554. **Arnold FW, Lopardo G, Wiemken TL, Kelley R, Peyrani P, *et al.*** Macrolide therapy is associated with lower mortality in community-acquired bacteraemic pneumonia. *Respir Med*. Epub ahead of print 2018. DOI: 10.1016/j.rmed.2018.05.020.
555. **Drago L, Nicola L, Rodighiero V, Larosa M, Mattina R, *et al.*** Comparative evaluation of synergy of combinations of β-lactams with fluoroquinolones or a macrolide in Streptococcus pneumoniae. *J Antimicrob Chemother*. Epub ahead of print 2011. DOI: 10.1093/jac/dkr016.
556. **Bosnar M, Kelnerić Ž, Munić V, Eraković V, Parnham MJ**. Cellular uptake and efflux of azithromycin, erythromycin, clarithromycin, telithromycin, and cethromycin. *Antimicrob Agents Chemother*. Epub ahead of print 2005. DOI: 10.1128/AAC.49.6.2372-2377.2005.
557. **Nilius AM**. Antimicrobial Pharmacodynamics in Theory and Clinical Practice. *Shock*. Epub ahead of print 2002. DOI: 10.1097/00024382-200206000-00018.
558. **Skardal A, Shupe T, Atala A**. Organoid-on-a-chip and body-on-a-chip systems for drug screening and disease modeling. *Drug Discovery Today*. Epub ahead of print 2016. DOI: 10.1016/j.drudis.2016.07.003.